



The
University
Of
Sheffield.

**Fabrication of Porous Copper using Metal Injection Moulding (MIM) in
Combination with Space Holder Technique**

SHAIFUL ANWAR BIN ISMAIL

Registration No: 160122680

A thesis submitted in partial fulfillment of the requirements for the degree of
Doctor of Philosophy

The University of Sheffield
Faculty of Engineering
Department of Materials Science and Engineering

February 2023

SUMMARY

The increased interest in porous metal fabrication is due to the multi-functional properties offered by this group of materials and grabbing numerous attention of industries. Porous metal offers outstanding properties, including lightweight material, optimum strength, excellent thermal conductivity, good energy absorption and many more. These porous metals can be applied in various applications such as structural, functional, biomedical, and many more. In this project, the porous copper was fabricated by combining the powder metallurgy approach, Metal Injection Moulding (MIM), with the space holder technique, MIM-SH. This technique combines the MIM benefits, which are capable of producing complex parts and high-accuracy design, and at the same time, the pore morphologies can be controlled. This project aims to investigate the capability of the MIM-SH technique for the manufacture of porous Cu with different space holder volumes between 50-75%. A new binder system was designed for porous Cu fabrication, and the removal process of the binder and space holder can be performed simultaneously. Furthermore, a new mixing method has also been investigated that suit the new SpeedMixer Machine. The fabricated porous metal has been investigated using selected analytical analysis to determine properties such as porosity, mechanical properties, and thermal behaviour. The study involves different types of manufacturing processes, such as Metal Injection Moulding machines and Pressing Machines. The analysis and characterization process involved high-end characterization machines such as Scanning Electron Microscopy (SEM) and X-ray Fluorescence (XRF). This study produced porous Cu samples with different porosity between 8.67 to 80.7% with irregular pore shapes. The porosity development was completely replicating the morphology of the KCl as the porosity increase with the increasing space holder volume.

ACKNOWLEDGEMENT

First and foremost, I would want to express my gratitude to my sponsors, the Malaysian Government and the Universiti Teknologi Malaysia, Melaka (UTeM), for allowing me to participate in research at the University of Sheffield by providing me with financial support and other assistance. Sincere gratitude to my primary supervisor, Professor Dr. Russell Goodall, who I believe has provided me with 100 percent support, encouragement, and direction throughout the study. I can assume that this dissertation would not have been completed without his patience, determination, and supervision. Thank you also to the University of Sheffield's Department of Materials Science and Engineering for granting me a Freshgate Trust Scholarship Award for research and support. Not to be forgotten is my beloved family, my father, Ismail Kamid and mother, Noraisah Osman, who have provided me with endless encouragement, prayer, and advice. Their support has provided me with the 'refreshment' and fortitude to manage and overcome any obstacles during my studies. Special thanks to my lovely wife, Azrina binti Arshad, for always being by my side and providing me with full support. Without her understanding and persistence, this work could not have been completed. I apologise to my children, Muhammad Adam Ehsan, Muhammad Akif Ehsan, and Aisyah Humairah, for "using" our family time for my research. Thank you for your support and understanding. Last but not least, I am delighted to meet the entire Malaysian community in Sheffield, who have treated us well and provided us with consistent support throughout my time as a student. May Allah grant you the highest place in Jannah, and the memories of our time here forever keep us together.

PRESENTATIONS AND AWARD

A. PARTICIPATION IN CONFERENCES AND SYMPOSIUMS

1. Shaiful Anwar Ismail, Muhammad Hussain Ismail, Russell Goodall (2021), *Porous Copper Production via Powder Metallurgy Routes*, 29th Scientific Conference of Microscopy Society Malaysia 2021 (SCMSM 21), Perak, Malaysia, 20-21th December 2021, 20-21th December 2021.
2. Shaiful Anwar Ismail, Muhammad Hussain Ismail, Russell Goodall (2021), *Microstructure and Performance Analysis of Porous Copper Fabrication*, Asia International Innovation Exhibition (AIINEX) 2021, Johor, Malaysia, 15-17th October 2021.
3. Shaiful Anwar Ismail, Russell Goodall (2019), *Porous copper- Modification and Improvement of Manufacturing Process; Metal Injection Moulding-Space Holder Technique (MIM-SH)*, Future Materials Conference 2019, University of Leeds, UK 17th December 2019.
4. Shaiful Anwar bin Ismail, Azrina Arshad, Russell Goodall (2019), “*Do Porous Metal Can Replace the Roles of Heatsink?*”, 2nd International Research Conference and Innovation Exhibition 2019 (IRCIE), Johor Bahru, Johor, Malaysia 25-27th November 2019.
5. Shaiful Anwar Ismail, Russell Goodall (2019), *Space Holder Technique on Porous Cu Fabrication*, National Student Conference in Metallic Materials 2019, Sheffield, UK, 24-25th June 2019.
6. Shaiful Anwar Ismail, Russell Goodall (2019), *Porous Copper by Using Metal Injection Moulding* Engineering Researcher Symposium 2019, University of Sheffield, UK, 25th June 2019.
7. Shaiful Anwar Ismail, Russell Goodall (2018), *Porous Copper by Using Metal Injection Moulding*, 10th International Conference on Material and Science Technology, BITEC, Bangkok Thailand 6-7th September 2018.
8. Shaiful Anwar Ismail, Russell Goodall (2018), *Porous Copper Fabrication Using Powder Metallurgy Routes*, Engineering Researcher Symposium 2018, University of Sheffield, UK. 26th June 2018.

B. AWARDS

AWARDS	DESCRIPTION
<i>Best Micrograph Award 2021</i>	29 th Scientific Conference of Microscopy Society Malaysia 2021 (SCMSM 21), Perak, Malaysia, 20-21 th December 2021 Micrograph entitled: The Origin of Life (Scanning Electron Microscope Category) Project: Porous Copper Production via Powder Metallurgy Routes
<i>Silver Award 2021</i>	Asia International Innovation Exhibition (AIINEX) 2021, Johor, Malaysia, 15-17 th October 2021 Project: Microstructure and Performance Analysis of Porous Copper Fabrication
<i>Reader Insight Special Award 2021</i>	Asia International Innovation Exhibition (AIINEX) 2021, Johor, Malaysia, 15-17 th October 2021 Project: Microstructure and Performance Analysis of Porous Copper Fabrication
<i>Gold Medal 2019</i>	International Research Conference and Innovation 2019 (IRCIE 2019), Johor Bahru, Malaysia, 25-27 th November 2019. Project: “Do Porous Metal Can Replace the Roles of Heatsink?”
<i>Research Funding 2019</i>	Freshgate Trust Scholarship Award, The Freshgate Trust Foundation, UK, January 2019 – April th 2019 Project: Porous Copper Fabrication by using Metal Injection Moulding (MIM) Process

DECLARATION

I, Shaiful Anwar bin Ismail, the author, confirm that the Thesis is my own work. I am aware of the University's Guidance on the Use of Unfair Means. This work has not previously been presented for an award at this, or any other, university.

TABLE OF CONTENTS

SUMMARY	ii
ACKNOWLEDGEMENT.....	iii
PRESENTATIONS AND AWARD	iv
DECLARATION	vi
TABLE OF CONTENTS	vii
LIST OF FIGURES.....	xiii
LIST OF TABLES	xix
Chapter 1 INTRODUCTION.....	1
1.1 Introduction	1
1.2 Research Aim and Research Objectives.....	4
1.3 Work Scope	5
1.4 Thesis Outline.....	6
Chapter 2 LITERATURE REVIEW	8
2.1 Chapter overview	8
2.2 Porous Metals- An Introduction	8
2.2.1 Overview of Porous Copper (Cu).....	14
2.2.1.1 General overview of Cu.....	14
2.2.1.2 Powder Cu production.....	15
2.2.1.2.1 The atomization process of Cu powder	15
2.2.1.3 Cu powder properties and metallurgy	16
2.2.1.4 Porous Copper (Cu).....	17
2.3 Porous Metal- The features and characteristics.....	18
2.3.1 Open-celled and Close-celled structure.....	20
2.3.2 Methods on how to measure porosity.....	23
2.3.3 Pore generated mechanism.....	25
2.3.3.1 Inherent pores or naturally pore generated.....	25
2.3.3.2 Intentionally pore generated.....	27

2.4	Porous Metal- Applications.....	27
2.4.1	Matching pores to application	28
2.4.2	Structural Applications.....	29
2.4.2.1	Automotive industry.....	30
2.4.2.2	Biomedical application.....	31
2.4.3	The application that exploits the material characteristics (Functional application)	32
2.4.3.1	Thermal management application	32
2.4.4	Porous Cu application	33
2.5	Processing method for Porous Metal.....	35
2.5.1	Liquid-State Processing Method	36
2.5.2	Solid-State Processing Method.....	39
2.6	Processing Porous Cu via Partial Sintering Technique	42
2.7	Processing with pore generating agent- Space holder assisted.....	43
2.7.1	Space holder technique with Compaction & Sintering (C&S) Method	46
2.8	Space Holder Technique with Metal Injection Moulding Process (MIM).....	50
2.8.1	Metal Injection Moulding (MIM).....	51
2.8.2	Important aspects to be considered in MIM	54
2.8.2.1	Material selection	54
2.8.2.2	The binder system	54
2.8.2.2.1	Binder system for copper.....	55
2.8.2.2.2	PEG-PMMA-SA System.....	56
2.8.2.3	Mixing Process	57
2.8.2.4	Injection Moulding Process.....	57
2.8.2.5	Debinding Process.....	57
2.8.2.6	Sintering Process	58
2.8.3	MIM with space holder technique.....	58
2.8.4	MIM-SH for porous Cu	61
Chapter 3	MATERIALS AND EXPERIMENT	63
3.1	Chapter overview	63

3.2	Preparation of main materials (Cu and space holder) and binder components.	66
3.3	Assessment of the raw materials	68
3.3.1	Morphology characterization by Optical Microscopy and scanning electron microscopy (SEM)	68
3.3.2	Particle analysis.....	69
3.3.3	Weight and density characterization	70
3.4	Powder-Space Holder-Binder system specification	70
3.5	Mixing of Feedstock.....	73
3.6	Injection Moulding Process.....	75
3.6.1	Mould design for the MIM process	75
3.6.2	Extrusion of Feedstock.....	77
3.7	Water leaching.....	80
3.8	Thermal debinding and Sintering	82
3.9	Sample physical characterization	84
3.9.1	Physical observation of samples.....	84
3.9.2	Thermal analysis.....	85
3.9.2.1	Differential Scanning Calorimetry (DSC) analysis	85
3.9.2.2	Thermo-Gravimetric Analysis (TGA).....	86
3.9.3	Chemical composition analysis	86
3.9.3.1	X-Ray Diffraction (XRD) Analysis.....	87
3.9.3.2	X-Ray Fluorescence (XRF) Analysis	88
3.9.4	Porosity Analysis.....	89
3.9.4.1	Volumetric porosity and density measurement	89
3.9.4.2	Measurement of density	90
3.9.4.3	Pores size and shape analysis	91
3.9.5	Microstructure analysis	92
3.9.5.1	Optical Microscope Analysis (OM)	92
3.9.5.2	Scanning Electron Microscopy (SEM).....	93
3.9.5.3	Energy Dispersive X-Ray Spectrometry (EDX)	95

3.9.5.4	Alicona Infinite Focus optical measurement device.....	95
3.9.6	Mechanical Testing by Uni-Axial Compression Test	96
3.9.7	Thermal Test.....	98
Chapter 4	COMPACTION AND SINTERING (C&S) METHOD	100
4.1	Motivation to produce porous Cu via Compaction and Sintering (C&S) Method.....	100
4.2	Processing of porous Cu by using the Compaction and Sintering Method	101
4.3	Space holder removal	104
4.3.1	Porosity measurement	105
4.4	Result and Discussion	106
4.5	Work planned for porous Metal Injection Moulding (MIM) with Space Holder Technique	113
4.5.1	The benchmark for porous Cu via Metal Injection Moulding and Space Holder Technique (MIM-SH)	114
Chapter 5	MIM-SH METHOD: PROCESSING OF POROUS CU FEEDSTOCK	116
5.1	Characterisation of initial materials.....	116
5.1.1	Particle features and shape	116
5.1.2	Particle density measurement.....	118
5.1.2.1	Effect of filling pressure of pycnometer on the density measurement	121
5.1.3	Particle size.....	123
5.1.4	The binder constituents	125
5.1.4.1	Thermal analysis of the binder system- TGA and DSC	127
5.1.5	Summary of starting materials properties.....	131
5.2	Optimisation of Powder-binder ratio.....	132
5.2.1	Tapped density measurement	133
5.2.2	The Rule of Mixtures (ROM).....	134
5.2.3	Discussion on powder-binder ratio investigation	135
5.2.3.1	Powder loading through Tapped Density Analysis	135
5.2.3.2	Powder loading through the Rule of Mixtures (ROM) Technique.....	137
5.2.3.3	The possible situations according to the powder loading identifying process	139
5.3	Identification of Binder System: PEG-PMMA-SA system.....	143

5.4	Feedstock preparation by Mixing Process.....	147
5.4.1	High-Speed Mixing Process with the Introduction of SpeedMixer Machine.....	148
5.4.2	Challenges for Successful Mixing.....	150
5.4.3	Preliminary testing	151
5.4.4	Findings and discussion on the proposed mixing procedure	153
5.4.4.1	The processing temperature analysis.....	157
5.4.4.2	The introduction of cylindrically shaped zirconia.....	159
5.4.4.3	The mixing speed and time.....	161
5.4.4.4	Mixing Procedure	162
5.4.4.5	Weight of Mixture	162
5.4.4.6	Mode of mixing	163
5.4.4.7	Summarisation of Mixing Parameters	165
5.5	Feedstock Characterisation.....	166
5.5.1	Physical observation.....	166
5.5.2	Thermal Analysis on feedstock sample.....	169
5.5.2.1	Discussion on thermal analysis of feedstock	172
Chapter 6	MIM-SH METHOD: POROUS CU PRODUCTION	174
6.1	Introduction	174
6.2	Pre-injection process - Free flow injection (without using mould).....	174
6.2.1	Identifying the shape of flow feedstock	174
6.2.2	Identifying the optimum holding time for feedstock melting.....	176
6.3	The Injection processes	179
6.3.1	Identifying the optimum injection temperature range	180
6.3.2	Identifying the holding time for moulding process	183
6.4	Assessment of the sample.....	186
6.4.1	Moulding evaluation.....	186
6.4.2	Physical observation.....	188
6.4.3	Microstructure analysis	189
6.5	Debinding Process	190

6.5.1	Water dissolution of the space holder and debinding process	191
6.5.2	Sample observation and microstructure analysis.....	194
6.5.3	The binder removal without water leaching process.	196
6.6	Sintering Process	199
6.6.1	Preliminary Testing	202
Chapter 7	POROUS COPPER ASSESSMENT.....	204
7.1	Physical Analysis	204
7.2	Microstructure Analysis	206
7.2.1	Porous structure morphology	207
7.2.2	Pore size analysis.....	211
7.2.3	Porosity analysis.....	213
7.3	Mechanical Properties of Porous Cu	214
7.3.1	Mechanical stress-strain curve toward porosity differentiation.....	216
7.3.2	Compression Yield Strength of Porous Cu	219
7.4	Thermal Assessment of Porous Copper	220
7.4.1	Temperature difference towards porosity and SH amount.....	220
Chapter 8	CONCLUSION	223
Chapter 9	RECOMMENDATIONS AND FUTURE WORKS	225
REFERENCE	227

LIST OF FIGURES

Figure 1.1; Multi-functional properties of porous metal [5]	2
Figure 1.2; The basic concept of the current Ph.D. work	6
Figure 2.1; Natural (a-b) and processing porous material structure (c-d); (a) Lotus root porous structure [20], (b) Cross-sectional of cancellous bone with interconnected pores structure [21], (c) Porous titanium structure made by space holder method [22], (d) Ti-HA biocomposite foams [23]	10
Figure 2.2; The combination of porous structure in the existing metal properties	11
Figure 2.3; The heat flow through the pores of porous metal via convection [26]	12
Figure 2.4; Works related to porous metal; (a) Numbers of publications from the year 2000 until 2019 related to porous metal works, (b) Numbers of publications from the year 2000 until 2019 according to the type of metals	13
Figure 2.5; Scanning electron microscope images of Cu powder with different atomization processes [34]; (a) air-atomized Cu powder, (b) water-atomized copper	16
Figure 2.6; Example of the microstructure of pure Cu, (a) Different grain size of pure Cu due to high cooling process [41], (b) Annealed pure copper [42].....	17
Figure 2.7; Commercial Porous Cu sheet as heat absorbing material [47]	18
Figure 2.8; Example of porous metal structure (porous Cu made by Lost Carbonate Sintering (LCS) [14] ...	19
Figure 2.9; Example of the open-celled and closed structure of porous metal; (a) The structure of open-cell Cu [62], (b) Closed-cell porous Aluminium [63].....	21
Figure 2.10; Example of the application according to pore shape- open-celled and close-celled [61]	22
Figure 2.11; Porous structure measurement method based on the pore size [65]	23
Figure 2.12; The image of porous Ti with different sintering temperatures (1173K (a), 1573 (b) and 1173K c)) under low compaction pressure, 10 MPa [66]	26
Figure 2.13; The application of porous metal according to the pore structure [15]	29
Figure 2.14; Cross-sectional view of AFS material [70].....	30
Figure 2.15; AFS application for material handling vehicle [70].....	30
Figure 2.16; Prototypes of crash absorbers based on extruded aluminium hollow sections [71].....	31
Figure 2.17; Natural and human-made porous structure (a) Structure of cancellous bone, (b) Cancellous structured titanium (CSTi) [74].....	32
Figure 2.18; Porous metals production methods according to their physical behaviour [15]	36
Figure 2.19; Example of pore structure made by liquid-state processing method, (a) GASAR technique [49] (b) Investment Casting of AlZn ₁₁ foams [92].....	37
Figure 2.20; A schematic diagram of partial sintering process	42
Figure 2.21; Neck formation between powder particles; a) Sintered Cu at 750 °C for 5min, b) neck formation between Cu particles, zooming at 100µm [110].....	43

Figure 2.22; Porous Al with 70% of porosity and fabricated with different pore shapes according to space holding materials, (a) Porous Al with spherical carbamide, (b) Porous Al with strip-shaped carbamide.....	44
Figure 2.23, The introduction of space holder processing method by Zhao (2001) [121]	45
Figure 2.24; Porous Cu with NaCl as space-holding material [101].....	45
Figure 2.25; Porous Cu fabrication by using the C&S method with different types of the removal process...	47
Figure 2.26; Redraw of the Venn diagram describes the application of the PIM process concerns about three important aspects [148]	52
Figure 2.27; The comparison of process routes of MIM, plastic, and compaction process	53
Figure 2.28; Schematic diagram of metal injection moulding process [151].....	53
Figure 2.29; Comparison between general MIM process and MIM process combined with space holder technique	59
Figure 3.1; Flowchart of experimental works	64
Figure 3.2; Summary of the flow of porous Cu fabrication by MIM with space holder technique	65
Figure 3.3; The current binders in solid form. (a) PEG 1500, (b) PMMA.....	67
Figure 3.4; Blowing direction close towards the top of the mounted powder sample for SEM inspection	68
Figure 3.5; The machine and tools involved in the mixing process. (a) SpeedMixer™ DAC 800 FVZ, (b) cylindrical zirconia dispersion media.....	74
Figure 3.6; Example of feedstock, (a) raw feedstock without shaping process (after mixing process) (b) feedstock after extrusion process before it is cut into small pellets (after injection moulding process)	75
Figure 3.7; (a) The customized mould design, (b) disassemble parts of the top plate and body, (c) the schematic diagram of mould design.....	76
Figure 3.8; The mechanism for the extraction of the green samples from the mould	77
Figure 3.9; Schematic diagram of benchtop operated vertical injection moulding machine MCP-100KSA, which was used for feedstock and green part fabrication.....	78
Figure 3.10; (a) The cavity of the mould is fully filled by feedstock, (b) Solidified cylinder green part of porous Cu	79
Figure 3.11; Examples of the physical form of extruded feedstocks at the pre-injection stage; (a) desired cylindrical shape of feedstock; (b) example of an unsuitable feedstock	80
Figure 3.12; Water leaching process by water bath equipment, WiseBath WB	81
Figure 3.13; The schematic diagram of debinding process for weight loss measurement using hot plate balance.....	82
Figure 3.14; a) Modified tube furnace, (b) schematic diagram of tube furnace and sample position	83
Figure 3.15; Schematic diagram of a heat treatment profile	84
Figure 3.16; X-rays Diffraction at crystalline lattice.....	88
Figure 3.17; Nomenclature used for sample dimensions	89

Figure 3.18; Schematic diagram of the main components inside the Helium Pycnometer, Micromeritics Accupyc II	91
Figure 3.19; An example of a 60% KCl sample for Image J analysis where the colour contrast was applied to the original image to differentiate pores and solid regions	92
Figure 3.20; Schematic diagram of sample preparation for OM observation	93
Figure 3.21; The signal produced due to the interaction of the electron beam on the sample surface [216] ...	94
Figure 3.22; Example of a 3D surface image of porous Cu (0% vol. KCl) via Alicona Infinite Focus	96
Figure 3.23; A schematic diagram of compression testing	97
Figure 3.24; A customized thermal testing setup for porous Cu using the Raspberry Pie 3	99
Figure 4.1; The fabrication process of porous copper by compaction and dissolution process	101
Figure 4.2; Mould die for Compaction and Sintering (C&S) method, (a) Mould die set, (b) after the compaction process	102
Figure 4.3; Manual compaction or pressing machine	102
Figure 4.4; Sintering profile used for porous copper production in this work	104
Figure 4.5; Water leaching process to remove KCl by using ultrasonic bath	105
Figure 4.6; Green sample of compacted porous Cu; a) The defect sample (10% vol. KCl) where the space holder was congregated at the bottom of the sample, b) Sample with 20% vol. KCl without defect.	106
Figure 4.7; (a) the compaction sample with compaction pressure below 9.81 MPa, (b) final compaction copper with the acceptable pressure range (9.81MPa and 25.78MPa).....	107
Figure 4.8; The removal of the space holder from the sample that was pressing at 2 tonnes (9.61MPa)	110
Figure 4.9; The relationship of compaction pressure and KCl volume % towards porosity percentage.....	112
Figure 4.10; The effect of porosity on the variation of KCl amount.....	113
Figure 5.1; Scanning electron micrograph (secondary electron mode) of as-received Cu.....	117
Figure 5.2; The as-supplied space holder material, potassium chloride (KCl), (a) photograph of particles, (b) optical microscope image of KCl by Nikon Optical Microscope, (c) Scanning electron micrograph ((secondary electron mode) of KCl by SEM Hitachi SU 3500	118
Figure 5.3; Schematic diagram of the apparent density measurement process	119
Figure 5.4; Effect of helium filling pressure on density measurement of KCl.....	122
Figure 5.5; DSC thermal analysis on the different binder constituents.....	129
Figure 5.6; TGA analysis of pure binder components	130
Figure 5.7; The structure of Cu feedstocks was clearly deteriorated after two-hour water debinding process at 60°C.....	132
Figure 5.8; The features of feedstock with more than 60% of powder loading	135
Figure 5.9; A schematic diagram of voids formation within powder particles	136
Figure 5.10; The critical and optimal powder loading estimation graph for feedstock preparation.....	138

Figure 5.11; Three conditions of the material mixtures, (a) excess binder, (b) critical binder concentration, (c) excess powder	141
Figure 5.12; Flashing problem on the feedstock due to excessive binder concentration	141
Figure 5.13; Feedstock with different powder loading ratio; (a) Powder loading with 55% volume, (b) Powder loading with 60% powder loading	142
Figure 5.14; Powder-binder ratio versus binder system	145
Figure 5.15; Example of the result of poor mixing, (a) The feedstock shows powdery form and incorrect shape, (b) separation of binder and Cu powder, (c) example of the desirable final feedstock of porous Cu ..	147
Figure 5.16; SpeedMixer schematic diagram	149
Figure 5.17; Schematic diagram of the top view of SpeedMixer	149
Figure 5.18; Poor mixing due to the binder not blending well with Cu powder.	151
Figure 5.19; Structural failure at the green sample stage after water debinding for one hour at 40°C	151
Figure 5.20; The investigation to find the optimum mixing speed and time to melt the binder. The process was carried out with a variation of speed and time (a) The binder was still in the solid state, (b) The shape of binder particles is clearly seen in the mixture of binder and powder (Cu, KCl)	152
Figure 5.21; The morphology of the mixing process at different speeds and total times,	155
Figure 5.22; Mixing built-up temperature	158
Figure 5.23; The schematic diagram of the movement of zirconia dispersion media inside the mixing container	160
Figure 5.24; A hole at the bottom of the mixing container, caused by overheating from high energy generation with mixing media used.....	160
Figure 5.25; Defect samples obtained from the Multi-Phase Mode Mixing	163
Figure 5.26; The feedstock particles after the mixing process; (a) Molten feedstock, (b) Solidified feedstock	166
Figure 5.27; Physical observation on feedstock made with different KCl volumes, (a) Feedstock with 0% vol. of KCl, (b) Feedstock with 60% vol. of KCl.....	167
Figure 5.28; The present study of Cu-KCl-Binder mixture, (a) Schematic diagram of the mixture, (b) Example of SEM image of cross-sectional feedstock with 60% KCl	168
Figure 5.29; DSC thermal analysis on feedstock	170
Figure 5.30; TGA analysis comparison between pure PMMA and feedstock	171
Figure 6.1; Cu feedstock, (a) Good feedstock quality in the form of continuous flow cylindrical shape, b) The feedstock was successfully filled inside the mould.	175
Figure 6.2; Example of defects on the feedstock during the pre-injection process, a) Watery-look of feedstock which easily flows out without given an injection pressure, b) Droplet-look feedstock that flows out without injection pressure, c) Binder separation from the feedstock	176
Figure 6.3; The Cu feedstock trapped inside the heated barrel.	177

Figure 6.4; Green sample, a) good quality of the green sample, b) failure sample.	179
Figure 6.5; The feedstock ‘stuck’ at the inlet and cannot flow to the mould.	181
Figure 6.6; The green sample that does not completely fill up the mould and solidified.	183
Figure 6.7; The polymer flow inside the cavity during the injection process [282].....	185
Figure 6.8; Mould parts quality checking, a) good mould sample, b) and c) defect samples of short shot and flashing	187
Figure 6.9; The transformation of feedstock into a green sample after the injection moulding process. The sample was made with 50% vol. KCl.....	188
Figure 6.10; SEM image of green sample of porous Cu that made with 50% KCl.....	189
Figure 6.11; Debinded sample (made with 60% vol. KCl) after 2 hours of the water dissolution process....	191
Figure 6.12; Results of water debinding and dissolution, (a) samples with different vol% of KCl at 60°C, (b) samples with 70% vol KCl that test at different dissolution technique)	192
Figure 6.13; (a) Cross-sectional of green part 60% powder loading 40% binder with 60% volume KCl, (b) Cross-sectional of debind sample after 3 hours water leaching process at 60°C (sample 60% powder loading 40% binder with 60% volume KCl)	193
Figure 6.14; Porous Cu sample after water debinding process, (a) poor sample, (b) good sample with 50% vol. KCl after 8 hours debinding process at 60°C.	194
Figure 6.15; SEM image of porous Cu (70%.vol. KCl) after the water leaching process	195
Figure 6.16; XRD analysis on the debinded sample	196
Figure 6.17; The flow of Porous Cu by MIM process, a) Water leaching process involvement in binder and KCl removal process, b) Water leaching at the end of the processing cycle for KCl removal	197
Figure 6.18; Debinding and sintering process on porous Cu samples, a) The samples without water debinding process, b) The sample with water leaching process on binder and KCl.	198
Figure 6.19; Crack problem on the sample that sintered without water debinding process.	199
Figure 6.20; The poor-quality sample after the sintering process, a) The sample consists of too much PEG, b) The sintering was performed with high sintering temperature.....	200
Figure 6.21; Good sintered sample, (a) Porous Cu without space holder, (b) Porous Cu made with different amount of space holder.....	200
Figure 6.22; SEM image of the porous sample that shows the sintering neck formation	201
Figure 7.1; (a) Sintered porous Cu made with 60% vol. KCl, (b) Cross-section of sintered sample (60% vol. KCl).....	204
Figure 7.2; Sample crack after the sintering process.....	205
Figure 7.3, A comparison of green sample stage (with 70% KCl) with sintered sample where it shows the pore generating by space holding method.....	206
Figure 7.4; Cross-sectional samples with extreme KCl volume after the sintering process	207
Figure 7.5; Porous Cu with 75% vol. KCl sintered at 850°C for 2 hours sintering process	208

Figure 7.6; 3D isometric surface image of porous Cu measured by Alicona Infinite non-contact Profiler, a) Sample with 70% vol. KCl, b) Sample with no space holding material	209
Figure 7.7; SEM images of various porous Cu sintered at 850°C for 2 hours sintering process	210
Figure 7.8; Manual measurement of pore size using SEM software.....	211
Figure 7.9; Example of Binary mode image of 75% vol. KCl sample.....	212
Figure 7.10; Pore distribution of porous Cu.....	212
Figure 7.11; The porosity of the sample under two different sintering temperatures	214
Figure 7.12; Compression experiment on porous Cu sample.....	215
Figure 7.13; (a) Compressive Strength curve of porous Cu with variation porosity, 2 hours sintering at 850°C, (b) Typical stress-strain curve for porous metal deformation [290]	216
Figure 7.14; SEM images of porous Cu made with different space holder volumes, (a) 0% vol. KCl (b) 75% vol. KCl.....	218

LIST OF TABLES

Table 1.1; Summary of the thesis outline	6
Table 2.1; Open and close-celled structure according to fabrication methods and pore cell distribution.....	21
Table 2.2; Example of techniques to calculate porosity	24
Table 2.3; Liquid-state processing of porous metal	38
Table 2.4; Example of solid-state processing method via space holder technique	40
Table 2.5; Other examples of solid-state processing method.....	41
Table 2.6; The space holder materials used to produce porous Cu by the C&S method	48
Table 2.7; Examples of the combination of metal powder and space-holding materials	49
Table 2.8; Example of porous metal by using MIM-SH.....	60
Table 2.9; The summary of previous works of MIM-SH with copper.....	62
Table 3.1; The characteristic of binder (polyethylene glycol (PEG), polymethyl methacrylate (PMMA), stearic acid)	67
Table 3.2; Overall volume fraction of Powder-KCl-Binder.....	72
Table 3.3; Estimation of porosity percentage according to space holder volume	72
Table 3.4; Weight Fraction for Binder System (PEG-PMMA-SA)	72
Table 4.1; Mixing parameters and compaction pressure.....	103
Table 4.2; Porous copper with different process parameter	108
Table 4.3; XRF analysis of leaching samples	111
Table 4.4; The porosity of each porous copper under different compaction pressure and KCl vol. %	111
Table 5.1; Density measurement of materials	120
Table 5.2; KCl particle distribution by Malvern 3000	124
Table 5.3; The summary of material specifications	131
Table 5.4; The prediction of feedstock density	137
Table 5.5; Examples of findings based on the binder system variation	143
Table 5.6; The proposed final mixing schedule for porous Cu fabrication.....	154
Table 5.7; Mixing Mode Phase Symbol	163
Table 5.8; Propose mixing parameters	165
Table 6.1; The identifying of the optimum time for filling the feedstock inside the heating barrel	178
Table 6.2; Injection testing to identify the suitable injection temperature for different sample conditions...	181
Table 6.3; Identifying the injection holding time.	184
Table 6.4; Samples trials to find sintering parameters	202
Table 7.1; Yield stress and relative density of porous Cu samples	219
Table 7.2; Temperature different variations of the operating temperature of Raspberry Pie 3 (average value)	222

Chapter 1 INTRODUCTION

1.1 Introduction

Typically, any materials that contain pores or voids within their microstructure might not be selected for applications requiring properties such as strength and hardness or where there is a risk of any impact. In some instances, any existing pores in a structure may lead to the formation of further propagating defects, such as cracks, which can lead to unpredictable accidents. Numerous examples can be cited from different areas of materials, such as that reported by Hardin and Beckermann [1], that the existence of porosity has a detrimental effect on steel casting, where stress concentrations around macropores promote the development of micro-cracks. Another study [2] reported that the porosity in a concrete structure is a significant cause of the formation of early-age cracking of concrete. This failure happens during concrete hydration and is a significant problem in the construction industry. While in joining, any trapped gas during a welding process results in porosity formation, which is identified as one of the extrinsic defects of welding. These features visibly impair their mechanical properties [3] and lead to the formation of cracks and fracture failure at the joining area. These defects must be avoided, particularly in high-strength applications such as aerospace and defence sectors, requiring comprehensive testing (e.g.; non-destructive evaluation (NDE)) for failure inspection purposes.

However, for several recent decades, continuous research on porous materials has revealed other positive impacts. It has been proven that a porous structure will not only reduce the weight of the product (as is evident), but it can also contribute various benefits towards structure performance and functional capability. Numerous studies [4]–[6] have revealed that porous metals may have unique properties and excellent performance at levels and combinations which are not offered by compact or dense materials.

Compared to bulk material, the existence of pores or voids within the material structure makes it light. If the pores are arranged appropriately, it can provide an excellent strength-to-weight ratio. The pores allow fluids (e.g.; air and water) to flow through to their structure and provide an excellent surface area to volume ratio, which may be ideal for some functional applications. As shown in Figure 1.1, porous metals can show several of these properties simultaneously (they are multi-functional), and these notable features have attracted high demands from numerous applications such as mechanical, electrical and thermal [5]. They have displayed outstanding performance features such as low density, high specific surface area, excellent permeability, good thermal conductivity, high strength, and energy absorption, and many of these at the same time.

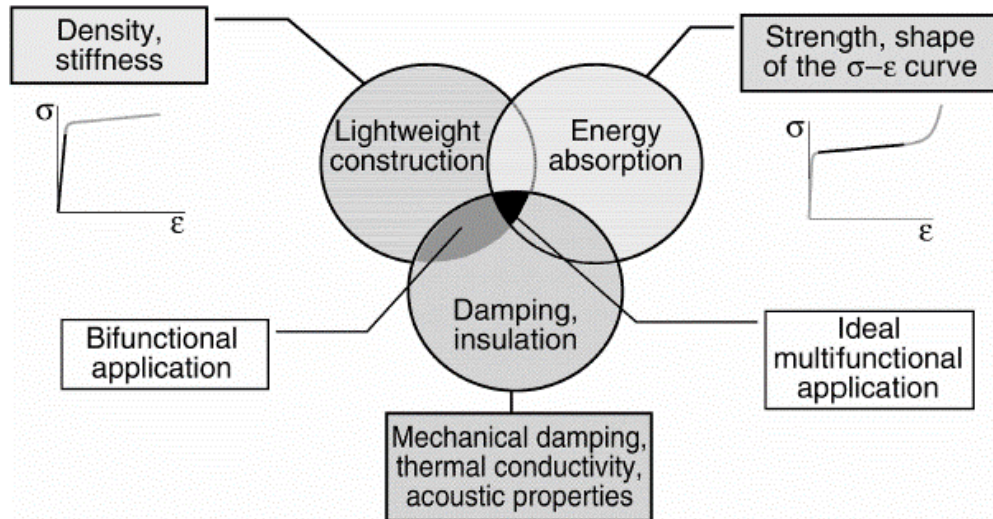


Figure 1.1; Multi-functional properties of porous metal [5]

The fabrication of porous copper may be particularly beneficial for functional applications, especially in the electrical and electronic industries. Recently, there has been an increase in high-density electronics production due to the high demand for multi-functional smart-portable devices such as laptops, smartphones, tablets, wireless devices, and portable gadgets of all kinds. These devices present challenges to the future electronics fabrication industry. Heatsinks are applied to assist the heat dissipation from the electronics, moderate the system temperature and thereby increase the lifespan of the electronic system. The selection of a suitable heatsink not only considers the factors of material properties (e.g.; thermal properties) but the physical properties (e.g.; size, shape). For example, copper is commonly selected as a heatsink due to its good thermal properties and ease of processing into different forms and shapes, thanks to its malleability. Thus, introducing porous copper as a heatsink could become a future trend to replace traditional heatsinks since it could offer excellent heat transfer management due to its large specific surface area and good permeability for fluids.

The identification of a fabrication method to produce porous copper becomes challenging since it considers many factors, including the capability of the manufacturing equipment available and controlling the porosity, pore size and other features of the structure. The proper selection of the processing method may not only transform the copper powder into lightweight materials but achieve appropriate material strength and thermal performance, as any detrimental changes may affect unique properties and prevent it from functioning as expected. Laboratory research on porous materials production has expanded rapidly over the last decade, and many researchers have investigated various techniques, from conventional ways (e.g., casting manufacturing) to the latest technologies, such as additive manufacturing, in order to achieve specific material properties. The investment and exploration of porous material fabrication are not always led by the final performance of materials but consider the constraints of being cost-effective, time, the market needed and the shortage of supplied materials. The production methods must be reliable and able to produce parts with different complexity in terms of shapes and size and achieve suitable properties.

Several researchers have tried producing porous copper with controlled pore sizes and morphologies using different techniques such as casting [7], compaction and sintering [8], GASAR-technique [9], and metal injection moulding [10], [11]. From previous literature [12], [13], some of the works on porous copper were performed by the powder metallurgy processing method. This method allows the precise control of part shape and thickness, low production cost, and good surface finish. Some researchers have employed a partial sintering technique [14] as the easiest way to produce porous copper. This method does not use any external media to assist with the formation of the pores within the structure of the material. The formation of pores in this process solely depends on the densification of the powder particles by controlling the sintering profiles (eg; sintering temperature, sintering time and atmosphere) to create a porous structure. Even though this technique is straightforward and easy to conduct, the final part usually displays lower mechanical properties due to insufficient bonding between powder particles. Other than that, by combining this technique with the assistance of a space holder material, makes it possible to achieve pore formation in part with a medium to high porosity percentage. However, this method cannot offer a wide variety of shapes and complex geometries for the final part. Furthermore, this technique, as well as the casting method, possibly requires a secondary process (such as grinding and machining) to shape these porous copper pieces into the final shapes. These grinding and machining processes can result in contamination of the foams produced and closure of the pores, thus significantly deteriorating their performance in different applications. The methods are not suitable for the high production volume. In addition, some common techniques in producing porous copper are relatively slow, high cost, require samples in liquid form, and do not offer the possibility of producing porous copper in large quantities, hence limiting these routes' viability on a commercial scale.

Therefore, there is a need to develop a process capable of manufacturing good quality material in a manner scalable for industrial processing. One promising method that could have the potential to address these issues is by combining the space holding technique with the powder metallurgy method, Metal Injection Moulding (MIM) in combination with a Space Holder (MIM+SH) technique, which is probably capable of fabricating near-net shape porous copper in large quantities. In this method, the use of the space holder itself can produce a wide range of porosity and control the development of pores through various sizes and complex shapes. MIM is a relatively well-known manufacturing technique for producing net-shaped complex metal parts and can be fabricated at a relatively lower cost. The combined technique is beneficial in terms of part size and shape, and the porous copper is also expected to perform with excellent thermal properties and exhibit a lightweight structure.

However, there has been a lack of comprehensive research on porous copper fabrication using metal injection moulding (MIM). Furthermore, the lack of availability of copper-MIM commercial feedstock due to the limited available binder systems as the current existing wax-binder type for copper production is not environmental-friendly and requires a longer binder removal process.

Therefore, the present work is needed to contribute critical technical data related to powder-binder-space holder combinations with different MIM parameters as well as to prepare alternative options to the existing production routes. A crucial study for the new binder system for copper (presented in this work) is to try and develop a water-soluble binder. Such a binder can be extracted via water solution; therefore, it offers the fastest and cheapest way to remove the binder. It should also be readily available in the market and non-toxic. In addition, the removal of binder and space-holding materials can be performed parallelly, improving production time and hindering resource waste. The introduction of new mixing procedures should also be investigated, and this study will also investigate the comprehensive studies of porous copper development via the MIM-SH method.

1.2 Research Aim and Research Objectives

The main purpose of this thesis is to carry out a feasibility study of the use of conventional powder metallurgy processes; Pressing and Sintering, and Metal Injection Moulding (MIM) in combination with the space holder technique to fabricate porous copper. By this combination, a near-net shape component of porous copper with a targeted volume percentage of porosity should be produced. This will require the development of specialized feedstock. The new binder formulation, which will be designed in the present work, forms a partly water-soluble binder system combined with the selected space holder material, potassium chloride (KCl). Since both the binder system and space holder can be removed by water, the process of debinding can be improved in terms of removal time through concurrent removal processes. Although the results may be useful in designing processes for a broader range of materials, this study focussed on the fabrication of porous copper at a laboratory scale with limited space holder material and binder components.

In order to achieve the aim of this research, several objectives have been identified;

- 1) To produce porous Cu by implementing the selected fabrication method and space holder material.
- 2) To design a binder system for porous copper fabrication.
- 3) To implement a non-conventional mixing method for feedstock preparation.
- 4) To analyze and characterize the designed feedstock.
- 5) To examine and characterize the produced porous copper.

1.3 Work Scope

The scope of work mainly focused on processing porous copper with MIM-SH techniques. The works involved the whole of the MIM process with additional modification procedures such as those required for the implementation of the space holder technique. Through the work, the identification and the development of the modified processing method are carefully designed and investigated to ensure this the combined technique (MIM-SH) is suited for porous copper production under specific parameters. The produced parts were assessed systematically at each stage of the MIM process. The activity is necessary as part of the ‘quality checking’ process since the MIM process is continuous, and each stage depends on the others. The formation of defects may influence the quality and suitability of the fabricated part for the subsequent MIM process, and it is difficult to remedy the problem. Finally, the successful part was physically examined and analyzed its properties.

The basic concept of the current Ph.D. work is illustrated in the flow chart shown in

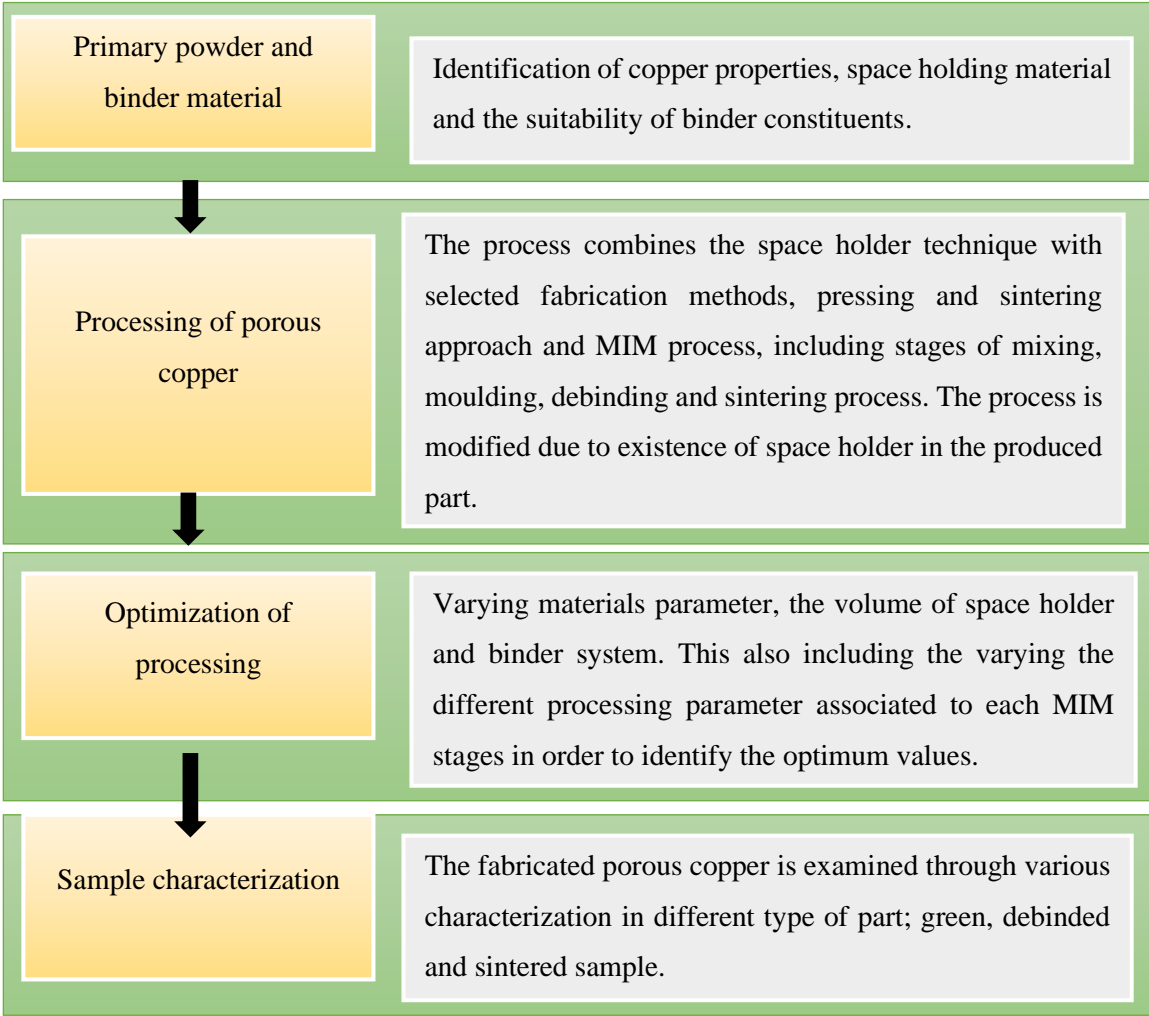


Figure 1.2; The basic concept of the current Ph.D. work

1.4 Thesis Outline

The present thesis is arranged into seven chapters. Each chapter is summarized in the following

Table 1.1;

Table 1.1: Summary of the thesis outline

Chapters	Contents
<i>Chapter 1: Introduction</i>	This chapter highlights the aims of the study, objectives, and work scope.
<i>Chapter 2: Literature Review</i>	This chapter covers the previous work on porous metal, focusing on porous copper and related research to date. This chapter also identifies the relevant information associated with the present work regarding relevant properties, processing techniques, and characterization analysis results on similar materials.
<i>Chapter 3: Experimental Methods</i>	This chapter focuses on processing porous copper, including sample preparation, fabrication method, and assessment technique used on final samples.
<i>Chapter 4: Compaction and Sintering (C&S) Method</i>	This chapter discusses the developments in this work on porous copper fabrication by the more basic Compaction and Sintering (C&S).
<i>Chapter 5: MIM-SH Method: Processing of Porous Copper Feedstock</i>	This chapter concentrates on the findings concerning the MIM process, with attention to the stages from raw materials until the part shape is achieved (mixing until metal injection stages).
<i>Chapter 6: MIM-SH Method: Porous Copper Production</i>	This chapter continues to report the work on the MIM process to produce porous copper with attention to the stages from debinding to heat treatment.

<i>Chapter 7: Porous Copper Assessment</i>	This chapter focuses on the porous copper assessment regarding microstructure, mechanical and thermal properties.
<i>Chapter 8: Conclusion</i>	This chapter concludes all findings
<i>Chapter 9: Recommendations and Future Works</i>	This chapter provides suggestions for further work.
<i>References</i>	References

Chapter 2 LITERATURE REVIEW

2.1 Chapter overview

In general, this chapter touches on the relevant information associated with the production of porous metals, which has previously been conducted. This chapter will focus on the introduction of porous metals, that the knowledge deals with the critical features and characteristics that are used to classify a porous structure, how this unique structure is being manufactured and the importance of the existence of porous metals in the modern manufacturing area, and the application of porous metal. This related information can be used as a reference and may act as an instant 'do and don't guidelines' for porous metal fabrication, particularly on porous copper (Cu). This chapter will discuss the potential manufacturing routes of porous copper, including the method that has been employed for the present study- the combination of Metal Injection Moulding and Space Holder technique. Finally, the associated properties towards the porous Cu development will be highlighted as this information is needed for the porous Cu analysis. Since the present study deals with solid material, this chapter, therefore, mainly covers literature related to the process of solid-state formation.

2.2 Porous Metals- An Introduction

Turning a bulk material into a pores structure material can be seen as a peculiar direction since the dense structure is well known has a rigid and strong solid structure. Some manufacturers might think this approach may expose the material to tonnes of failures related to the structure integrity. Fabricators work hard to produce pore-free parts, with it is considered ideal conditions in powder metallurgy-type products, weld joining parts, and building wall bricks. With the mindset of pore presence, would preparing the material in a weak stage and deteriorates the material structure. This condition may encourage the formation of unwelcome defects such as cracks, which leads to low mechanical properties [15] and difficulty withstanding a higher load. This limitation will lead to other problems, such as brittleness and joining problems. Due to these problems, how these voids structures perform an important role in the development of useful features instead it only be seen as a 'source of failure' in specific applications, especially in a critical industry such as welding and building construction.

However, numerous existing natural creatures, such as coral, demonstrate optimum mechanical strengths and give other benefits and cannot be ignored even though it contains large numbers of pores. Thus, because of the potential advantages observed from cellular-structure type creatures, the extensive research on

porous materials revealed other impacts and denied these 'bad perceptions' of porous material previously. The 'deficiency structure' of porous material has been manipulated into something valuable and indirectly denied the claimed made on this class of material. Furthermore, this class of materials may stand with optimum strength under a minimum load applied.

The dictionary definition of porous is something that contains many holes in its structure that allows any liquid or air to pass through it. This definition means that it must be a permeable structure which is according to scientific description; it can refer to materials with open-pore structures as well as porous materials can be found with close-pore structures. These pores (also known as voids, cavities or interstices and may also be called a matrix or frame) may differentiate according to their size, shape, and could be present with different degrees of volumes; commonly filled with fluids in secure close-structure or open-structure that allow liquid or gas to flow through them. Stanev [16] defines porous material is a material achieved via specific processing, while foam material is made with closed pores structure produced by gaseous substances. In the field of metal fabrication, Ashby [17] describes porous metal as a group of low-density metallic materials with a large specific area. Due to the porosity characteristic, they demonstrate novel mechanical, thermal, electrical, acoustic, and physical properties. Banhart [18] referred them as cellular metals that contain gaseous voids, whereas porous and foam metals are classified as one kind of cellular metal. Both of them (porous and foam metals) are exhibited in isolated close-celled structures divided with a thin film. In contrast, cellular metals with interconnected cells are referred to as metal sponges. From another point of view, Lefebvre [6] referred foam metals as metal that is engineered under a specific manufacturing process to obtain porous structure, and porous metal defines as a metal that has a high percentage of porosity. Although many researchers have also defined them with different terminologies, such as sponge metal, cellular metal, or scaffold metal, these all have similarities with a structure containing several pores.

Porous materials can be noticeably identified in natural materials (such as wood, plant, soil, rock, shell and human bone or animal). Frequent reference has been made to the peculiar mixed-mode structure (dense and porous) that can be seen from natural structures. The pores are purposely designed to obtain a certain level of material performance. In technological applications, efforts have been made to create similar materials for various roles and functions. In each case, this is optimised by control of their structure, which displays and contains numbers of pores, voids, and cavities in different shapes, sizes, and types of connectivity. Porous metal has been made for various applications, including ceramic, bricks and cement for building construction materials, or from metals, for example, medical applications (e.g.; an alternative Ti-foam for biomedical applications) (Figure 2.1) or to serve as a simple role in household application such as in cleaning sponge in the kitchen and purifying drinking water. The pores may vary according to the pore arrangement and distribution, geometrical shape (e.g.; spherical, cubic, irregular, needle-hopper), size, specific surface area as well as total porosity volume and these morphological properties have significant benefits for their physical, mechanical, chemical properties and definitely changes the material density.

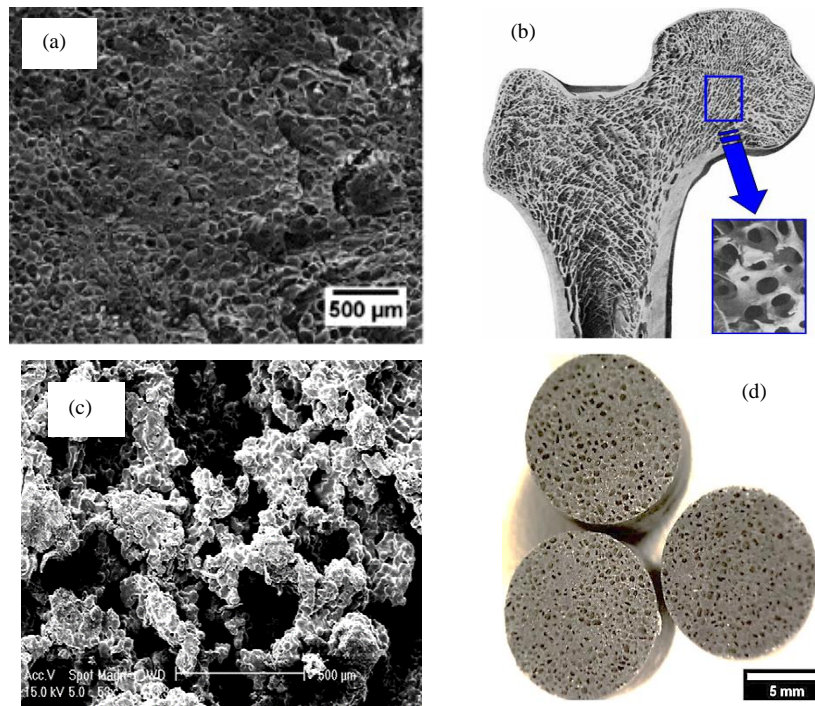


Figure 2.1; Natural (a-b) and processing porous material structure (c-d); (a) Lotus root porous structure [19], (b) Cross-sectional of cancellous bone with interconnected pores structure [20], (c) Porous titanium structure made by space holder method [21], (d) Ti-HA biocomposite foams [22]

The combination of a different phase of material structure and the integration of different material properties would be one of the solutions due to the increasing cost of material production nowadays, besides the pressure to meet the rising market demands. As simplified in Figure 2.2, the penetration of porous structure morphology into the structure of the existing material turns the final product with multi-functional features, which is valuable for many applications.

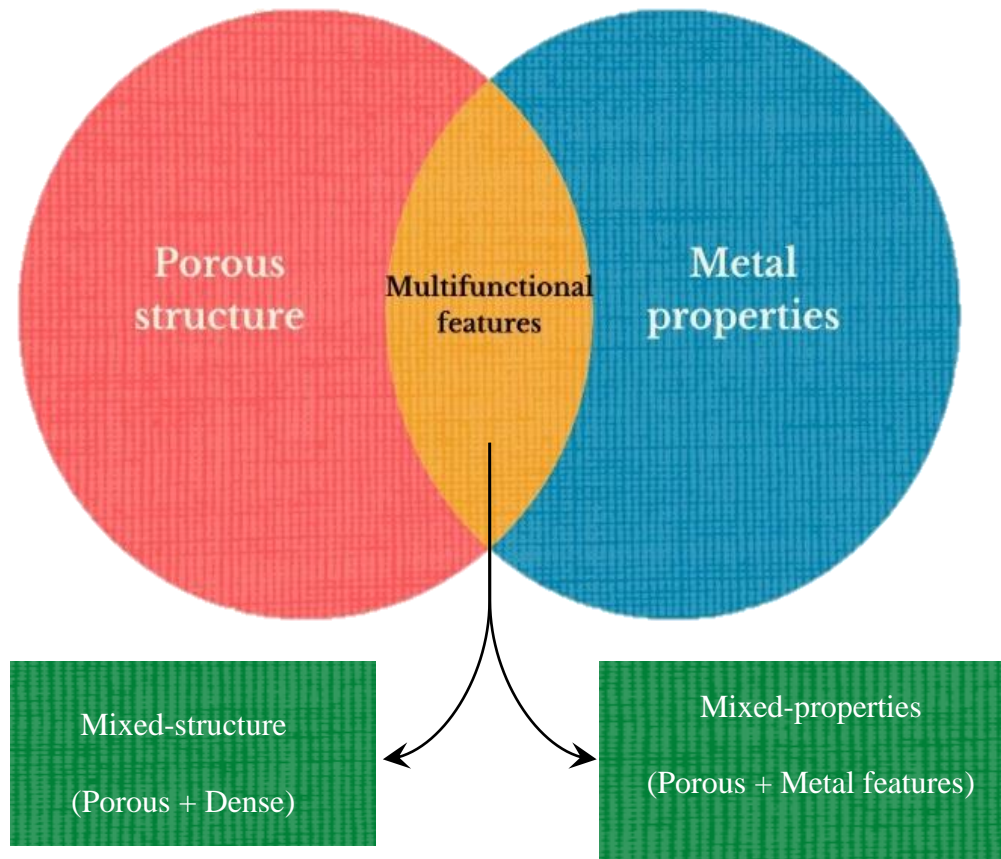


Figure 2.2; The combination of porous structure in the existing metal properties

These new features have contributed through a mixed porous-dense structure and a combination of properties. Mixed-structure regions (porous and dense) may reduce the weight of the part produced, which is credited with regard to the cost of production and the utilization of material resources. In addition, lightweight materials are needed in many fields, including the construction and automotive industries. Previously, manufacturers depended mainly on the use of lighter alloys and the use of new manufacturing technologies [23] to obtain lightweight products. Thus, employing porous material production will be another alternative for lightweight part production, as long as the porosity gain does not reduce the essential properties of the materials. It has been proven that porous structure will not only reduce the weight of the product, but it can also contribute various benefits towards structure integrity due to high specific strength [6], [14] compared to fully dense metal. Banhart [14] claimed porous metals were good in mechanical performance, and many researchers have passed many assessments regarding strength. Low density, high stiffness, good energy absorption once it is subjected to any load or force and then transmitted to fracture behaviour or bending of pore struts. They could usually withstand the maximum force but less than any force provided by a dense body. This makes them can be adopted in real products and different fields [14], such as structural application, building, railway, ship industry, transportation machinery, sporting equipment and automotive.

The integration of porous material structure properties (e.g.; large surface area, fluid flow passage, low density) with the basic properties of base metal, such as thermal conductivity, chemical stability, high strength, biocompatibility etc., give an outstanding value-added to these metals. As result, they have been exploited in multi-functional applications from the heat exchanger to the heavy objects of building construction walls. These properties may not be offered by compact or any dense materials, and in certain aspects, porous material has far better performances than other class of materials. Through mixed-combined properties, porous metals can deliver good combinations as numerous studies [4]–[6] reveal that porous metals have excellent performance, such as high energy absorption, higher surface area to volume ratio, efficient heat transfer, and excellent permeability properties that match for functional application. They can be found in energy management, silencers, filtration, fluid flow control fields and thermal management. Thermal management issues on highly advanced products requiring high processing speed would become ‘headaches’ to the manufacturers. The high amount of heat generated must be handled efficiently, where porous metal may become one of the solutions for this issue. The designed pores structure of porous metal was definitely exhibited with a high specific area-to-volume ratio, which is beneficial for thermal management applications. The high surface area allows the flow of fluids (e.g.; air and water) due to excellent permeability properties [24] and tortuosity obtained from porous metal, where the massive heat amount can be transferred efficiently via convection (Figure 2.3). Thus, this unique property makes them ‘fit’ to be applied as heat exchangers, heat pipes wicks etc.

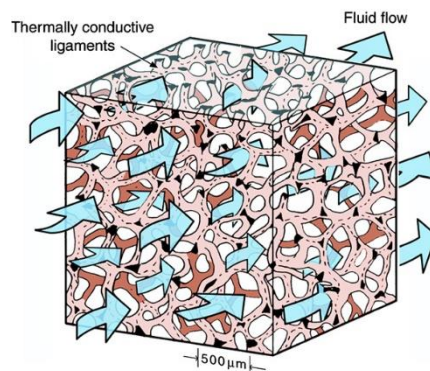


Figure 2.3; The heat flow through the pores of porous metal via convection [25]

Porous metal has been produced over many years and has experienced numerous variations and improvements. Various methods have been used, but with the same objectives of managing and controlling the production of pores. Due to the multi-properties offered by the porous material, it has produced a high interest among researchers. There has been an enormous increase in work related to porous metal for almost 20 years (refer to Figure 2.4). As the ScienceDirect search database shows, the frequency of publication in this field has increased rapidly to 1567 publications in 2019. It could also be found in another academic search database.

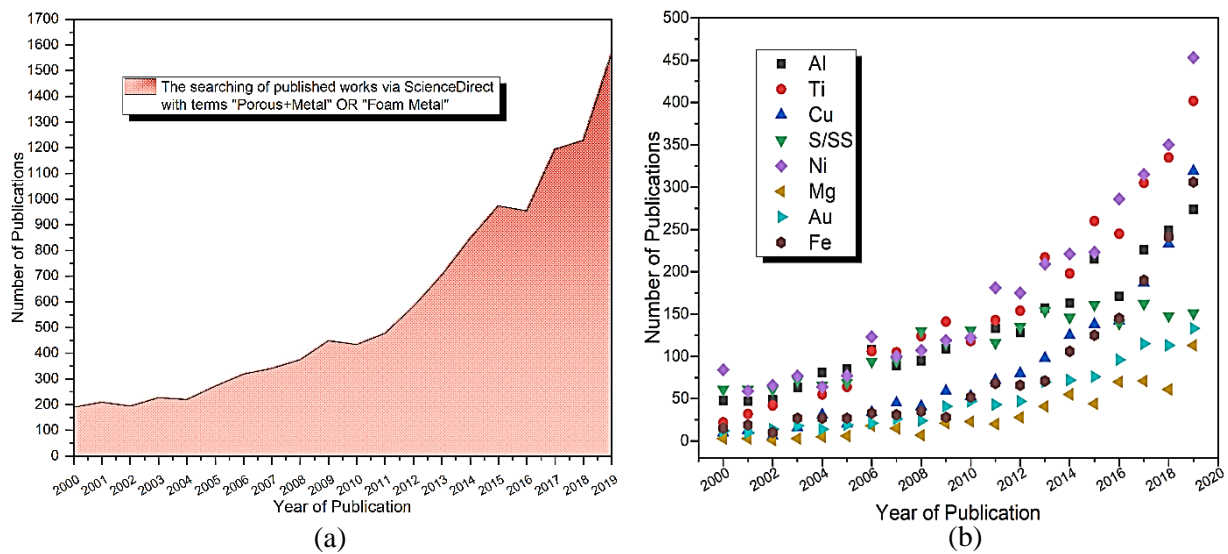


Figure 2.4; Works related to porous metal; (a) Numbers of publications from the year 2000 until 2019 related to porous metal works, (b) Numbers of publications from the year 2000 until 2019 according to the type of metals

Figure 2.4 (b) shows the number of publications of porous metals by segregation into the type of metal. The nature of the research in each publication may, of course, be very different (the data are collected using the ScienceDirect platform); with the search word “porous metal” and the word "metal", is replaced by specific metal types such as Al, Mg, Cu etc. According to the graph projection, Al and Stainless steel were popular at the beginning but have now been overtaken by other materials such as Ni, Ti, Cu and Fe. Porous Ni work remains consistent, possibly resulting in its roles in the medical and electrochemical fields. While for Ti, there has been an outstanding increase in interest over these 20 years, possibly due to biomedical interest. Fe and Cu are constantly evolving over the years, with these materials having their advantages in terms of low cost, strength offered, good biodegradable properties (Fe) and excellent thermal properties (Cu). Fe can be found in biomedical applications, while Cu is very common in functional applications.

Porous Al initially attracted many researchers since it can be processed with higher porosity of up to 90% at a lower cost for large quantities. Molten Al has undergone inert gas injection or been mixed with secondary materials (e.g.; TiH_2 , $CaCO_3$, etc.) for phase decomposition techniques to release gas and create pores within the structure. Since porous Al can be made in a larger size, they are significant materials and can be found in lightweight structure applications such as sandwich panels [26] as well as for automotive purposes. The combination of mechanical properties and biocompatibility properties makes Ti and Mg [27]–[29] interesting materials to be applied as porous metals. These metals can be used as bone tissue scaffolds [30] and implants [27], [31] as the porous structure can reduce the mismatch effect of elastic modulus between

implant and host bone tissue. Other metals, such as stainless steel and cobalt-chromium alloys, have a limitation due to their high elastic moduli that can lead to stress shielding.

2.2.1 Overview of Porous Copper (Cu)

2.2.1.1 General overview of Cu

Cu is renowned for its distinctive properties relevant to various applications, including the chemical, electrical, electronic, coating, paint, and lubricants industries. Instead of its extensively used electrical and electronic applications, this material is also used in other applications such as joining purposes (soldering and brazing), industrial products, and other fields like the chemical industry and medicine. Cu is mainly contributing to the application related to thermal and electrical conductive applications. It is also applied as a heat sink for power electronics, regenerators etc.

Pure Cu is soft and malleable, demonstrates low hardness but excellent ductility across a wide temperature range, and has excellent corrosion resistance. The melting point of Cu (1084.62 °C) is twice that of Al and Mg, and at the highest density, its thermal conductivity is superior to Al, Ni, and Sn but lower than silver (Ag). This outstanding thermal conductivity (391 W/(m·K) [32]) makes them indispensable for numerous applications. The 8.96 g/cm³ density of copper makes its weight equivalent to brass, nearly three times higher than aluminum but lighter than gold and silver. Pure Cu powder is typically available in a high purity grade, usually 99.4% Cu [32], as most commercial Cu alloys include 99.2 to 99.8 percent Cu or more, depending on production and handling processes [33]. The surface oxygen impurity affects the degree of Cu purity and typically makes up 0.1-0.5% of the weight of Cu powder. As pure Cu exhibits in soft form, thus Cu is purposely alloyed with elements such as zinc and tin to improve the material's strength and formability, resulting in more Cu alloy families (brass and bronze). These elements act as hardeners and change pure Cu's colour from reddish brown to yellow (zinc addition) or silver (Ni addition). Nonetheless, this addition would reduce the specific performance of Cu, such as thermal conductivity (relative to pure Cu), based on the element amount and alloy selection.

Pure Cu is generally available in a high purity grade as commercial Cu alloy consists of 99.4% or higher depending on production methods and handling techniques [34]. The surface oxygen impurity influences the Cu purity level, and oxygen often makes up around 0.1-0.5% wt. of Cu powder. Pure Cu has soft and malleable properties, with alloys containing additional elements such as zinc and tin helping to strengthen the material, leading to other Cu alloy families (brass and bronze).

2.2.1.2 Powder Cu production

Cu powder was commercially made by various production techniques [35]; atomization (water and gas), chemical routes by reduction of Cu oxide and electrolysis. Each process prepares the Cu powder with different physical properties. Cu powder can be processed by chemical reduction (electrolysis deposition), reduction of Cu oxide, and atomization with gas or water. Each technique generates copper powder with varied physical qualities and is closely monitored to control impurities and oxygen levels that could impair the conductivity and performance of Cu while maintaining its high density.

2.2.1.2.1 The atomization process of Cu powder

The production of Cu by atomization routes was commercially available in the 1950s [33], where the molten metals were dispersed into particles either by gas or liquid processing medium. The high velocity of these mediums breaks the molten Cu and, with rapid solidification, has transformed into particles. Water atomization disintegrates liquid Cu into smaller particles using high-pressurized water, resulting in slurry Cu, which needs a drying process. In contrast, the gas atomization process uses jets of air or gas to break the liquid Cu into particles and normally produces a spherical shape of Cu particles with high density. Then the solidified particles may require a second treatment process, such as milling procedure, to transform the particles into specific particle sizes. During the atomization process, substances like phosphorus and oxygen may alter the characteristics of Cu and should be carefully controlled. For example, low oxygen content tends to create more spheroidal particles [33]. Otherwise, high content of oxygen produces an irregular shape of Cu powder. The atomized Cu powder is often suitable for powder metallurgy applications due to its high density, low flow rates, and high green density [36]. The characteristic of Cu particles, such as their form, size, density, and green strength, may vary according to the atomization medium used, flow rate, and pressure. Figure 2.5 shows the images of Cu powder produced by using the air and water atomization method.

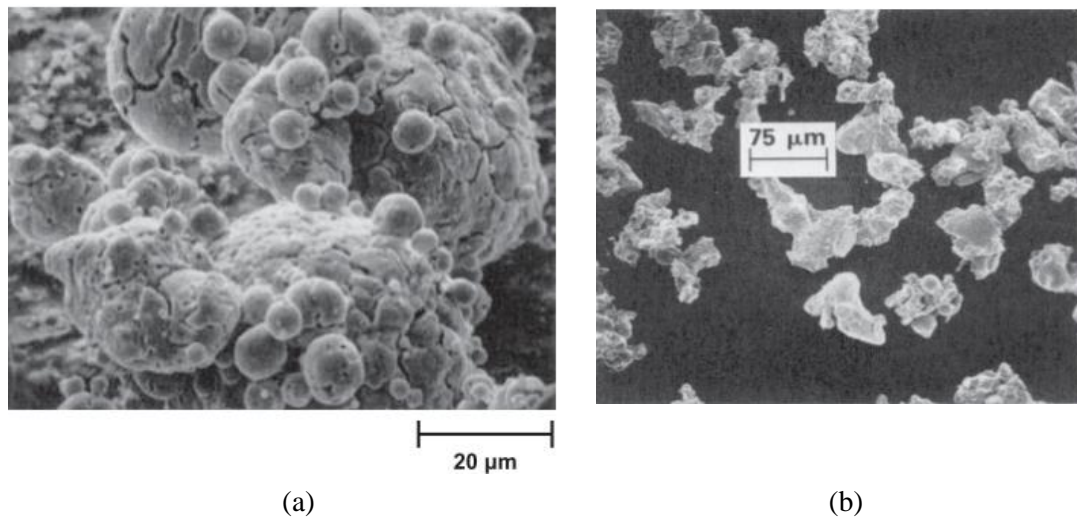


Figure 2.5; Scanning electron microscope images of Cu powder with different atomization processes [33];
 (a) air-atomized Cu powder, (b) water-atomized copper

2.2.1.3 Cu powder properties and metallurgy

The Cu powder could be spherical, irregular, dendritic, acicular, and angular, according to their synthesis process. For example, the atomization process often results in spherical (gas atomization) and irregular (water atomization) shapes, while electrolysis and other chemical reactions typically produce dendritic structures. Cu powders also come in other shapes, such as cauliflower-like particles, due to the different conditions of the electrolysis process, while non-uniform aggregate particles shape is obtained through the polyol process [37]. The particle size of Cu may vary according to various applications between the range of 1 mm down to 10 μm [38] and could be the finer size as 2 μm.

This metal has a melting point of 1084.62 °C, a density close to 8.96 g/cm³, and outstanding thermal conductivity (391 W/(m·K)), making them indispensable for numerous applications as lubricating bearings, heatsinks, etc. The good features of Cu (e.g.; ductility, thermal conductivity) are defined by its structure. The Cu atom arrangement is face-centered-cubic (FCC) and twelve dislocation slip system [39], where the copper atom exists in the centre and corner of the cube face. This FCC arrangement makes Cu easy to form and fabricate and poses with good ductility and toughness at room temperature. The microstructure of Cu consists of non-uniform grains with different shapes and sizes. Figure 2.5 shows examples of pure Cu microstructure [40], [41].

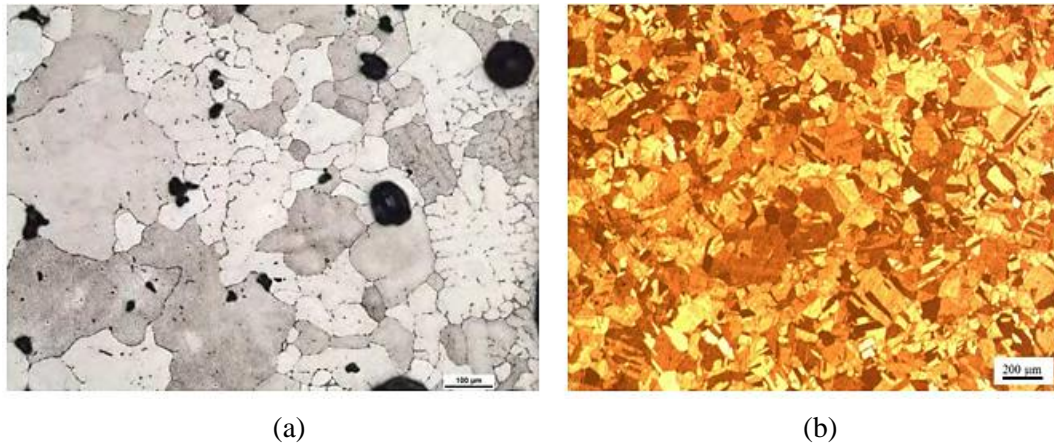


Figure 2.6; Example of the microstructure of pure Cu, (a) Different grain size of pure Cu due to high cooling process [40], (b) Annealed pure copper [41].

2.2.1.4 Porous Copper (Cu)

These superior features of Cu, combined with the outstanding properties offered by a porous structure such as lightweight, excellent permeability to fluids, and good mechanical properties, could be potentially applied for structural and functional applications. Porous Cu may exhibit in low-density range (3-12% that of the dense Cu), a high surface area, and at the same time, offer multi-functional properties such as thermal and electrical properties [42]. The demands on this porous metal keep attracting many industrial players because of its advantages based on the multifunction properties such as excellent thermal and electrical properties [42] and corrosion protection. Due to its porous structure, porous Cu exhibits a low-density range (3-12%) and may have outstanding characteristics such as high surface area, high strength, and thermal conductivity and can be physically modified by various processes such as coating, plating and brazing. Various commercial products are made from porous Cu, such as heat exchangers, filtration, batteries, porous electrode [43] and commercial porous Cu that used for electronics application (Figure 2.7).

Furthermore, porous Cu has great potential to be applied as a noise reduction, catalyst, and thermal management product [44]. Theoretically, the solid Cu metal that contains a higher amount of metal may offer higher thermal properties, such as thermal conductivity, compared to the porous metal [45] due to the high amount of Cu. However, the metallurgical properties of porous Cu offer high surface area. Thus, it has better thermal properties and is suitable for a heat sink in high electronic devices [45], [46] due to its excellent thermal conductivity properties.

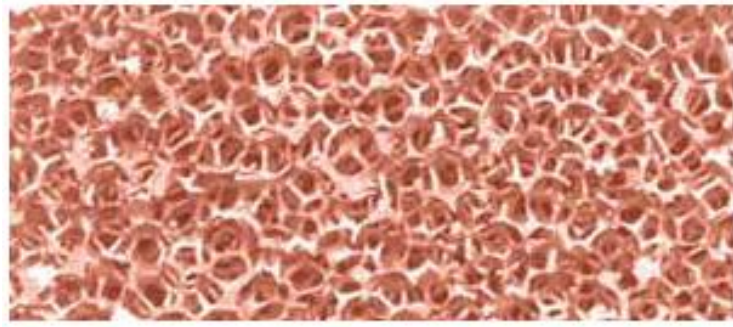


Figure 2.7; Commercial Porous [47]

Any decision that converts a bulk Cu into porous Cu must not damage its soft-ductile structure while maintaining its essential properties in order for it to function and perform as expected. Generally, the liquid-state processing method is implemented on metals with lower melting points, such as aluminium. For high melting material such as Cu, it also can be done by liquid-state of processing type (e.g.; investment casting), but commonly this material is produced via a solid-state processing route [8]. Since the liquid-state processing method requires high cost and advanced technology, it is suitable for larger production and involves massive material resources; thus, the researchers engage with solid-state processing techniques. Processing methods such as the gas-saturated melts technique (lotus-type porous metal) [48], [49] known as GASAR [50] give limitations in terms of pore size and material availability as well as the issue of safety instead of parts can be produced with uniform pores

Mark and his colleagues [51] reported that porous Cu through solid-state processing had attracted many researchers because it provides more versatility in terms of porosity control options and more flexibility in controlling the shape complexity and product size. Porous Cu can be fabricated through the powder metallurgy technique [52]–[54], which combines powder metal with space-holding material (as pores agent formation) [8], [55]. The manufacturing routes will be discussed in detail in the next section.

2.3 Porous Metal- The features and characteristics

The defining on the application that the porous metal can suit and perform in the right area is by assessing its material structure (2008) [6]. Thus, it is important to understand the basic features of porous structures which specifically designed for the target application. Different phase regions of structures are displayed in porous metal, where the space regions, known as pores or cells, are surrounded by the solid structure. This solid structure can be called a dense structure. The network structure known as struts connects the pores, which exhibit a thin structure (Figure 2.8). There are several ways to identify the types of pores,

typically by referring to the structural connectivity of cells and cell features. The thin structure that connected each pore can be identified as struts, while the connectivity of the pore can be distinguished as either close or open-celled.

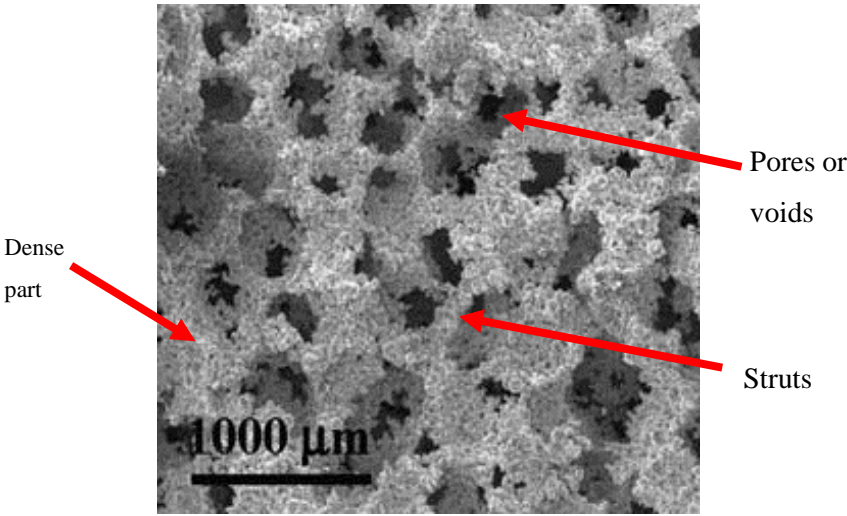


Figure 2.8; Example of porous metal structure (porous Cu made by Lost Carbonate Sintering (LCS) [13]

In general, the porous metal can be simply identified through its structure, which is displayed through pore properties such as porosity volume, pore size, shape, distribution and connectivity. The pores may form the result of the spaces obtained from the arrangement of powder particles, and the shapes and size of generated pores rely on starting powder particles. When speaking about porous material, most researchers intend to produce a part with larger porosity. Commonly the porosity volume plays dominant properties in porous metal, but [56] claimed pore size gives more important, especially for practical use in different applications.

The porosity represents the volume of pore or void within the material structure, which is generally expressed by porosity percentage, in the range of low 25% to 95% porosity volume [15]. Porous metals may contain a high percentage of volume fraction pores, usually in the range of 75-95% [57]. Zhang and Wang (2005) classified the three types of porosity volume in solid material. First, the material with a very low porosity volume (below 1%) can be neglected. The second group has very high porosities, which is more than 70% and comes from corals, woods and foam materials. The last group contains porosity volume between 10 to 70 % and is applied in various industries. Porous metals are often characterized through their common porosity properties and which may determine by their relative density (equation 2.1);

$$\rho R = \frac{\rho}{\rho_s} \quad (2.1)$$

Where ρR is the relative density, ρ is the porous material density, ρ_s is the bulk material density.

This relative density measurement and other porosity properties (e.g.; volume, morphology) strongly dictate the structure of porous metal and are connected to different features such as excellent thermal conductivity, high strength and ideal elastic stiffness, etc. These features respond to different needs in different applications, such as structural or functional fields. The pore size of porous metal also determines its application [56] and can be grouped into (i) macropores (more than 1000 nm) and (ii) micropores (100 r<1000nm). However, porosity will decrease in decreasing powder size due to rapid sintering. Meanwhile, the matrix powder with an angular shape has the potential to produce samples with larger pore sizes and higher porosity compares to spherical powder [59]. Furthermore, the sample compacted with spherical powder particles has low mechanical interlocking and makes the samples easily collapse during space holder removal.

2.3.1 Open-celled and Close-celled structure

The porous metal structure can be divided into two distinct groups; close-celled and open-celled structures. A simple identification of the feature of open cell, the base metal structure framework builds with the interconnected struts (without wall) and nodes where these pore networks are accessible by outside surrounding. As shown in Figure 2.9, open-celled pores exhibit continuous open pore networks [60], and the joining of the open pores acts as a pathway for fluid and air flow through these pores. They can be formed either from the leaching process of the space holder or the burning of pore-generated agents under a specific heating process. The close examples of the manufacturing process are powder metallurgy approaches combined with the space holder technique.

In contrast to the open-pores structure, the close-celled structure is not linked to each other, and this non-interconnected network has prevented it from external connectivity. This means their celled feature represent individual enclosures, isolated close boundaries [24], [61] and surrounded by a separated cell wall, and no fluid or gas can flow through them. The sealed pores, like bubbles, generally contain gases obtained from the processing stage. Both open-celled and close-celled structures can differentiate their pores distribution according to the assigned fabrication method (Table 2.1). The close-celled structure seems distributed randomly compared to the open-celled, which is more structured and organized.

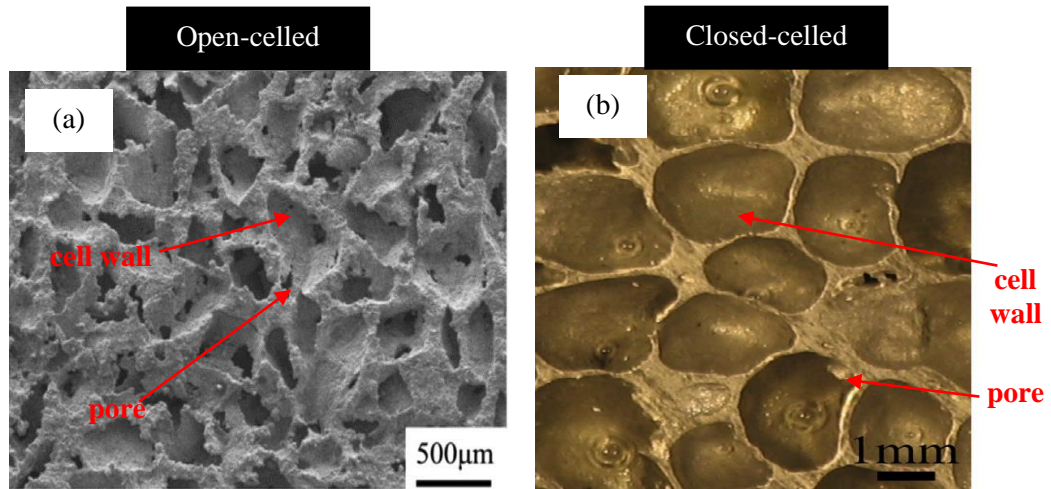


Figure 2.9; Example of the open-celled and closed structure of porous metal; (a) The structure of open-cell Cu [62], (b) Closed-cell porous Aluminium [63]

Table 2.1; Open and close-celled structure according to fabrication methods and pore cell distribution

Cells types	Processing type	Pores Homogeneity	Pores; Non-homogenous / random	Pores Orderly, designated, functional graded
Open-cells	Powder sintering		✓	
	Space holder	✓	✓	✓
	Rapid Prototyping	✓		✓
	Press and Sintered	✓	✓	
	Scaffold			✓
	Replication		✓	✓
Close-cells	Gas injection to molten metal		✓	
	Foaming agent decomposition		✓	

These different cell morphology structures have pursued them with a different area of application, combined with their key characteristics, the weight reduction of materials. The high surface area to volume ratio makes the open-celled porous metal contribute more in functional roles than structure fields, and their lightweight structure may give extra value. The open-celled porous metal widely penetrates biomedical implants as an open-celled structure promotes bone tissue growth. Furthermore, its permeability properties improve the thermal conductivity properties, which is practically suitable for thermal management areas as commercially applied in the heat exchanger and heat sink. Other applications can be found in refrigerators and electrodes for batteries etc. [17] and favourable candidates as sandwich panels core. However, the strength structure may gradually decrease with increasing the porosity volume fraction.

Meanwhile, the close-celled porous metal is usually needed in the application with sufficient mechanical strength with low weight structure [4], [57] compared to heavy solid parts. They are familiar with structural-related applications such as porous steel in the frame design of automobiles, while porous Al commercializes for sound absorbers for elevated viaducts to absorb vehicle noise [64]. It may also utilize for high-impact applications (e.g.; railway absorption cushion) owing to its deformation behaviour under low stress. As reported by Banhart J. [14], the infiltration method is usually applicable to produce close-celled porous metal beside the popular method, the GASAR technique. The thin cell walls may become the weak structure spot of close-celled porous metal when subjected to a different degree of compression load, and it is challenging to reproduce with consistent properties. As shown in Figure 2.10, the application can be designated according to its cell morphology. It shows that open-celled pore is more applicable for functional applications related to its optimisation of material properties. While the close-celled structure is suitable for structural applications that require strength and mechanical properties.

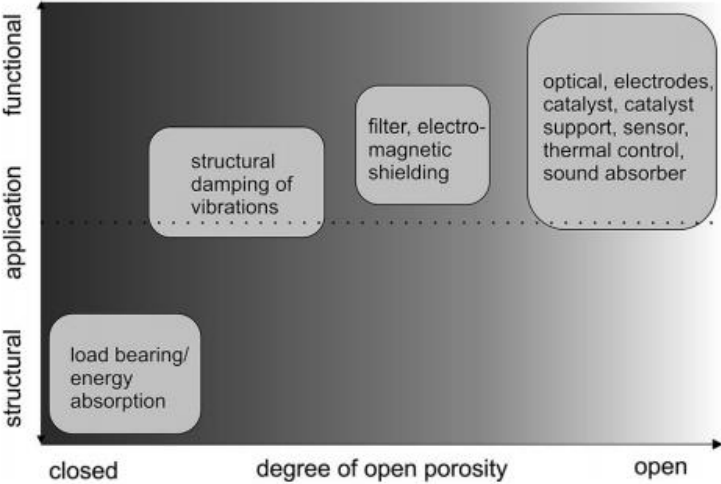


Figure 2.10; Example of the application according to pore shape- open-celled and close-celled [61]

2.3.2 Methods on how to measure porosity

The porosity of materials can be measured in various ways, and each measurement technique has a different principal mechanism. These techniques were applied according to material characteristics, pore size [65] (Figure 2.11), instrument capability, specimen geometry and the application of the sample.

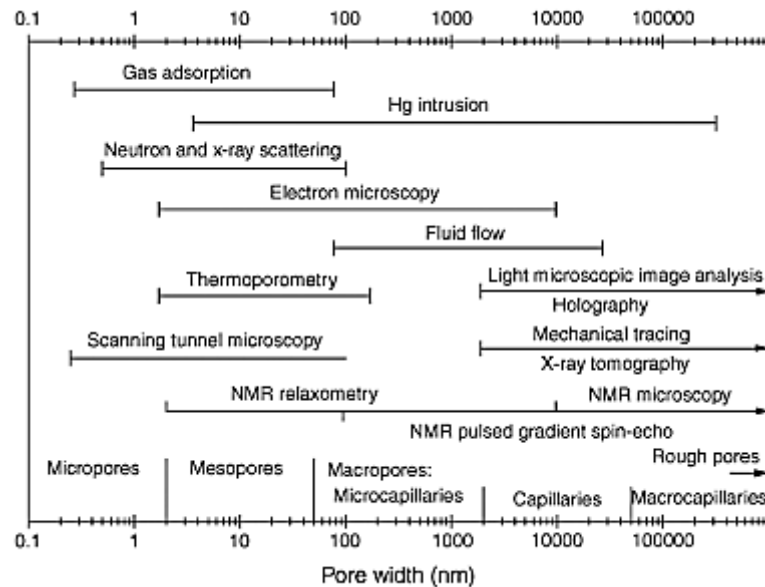


Figure 2.11; Porous structure measurement method based on the pore size [65]

The methods of porosity measurement, either for open-celled or close-celled porous metals, may vary according to the measurement media or depend on the morphology of the pore. The measurement technique uses different media such as gas (e.g.; helium gas) or liquid (e.g., mercury, water) to assist in porosity measurement, which this technique may damage the sample. Then, the visualization technique via optical devices such as scanning electron microscopy (SEM) and microscope may become the non-destructive measurement in contrast to the previous approach. The drawback of this method is that it requires specific sample preparation, such as grinding, polishing or coating, which may affect the sample quality. Another more extensive and detailed image analysis, such as X-ray tomography, can be applied to measure the porosity directly on the specimen with high accuracy. However, this technique is advisable to be applied for any usage that requires a critical and detailed material characterization. In addition, this process is quite costly, leading the researcher to implement the more simple and cheaper approaches such as the Archimedes technique. Here are examples of porosity measurement techniques, as shown in Table 2.2.

Table 2.2; Example of techniques to calculate porosity

Technique	Pore cell types (Open-pore or Closed-pore)	Measurement media	Description
Archimedes method	Both	Water, ethanol	The samples were dipped into the water as part of this procedure, which is based on the buoyancy principle. After water immersion, the weights of the dry and wet specimens were used to calculate the sample weights. Typically, the fluid (measurement medium) is ethanol or deionized water.
Mercury porosimetry	Open only	Mercury	This destructive measuring method was used in a closed chamber that was filled with mercury. Under specified pressure, mercury was injected into the specimen, allowing the pore volume to be measured. Since the measurement method involves easily evaporating mercury fluid, it must be handled cautiously.
Helium pycnometer	Both	Helium gas	This method, which was carried out in a sealed container filled with helium gas, was popular among researchers. The measurement needs small size of specimen and the density was measured according to Boyle Gas Law due to different of volume-pressure reading. From this value, the porosity percentage can be calculated.
Optical visualization analysis	Both	Image of specimen	This measurement technique uses an optical device such as an optical microscope or a higher image analysis machine such as SEM. The analysis relies on specialized analytical software and requires careful sample preparation to avoid any sample destruction. The accuracy of porosity measurement is based on the quality of the image taken.

Envelope volume	Closed only	-	The measurement focuses on the volume reading before the density and porosity can be estimated.

2.3.3 Pore generated mechanism

The generated pores may come with different sizes, geometrical shapes, volumes, and pore arrangements. These attributes influence how they can ‘serve and fit’ with suitable applications. According to [56], the pores generated can be grouped into two different mechanisms, (1) *inherent pores or naturally pore generated*. The pores were formed without any assistance from external pore-forming media. (2) *internationally pore generated*.

2.3.3.1 Inherent pores or naturally pore generated

This technique is described as the easiest way to create a porous structure without any ‘investment’ and requires no extra effort. Without the involvement of any assistant of external media or any pore generated driven to ‘forcibly’ generate the pores structure. The pore formation entirely depends on the intrinsic characteristics of powder materials, especially the physical properties of starting powder (density, size of powder particle, shape or particle distribution). They may also influence due to reactions towards processing setup, such as initial compaction, densification temperature, and sintering time.

For example, through the powder sintering approach, the porosity percentage can be naturally developed up to 35% [66], and the porous structure (pore size and shape) depends on the powder particle size [67]. The pores were obtained through the adjustment of the processing parameters, such as the heating process or compaction pressure, with the aim of reducing the density of produced parts. This can be done by lowering pressing pressure or reducing the sintering temperature or time with minimum setting parameters. Figure 2.12 shows the cross-section of porous Ti under different sintering temperatures and low compaction pressure. It found out that, the pores may develop with low compaction and reduce its porosity percentage, in line with the increasing sintering temperature.

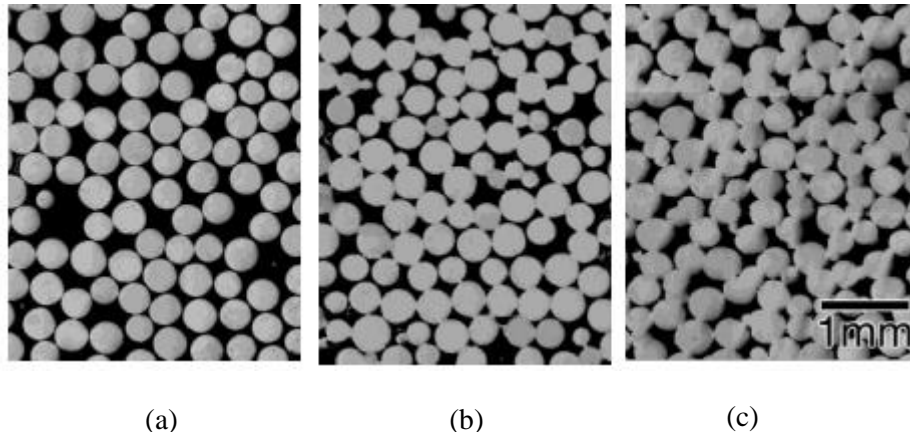


Figure 2.12; The image of porous Ti with different sintering temperatures (1173K (a), 1573 (b) and 1173K c)) under low compaction pressure, 10 MPa [66]

Low compaction pressure would promote spaces between powder particles and neck formation. In extreme conditions, some researchers [68] applied the non-pressured process and managed to achieve porosity between 40 to 60% volume but faced high risk to the structural integrity due to poor mechanical bonding among powder particles.

Since this method depends on the adjustment made to the processing setting for porous structure readiness but may pay a high price in some aspects. The pore properties formation seems uncontrollable, and difficult to obtain the targeted specific states in terms of total volumes, shapes or distribution. Furthermore, this mechanism commonly comes with low output of porosity volume where required to be coupled with additional technique (e.g.; space holder technique) to reach a higher porosity degree. Moreover, since the processing happens under the ‘satisfaction’ stage of microstructure development, it may face structure integrity. As the processing stage is performed below normal densification points or compaction pressure, it exposes insufficient bonding of powder particles, resulting in poor mechanical properties. This situation affects the part reliability, limits the performance and application of potential parts, and becomes a major obstacle for broad industries.

2.3.3.2 Intentionally pore generated

The pores development of the aforementioned method (powder sintering process) manages to obtain porosity less than 30% [68] with a small pore size. Since the pore was naturally developed, the slow production requires more time and is non-efficient result oriented. In some cases, this can be displayed with the uncontrolled design of pores shape, size and pores distribution, and it comes with fragile structure due to poor mechanical properties.

Therefore, these problems lead the researchers to move to another alternative method to increase and speed up the pore's formation. The pore structure is intentionally generated in various ways, for example, by coupling the conventional metal processing method with a special technological technique such as the space holder [68]. Through these efforts, the target pores can be obtained with designated properties and features such as pore size, shape and volume. This process gives freedom to manufacturers to manage and control the final specific outcome of pore structures according to the 'command' that is being set up. Furthermore, the fabricated porous structure is not only dynamically controlled (e.g.; increase or decrease), it can be tailored to the specific properties to achieve target performance.

The selection of the right method depends on many factors, such as pore generating media itself, the suitability of the fabrication method, the outcome of the final product, porosity properties and many more. Any 'hired assistant' in generating pores must take notes on any possibility and consequences before it unites with the base metal.

2.4 Porous Metal- Applications

The introduction of pores into the material structure not only changes the material physically, but the drastic weight reduction and lower density also lead them to material saving, performing with outstanding properties and flexibility usage in various applications. They can be designated to specific needs, especially in critical fields and disciplines, either from industrial usage or for medical implants. However, this group of materials commonly suits and matches specific applications by assessing the relationship between base metal properties and the formed porous structure performance. [61] claimed the aspect of pore structure properties (the density, pore size, pore connectivity, pore shape etc.) besides other factors; the metal composition and macroscopic shape need to examine before it is ideal for suitable application. According to [24], two essential characteristics to stress that the porous metals may play roles in the specific application; *are the combination of properties and property customization.*

The **first aspect** is how the base material and porous structure can get along to perform the targeted behaviours. Theoretically, the selected base metal is predicted to serve its original and intrinsic properties (such

as strength, elasticity, machineability, chemical stability, electrical or thermal conductivity etc.). For example, the thermal conductivity features commonly obtained from Cu and Al, the biocompatibility behaviour of Ti and Mg, as well as Stainless steel for its strong structure. Then, combining these essential features with the beneficial characteristic of porous metal properties (such as lightweight, low density, permeability behaviour, large specific surface area etc.) will definitely ‘upgrade’ the material and turn metal with multifunctional behaviour compared to other classes of materials. For example, the permeability properties of porous Cu may pose excellent thermal conductivity properties, which would be possible to apply as a heat exchanger.

The second aspect relates to the adjustment of properties. Since porous metal exhibit mixed structure properties (dense and porous), the metal properties can be customized to meet the required application within its limits. The properties tailoring is made on the structure to obtain optimum and reliable structure to be used on the target application. This aspect can be seen in automotive and building construction. The lightweight automobile body structure reduces production costs and saves raw materials while also improving mileage-to-gas ratio consumption.

2.4.1 Matching pores to application

Banhart [14] classified applications of porous metals into two main groups, structural and functional, according to the material properties. Structural applications commonly exploit the benefits of light-weight and mechanical properties while functional depends on the specific characteristics of the material itself combined with porous structure advantages. For example, the excellent conductivity of Cu [45] may contribute to its good thermal properties and combine with a large surface area for larger heat transfer capability. The easiest way to identify the relevant application, in general, is mainly by the cell type structure (as discussed in the previous section). According to Figure 2.13, a shift from structural into functional applications for porous metal occurs according to how open the pore structure is. By adjusting the pore structures into an open interconnected structure, the porous metal is generally more suitable for functional applications. The open-celled structure dominates for functional-type applications where their continuous pore channel [57] is utilised and applicable for applications such as thermal control, filtering, sound absorption etc. On the other hand, the air-trapped close-celled porous metal is reserved for structural applications, such as impact absorbers in automotive applications and frequently, such as sandwich panel cores due to the lightweight structure.

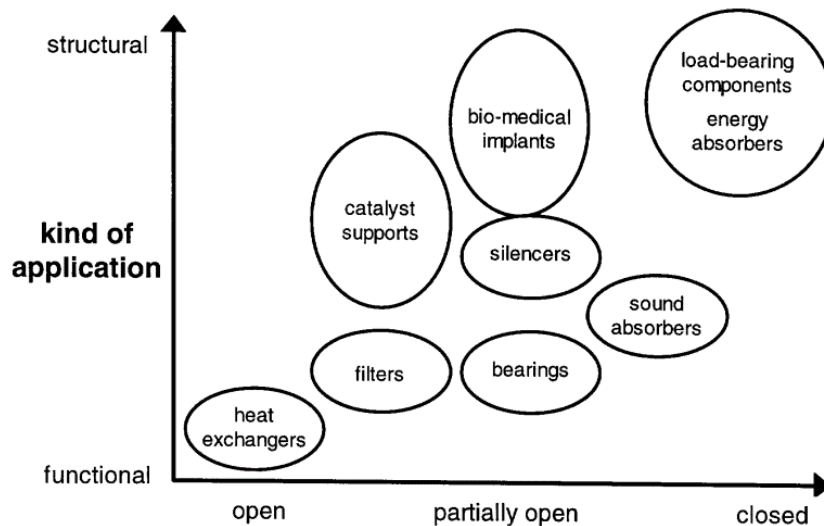


Figure 2.13; The application of porous metal according to the pore structure [14]

The revolution of solid-state batteries with high storage capacity and shorter charging time has pulled a variety of foam materials into this potential area. Porous metal, such as Cu, is a good choice for the development of new batteries since the need for batteries (particularly for transportation) necessitates materials that are lightweight, highly flexible in the shape, safe, and environmentally friendly, for example, in components such as electrodes.

2.4.2 Structural Applications

Although fully dense materials may withstand higher loads and stresses than porous versions, their weight may make them less suitable for some situations, such as transportation. Porous metal has the benefit of being lightweight while remaining mechanically efficient. For certain loading geometries, porous metals may offer better weight-specific properties. Additionally, dense and porous structures (mixed structures) may be modified and tailored to get the required property combination.

Aluminium foam sandwiches (AFS) [26] are one example of porous metal-type products for structural applications. AFS was developed by Fraunhofer-IFAM, an aluminium foam sandwich where the porous metal is placed between sheets of dense material. AFS can reduce the overall weight with higher bending stiffness characteristics (Figure 2.14) [69]. AFS can be used as support frames, platforms, or a variety of panels (e.g.; wall, solar etc.). Furthermore, AFS is reportedly stronger than other sandwich structures due to the formation of direct metal bonds between the foam and the dense material instead of using adhesives. In the building industry, AFS can be used as wall and ceiling structures, for load bearing purposes and can act as sound insulation to reduce noise and sound and potentially serve as fire protection. In railway construction for

example, AFS was used in the prototype of a power head cover for an Intercity-Express-Train (ICE) train. This led to an 18% decrease in weight for the same stiffness, without the need for an additional manufacturing step.

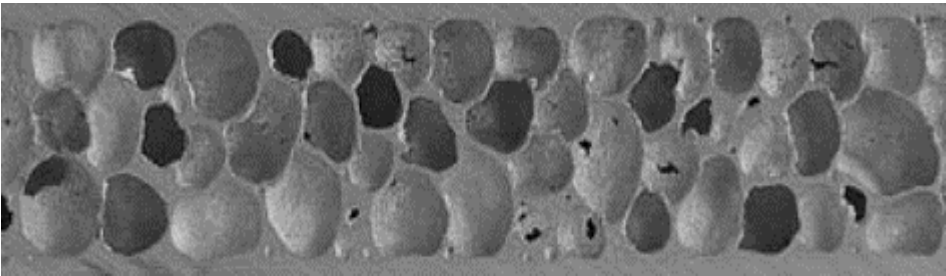


Figure 2.14; Cross-sectional view of AFS material [69]

2.4.2.1 Automotive industry

According to [70], the engaging of porous materials in automotive applications with respecting to lightweight construction, energy absorption and acoustic properties. These features are pertinent to this field and can be found in car body development, like car doors and body frames, as well as the floors. The fabrication of car components with porous structures is driven by the need for lightweight construction where the volume reduction may lead to other benefits such as minimising fuel consumption, saving the usage of raw materials etc. This direction may not miss considering the safety factor where the final product must possess high-strength protection instead of a lightweight structure. AFS for automotive application can easily reduce the weight of car components, acts as a vibration damper [70], facilitate the assembly and has the potential to replace the conventional car body. The usage of AFS can replace the conventional heavy-weight stamped steel parts of the car. AFS also was applied for telescopic working platforms for material-handling vehicles (Figure 2.15).



Figure 2.15; AFS application for the material handling vehicle [69]

Instead of the development of a lightweight car frame, the other application is the design of the bumper beam, as it has been designed as a crash absorber component. This element is critical to minimize the impact of vehicle collision through energy absorption and protect the passenger through rigid frame-matrix. Fuganti [71] experimented with the impact of 15km/h on porous aluminium, where it was observed the energy absorbed by a crash box with foam structure is nearly twice higher compared to a conventional crash box with 38.8kN of average force. In terms of structure design, it took 10% of weight saving and reduced almost 30% of crash box dimension length. Manufacturers foresee this way to reduce vehicle weight and come up with a new design of the crash box as well as a savvy approach to minimize production costs. Porous material can absorb large quantities of mechanical energy by plastic collapse when deformed in crash and collision situations. Studies [70] shows close-celled Al foam has an impressive impact energy-absorption capacity and has been implemented in high-speed trains and car as a “safety or crash box”. Figure 2.16 shows an example of a crash absorber that is designed in thin-walled tubes filled with aluminium foam. When it is positioned between the impact beam and the front rail of the vehicle, the use of a foam-filled crash box will decrease the repair cost because it can mitigate or absorb the collision energy and then simply be replaced.



Figure 2.16; Prototypes of crash absorbers based on extruded aluminium hollow sections [70]

2.4.2.2 Biomedical application

An extraordinary feature of porous materials has breakthrough them into biomedical, pharmaceutical and dental applications. Porous metal was used in the biomedical industry in the late 1960s as a solution to improve long-term implant stability where the bone tissue has grown within the porous surface successfully [6]. The porous implant comes with suitable pores volume fraction to encourage the ingrowth of bone tissue [31] and also gives strong support to the bone with sufficient strength.

Since they were going to serve for a long-term period and be permanently installed together with live tissue or human organ, it is obligatory for those metal implants to demonstrate 'human-friendly' characteristics. The properties such as non-toxicity, biocompatibility & bioinert properties, and resistance to corrosion

properties are important to prevent body denial, and they are homogeneously uniform and work with live bone. Furthermore, it is essential for the selected metal implant to encourage cell attachment growth and bone tissue, bone matrix formation and facilitate tissue regeneration.

Due to aged-related bone loss, such as bone density reduction, it decreases the loading ability, and the huge mismatch of Young Modulus (YM) between bone and implant makes its worst condition. The bone naturally exhibits high stiffness between 10-30 GPa of YM, much lower than Ti (110 GPa) or cobalt-chromium (220 GPa) [72]. The stress-shielding effect becomes obvious due to this large gap in modulus properties, which leads to poor bonding of bone and implant, resulting in a loosening problem between them. Therefore, the demand for low-stiffness implants is necessary to lower the bone stress-shielding effect, which it can clearly be found in the outcome of porous implant usage. The porous implant shows properties close to the nature features of bone with structure porosity in the range of 50-75% volume [73] and manages to imitate the bone features (as depicted in Figure 2.17). Furthermore, compared to conventional approaches in terms of screws and pins usage, porous implants may solve the issues of fixation and stability and eventually avoid implant loosening.

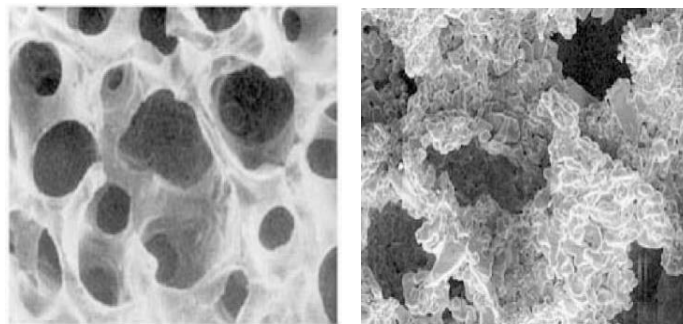


Figure 2.17; Natural and human-made porous structure (a) Structure of cancellous bone, (b) Cancellous structured titanium (CSTi) [73]

2.4.3 The application that exploits the material characteristics (Functional application)

2.4.3.1 Thermal management application

Porous metal that combines the features such as good conductivity with the high surface area can be considered to be applied in various thermal applications, for example, heat exchangers and heat-sink). Many types of research that were working on heat transfer analysis via porous metal [46], [74]–[76] where the features influenced the different types of porous structure parameters (e.g.; pore volume, cell connectivity,

material density, pore size etc.) and still on-going research on these topics which the finding may give a better understanding in utilizing porous metal towards thermal application. High performance of power electronic system entails an efficient cooling system to dissipate the generated heat via heatsink, for example.

The transfer of heat can be carried out with different mechanisms, either conduction, radiation or convection. As explained by [74], the mechanism of heat transfer in the porous metal can be made by heat conduction and convection via cell walls and heat conduction through pores. For porous metals, solid conduction is the most dominant mechanism of heat transfer [74]. It was also reported that factors such as thermal properties (e.g.; thermal conductivity) and the choice of porous material have significant influences on the heat transfer performance of heat exchangers. Besides, porous properties such as porosity, surface area and pore size give the greatest weightage toward heat transfer performance. The heat transfer of devices is controlled and dominated by the material's thermal conductivity properties, which can be increased as a consequence of the increasing porosity, pore size [77] and the presence of cell walls. [76] found out that a higher porosity structure offered better heat transfer performance with fluid flow. The investigation was done on the different porosity levels of vertically stacked layers placed near heat sources. Thus, the interest in porous metal development for thermal management fields was inspired by porous metal structure optimization to improve its thermal properties performance.

The allied fluid flow and porous metal structure can improve the heat transfer of products or systems such as electronic devices, combustion systems, as well as other cooling systems for devices. As reported by Boomsma [78], the experimenting with the porous structure of the Al heat exchanger, the device has better thermal management properties up to three times better compared to the existence commercial heat exchanger. This finding similar agreement by [79], where porous heat exchangers could replace conventional devices due to heat transfer performance.

2.4.4 Porous Cu application

Low cost, availability with a variety of shape, high thermal conductivities (~ 400 W/m K) [80] and high ductility possessed by porous Cu [42] has made this material get a place in the application fields such as electronic engineering, sensors, noise reduction and catalyst and high performances battery technologies [42], [81]. For example, Liu [42] has replaced the common flat Cu foils for Lithium-Ion batteries with porous material that has improved the specific capacities and performances due to the integration of porous Cu and active electrode materials. The lightweight of porous Cu has improved in terms of thermal shock resistance as well as noise reduction [68] with the existence of pores within its structures. Porous Cu is ideal to be applied for thermal devices such as heatsinks and heat exchangers that can be found in high electronic devices [45], [46] and electrodes. The development of advanced technology in computing engineering and electronics-

related products, as well as the increasing demand for miniaturization products, requires massive improvement and upgrading in the performances of components (e.g.; microprocessor, chips, CPU). This enhancement, not to mention the product or component roles, also penetrates the aspect of the thermal management system, which requires an efficient cooling system to cater to high heat generation due to high load and heavy usage. The employment of an efficient cooling system may maximize the performance of electronic devices and also contributes towards the extension of their lifespan. However, inadequate thermal handling may expose problems of poor heat dissipation, increasing hot spot area, and the worst scenario will lead to malfunctioning of the product. Furthermore, miniaturization products may face space-constrained issues that need to solve without sacrificing their performance.

Therefore, many researchers have proposed competitive solutions to improve the heat transfer performance of thermal devices such as heatsink and heat exchangers. The improvement is mainly focused on the alteration of the size, shape, and arrangement of the devices [82] to improve the contact area with the cooling fluid that may be able to transfer out the heat in a larger amount. One of the possible ways to enhance the heat transfer capability is by introducing a porous structure within the thermal device, such as a heatsink. The ‘participation’ of porous material is expected to upgrade the features of the heatsink as it is associated with a high surface-area-to-volume ratio, low density and high fluid permeability [74].

Several findings focus on the performance of porous metal as potential heatsinks, especially porous Cu. A porous Cu heatsink was initially developed by Zhao [13] with the method known as Lost Carbonate Sintering (LCS). Various investigations were taken place to examine the heat transfer performance of the innovative porous Cu heatsink, as reported in [75], [76], [83]. Porous Cu structure has shown an enhancement in thermal properties as reported by [75], [84] and [85], where the heat transfer performance improves with increasing porosity as a result of greater surface area. The comparison of the different types of Cu heatsink by [46] found that porous Cu heatsink has four times better heat transfer capacity than microchannel heatsink with similar power.

Porous metal heatsinks such as steel, aluminium and copper can combine with an identified fluid such as water or air as cooling media manage to transfer heat by forced convection. The designing of the heatsink associated with a large surface area allows the flow of fluid to remove the heat via convection [78]. Cu and water combination offered a good quality cooling system due to chemical compatibility as well excellent heat transfer performance due to the higher surface area [17] as a result of the increase in the contact area with the coolant fluid. This will boost the heat transfer capacity due to the larger surface area permitting larger heat can be transferred. Singh [86] investigated the Cu heatsink with 40% porosity and water as a coolant medium to study the heat transfer performances of the high-powered microprocessor. The finding shows an effective result of thermal conductivity that managed around as high as 32 W/m K from porous heatsink water saturated with heat fluxes of 2.9MW/m² being removed. While Jiang [87] examined the porous plate of bronze on the capability of the heat transfer process with air and water acting as heat transfer media. The finding shows the

heat transfer coefficient of the porous medium has improved 30 times better by using air and 15 times by water instead of operating under an empty channel. Ould-Amer [88] includes the porous material within the heat-generating blocks, which has lowered the maximum temperature, which is also similar outcome with [76] that porous heatsinks manage to reduce the operational temperature of the electronic devices.

2.5 Processing method for Porous Metal

The methods available for porous materials production have expanded rapidly over the last decade, and many researchers have investigated various techniques, from conventional ways (e.g.; casting manufacturing) to the latest technologies, such as additive manufacturing (e.g.; 3D printing), in order to achieve specific material properties. From the perspective of the application, the selected method should consider the features of the end products, such as pore distribution and pore features [89], that can meet the needed of the application. The investment and exploration of porous material fabrication have also not only been led by the final performance of materials but also considered the constraints of being cost-effective production and raw material, time limitation, the market needed and the shortage of supplied materials as well as the health and safety aspects. The production methods must be reliable with the part complexity in terms of shapes and size in order to achieve appropriate porous properties, characteristics and performances.

In general, the fabrication of porous metals can be classified according to the physical characteristics of selected metals, either in solid form, liquid, vapour or ion. Figure 2.18 [14] shows several fabrication techniques that are based on their original state, as each method has its own method, advantages and constraint. For example, the liquid-state processing technique considers metal which has a lower metal point, such as aluminium, magnesium, as well as Cu, that some works reported by liquid-state of processing type (e.g.; GASAR process) [48], [49] instead of its high melting point. Although this approach has advantages in terms of high porosity features, uniform pores etc., this process also demonstrates some drawbacks. For example, molten Mg and Al are easy to react with air, which may reduce their quality due to the oxidation effect. While the high melting temperature of Ti requires to appoint advantage advance equipment besides the challenges of controlling its composition in exposing conditions to the air.

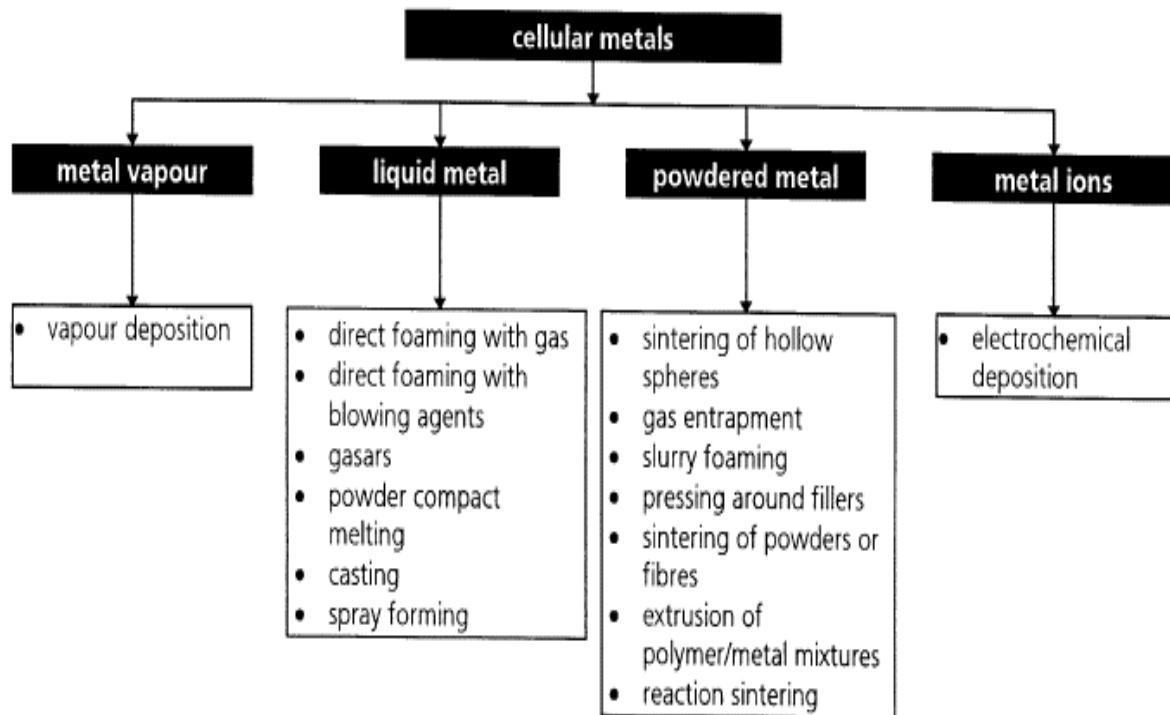


Figure 2.18; Porous metals production methods according to their physical behaviour [14]

2.5.1 Liquid-State Processing Method

The metals should be in the liquid state (molten) and normally conducted for large production. The liquid-state processing technique considers metals with lower melting points, such as aluminium, magnesium, and copper. The introduction of pores into this molten metal can be conducted through gas injection, introducing a blowing agent, gas eutectic solidification (GASAR) [49], and the use of space holder materials during the casting process [90] to preserve space within its microstructure. Figure 2.19 shows examples of a pore structure made by the liquid-state processing method.

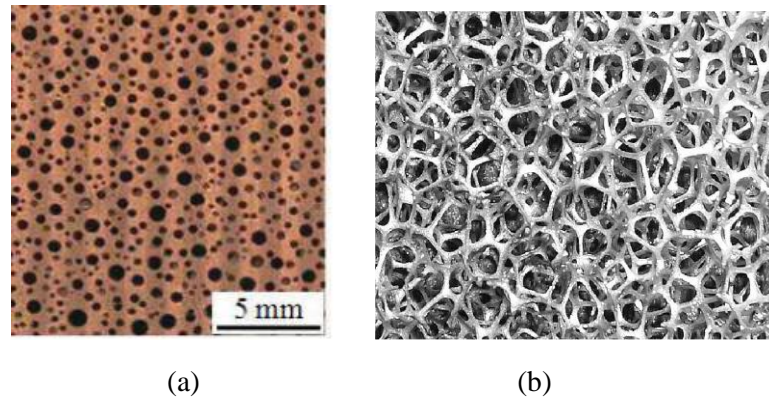


Figure 2.19; Example of pore structure made by liquid-state processing method, (a) GASAR technique [49]
 (b) Investment Casting of AlZn₁₁ foams [91]

The pore formation by gas injection method would be assisted by the roles of gas bubbles introduced to molten metal. These techniques are most likely ‘comfortable’ with the entrapped gaseous as pore-generating media that sources from various types of gaseous (e.g.; nitrogen, hydrogen, air, argon). These gaseous are intentionally injected into the molten metal under specific pressure, and by using the mechanical mechanism of the nozzle vibration or impeller rotation [18], the viscous bubbles of gas are uniformly distributed in the molten metal. The gas bubbles then will float on the molten metal surface, and the pore is created once it is solidified. High-reactive metal such as titanium is not recommended due to impurities, and the pore morphology is difficult to control. The porosity can be achieved at 80-98% with a close-celled pore structure [14].


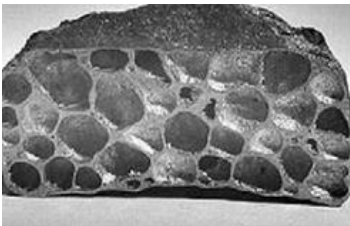
The previous method mainly used injected gas such as air, argon, etc. But for this second method, the gas was supplied and released by the decomposition of the blowing agent during the heating process. The common blowing agents are titanium hydride (TiH₂) [92] and zirconium hydride (ZrH₂), and calcium carbonate (CaCO₃) powder. This blowing agent, titanium hydride (TiH₂), is mixed and stirred together with the molten metal before decomposing and releasing a large volume of gas and hydrogen after exposure at a particular temperature. The process is cooled down below the melting point after mixing to inhibit any premature formation of hydrogen gas. This process was commercialized and patented under the terms of ‘Alporas’ for porous Al production. Although this process has advantages in terms of production scale, porosity, and mechanical properties, however, the bubble gas process is not ideal for any material as it easily reacts to air [17]. At the same time, it requires high pressure to control and maintain the uniform pores. Furthermore, the process has limitations in fabricating a complex shape and makes it difficult to control the foaming structure.

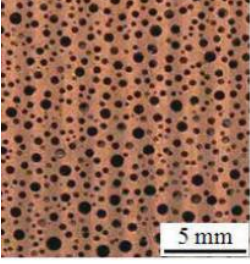
Another common technique in the liquid state processing method is the GASAR method [93] which is carried out at the solid-gas eutectic phase. This method relies on a eutectic system produced by molten metal

with high-pressure hydrogen gas. Once the molten metal solidifies, the absorption of hydrogen gas into the metal structure will create pores. The morphology of the porosity depends on the gas pressure, gas content, cooling rate, etc.

Liquid-state processing method has advantages in terms of high porosity features, uniform pores etc. This process also demonstrates some drawbacks. For example, molten Mg and Al easily react with air, which may reduce their quality due to the oxidation effect. While the high melting temperature of Ti requires to appoint advantage advance equipment besides the challenges of controlling its composition in exposing the condition to the air as it will promote contamination of the Ti element [94]. Table 2.3 shows an example of the liquid-state processing of porous metal.

Table 2.3; Liquid-state processing of porous metal

Method used	Mechanism	Pores metallurgy	Metals	Characteristic	Benefits
Gas injection	Gas injection into molten metal to create bubbles and preserve spaces (pores)		aluminium alloy [95]	Porosity with 80-98% [14], closed-celled	Suitable for large production, low densities porous metal
Blowing agent- TiH ₂ , calcium carbonate (CaCO ₃) powder	The gas was released from the blowing agent as this gas acts as a pores agent	 Sample width: 36mm	Aluminium [92], Commercial Mg ingot	Closed-celled structure	Low melting material

Solid-gas eutectic (GASAR)	Unidirectional solidification		Copper [49]	Closed-celled structure	High porosity
----------------------------	-------------------------------	-----------------------------------------------------------------------------------	-------------	-------------------------	---------------

2.5.2 Solid-State Processing Method

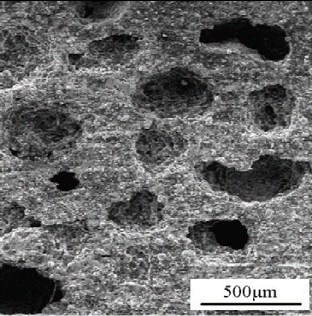
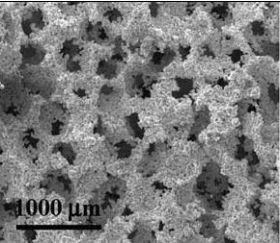
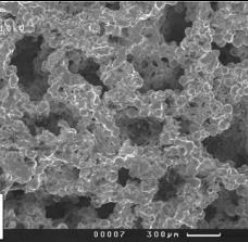
Although most of the commercialized process employing liquid-state processing technique such as ALPORAS [64], the accelerating work on the solid-state processing approach keeps increasing not only on the output volume, this process is more practical and functional and meet the acceptable quality. The processing through solid-state type deals with metal powders and the sintering process. The significant difference between solid-state and liquid-state processing methods is in the morphology of the selected metals, and the solid-state tends to produce open-celled pores, as liquid-state focus on close-celled pores.

This processing method is suitable for numerous metals, including high melting and reactive such as Titanium. This approach offers benefits in terms of pores design and application, and at the same time, this method is safer than the liquid-state processing method. The porosity degree can vary from 50% to a maximum of 90% volume, and the pore size and shape can be modified. The solid-state processing method receives huge attention from manufacturers because it produces a good-quality porous structure. This approach is based on the powder metallurgy process, which can produce complex, near-net shape parts and minimise the need for a secondary operation. The simple processing method is the sintering process on loose powder. This method depends on the sintering parameters and the pores influenced by the features of the metal powder used.

One of the promising methods is by introducing temporary external material to create pores which are known as space holders. This material is added to the metal powders with a combination of conventional fabrication machines such as pressing machines and then turned into a specific shape of part or component. Then, the part will undergo a leaching or pyrolysis process to remove these space-holder materials that will create the targeted pores and porous structure. There are a variety of space holder materials such as Sodium chloride (NaCl) [96], Potassium Carbonate, K_2CO_3 [53], urea [97], and ammonium bicarbonate $(NH_4)HCO_3$ [98], and many more, as they are selected based on factors such as solubility features, degradation temperature as well as their physical shape, size, and volume. NaCl is usually preferred due to its good

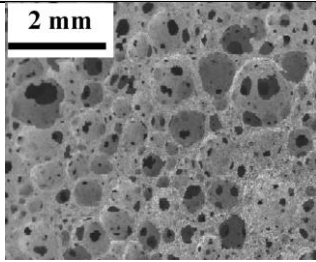
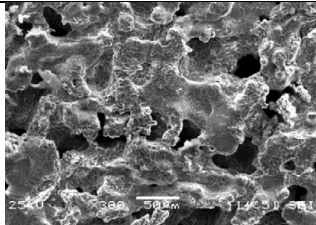
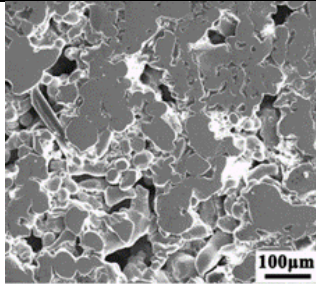
solubility and non-chemical reaction material. Previous works by [99], [100] produced porous Cu with PVA as a binder under 375 MPa of compaction and sintered at 850 °C. Table 2.4 shows the example of a solid-state processing method via the space holder technique

Table 2.4; Example of solid-state processing method via space holder technique

Processing type	Porous mechanism	Descriptions	Porous Structure
Space Holder Technique in combining with the conventional method	Compaction with space holder technique	Space holder technique (Porous Ti with Carbamide, 55–75% porosity)	 <p>Open-cell pores [101]</p>
		Porous Cu by using the LCS method with 80% porosity and cell sizes of 53–1500µm	 <p>Porous Cu by Lost Carbonate Sintering (LCS) [13]</p>
	MIM with space holder technique	Porous Ti with 50% porosity fabricated with KCl as a space holder	 <p>Porous Ti made with the MIM process [102]</p>

Besides the mentioned processing methods above, there are various techniques for porous metal production in the solid-state category, either requiring simple or sophisticated techniques (summarized by Table 2.5). The introduction of additive manufacturing methods such as selective laser sintering (SLS), direct metal typing or 3D direct metal printing, and Electron Beam Melting (EBM) [57], [103] in this processing method category makes them more reliable and capable for complex shape porous metal fabrication.

Table 2.5; Other examples of solid-state processing method

Processing Method	Porous microstructures	Powder Metal	Foaming media	Porous structures	Ref
Metal powder slurries (316L stainless steel powder with aeration, 2 minutes)		316L stainless steel powder	Methylcellulose	Open-cell pores	[104]
Pressureless Sintering (Ni-30 wt% Al at 1000°C)		NiAl	-	Open-cell pores	[105]
Selective Laser Sintering (SLS) (Porous 316L SS sintered at 1100 °C)		316L SS	Ethylene-vinyl acetate copolymer (EVA)	Open-cell	[106]

Solid state processing method receives huge attention from manufacturers owing to its capability to produce a good quality porous structure. This approach is based on the powder metallurgy process, which offers many benefits, such as producing complex and near-net shape parts and minimising the need for a secondary operation. Studies show that Cu is frequently processed using solid-state methods [8], [100], [107] due to its properties.

2.6 Processing Porous Cu via Partial Sintering Technique

The easiest way to fabricate porous Cu fabrication is by utilising the control sintering process in the powder metallurgy approach (refer to Figure 2.20) to meet the desired pores properties. In general, the sintering process can be referred to as a densification process that heats the parts to obtain the densification stage from a porous structure [108]. The process must carry out in a certain condition before full densification is taken place. This technique is relatively interrupting the inter-particle bonding that prevents them from obtaining near full density and achieves an incomplete densification stage [103]. The sintered part was created with small necks formation [103], and the pores were formed upon sintering and cusped between powder particles at the necking area (Figure 2.21). This process is known as the partial sintering process [24]. The sintering parameters, such as temperature and time, must be controlled for a certain porosity level.

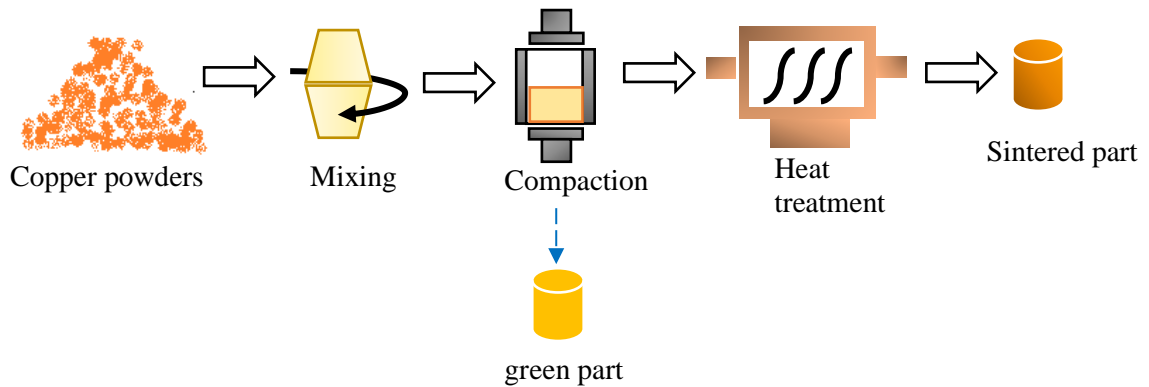


Figure 2.20; A schematic diagram of partial sintering process

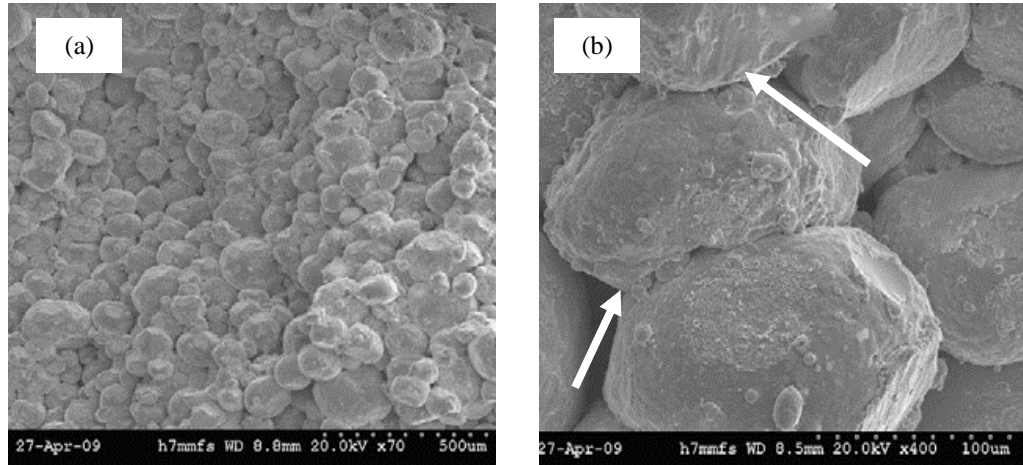


Figure 2.21; Neck formation between powder particles; a) Sintered Cu at 750 °C for 5min, b) neck formation between Cu particles, zooming at 100µm [109]

Thus, controlling the sintering profiles, such as temperature and heating time, will minimize the particle bonding formation. Studies by [110] have detected a close pores shape with 10% at 1000°C on Cu compact, while other works on porous bronze ($\text{Cu}_{89}\text{Sn}_{11}$) have obtained porosity between 20 and 50% for [14]. However, this process is limited to work with low porosity formation and is challenging to achieve with high porosity samples. Previous work reported the porosity constrained to 50% [67]. Furthermore, the generated pores features are not tailored to the desired shape and size as it depends on the formation of the voids near to the necking area. The other drawbacks are this process produces parts with low mechanical properties due to insufficient particle bonding. Lower sintering temperature produces insufficient bonding between powder particles, e.g.; for porous Al fabrication at the lower sintering temperature, 550°C [111] will possess lower mechanical properties. To sum up, although this powder sintering technique has managed to produce numerous porous metals and suit with different metals, most of the part comes with low fraction of porosity and has disadvantages in terms of mechanical performance. In addition, this technique unable to control its own pores formation and prevent them being applied broadly in porous metal application.

2.7 Processing with pore generating agent- Space holder assisted

Although powder sintering has produced a number of parts with different types of metal powder in terms of porosity behaviour, most of the final samples come out with a lower fraction of porosity volume. Moreover, this technique has weakness in controlling porosity properties such as pore shape, sizes, and porosity distribution. These constraints have prevented them from being applied widely in porous metal applications.

If any part can secure its own pores and preserve the space in the structure, this means the pores structure can be controlled and achieved with the desired characteristics. Therefore, it would be good to find certain methods to achieve this condition. Essentially, the porosity and pores formation can be increased by preserving some regions and spaces within the microstructure. To achieve this condition, the metal should integrate with external agents or particles to obtain some degree of porosity. The external particles should not give any chemical reaction or change the metal performance, and the most important thing and the particle can be eliminated without degrading the material structure.

Porous metals can be fabricated by a method such as the space holder technique [24], [103]. This technique has been proven as one of the promising methods in controlling porosity formation, but it also can be merged and paired with various processing methods, for example, the conventional pressing method [112], [113], spark plasma sintering [114]–[116] and investment casting [117]. The different and independent material content of the space holders makes them easily removed and creates pores [61]. The polymer grains, ceramic particles, salts, or metals can all be used as space holders [74]. This temporary material plays a noteworthy task in ‘preserving’ space in the metal once it is eliminated without altering the material composition or chemically reacting and produces a distributed open and interconnected pore. The space holder material in some works is called other names such as placeholders [118], substances [89], and porogen [119], but they serve similar roles to generate pores. The developed pore structure replicates and imitates the physical properties of the selected space holder. Therefore, the aspect of porosity degree can also be easy to be controlled and designed to obtain the intended value. This means the final porosity volume is expected to be proportional to the amount of space holder that being setup besides its shape and size. Figure 2.22, demonstrate the pores formation are exactly similar to the space holder properties. The created pore shape and size is based on the morphology and size of the sacrificed particles [120].

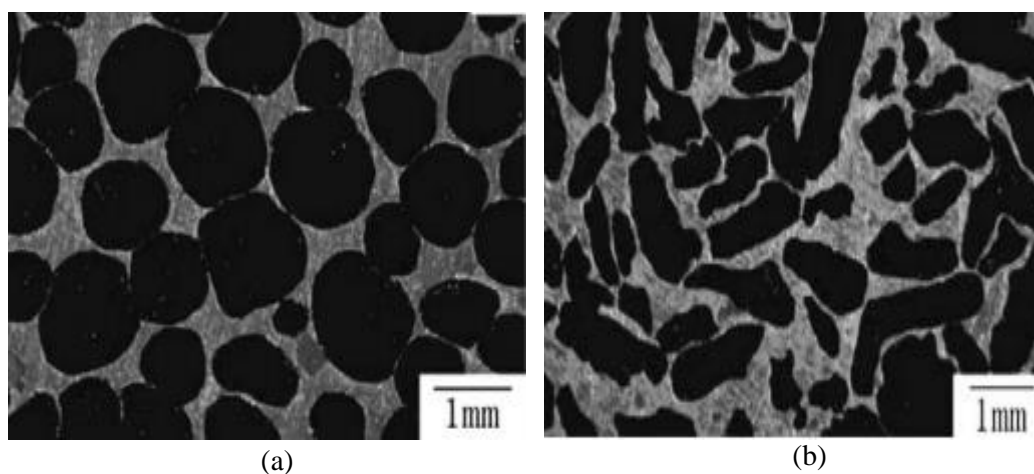


Figure 2.22; Porous Al with 70% of porosity and fabricated with different pore shapes according to space holding materials, (a) Porous Al with spherical carbamide, (b) Porous Al with strip-shaped carbamide

Zhao and his team [13] [120] have developed a remarkable technique that the formation of the pores can be preserved and designed in the development of aluminium foam. As shown in Figure 2.23, this method requires the space holder (Sodium Chloride (NaCl)) that is incorporated and mixed into the present metal structure, followed by the shape formation process and finally these space holder particles will be removed by water leaching. This processing method managed to produce pores with similar morphology to the selected space holder and pore size in the range of 300-1000 μ m. Figure 2.24, shows the porous Cu made by space holder technique.

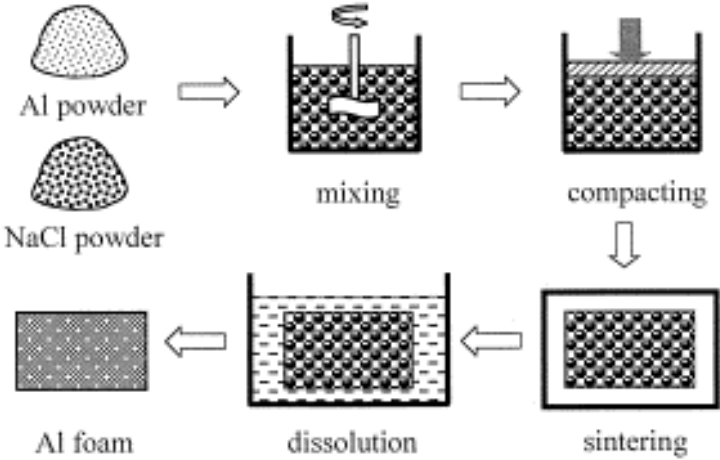


Figure 2.23, The introduction of space holder processing method by Zhao (2001) [120]

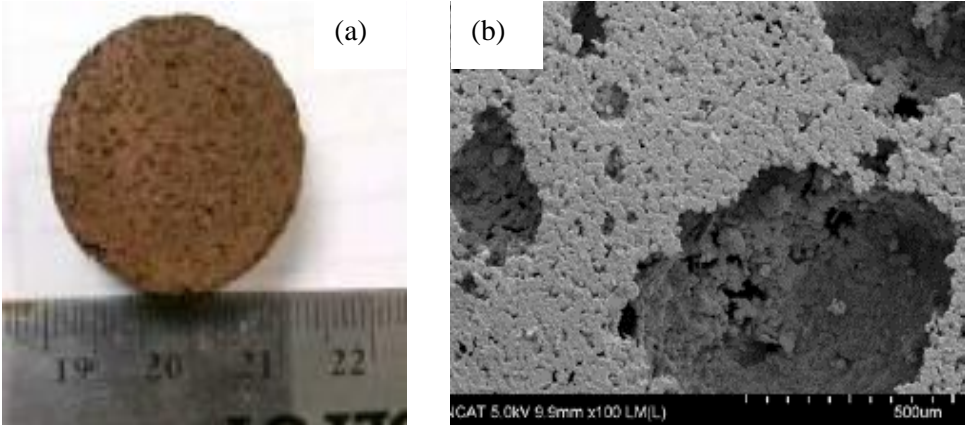


Figure 2.24; Porous Cu with NaCl as space-holding material [100]

In terms of porosity volume, this technique is capable of achieving a higher percentage of porosity, e.g. porous Al with carbamide as space holder has successfully been fabricated with porosities between 50-80% [111]. Numerous space holder materials have been attempted for porous metal fabrication, such as ammonium hydrogen carbonate (NH_4HCO_3) [121], [122], carbamide [101], [123], [124], magnesium [125], [126], urea [127], and sucrose [128]. For porous copper fabrication, previous studies have demonstrated numerous space-holding materials such as NaCl [100], [129], Carbamide [130], [131], and PMMA [58]. For reasons related to environmental friendliness and reduced toxicity, some space-holding materials, such as rock candy and sugar cane [132], have been used in the processing of porous copper. The introduction of organic space holders was driven by the concern for the toxicity effect on the human body and environment caused by the chemical reactions of space holders. For instance, sugar pellets [133] have been proposed as space holder material due to excellent biocompatibility behaviour which is suitable for biomedical application. While tapioca starch [21] in processing porous titanium has been chosen since starch is considered an environmentally friendly material.

2.7.1 Space holder technique with Compaction & Sintering (C&S) Method

This process technique can be identified as one of the easiest ways in powder metallurgy (PM) and possibly the fastest technique to fabricate parts without considering the involvement of complicated attributes that require some processing. As the initial mixing process is inevitable in all powder metallurgy processes, including the compaction method, then the mixture of powders is subjected to forces or pressure to transform the packed powders into certain shapes and designs. The created green part's design replicates the assigned mould shape and then may be heated to a certain temperature to strengthen the structures, and the secondary process may or may not be carried out on the sintered sample. This straightforward processing technique does not require any multiple binder components as its vital for other PM processes such as metal injection moulding (MIM). Figure 2.25 shows the methods and examples of porous Cu fabrication by this method with different removal processes, either by dissolution process or thermal degradation. In contrast to other powder metallurgy approaches, the C&S method is relatively easy and straightforward, which no need to have any specific requirements or other compulsory materials during their fabrication, such as MIM requiring binder components. This method, as well as other powder metallurgy approaches, generally depends on the characteristics of the powder (size, shape, and distribution). For example, irregular powders, through their good interlocking mechanism, give benefit in retaining the part shape and eases the part handling. Generally, the higher the compaction pressure, the lower the porosity formation. After sintering, the porosity might be increased or decreased depending on the sintering profile.

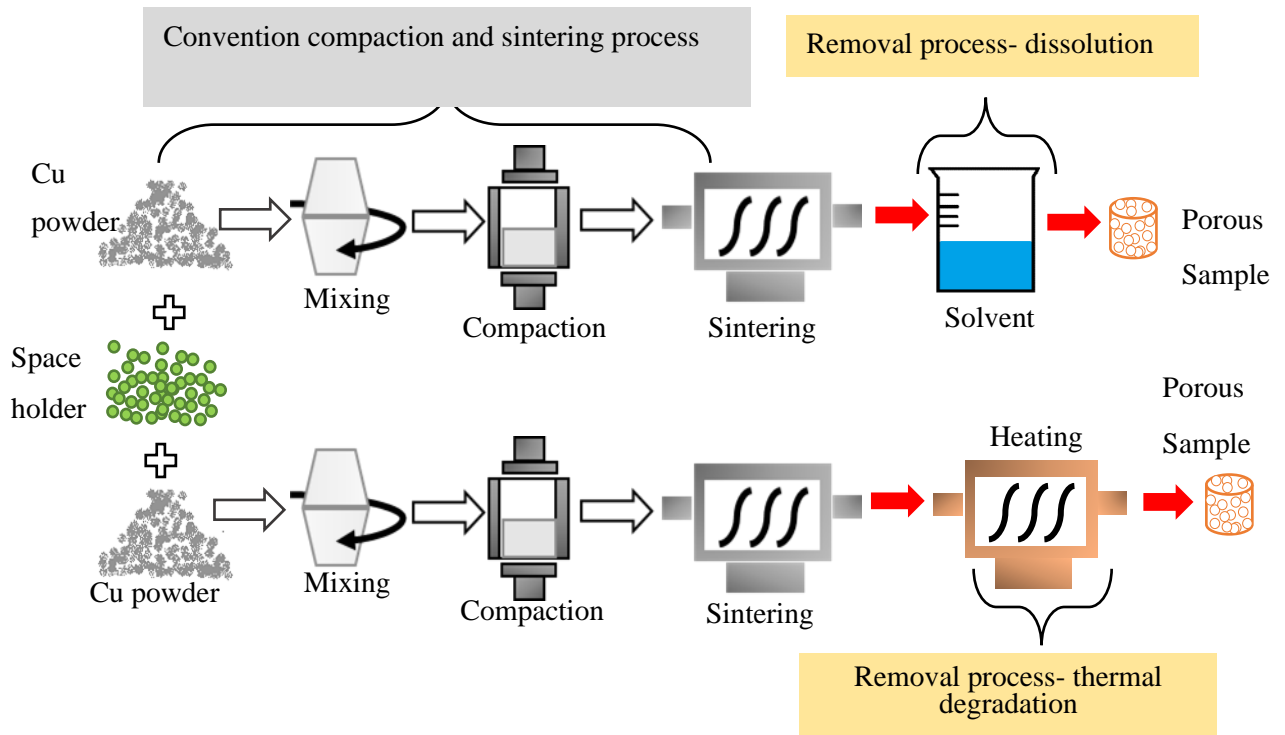
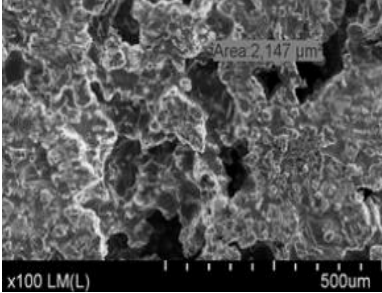
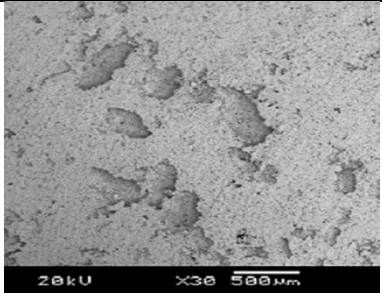
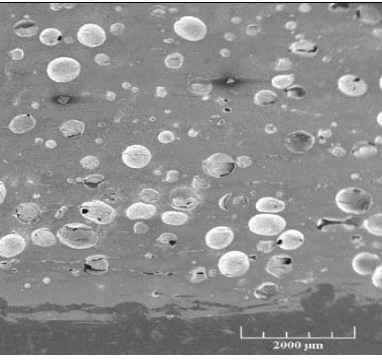
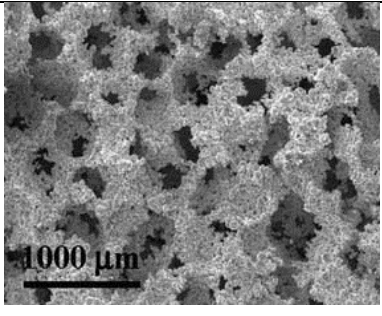
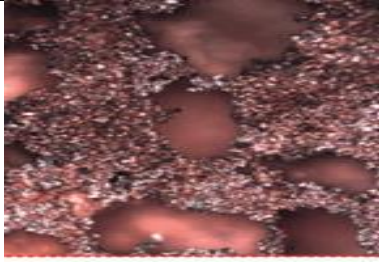


Figure 2.25; Porous Cu fabrication by using the C&S method with different types of the removal process

A study [134] has been carried out assessing the different types of spacing-holding material in fabricating porous copper, including NaCl, potassium carbonate (K_2CO_3), and polymethyl methacrylate (PMMA). The pre-sintering is done at $770^\circ C$ before the sintering process takes place at $900^\circ C$, and finally, leaching in hot water. From the findings, porous copper samples with PMMA faced a shrinkage problem due to the sintering process, which might lead to material collapse. In another study, porous copper with a porosity between 50-85% [13] has successfully fabricated with pores sizes between $53-1500\mu m$. The appointment of K_2CO_3 as a space holder due to high solubility in water ($112\text{ g}/100\text{ mL}$ ($20^\circ C$)) [135]. By using the same technique, a study by [136] produced porous copper with better mechanical strength and 33.9 % of porosity at a sintering profile of $450-850-950^\circ C$. Table 2.6 below shows an example of porous Cu production using the C&S method.

Table 2.6; The space holder materials used to produce porous Cu by the C&S method

Space-holding Material	Method	Removal	Morphology structure	Porosity	Ref.
Sodium Chloride (NaCl)	Compaction	Dissolution in water for 2 hours at 70°C		42.2-57.79%	[100]
Carbamide (Urea)	Compaction	Decomposed at 200 °C, 4 hours		71.75% porosity at 30 wt.% space holder	[130]
PMMA	Compaction	-		5.9–55.5%	[58]
Potassium Carbonate	Compaction	Water for 5 hours Decompose at 950 oC, 2 hours		50-85% porosity	[13]

Sugar cane	Compaction	Water at room temperature		60-80% porosity	[132]
------------	------------	---------------------------	------------------------------------------------------------------------------------	-----------------	-------

The properties of space-holding materials, such as melting point and solubility level, determine how the removal process will be carried out. Previous studies reported that the selection of space holder material is based on how the space holders can be removed from the structure either by evaporation or dissolution during the processing stage (according to Table 2.7). For example, in the processing of porous copper, soluble NaCl is preferred to be eliminated via the dissolution process [129], while the low decomposition temperature of carbamide makes this type of material suitable to be removed by thermal treatment [130]. However, the process was reported to face poor structural integrity due to the lower sintering process since this low decomposition space-holding material cannot withstand the higher sintering process. Therefore, proper sintering parameters (e.g. sintering time) need to be carefully controlled [137] to limit the potential failure. Special space-holding material such as K_2CO_3 is capable of being removed in both ways, but research [8] has compared the preferable removal processes for this kind of material. They found that porous copper will have excellent material strength if K_2CO_3 is removed by the decomposition process.

Water soluble space holder materials such as sodium chloride (NaCl) [138], potassium chloride (KCl) [139], and potassium carbonate (K_2CO_3) [13] are easy to dissolve in water. For example, NaCl has a high solubility in water, 359g/L at room temperature [112], and sucrose (211.5 g/100ml) [128]. While space holders such as polymethylmethacrylate (PMMA) [140] and ammonium bicarbonate are removed by thermal treatment due to their low decomposition temperature.

Table 2.7; Examples of the combination of metal powder and space-holding materials

Porous Metals	Space-holding materials	Type of removal process	Solvents / Decomposition Temperature	Ref.
Copper	Potassium Carbonate	Dissolution Thermal treatment	Water for 5 hours Decompose at 950 °C, 2 hours	[13]

Aluminium	Carbamide PMMA	Dissolution Thermal treatment	Water at 80°C.for 5 hours Decomposed at 450°C for 1 hour	[111] [140]
Ti TiNi	Sodium Chloride (NaCl) Magnesium	Dissolution Thermal treatment	Water for 2-3 hours Decomposed at 1100°C for 1 hour	[112] [126]
Stainless Steel	Ammonium bicarbonate	Thermal treatment	Decomposed at 200 °C for 2 hours	[121]
Magnesium	PMMA	Thermal treatment	Decomposed at 400-550 °C for 2 hours	[141]
Tantalum	Sucrose	Dissolution	Water at 20°C	[128]

Although the process is able to achieve high accuracy in geometrical shapes, the limitation of shape tooling and ununiform compaction contributes to the constraints [142]. Additionally, because the process commonly deals with high-pressure levels, this will expose the space holder to high compaction pressure. If this projected pressure is over the limit of critical strength of the space holder particle, then it will deteriorate the space holder shape. Thus, the created pores are not fully replicate the original shape of the space holder. In the worst case, the space holder materials tend to deform and break due to the deformation process [59] as carbamide [143], [144] was reported to fracture when the compaction pressure exceeded more than 100 MPa while ammonium hydrogen carbonate and NaCl show the same result at 350 MPa [138], [145]. The pore shapes also change from the original spherical shape into an elliptical shape resulting from high compaction pressure [144]. However, too low compaction pressure will produce the final part with structural integrity problems, as found on Ti-6Al-4V if the compaction pressure is lower than 300MPa [146]. Therefore, an optimum compaction pressure is necessary to avoid defects in the final part and maintain the shape of the space holder.

2.8 Space Holder Technique with Metal Injection Moulding Process (MIM)

As reported in the previous section, mixed space holder materials and metal powder have been shaped by using a simple pressing technique, either cold or hot-pressing. The ‘green samples’ then need to be hardened in the heat treatment process, called the sintering process, under specific atmospheres; inert gases (e.g. argon) or vacuum atmosphere. Conventional pressing methods (cold or hot) have successfully produced samples with up to 80% porosity. Nevertheless, these processes have major weaknesses on their part due to geometrical

limitations. This process is capable of producing conventional cylindrical parts, but some research has enhanced the shape of the final part. However, these improvements are still within the limit of shape and size.

Additionally, because the process commonly deals with high-pressure levels, this will expose the space holder to high compaction pressure. If this projected pressure exceeds the limit of the critical strength of the space holder particle, it will deteriorate the shape of the space holder. Thus, the created pores are not fully replicate the original shape of the space holder. In the worst case, the space holder materials tend to deform and break due to the deformation process [59] as carbamide [143], [144] is reported to fracture when the compaction pressure exceeds more than 100 MPa. In comparison, ammonium hydrogen carbonate and NaCl show the same result at 350 MPa [138], [145]. The pore shapes also change from the original spherical shape into an elliptical shape resulting from high compaction pressure [144]. However, too low compaction pressure will produce the final part with structural integrity problems, as found on Ti-6Al-4V if the compaction pressure is lower than 300MPa [146]. Therefore, an optimum compaction pressure is necessary to avoid defects in the final part and maintain the shape of the space holder.

Because of the limitation of former methods, the ideal potential process to be paired with space holder technique in a similar category (powder metallurgy) is metal injection moulding (MIM). MIM is the closest candidate to fabricate porous parts, which not only can fabricate porous metal but at the same time, the parts can be processed with high precision and complex shape design. This process is mostly known as a near-net shape method, where typical additional processes such as machining can be avoided or reduced. These advantages provide a beneficial impact, especially in minimizing the production cost and can also produce large volumes of part production.

2.8.1 Metal Injection Moulding (MIM)

Metal injection Moulding (MIM), or, in some cases called, Powder Injection Moulding (PIM), where the process was adapted from polymer-based industries. MIM products are widely used in many industries, such as automotive, building, manufacturing, aerospace, medical, etc. MIM fabrication has received a lot of attention from industrial players due to its benefits. [147] reported that, with MIM, these three features have been ‘taken care of’, which consists of shape complexity, performance, and low-cost factor (Figure 2.26). MIM not only accommodate high-volume production [148], but this process has reduced the need for the secondary process (e.g.; cutting, grinding, drilling etc.), which helps to minimize industrial waste.

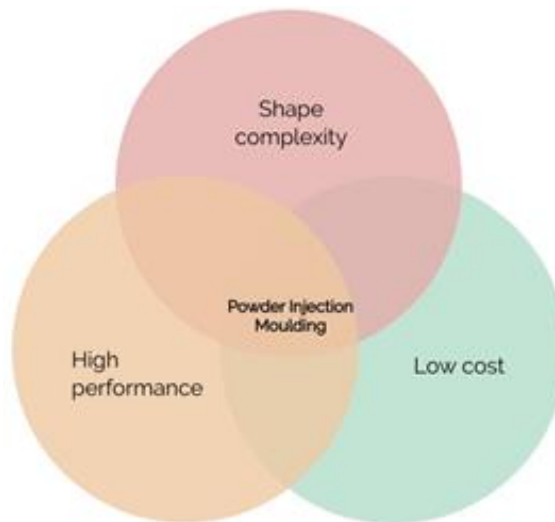


Figure 2.26; Redraw of the Venn diagram describes the application of the PIM process concerns about three important aspects [147]

MIM process is purposely used metal powder as the main material along with the binders in its production. Thus, it is essential to understand each processing stage in MIM in order to produce good-quality parts. MIM consists of four main stages; mixing, injection moulding, debinding, and sintering. Each stage is dependent on the others, which is any defect in the previous stage will cause a problem in the subsequent stage. Compared to other powder metallurgy approaches, MIM requires the use of polymeric binders that consist of approximately 30-50% [149] of the overall composition. The binder will be mixed with the parent metal during the mixing process and then turn them into feedstock. As shown in Figure 2.27, the MIM process is a combination of metal compaction and plastic injection moulding (PIM). Previously, the PIM process has been proven to produce plastic parts with high accuracy and a large volume of production. Thus, adopting the process mechanism of PIM with compaction metal powder has introduced the MIM process in the fabrication method.

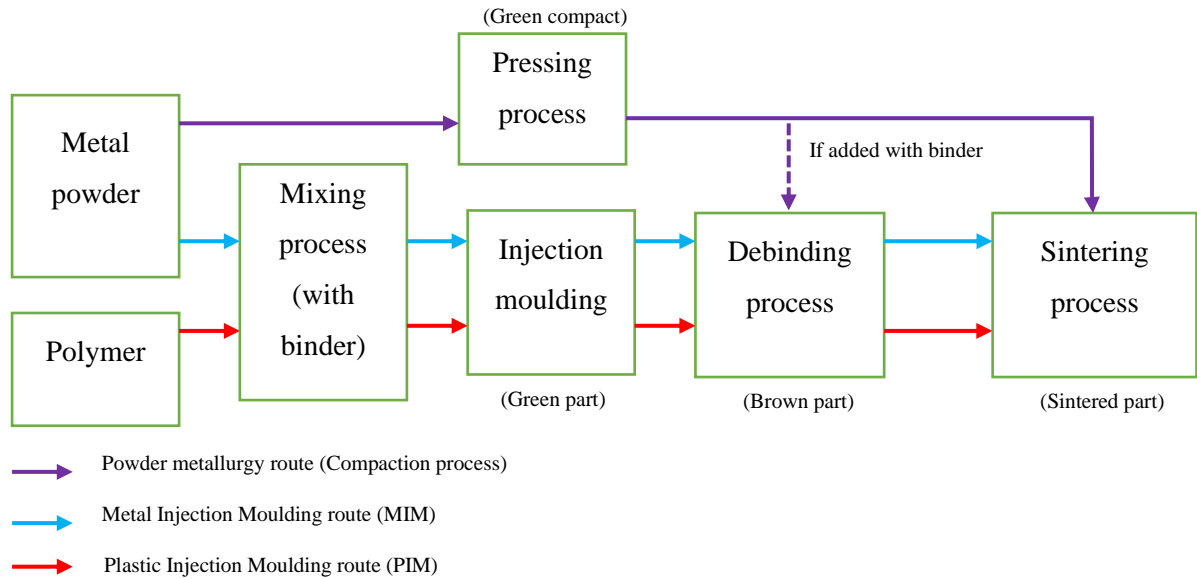


Figure 2.27; The comparison of process routes of MIM, plastic, and compaction process

Similar to conventional powder metallurgical processes, MIM starts by defining the appropriate metal powders and binder system, which will then be blended together in a specific mixing machine. As a result, the uniform powder-binder mixtures will be produced in paste form and then transformed into pellet particles (can be called feedstock) in order to be processed through an injection moulding process. The raw parts in specific shapes, known as ‘green parts’, are produced based on the die shape. Subsequently, the green part requires a debinding process to ensure the binder within the structure can remove away. Finally, the densification process will occur in high-temperature sintering, and the heating process activity is generally done in a furnace. Additional processes, such as post-sintering, are necessary for improved part structure. The summary of the process is shown in Figure 2.28.

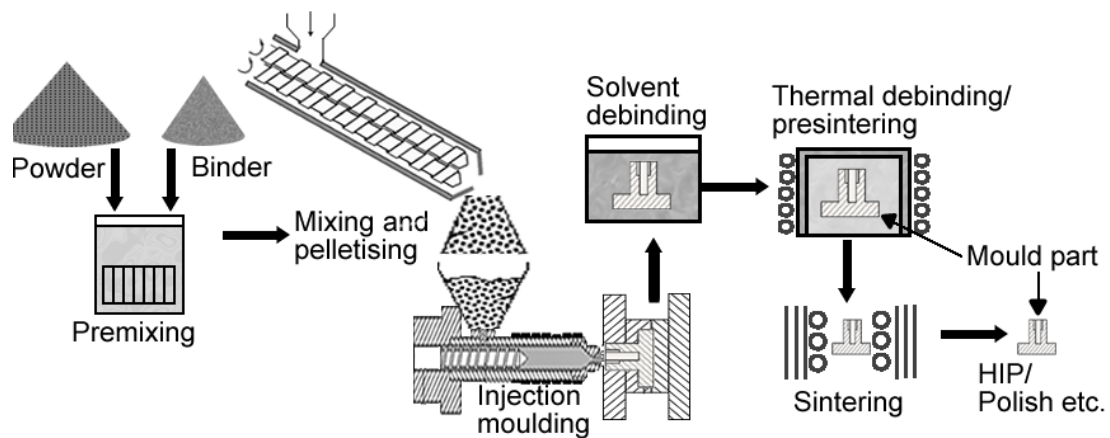


Figure 2.28; Schematic diagram of metal injection moulding process [150]

2.8.2 Important aspects to be considered in MIM

2.8.2.1 Material selection

For the MIM process, it is compulsory to understand and identify the material, especially the metal powder itself. The properties such as shape, size, and composition play important roles in the successful MIM process [147]. The powder shape, for instance, has come in a wide variety of shapes such as spherical, irregular, flaky, and needle-shape, which is based on how they are being manufactured. According to [151], powder particles with spherical shapes and less than 20 μ m are suitable for the MIM process the reason of better mouldability and low viscosity, but this group of powder particles is quite costly. However, the selection of metal powder is mostly motivated by the application and its processing capability.

According to [151], powder particles with a spherical shape and less than 20 μ m are suitable for the MIM process for the reasons of better mouldability and low viscosity, but this group of powder particles is quite expensive. Torres [138] preferred the size of the metal powder to be much smaller than the space holder size to promote the sinterability of the sample. In contrast, larger particle size has the potential to have a problem regarding flowability behaviour.

2.8.2.2 The binder system

The difference between the MIM process rather than other powder metallurgical approaches is this process requires a binder system in the processing stage and is an important aspect that contributes to the successful fabrication. Generally, the binder system consists of multi-component materials of polymer and wax. According to German and Bose [151], MIM binders must be able to mould the sample without any defects, have good shape retention, be low cost, and can be removed either by solvent or thermal removal process with minimum environmental impact. The appointment of binder in the MIM fabrication process contributes to two types of roles; transportation of feedstock by reducing the viscosity behaviour and maintaining the feedstock structure before the thermal process. The ideal binder systems in MIM consist of three components; the main binder controls the flowability of feedstock. This binder commonly comes from waxes-type binder such as Paraffin Wax (PW) [152], which needs to be removed by solvent debinding resulting in pores creation. Moreover, the pores act as a channel for the remaining binder to flow out during thermal debinding [147]. However, the higher content of PW will have poor mechanical feedstock because, in the extrusion stage, the shape of the part was not maintained by PW [153]. As discussed by [154], paraffin wax and stearic acid have a tendency to create a crack in the structure from the heating process before proper pore channels to the surface are developed. Thus, by the solvent debinding process, channels can be formed, and

the removal of the remaining binder via thermal debinding can be processed without demolishing the structure. Although wax binder has prepared feedstocks with less defect, a previous study has reported that this binder contributes towards environmental problem since wax binder need to be removed by solvent liquid rather than water. The toxicity of solvents may promote problems for the environment and humans. Therefore, a water-soluble binder, such as PEG, has become the ideal replacement to solve the problem related to chemical hazards.

The second component of binder which is designed to maintain the material structure (known as backbone binder) and thermoplastic binders, e.g. polyethylene (PE), polystyrene (PS), polypropylene (PP), Poly(methyl methacrylate) (PMMA) are frequently used as a backbone binder.

Finally, the surfactant is used to enhance the interaction between metal powder and binder and improve wettability behaviour by avoiding particle separation in the mixture [155]. Usually, a surfactant such as stearic acid (SA) is used in lower content since previous research reported that a higher volume of surfactant would lead to crack problems [156]. Higher content of the wax-based binder in feedstock will have better lubrication behaviour, especially in combination with polyethylene.

2.8.2.2.1 Binder system for copper

This binder for Cu production is commonly made from waxes-type binders such as paraffin-based binders; Paraffin Wax (PW) [152]. This binder is being removed through solvent debinding, and the process will create pores and act as a channel for the remaining binder to flow out during thermal debinding [147]. However, the higher content of PW will have poor mechanical feedstock because, in the extrusion stage, the shape of the part was not maintained by PW [153]. As discussed by [154], paraffin wax and stearic acid have a tendency to create a crack in the structure from the heating process before proper pore channels to the surface are developed. Thus, by the solvent debinding process, channels can be formed, and the removal of the remaining binder via thermal debinding can be processed without demolishing the structure. Although waxes binder has prepared feedstocks with fewer defects, the previous study has reported that this binder contributes to an environmental problem and is toxic to organisms [94] as it must engage with a chemical solution. The toxicity of solvents may promote problems for the environment and humans. Therefore, a water-soluble binder, such as PEG, has become the ideal replacement to solve the problem related to chemical hazards.

Previous studies reported that the fabrication of copper by the MIM process had used different types of the binder system, for example, wax-type binder systems (Paraffin Wax, HDPE or PE, Stearic Acid) [157][158][159]. A study by [160] focusing on Cu-MIM fabrication for heat sink purposes where wax-type binder (paraffin wax) as a main binder combined with polypropylene and stearic acid. The heat sink part shows a density between 93-96% of theoretical density and 280-320 $\text{Wm}^{-1}\text{K}^{-1}$ of thermal conductivity. [159] also

employed a similar binder system to fabricate 66% of Cu with lower injection pressure and 980°C of sintering temperature. The process has successfully produced the part without any defects, but the shrinkage needs to be carefully controlled. Another study by [157], which combined the paraffin wax with 40% wt. of high-density polyethylene (HDPE), produced MIM Cu with a lower volume (59%). Since 70% of paraffin wax has been removed during debinding process through solvent debinding (heptane solvent) has resulted in a faster thermal debinding process. However, the employment of solvent liquid, such as heptane, in these studies has led to the environmental problem [161] since the wax binder must be removed by chemical solvents such as hexane, heptane or ethanol. Therefore, an alternative binder system needs to be proposed to replace the current binder system for MIM Cu fabrication. Other researchers implemented an organic binder such as palm stearin (PS) in the porous copper fabrication [162], [163] with the role of improving the flowability behaviour of feedstock. However, the study focuses on viscosity behaviour and lacks characterization of certain aspects that are related towards debinding behaviour and the sintering process.

For the present porous Cu fabrication study, using a water-based binder system such as PEG-PMMA-SA will give credit for the time reduction of processing since the appointed space holder-KCl also can be eliminated via the water leaching process. Therefore, both binder (PEG) and KCl can be removed simultaneously, which may speed up the processing process of porous Cu. This binder system can be the best candidate for porous metal fabrication.

2.8.2.2.2 PEG-PMMA-SA System

This binder system was applied in a wide range of materials as they have been used in many works [164]–[167] due to its advantages. This binder system consists of polyethylene glycol (PEG) with a major fraction, followed by polymethyl methacrylate (PMMA) and stearic acid (SA). This binder system has been used in feedstock fabrication, such as titanium [168], [169], stainless steel [170], Inconel [161], and also metal alloys such as NiTi [171]. The main advantages of the binder system are this binder gives a shorter debinding process [170] compared to other binder systems. It has been proved that the PEG component is capable of being removed rapidly with water dissolution. This is followed by the thermal degradation of PMMA and SA. This binder system is also environmentally friendly [167], [172] since it is contacted with a water-based solution rather than other chemical solvents. For the present study of porous Cu fabrication, the use of a water-based binder system such as PEG-PMMA-SA will give credit for the time reduction of processing since the appointed space holder-KCl also can be eliminated via water leaching process. Therefore, for both binder (PEG) and KCl can be removed simultaneously which may speed up the processing process of porous Cu. This binder system can be the best candidate for porous metal fabrication.

2.8.2.3 Mixing Process

Initially, the MIM process starts with the preparation of feedstock by mixing metal powder and binder. The mixture is blended together based on a specified ingredient ratio in order to have a homogeneous mixture. Poor mixing will lead to the separation of the metal powder-binder, and the part will have defects such as cracks and porosity. In addition, the feedstock must have a suitable metal powder-binder ratio to produce good MIM parts.

Metal powder usually occupies between 50-65% of the total volume [173], and the rest of the volume is covered by binder content. Previous studies reported that the metal powder is advisable in higher content to ensure the part can have the maximum properties offered by the metal powder. The feedstock also requires sufficient binder content to control viscosity behaviour and keep the shape of the part before proceeding to debinding process. Therefore, good balancing of the ratio between metal powder-binder is necessary to have good MIM parts. Another point of view is that the right ratio will limit potential defects in the final MIM product. For example, a higher metal-powder ratio will face difficulty in sufficiently filling the mould, and in contrast, the (high binder volume) may not be able to maintain the shape of the part due to metal powder-binder separation.

2.8.2.4 Injection Moulding Process

Once the feedstock is ready, it will be injected into the mould die by using an injection moulding machine. In this process, the important parameters such as injection pressure, injection temperature, and mould size are carefully defined to ensure the injected part has a good shape without any defects such as warping, bending or voids in the structure. Generally, defects can occur during injection moulding due to improper injection settings and may also result from an insufficient mixing process. Furthermore, the flowability of feedstock is also one of the crucial aspects in determining a good moulding process, which is dependent on the rheological characteristic.

2.8.2.5 Debinding Process

The binders play important roles in holding the part until the densification stage. However, the binder elements need to be extracted from the microstructure. Failure to completely remove the binder system will promote a large number of defects, such as corrosion and poor mechanical strength [174]. Therefore, the aim

of debinding process is to remove the binder component at an appropriate time without affecting the component properties. The wide debinding processes among researchers and industry are thermal debinding and solvent debinding. Each activity has its own mechanism, such as the solvent-type binder being designed with the capability to be removed by water or any chemical solvent through the dissolution process without affecting the existing backbone binder. Examples of solvents are heptane, hexane, or ethanol, performed within a certain temperature range. Depending on the MIM process, the binders can be eliminated by dual stages of debinding process (solvent debinding and thermal debinding), or they can be fully removed by the thermal debinding process alone. In another part, the thermal debinding process, which is a different mechanism than the solvent debinding process, is the process where the part will be heated in a specific atmosphere to remove the remaining binder. This process is normally carried out simultaneously with the sintering process.

In this study, the assigning of water-soluble binders is based on certain factors. The main reason is related towards the debinding process. Since KCl is used as a space holder, which is classified as a water-soluble type space holder, the removal of both components (space holder and binder) can be performed at the same time. Thus, this concurrent process will save time by using the same removal platform. Another reason, water-soluble binder, such as PEG, is known to be a non-toxic binder since this binder is removed by using water rather than other chemical solvents.

2.8.2.6 Sintering Process

The sintering process, or known as the thermal treatment process, is normally carried out after the debinding process with the purpose of improving the strength of the part by enhancing the powder particle bonding. The size of the green part is normally larger than the potential shape since the shrinkage will take place around 14-20% from the initial dimension [175]. The sintering temperature must keep at a lower temperature than the melting point of the metal, which is usually within 70-90% of the melting point of the parent metal. This process is continuously performed exactly after the thermal debinding process with the same or different atmosphere (inert gas or vacuum). High-purity inert gasses such as argon and nitrogen assist in the heating process, while vacuum sintering is helpful with a clean atmosphere to avoid any oxidation effect on the samples.

2.8.3 MIM with space holder technique

MIM is the closest candidate to fabricate porous parts, which not only fabricate porous metal but also can be processed with high precision and complex shape design. This process is mostly known as a near-net shape method, where typical additional processes such as machining can be avoided or reduced. These

advantages provide a beneficial impact, especially in minimizing the production cost and can also produce large volumes of part production. The ‘joint venture’ of space holder technique with metal injection moulding (MIM-SH) benefits large production volumes and net-shape porous parts. With the assistance of space holder materials, the porosity and the pore morphology can be controlled, and the end product will have an accurate dimension without submitting for an additional machining process, as this process could destroy the pore structure [176]. The process is similar to the conventional MIM process, and the only difference is in introducing space holder material into feedstock fabrication (Figure 2.29).

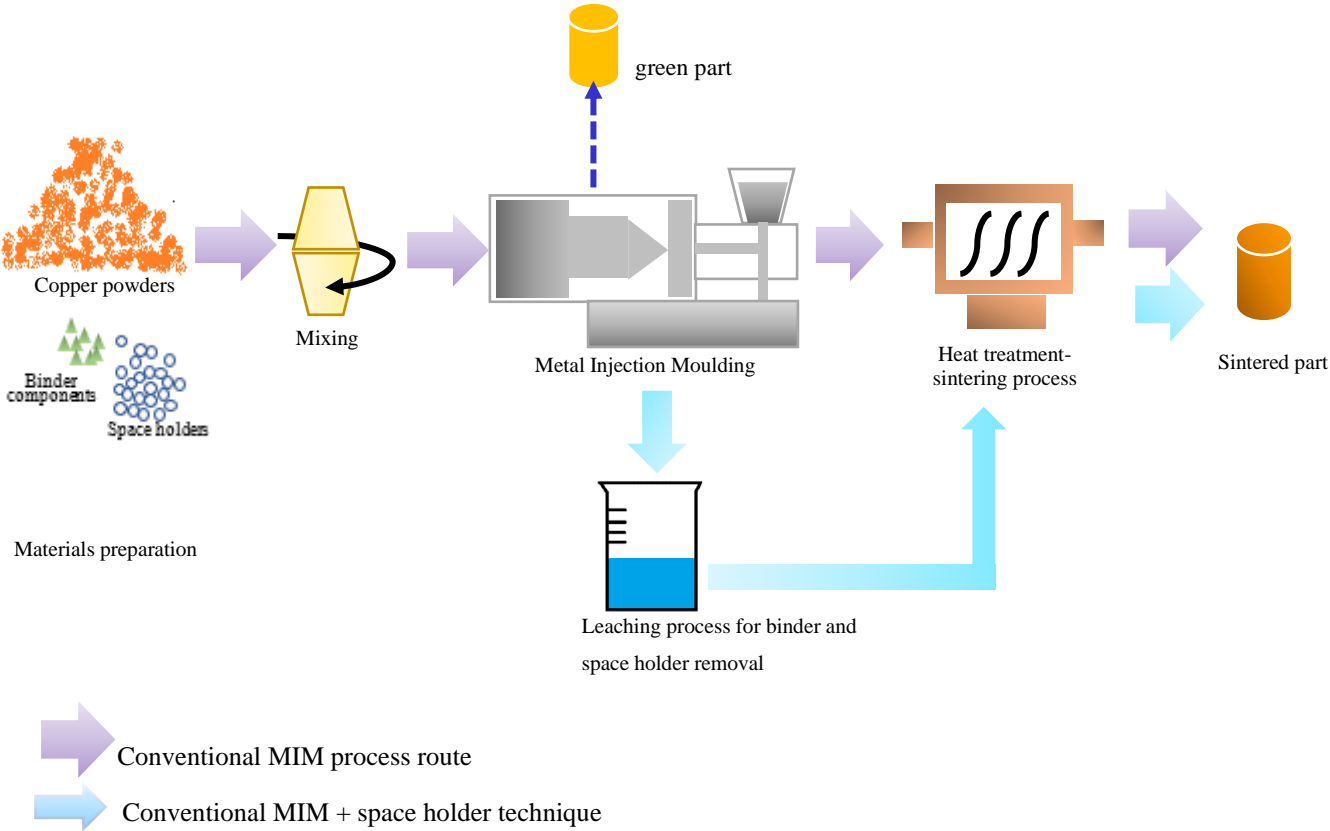


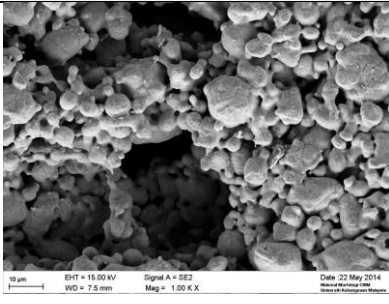
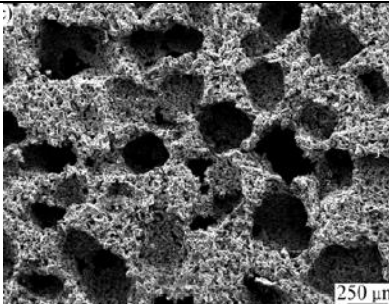
Figure 2.29; Comparison between general MIM process and MIM process combined with space holder technique

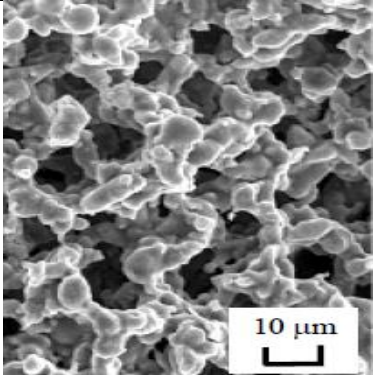
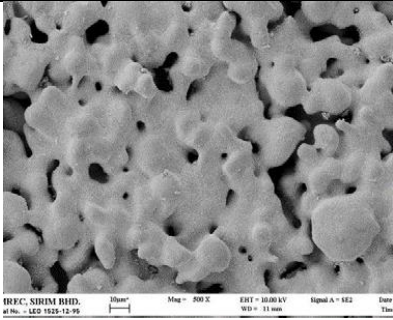
Previous studies on MIM-SH [102], [139], [154], [177]–[179] show promising results in producing high-precision parts while controlling their porosity. This MIM-SH technique can be conducted with numerous types of materials such as Titanium [180], [181], Stainless Steel [154], [182], Aluminium [183] [183], Copper [158] etc. Nishiyabu and his teams [182] fabricated components with micro-sized porous structures using the MIM-SH technique, but it requires some improvement in powder particle size and the sintering temperature.

The components demonstrated 2.39 to 9.58 μm of pore size. Some works adopted this technique to produce products beneficial to biomedical applications. [184] managed to fabricate porous titanium with an excellent elastic modulus close to the human bone. The performance of the MIM-SH technique should be investigated to ensure the quality of the end product. [179] has examined the rheological performance of 316 stainless steel. The tested feedstock demonstrated high viscosity and voids with increasing space holder content. However, this problem was overcome by controlling the parameters of MIM mixing steps to enhance the flowability of feedstock under the higher volume of space holders.

Since the space holder materials are part of the MIM-SH technique, selecting the right space holders is crucial to obtain a good quality product. Many factors need to be considered in terms of the physical properties of the space holder, removal method, level, safety issues, and processing parameters. Previous works showed that numerous types of space holder materials could be paired with MIM, as summarised in Table 2.8.

Table 2.8; Example of porous metal by using MIM-SH

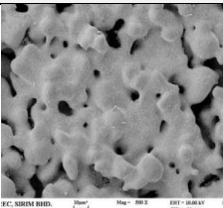
Metal	Space holder	Binder system	Porous microstructure	Finding	Ref
Stainless steel	Glycine	paraffin wax (60% wt) and polythene (40% wt)		Porosity volume; 37.7%- 53.9%	[185]
Titanium	NaCl	paraffin wax (PW) + polypropylene (PP) + stearic acid (SA))		porosity in the range of 42.4%–71.6%, pore size 300 μm	[176]

Aluminium	PMMA	Polypropylene, Poly-acetyl, Paraffin wax		55-60% volume of pore	[183]
Copper	potassium carbonate	potassium carbonate		Porosity volume; 53%	[186]

2.8.4 MIM-SH for porous Cu

Compared to titanium and stainless steels, MIM-SH with copper materials was limited, and most of the works were conducted with traditional methods such as compaction [13], [45], [107]. However, due to some limitations regarding geometrical limitation, ununiform pressure, and deterioration of the shapes of the pores, porous copper fabrication by the MIM-SH technique can be an alternative solution. Previous studies found that the MIM process with space holder technique (MIM-SH) has been successfully fabricated with porous copper [163] where NaCl is space holder material and binder system of palm stearin (PS) and low-density polyethylene (LDPE). The addition of NaCl has increased the feedstock viscosity. However, this research only concentrated on rheological behaviour rather than porosity properties. Jabir [158] has blended potassium carbonate with paraffin wax binder and produced porous copper with a suitable range of rheological behaviour. While the study by [186] investigated the effect of space holder volume on porous copper fabrication by using the MIM-SH process. As expected, increasing the amount of potassium carbonate from 0% wt. to 40% wt. has increased the porosity percentage from 14.88 % to 52.9%. Table 2.9 summarizes some works of MIM-SH with copper.

Table 2.9; The summary of previous works of MIM-SH with copper

Copper (Size, shape)	Binder system	Space holder (Type)	Solid loading (vol%)	Space holder (Volume/weight, Shape)	Porosity (%)	Pores	Finding	Ref
Spherical	palm stearin (PS), polyethylene (PE) and stearic acid (SA)	K ₂ CO ₃ ,	63	0,30,40 wt%	52.99% porosity with 40 wt% of K ₂ CO ₃ , 14.89% (0%), 40.11% (30%)		Short removal of binder and space holder	[186]
22 μm, Spherical,	Polyethylene (PE), Paraffin Wax and Stearic Acid (SA),	K ₂ CO ₃ ,		0.4-0.6 vol%	-	-	Copper feedstock exhibits a shear thinning or pseudoplastic behaviour based	[158]
14.2μm	LDPE and PS	NaCl	63	20 vol%	-	-	Demonstrate with the highest viscosity of 657.67 Pa.s	[163]

Therefore, the fabrication of porous copper by the MIM-SH process still needs to be investigated due to the lack of information about this fabrication route. The introduction of a potential water-soluble binder system such as PEG-PMMA-SA may offer a processing method with a more environmentally friendly, shorter processing period and applicable for industrial applications.

Chapter 3 MATERIALS AND EXPERIMENT

3.1 Chapter overview

This chapter points out and reviews the details of materials, equipment and tools used in the present study as well as the experimental process. The methodology of the study is briefly discussed, starting from the preparation of raw materials until it becomes a successful part before the assessments are made to evaluate the product. Since the present study involved the use of different powders, it is necessary to understand the behaviour from the particle form through to porous metal. Porous Cu manufacturing routes incorporate two main techniques: MIM manufacturing as the major manufacturing process, together with the space holder technology that is employed as a porosity-generating mechanism. Since the process uses novel materials (e.g.; the space holder) instead of standard MIM ingredients (metal powder and binders), there has to be some alteration and modification of some processing parameters to obtain the correct porous structure. This powder metallurgy approach incorporates three primary ingredients; primary metal (Cu) powder, potassium chloride (KCl) as space holder material and binder constituents, and these have to operate together in the right way to get a homogeneous mixture. The process begins with the preparation of the powders before the MIM process takes place. The mixing process works by combining the powders and binders to form a feedstock. These feedstocks, which are a mixture of powders, KCl and binders, are then converted into green components through a shaping process by injection moulding of the MIM process. Next, the debinding stage will be performed, where the green parts are immersed in water to extract the binders and dissolve the KCl under a certain temperature and time. These debind samples will be heated gradually in the final step of the MIM cycle using a furnace to remove the remaining binder, sinter the samples, and finally convert them into porous Cu. The fabricated porous Cu will undergo a series of tests that involve physical, mechanical, and thermal assessments to characterize the relevant behaviours.

Figure 3.1 shows the flowchart on the experimental process for porous Cu production, and Figure 3.2 outlines a summary of the entire porous Cu development process. Because of its advantage, the introduction of an alternative high- mixing machine may become a value- to the current process, rather than a traditional mixing method in MIM research. This gives a 'refresh' to MIM's typical mixing process, which faces many issues concerning part cleanliness, mixture quality, and lengthy process time. The introduction of a water-soluble binder system can also be seen as one of the alternatives in the development of a binder system, particularly for porous Cu.

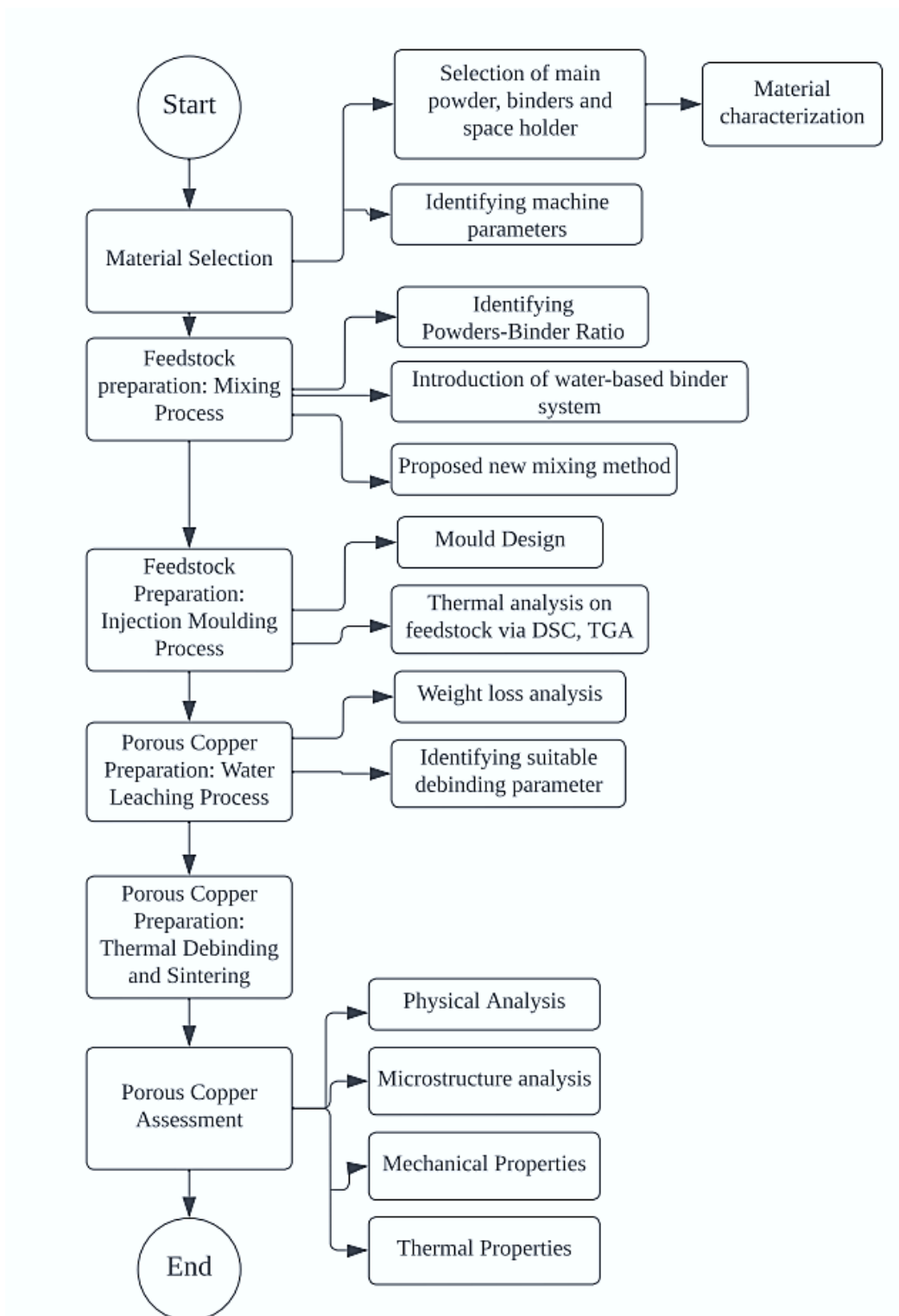


Figure 3.1; Flowchart of experimental works

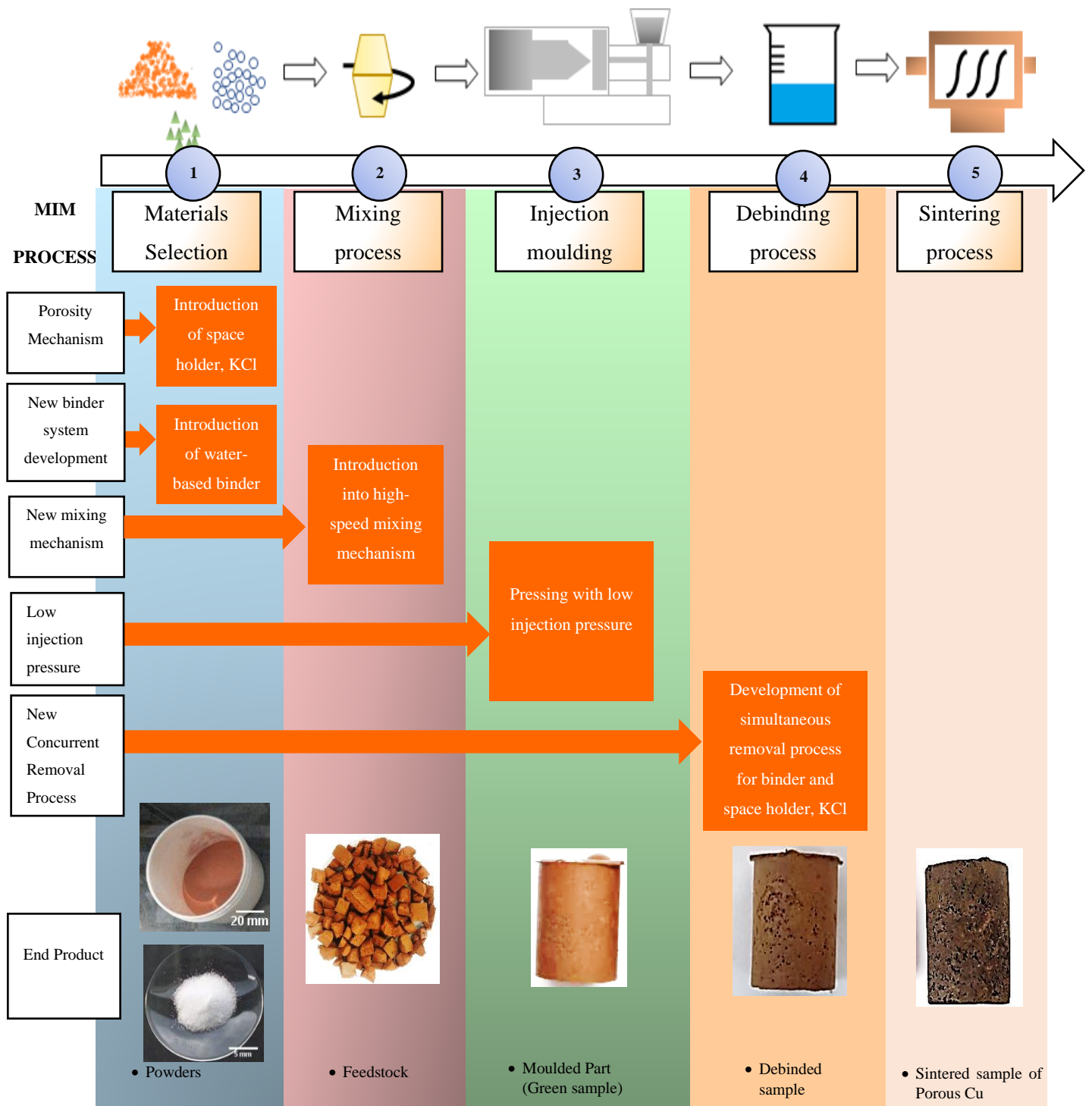


Figure 3.2; Summary of the flow of porous Cu fabrication by MIM with space holder technique

3.2 Preparation of main materials (Cu and space holder) and binder components.

The MIM method exploited the benefits of powder metallurgy as it can monitor and control the composition and features of main materials, the cost-effectiveness of production, better dimension tolerance and the capability to control the porosity properties. Therefore, this gives freedom to choose and specify the properties of the suitable material for porous Cu processing. The copper (Cu) powder comes in the coarse form, 99.4 per cent pure form supplied by Sandvik Malaysia Sdn Bhd, used as the main metallic material in this study.

In the case of space-holding materials, potassium chloride (KCl) is selected to assist in the promotion of porosity. The KCl used here is supplied by Qrec (Asia) Sdn. Bhd. Instead of the popular choices of sodium chloride (NaCl) [100], [107], [187] and potassium carbonate [13], [188], [189] for porous Cu production, the introduction of KCl can be an attractive alternative. KCl is not only safe to handle, but its rapid water-soluble characteristics can speed up the process of dissolution. In addition, paired with a water-type binder system in metal injection moulding (MIM), it may contribute to lower processing costs and save time.

The third main components for the development of porous Cu through the MIM process are the binders for the roles of material transport and moulding. Porous Cu processing is synonymous with the paraffin wax binder system [159] due to its good flowability behaviour. However, this binder may have an environmental impact in addition to the process complexity of the extraction process [190]. This wax-type binder requires external chemical solvents such as hexane and heptane.

The use of water-type binder components may become an ideal option to overcome these limitations. The water-soluble binder system has been used in feedstock fabrication for its benefit towards environmentally friendly [172], [191] as it can easily be extracted by water. Furthermore, this binder system provides a shorter time of debinding process [170], non-toxicity [190], and is also compatible with several metals such as Inconel 718 [192], [193], stainless steel [170], [194], titanium [167]–[169]. One of the promising water-based binder components that are comprehensively used is polyethylene glycol (PEG). This binder is a crystalline polymer that is soluble in water due to its open helical structure ($\text{H}(\text{CH}_2\text{CH}_2\text{O})_n\text{OH}$) [190] and has a low melting temperature (e.g.; 57-63°C for PEG with 1500 g/mol of molecular weight).

Therefore, for the present study, the water-based binder systems consist of three polymeric binder constituents, starting with polyethylene glycol (PEG) flakes, which contribute to the flowability of the feedstock. PEG 1500, which has a molecular weight of 1500 g/mol, was chosen for this study as this binder has a high solubility in water [193] and can be fabricated with low melting temperatures. The second binder component is a fine dispersed crystalline polymethyl methacrylate (PMMA) powder used to maintain the sample shape. The third component is a minor addition of stearic acid (SA) to improve the lubricity of the blended powders. These binder components were supplied by System Chemicals (SA), while both PEG and

PMMA were supplied by Alfa Aesar, Lancashire, UK. PEG and SA are easily dissolved by water during the debinding process. However, PMMA is an insoluble binder that can be thermally decomposed in the subsequent sintering process. In this situation, PMMA serves as a backbone binder to maintain the strength of the green sample during the water debinding process for PEG, SA, and KCl. As reported by [195], the solution and emulsion form of PEG and PMMA is preferable since it produces homogeneous feedstock. However, due to the additional cost of emulsion-type binders, the present study used solid-form binders (Figure 3.3), and this may require several experiments to obtain a homogeneous mixture. The design of the binder system was adapted from various experimental studies (which will be further discussed in Chapter 5). Table 3.1 displays the characteristics binder system used in the present study. PEG and PMMA that comes in the form of emulsions or solutions are preferable, as they can easily produce homogeneous feedstock, as stated by [195].



Figure 3.3; The current binders in solid form. (a) PEG 1500, (b) PMMA

Table 3.1; The characteristic of binder (polyethylene glycol (PEG), polymethyl methacrylate (PMMA), stearic acid)

Binder components	Manufacturer	Molecular Formula	Density (g/cm ³)	Colour	Melting point (°C)
PEG 1500	Alfa Aesar, UK	H(CH ₂ CH ₂ O) _n OH	1.125	White	57-63
PMMA	Alfa Aesar, UK	[-CH ₂ C(CH ₃)(CO ₂ CH ₃)-] _n	1.18	White	130-140
SA	System Chemicals	C ₁₈ H ₃₆ O ₂	0.941	White	70

3.3 Assessment of the raw materials

3.3.1 Morphology characterization by Optical Microscopy and scanning electron microscopy (SEM)

The morphology of copper powder and KCl was characterized by the Nikon optical microscope and the Hitachi SU 3500 scanning electron Microscope (SEM) under various magnifications. The physical properties of these powders can be easily derived from the analysis, such as the shape and size of the material. In addition, an SEM observation procedure provides an overview of the physical condition of powder to be examined either in a suitable form (e.g.; with good regularity and sphericity) or poor morphology that can impact the effective production process of MIM.

For SEM characterization, the process begins by sprinkling the powders onto a carbon adhesive sticker attached to the base of the sample holder. Some loose powder that does not stick to the tape can be removed with a blower (Figure 3.4). The stuck powders were then coated with gold by Sputter Coating Machine Polaron SC7620 at a current of 10 mA prior to SEM observation. This phase is crucial to lowering the sample charge and completing the circuit connection between the sample holder and the sample surface. This coating process was also applied to green feedstock and sintered specimens.

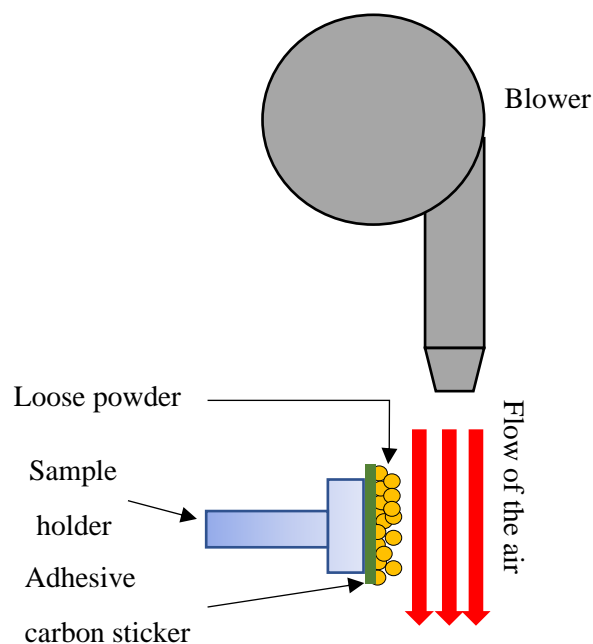


Figure 3.4; Blowing direction close towards the top of the mounted powder sample for SEM inspection

Cu powder and KCl are also chemically analyzed in the subsequent process using Energy Dispersive X-Ray Spectroscopy (EDX) via Hitachi SU 3500 (the same machine used for SEM analysis). The results are then compared to Panalytical Zetium, an X-ray fluorescent (XRF) machine analyzer. The aim is to monitor

the chemical elements of the samples and ensure these are consistent with the material specification data provided by the supplier. Details of the analysis using these machines will be discussed in later sections.

3.3.2 Particle analysis

MIM typically employs powders of less than 22 μm in size, as finer particles have been found to have advantages for retaining structure, minimizing defects in moulding [196], better viscosity and better surface finish. Owing to a greater number of particle-to-particle contacts, finer powders with spherical shapes have been able to control and preserve the structure resulting in better mechanical performances. With a larger powder, it is more difficult to maintain the part shape, especially during debinding and sintering. However, small-size powders face higher shrinkage rates and agglomeration problems due to the larger surface area, resulting in a higher driving force for sintering or ease of mutual bonding. In addition, it is noted that finer powders come at a cost. This downside is clearly not economically friendly to larger production.

For this reason, further investigation of coarser powders is worthwhile since it not only provides alternatives for a low-cost study but may improve the processing where it offers lower sintering shrinkage rates and lower debinding times [196] and may help to generate and promote the structure of micropores. As a result, the present study will use coarser Cu powder to manufacture porous materials. In the present study, the Cu powder has a size of approximately 50 μm which is still suitable for porous metal processing. This powder size was also used in Ref.[189] which has proven effective in the development of porous Cu. While, for the space holder, KCl, the particle size is larger than Cu powder which undergoes a sieving process using a vibrating sieve shaker to select a fraction with a uniform particle size.

Although the purchased powders come with the manufacturer's specifications, particle size analysis must also be performed to ensure that the powder meets the size range specified. Accordingly, the particle size of the two powders, Cu and KCl, was determined using the rapid particle analysis method and the Malvern Mastersizer 3000. For the present study, the particle size measuring range has been defined in the 0.01 μm -3 μm range. This instrument has the capability to analyze numerous types of powders with size ranges of 0.01 μm -3500 μm . Two types of measurement methods, emulsion and dry dispersion methods, are offered via this analytical instrument. Since KCl is easy to dissolve in water, it is not recommended to be analyzed by wet dispersion. The measurement, therefore, was performed using the dry dispersion technique, which operates through laser diffraction. As the dispersed particles move through the measurement area, they are screened, resulting in a dispersed light pattern with different intensities. These patterns are then detected, and the Mastersizer program is used to determine particle size and distribution.

3.3.3 Weight and density characterization

Initially, the weight of powders was determined by a weight balance with 0.0001 g precision, with the procedure repeated three times to achieve an accurate reading. The measurement operation involves calculating the powder weight (Cu, KCl and binders) or alternatively of solid samples in order to carry out assessments such as measuring density and calculating porosity and weight of the sample.

In the present study, three techniques characterized the density of the received powders, known as tapped density, apparent density and true density or theoretical density. Measurement of tapped and apparent density referred to standards 46 and 43 of the Metal Powder Industries Federation (MPIF). While the true density was calculated as per MPIF Standard 35. The theoretical density of powder was calculated using a 10-cycle calculation with Helium Pycnometer, Micromeritics Accupyc II (M06) filling pressure of 10psi. This non-destructive technique uses an inert gas, helium, as a displacement medium for measuring the volume.

For the powders, a range of measurements was applied, as above. These involved adding the powder to a measuring cylinder. The apparent density is the density of the material, measured without agitation in a loose state setting. 10ml of powder was poured into the cylinder according to MPIF 43 standard, and the total weight of both powder and cylinder was determined. Then, true powder weight can be determined by deducting cylinder weight from the total powder and cylinder weight. Lastly, the apparent density can be determined by dividing the weight of the powder by the amount of powder in the container. Finally, the tapped density of the powder was measured by hand-tapping with about 200 taps per minute of tapping frequency [197], using the same powder. Then, the density value was obtained as in Equation 3.1,

$$\rho_t = m / V_t \quad (3.1)$$

Where ρ_t is tapped density (g/cm^3), m is the weight of the powder (g), and V_t represent the tapped volume (cm^3)

3.4 Powder-Space Holder-Binder system specification

For feedstock development, the right selection of ingredients is vital to avoid failure in the subsequent process. Lower powder loading percentage may cause a problem of shrinkage [161], especially in debinding and sintering, leading to the poor dimensional accuracy of sintered samples. On the other hand, excess powder loading may lead to difficulties in filling the die cavity completely [198]. Thus, having the optimum powder-binder ratio is crucial.

With limited resources of Cu powder, KCl, and binders, a systematic procedure for successful feedstock development was required. Trials and experiments were carried out with caution to prevent any potential wastage. In the event of any unsuccessful trials, the quality of the materials must be verified in order to prevent any contaminants from being reused in the process.

By knowing the optimum powder loading volume and the weight fraction percentage of the binder constituent composition, the mixing process began by weighing all the powders, including the space holder material and each binder component, using a weight balance. The powder measurement was made three times in order to obtain an average reading as well as to obtain a constant reading. The optimum powder loading is based on the tapped density measurement to identify the initial ratio of powder-binder loading. The rule of mixture (ROM) is also being used to find the optimum volume, which is based on Equation 3.2 ;

$$\rho_{mix} = \Phi\rho_p + (1 - \Phi)\rho_b \quad (3.2)$$

where ρ_{mix} is the theoretical powder-binder mixture density, Φ is powder loading volume fraction (%), ρ_p is a density of powder mixture and ρ_b is the density of the binder. This equation will show a linear relationship between the volume of powder loading and the mixture density.

The powder-binder volume fraction was decided at 60% vol. for powder loading, while the remaining portion is allocated for binder components. Powder loading includes the Cu powder and KCl as a space holder material with variable fractions, as stated in Table 3.2. Table 3.3 shows the varying space holder fraction that would initially estimate the possible porosity formation and the overall powder-binder-space holder volume ratio. For 40% vol. binder system consists of PEG, PMMA and SA with 70%, 25% and 5% wt., respectively, as shown in Table 3.4. The estimation and assessment of porosity percentage are based on the volume of space holders used in the present study since previous studies [199]–[201] have shown that the use of space holders has influenced the development of sample porosity, pore shape and size. According to Table 3.3, 60 % of the volume of solid powder consists of a combination of copper powder and KCl, where the volume of both powders can be adjusted to control the porosity. For example, 30% by volume of KCl out of 60% solid powders is equivalent to 50% by volume of its solid powder. Hence, this volume represents a 50% porosity, which might be obtained as KCl, and will be eliminated via the water dissolution process.

Table 3.2; Overall volume fraction of Powder-KCl-Binder

Copper (vol. %)	KCl (vol. %)	Binder (vol. %)
	(60 %)	(40 %)
60	0	40
30	30	40
24	36	40
18	42	40
12	48	40

Table 3.3; Estimation of porosity percentage according to space holder volume

Solid powder (60% vol.)		Estimation of porosity percentage by space holder amount
Copper (vol. %)	KCl (vol. %)	(vol.%)
60	0	0
30	30	50
24	36	60
18	42	70
12	48	75

Table 3.4; Weight Fraction for Binder System (PEG-PMMA-SA)

PEG (wt. %)	PMMA (wt. %)	SA (wt. %)
70	25	5

3.5 Mixing of Feedstock

In addition to the slow processing offered by the conventional mixing machine, the issue of the cleanliness of ready-mixed samples has become a motivation for the introduction of other efficient mixing instruments. Thus, the high-speed mixer machine was explored for the mixing process in the present study. The introduction of a high-speed mixing process is expected to positively impact the development of porous material, and the findings of this study may become a future reference, particularly in the preparation of porous Cu. In addition, the question of mixing homogeneity due to rapid mixing, where the mixing speed can reach up to 2000 rpm, will be answered.

This high-speed mixer machine is known as SpeedMixer DAC 800 FVZ, Hauschild, UK, laboratory-sized rapid mixing equipment supplied by Synergy Devices Ltd, UK, with a size of 400 x 529 x 610 mm (Figure 3.5a). The machine can be moved easily with four stable wheels, which are securely locked during the process. The mixing area is securely protected by a durable transparent cover, automatically locking the mixing process. A special mounting system is built inside the mixing area, where the mixing container is tightly held during the process. The mounting system can be paired with different size holders where the mixing container is placed.

The machine uses a mechanism known as a Dual Asymmetric Centrifuge, which allows simultaneous counter-rotation and a mixing range from 800 rpm to a maximum of 2150 rpm. The machine operates in two modes of operation: single and multiple-phase modes. Single-phase mode allows 2 minutes of operation with set conditions before moving on to the next stage of a set mixing program. Alternatively, the machine can run continuously for up to a maximum of 10 minutes. The machine can be stopped immediately by an emergency stop button, and the process can also be interrupted to check the current mixing status in case changes to the conditions are needed.

Conventional mixing machines, such as the sigma blade, are outfitted with a temperature controller and mixing blades to facilitate the mixing process. The heat during mixing might originate from the temperature controller and the thermal energy generated by particle shearing during the mixing process. However, the present high-speed mixer machine is not equipped with a temperature controller (which other similar machines, such as the sigma blade, do). Thus, the heat is generated by the inter-particle friction between the powder particles and two cylindrical zirconia dispersion media (refer to Figure 3.5b) during the high-speed rotation of the machine. This combination of external mixing media and high-mixing speed [202] could improve the mixing capability and facilitate the coating of Cu and KCl with binders.



(a)



(b)

Figure 3.5; The machine and tools involved in the mixing process. (a) SpeedMixerTM DAC 800 FVZ, (b) cylindrical zirconia dispersion media

The feedstock was prepared to start by weighing each powder according to the determined powder-binder-space holder ratio. In the present study, the total weight of the mixture was constantly set at 150 grams per mixing cycle, although the machine can accommodate up to 250-300 grams. A few testing show that in some cases, if the weight of the mixture is more than 150 grams, the mixing machine tends to vibrate heavily and suddenly shut down on its own, so this value was used as a limit. Two cylindrical zirconia dispersion media were used to improve the blending and promote the uniformity of the mixture. The use of a large number of these ceramic media per mixing cycle is not recommended since it generates extreme heat that will lead to mixing failure.

After several trials, a few modifications to the mixing method were made to obtain a good-quality mixture. The MIM ingredients (Cu powder, KCl and binder components) cannot simply be mixed and blended without mixing plans and sequences. Trials to identify the optimum mixing sequence will be discussed in Chapter 5. The mixing process was repeated three times to obtain a consistent performance and avoid agglomeration among the powder. A suitable feedstock may have flow characteristics similar to toothpaste in hot conditions, but on cooling, it can turn into a hard-fragile sample that needs to be crushed into small particles. To ready it for injection, a crushing must be carried out, producing particles of an uneven, rough and large shape (Figure 3.6a). Sometimes it is difficult to insert these particles into the injection barrel, which has a small inlet opening. Hence, pelleting of the feedstock is needed to resize and reshape it for easy moulding and to stockpile it for further testing. The pelleting process is where the feedstock is directly

injected into a steel plate platform without flowing through the mould die attachment at 150°C. The feedstock (Figure 3.6b), which then has a uniform long cylindrical shape, was immediately cut by using a small cutter into a small pellet size approximately 3-5mm in length before it began to harden. The feedstocks then need to be dried at room temperature to remove any moisture.

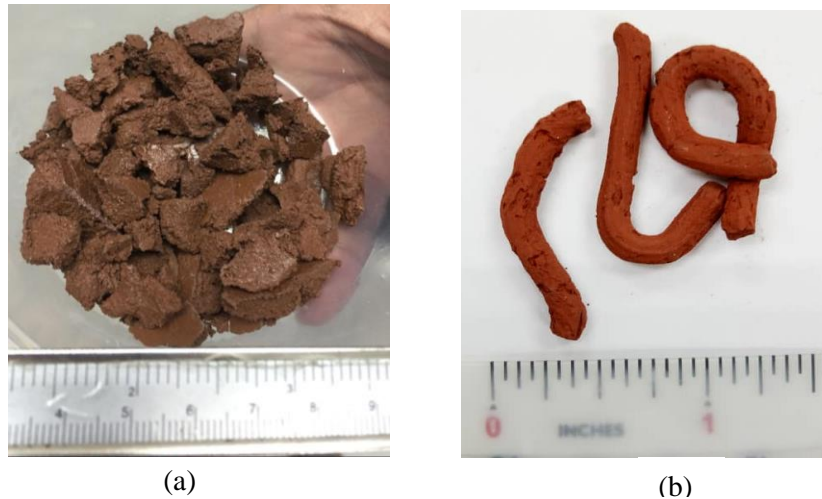


Figure 3.6; Example of feedstock, (a) raw feedstock without shaping process (after mixing process) (b) feedstock after extrusion process before it is cut into small pellets (after injection moulding process)

3.6 Injection Moulding Process

3.6.1 Mould design for the MIM process

A mild steel mould die was built with a 10 mm diameter twin-cavity cylindrical shape (Figure 3.7a,b). The height of the mould can be controlled, as shown in the schematic diagram (Figure 3.7c), by controlling the screw at the base of the mould. The maximum height can be up to 20 mm. The mould is designed for use with a benchtop-operated vertical injection moulding machine (Figure 3.9), where the size and shape of the mould fit into the injection area. The gating system was positioned at the centre of the cavity for uniform distribution of feedstock. The top cover was tightly secured with four screws to minimize flashing problems during the injection process.

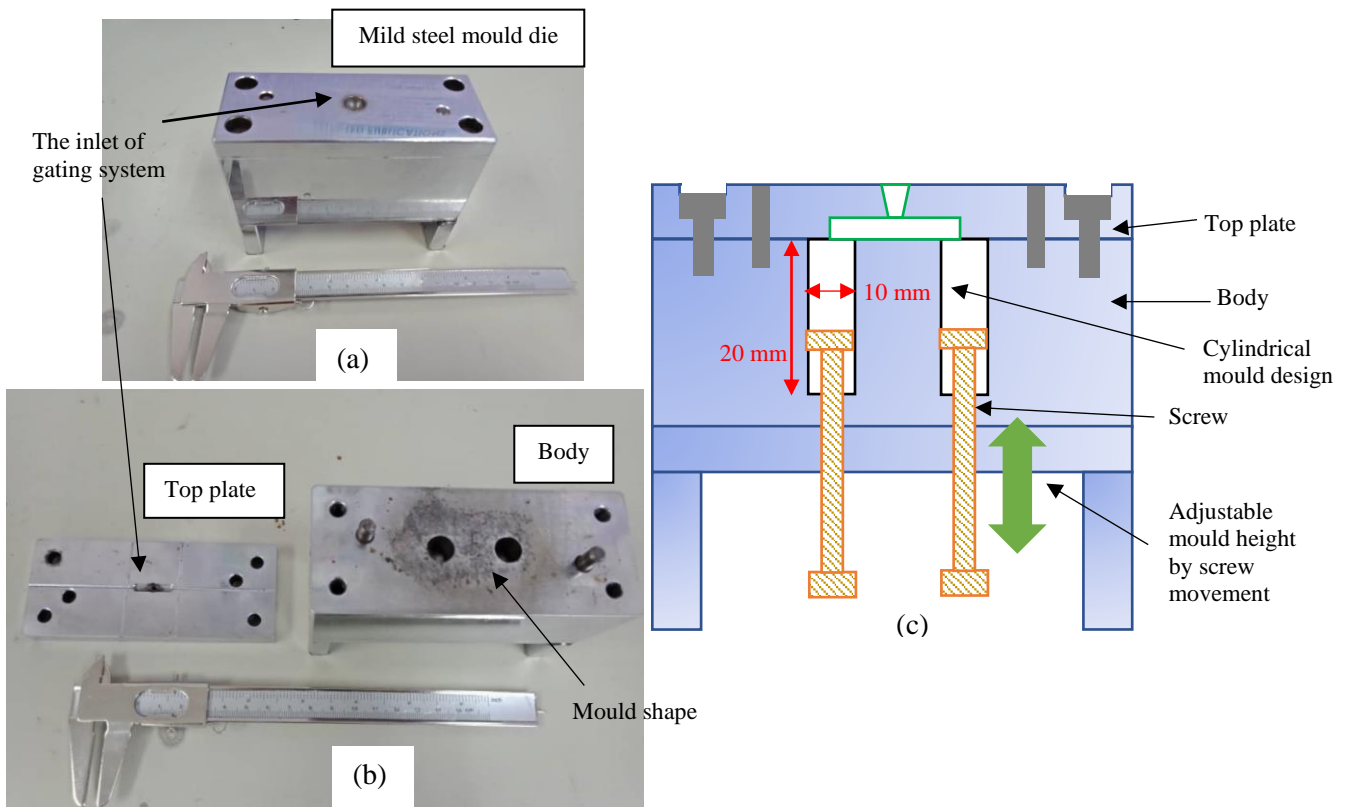


Figure 3.7; (a) The customized mould design, (b) disassemble parts of the top plate and body, (c) the schematic diagram of mould design

The new mould is more practical than the current one in three respects. First, the height of the cylindrical mould can be adjusted accordingly, and the green part dimensions can be altered. The new design also improves the production rate of green parts, as two samples can be fabricated per extrusion. Thirdly, sample extraction is facilitated (which is important as the green parts can easily become damaged) by adjusting the screw at the bottom of the mould to eject the parts (Figure 3.8).

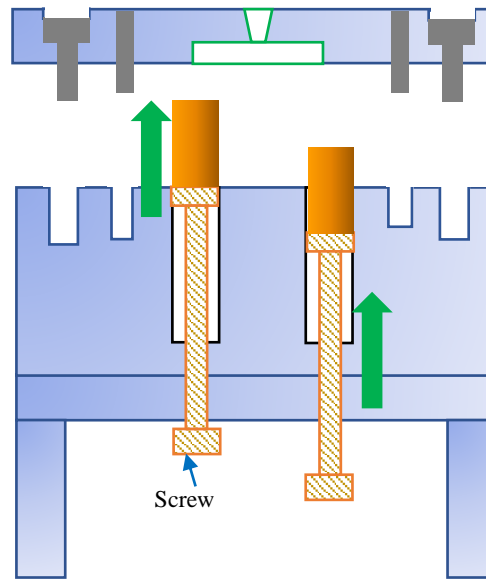


Figure 3.8; The mechanism for the extraction of the green samples from the mould

3.6.2 Extrusion of Feedstock

All tools involved in MIM processing, including the machine parts (such as the hot barrel, nozzle and mould), were cleaned using acetone to prevent any potential contaminants that could affect the quality of the final green product. The entire injection process was carried out by a customized vertical injection moulding unit, MCP-100KSA (Figure 3.9). The MIM benchtop machine comes with a main control box that monitors the main MIM parameters, such as the temperature and pressure of the injection. The cylindrical barrel is heated according to the temperature that has been set at the main controller before the injection process is carried out. The temperature of the cylindrical barrel is monitored during processing using the laser thermometer to ensure that the feedstock is fully melted within the appropriate temperature setting.

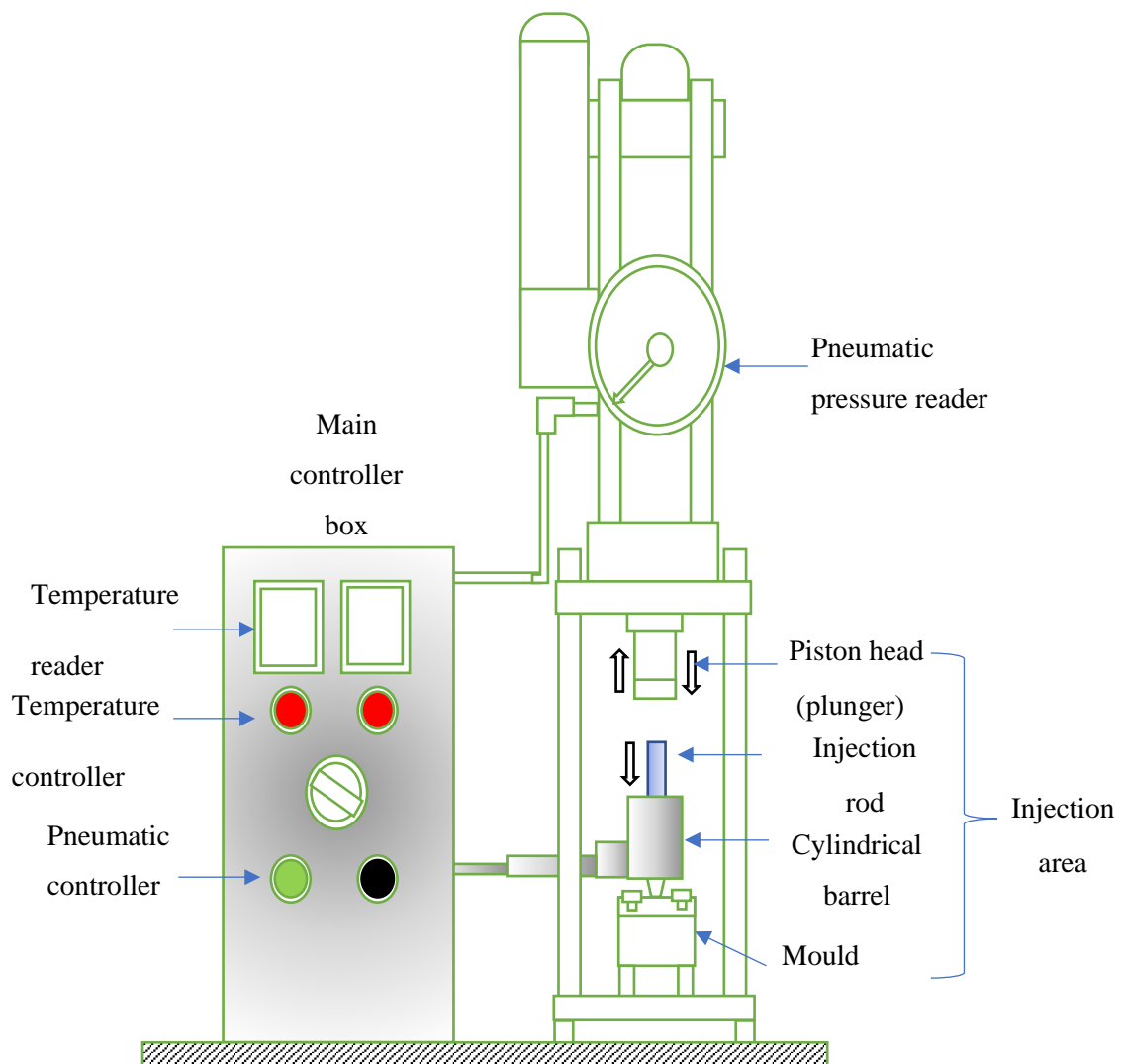


Figure 3.9; Schematic diagram of benchtop operated vertical injection moulding machine MCP-100KSA, which was used for feedstock and green part fabrication

Before the injection process began, the mould die and the cylindrical barrel were positioned in the injection area and aligned with the injection plunger, as shown in (Figure 3.9). The cylindrical barrel was then heated until it reached the required temperature set for injection. The temperature was conducted at 150°C according to the findings of the DSC analysis. Once the temperature is stable, feedstock loading will begin until the heated barrel is full of feedstock. The feedstock was left inside the heated barrel for at least 10-15 minutes to ensure it was fully melted and ready for injection. Next, the injection rod was installed vertically at the opening of the cylindrical barrel to push the feedstock out of the cylindrical barrel to the mould gate. The feedstock was extruded at a constant pressure of 45 MPa, as this laboratory instrument can only accommodate a lower injection pressure range, unlike in other work [9]. This previous study suggested

that the injection should be carried out at high pressure as the feedstock is expected to fill the mould cavities. In the present case, the extrusion process was conducted at a lower pressure since the results of the initial tests show the molten feedstock did fill the cavities, as shown in Figure 3.10a. The successful green part shows a precise cylindrical shape (Figure 3.10b) without any flashing or dimensional defect, or incomplete filling.

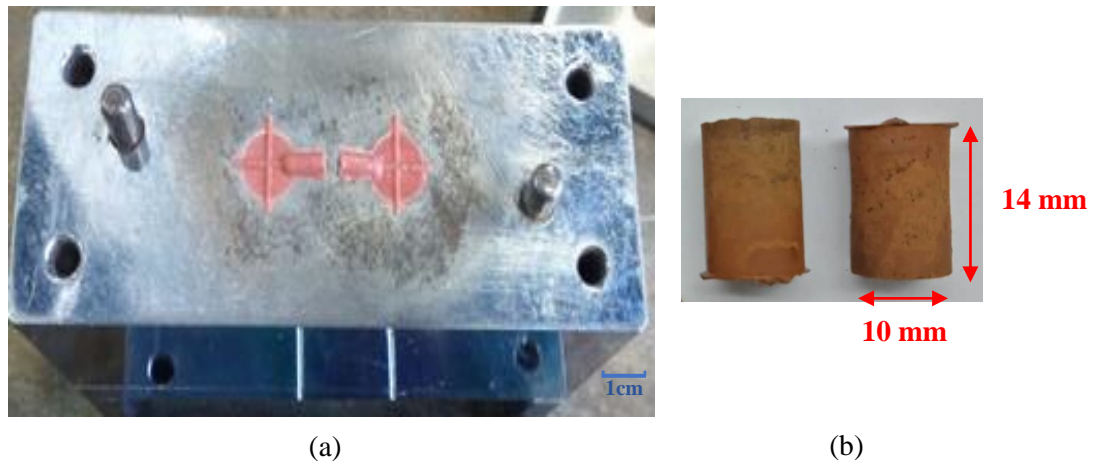


Figure 3.10; (a) The cavity of the mould is entirely filled by feedstock, (b) Solidified cylinder green part of porous Cu

A pre-injection session was performed for visual inspection purposes, and this activity was found to be crucial before the complete injection process. A small quantity of feedstock is extruded out of the heated barrel without flowing into the mould. The feedstocks could be evaluated based on the physical features of the extruded feedstock (in terms of shape, colour, abnormality in the structure, and moldability). The injection process itself, specifically if the feedstock is difficult to inject or demonstrates free-flowing behaviour due to inadequate viscosity behaviour. This assessment detects the possibility of defects in the poor quality of extruded feedstocks due to many factors, such as poor feedstock mixture, material shortages, incorrect injection setting and insufficient feedstock heating. Any deficiencies need to be examined to determine the cause behind them and what adjustments are needed to maintain feedstock quality. Figure 3.11a shows an example of good-quality injected feedstock in a long continuous cylindrical shape, while Figure 3.11**Error! Reference source not found.**b displays an example of poor-quality feedstock.



Figure 3.11; Examples of the physical form of extruded feedstocks at the pre-injection stage; (a) desired cylindrical shape of feedstock; (b) example of an unsuitable feedstock

3.7 Water leaching

Separating the binders from the mixture is not easy; the feedstock may deteriorate due to water or thermal exposure. Once the feedstock has been shaped through the injection process, binder components must be removed. The removal of KCl is also carried out at this stage as it is correlated with the preparation of porosity.

This stage can reveal whether the green parts exhibit a good mixture even though the fabricated feedstock has been successful in the previous MIM stage. Improper handling of the debinding stage may expose samples to unwelcome defects (e.g.; cracking, bloating, etc.) and residual contaminants [203] due to poor removal of space-holding materials. Previous studies have been carried out to find optimum routes for debinding purposes [161], [195], [204]. There can also be difficulties if binder and space holder materials require different solvents. Thus, one of the objectives of the present study is to solve this problem, as both the PEG binder and KCl can simultaneously be eliminated in a single process. This concurrent removal process can save time, and the process does not involve the use of different solutions or solvents [198], [205] as well as avoiding chemical solvents [161].

The debinding process (Figure 3.12) was performed using a water bath, WiseBath WB, supplied by Laboratory Instrument. The machine can operate with an accuracy of ± 0.1 ° C from ambient temperature to

a maximum of 100 °C and can continuously operate for up to 100 hours. The water tank can handle the number of samples needed, and the temperature setting controls the process. The water leaching process could take 10-14 hours to completely eliminate all binders and KCl. Through weight loss analysis, the actual duration of the water-leaching process for the samples to be entirely removed will be determined. The process starts with the water tank being filled with water and heated to a specific temperature. Two specific temperature levels, 50°C and 60°C were set for the debinding process to examine the temperature influences towards the removal rate. The testing temperature range was chosen according to the binder (PEG) DSC analysis test. Once the water temperature had reached a stable reading, the green parts were carefully submerged in the beaker. The procedure was carried out for about ten hours for analysis purposes. Finally, the debind sample was dried in an oven and kept safely in a closed container.



Figure 3.12; Water leaching process by water bath equipment, WiseBath WB

SEM analysis was conducted on samples to determine the formation of pore structures during water leaching. For weight loss monitoring activities, the green parts were hung with a custom-made basket (Figure 3.13) and soaked at different temperatures, speeds and times. The samples were used for weight calculation after drying using a density balance with a resolution of 0.001 mg. The green parts were weighed three times at different time intervals to ensure consistent measurement readings. Any physical changes in the debind sample were also observed for any changes.

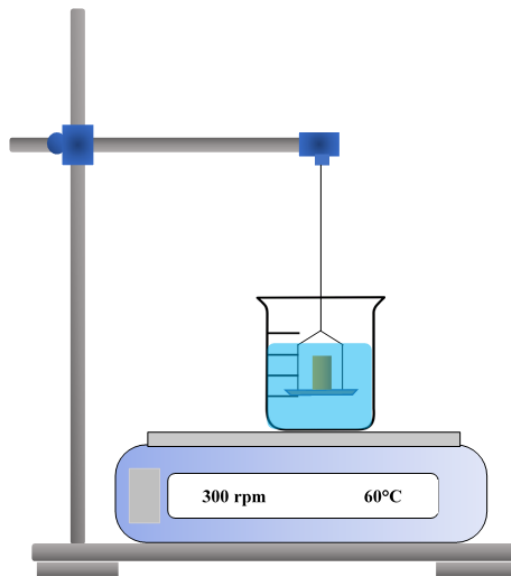


Figure 3.13; The schematic diagram of debinding process for weight loss measurement using hot plate balance

The debinding process used two different techniques. The first technique is where the green part goes through the process of 'static dissolution' without any mechanism to accelerate the removal rate. This technique allows the sample to dissolve in different operating temperatures (50°C, 60°C). The weight loss was recorded over time via the density balance after drying. The second approach introduced a minor adjustment that allowed agitation of the solvent. Two magnetic bars were put inside the beaker, and the water was forcefully mixed with increasing the dissolution rate. These two magnetic bars were rotated at a setting of 900rpm in the bottom of the 100ml beaker. Finally, the measurement was carried out similarly to the previous technique.

3.8 Thermal debinding and Sintering

All debind samples were sintered to reinforce their structure due to inter-particle bonding of the loose sample structure (brown part). In the present analysis, the PMMA binder and sintering processes were eliminated in the same cycle but with different heating profiles. As the technique was adopted from [102], the high viscosity binder (PMMA) was removed through thermal debinding. The temperature for sintering should be 70-90 per cent of the melting point. The characterization of the sample was carried out on the sintered part only and was not feasible on any sample taken after thermal debinding, since the heat treatment is a continuous process using the same equipment, a modified CMTS high-temperature tube furnace. This modified tube furnace was supplied by UQ Industries Sdn Bhd (Figure 3.14a) and can operate at a temperature of up to 1100 ° C under argon gas flow. Several trials were carried out to achieve an adequate heating profile, which can be seen in Figure 3.15.

The sintering process can only be carried out with restricted access since it depends on the availability and accessibility of the equipment in the laboratory. The design of the experiment must consider this factor and other considerations, such as the number of samples, safety issues, operating costs and the high consumption of argon gas. Due to these restrictions, the heating process could only be carried out with a limited number of samples, and it required an extensive adjustment of the heating profile for the next testing cycle. The prepared samples were placed on an aluminium crucible and carefully positioned inside the tube furnace, as shown in the schematic diagram (Figure 3.14b). Both sides of the tube furnace were closed and locked to ensure no gas was leaking out of the furnace. The samples were heated at a constant heating rate of $0.5^{\circ}\text{C} / \text{min}$ to reach 450°C . The temperature was set according to the results of the TGA, and the thermal debinding process was run for one hour to ensure that all PMMA components were completely removed. Then, the temperature increased gradually to the specific sintering temperature (800 and 850°C) at $5^{\circ}\text{C} / \text{min}$. The sintering process was conducted for two hours before cooling under argon gas flow at a rate of $5^{\circ}\text{C} / \text{min}$ until room temperature. The total duration of the heating process was taken place around 3 hours.

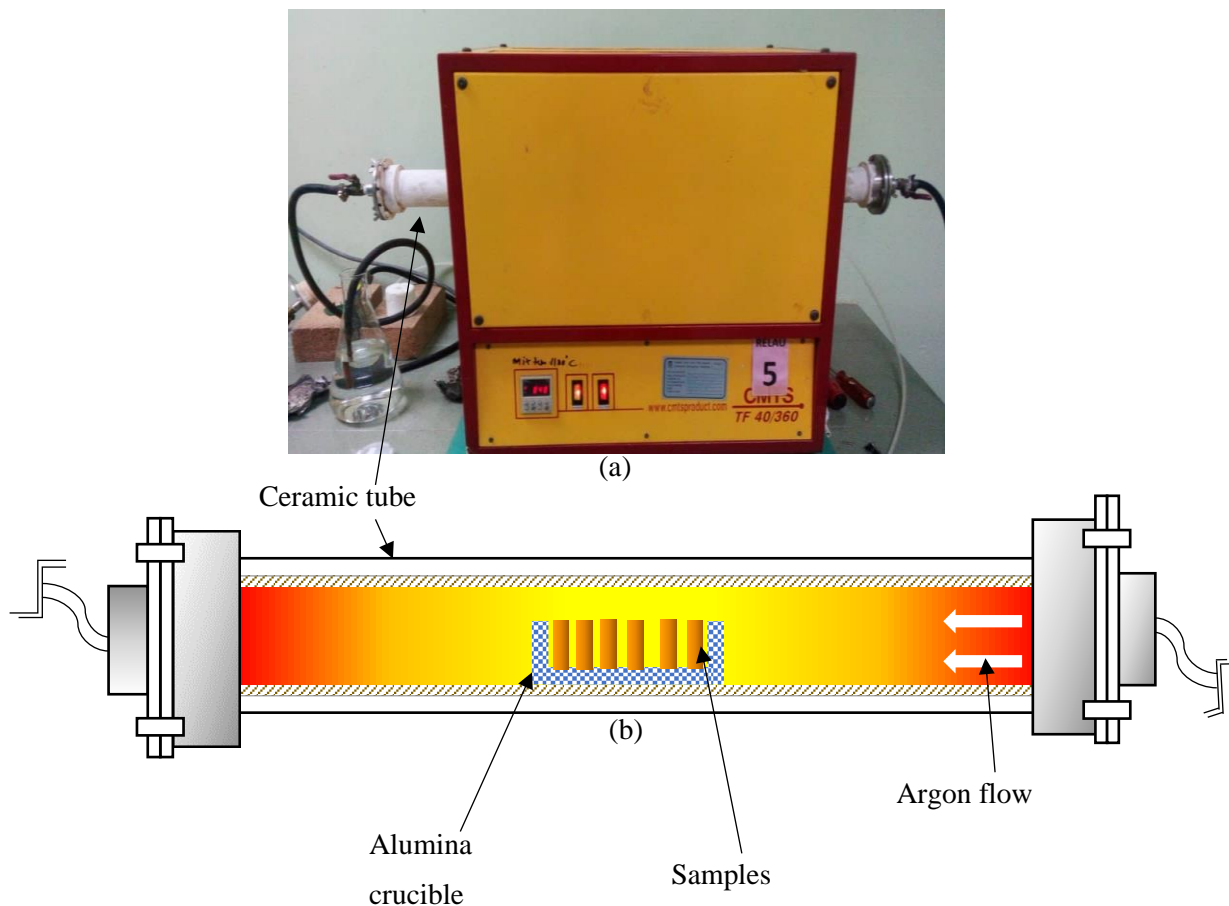


Figure 3.14; a) Modified tube furnace, (b) schematic diagram of tube furnace and sample position

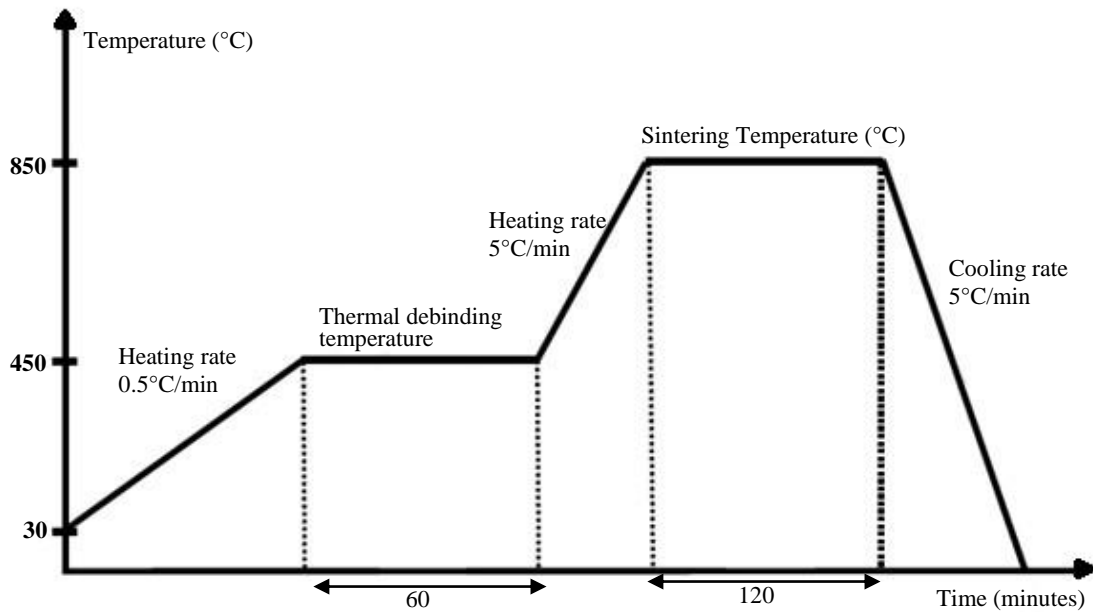


Figure 3.15; Schematic diagram of a heat treatment profile

3.9 Sample physical characterization

3.9.1 Physical observation of samples

Visual inspection was used in the first instance for all sintered samples to assess general changes. Dimensional (diameter and height) measurements were performed to describe the physical changes in the samples and applied to all types of samples, including green, debind and sintered samples. Any defects and physical anomalies identified were further examined and analyzed by visual inspection. Then it was necessary to separate the defective parts and investigate the cause of this failure before developing new parameters for subsequent processing sessions. This physical observation is important for the 'first impression' of the fabricated component, which gives a sign of the success or failure of the samples. These observations can also be used to find an optimal processing technique.

For the weight of green parts, the measurement was performed by using a standard analytical balance with an accuracy of $\pm 0.0001\text{g}$, and the green part dimensions (height and diameter) were measured using a Vernier calliper with an accuracy of $\pm 0.01\text{mm}$. Repeated measurements for both characterization exercises were carried out to evaluate the distribution of results. The density measurement process was conducted using a pycnometer, as discussed in the previous section. The morphology of the samples was analysed by using SEM, while the chemical properties were comprehensively examined using XRF and XRD. The tested sample requires ultrasonic cleaning before proceeding to these analysis processes.

3.9.2 Thermal analysis

The manufacturing of the MIM part requires the feedstock to be heat-treated at various stages of MIM, such as debinding, injection moulding and sintering. As a result of this, the feedstock can face transformation as a physical reaction to each MIM stage. For example, the solid feedstock may change to a molten state after exposure to the appropriate temperature range for injection purposes. The chosen parameter for injection depends on the molecular structure of the polymer (binder) and the melting point that results, and the upper temperature, which is correlated with the thermal decomposition properties [206]. Therefore, it is essential to understand thermal behaviour.

3.9.2.1 Differential Scanning Calorimetry (DSC) analysis

Differential Scanning Calorimetry (DSC) measures the heat amount required to increase the temperature of a material, and it can show the endothermic and exothermic activity, the glass transition temperature (T_g) and also calculate the melting point of the sample. For the present study, the finding from this thermal analysis tool helps to identify the optimum processing temperature range.

The DSC analysis was performed using PYRIS-1 Perkin Elmer Differential Scan Calorimeter (DSC 6). This machine is capable of controlling the heating and cooling rate as well as setting the temperature to 445°C. However, for the present study, the temperature range for analysis was set from room temperature to a maximum temperature of 200°C. All binders were expected to decompose completely after 200°C. Measurements were performed on two types of the sample group. The first group is the single binder components, while the second group is the feedstock where the binder has been mixed with Cu and KCl. This arrangement aims to monitor the transition between these two materials at any temperature.

A small sample with a weight of approximately 4-5 mg was cut into small pieces that could easily fit into the DSC aluminium pan before being sealed with an aluminium cap using a pressing tool. Pressing must be done with moderate force because it is possible to damage the pan and the cap. Following this, the sample was placed on the first side of the heating chamber, while the reference sample (empty aluminium pan) was placed on the other side. Both samples were concurrently heated or cooled at a constant rate. The samples begin to be heated from 25 °C to 200 °C at a heating rate of 5 °C / min under an inert gas atmosphere. DSC calculates the difference in the temperature flow rate between the test material and a reference sample. This activity was recorded by the DSC software, and the result is the thermal energy released or absorbed from the sample tested. To ensure a consistent result, at least three samples were measured, and the generated result is shown as a function of heat flow versus temperature. The thermogram indicates the heat flow versus the temperature and provides important information such as transitional information (melting region,

crystallization, phase change, glass transition). This can be relatively useful in predicting the melting point of the binder and its components [45], followed by determining the injection temperature.

3.9.2.2 Thermo-Gravimetric Analysis (TGA)

Thermo-Gravimetric analysis (TGA) has been used to characterize another thermal parameter correlated with the processing stage of binder and feedstock. Similar to DSC, both approaches are carried out under inert gas, where the sample is gradually heated in a specific temperature environment. TGA performs quantitative measurements associated with weight changes due to dehydration, gas absorption, evaporation, and decomposition [207]. Thus, TGA predicts the decomposition pattern of the respective binder and feedstock for the MIM cycle. The finding is useful in designing the sintering profile associated with temperature debinding. The study was performed using Perkin Elmer with Pyris 1 TGA, where the tested material is subject to heat with different temperatures and times, which is controlled by thermobalance [208]. Thermobalance determines the sample mass as a function of temperature and time.

The sample was prepared with 10 mg of sample, put in a platinum pan and then placed inside a furnace (heating area) where it was supported by a precision balance. The sample was gradually heated from room temperature with a constant heating rate of approximately 5°C / min to the maximum temperature of 600°C. The PMMA components were estimated to burn out at approximately 400°C, and the test heated beyond this in accordance with [189]. Concomitantly, argon gas was purged into the heating area where the sample was located to control the heating atmosphere before it flowed out through the exhaust. Subsequently, any change in the sample weight will be recorded and registered as either a loss or a gain from the heating process depending on temperature and time. The changes in weight may provide important information related to decomposition, phase transition, chemisorption, oxidation, pyrolysis or loss of solvent. The data collected from the analysis was plotted as a function of temperature changes by mass percentage changes, as TGA curves, through Pyris software.

3.9.3 Chemical composition analysis

Since the samples have been subjected to different MIM processing processes, it was appropriate to conduct a chemical analysis of porous samples to determine the sample elements. Chemical analysis was performed on different types of samples; green, debind and as-sintered samples using Ultima IV Rigaku X-Ray Diffractometer for X-Ray Diffraction (XRD) analysis and PANalytical Zetium for X-Ray Fluorescence (XRF) analysis.

3.9.3.1 X-Ray Diffraction (XRD) Analysis

The X-Ray Diffraction (XRD) technique is widely used as a rapid analytical tool specifically designed for crystalline material characterization [209], [210] providing valuable technical details related to phases and structure of the materials, texture, grain size, crystallinity, phase composition identification, sample purity determination, lattice strain measurement etc.

The XRD in the present study seeks to characterize the porous Cu material for any chemical reaction and phase transformation that occurs when the samples are subjected to different MIM stages. Previous studies set out the XRD analysis to define any changes in the material during the powder mixture process [140], while [211] used XRD measurements to identify the composition of the manufactured steel foam. In addition, the effectiveness of the dissolution process can be validated by means of XRD as carried out by [212], and this may indicate failure of the leaching process.

XRD machine, Rigaku Model Ultima, is used to perform XRD analysis. The sample was cut into suitable sizes, mounted in the sample holder, and flattened using a glass slide. The sample was then placed in the measuring chamber, and the analysis was performed with CuK α -007 radiation and operated under 40kV/40mA. Samples were scanned in a range of 30° to 80° at a count time of 10° per min of scanning speed with a diffraction angle of 2 θ . The XRD peaks were identified and matched to the standard database called the Powder Diffraction File (PDF) provided by the International Center for Diffraction Data (ICDD). The XRD analysis provides valuable information on phase analysis.

The basic measurement of XRD is based on the constructive interference of the monochromatic X-Rays which has been subjected to any crystalline sample. These X-rays were produced by a cathode ray tube by filament heating. The generated monochromatic X-rays were collimated to make them focused and concentrated directly on the samples. The interaction of incident X-rays on the samples causes an interaction with the electron in the atom of the structure of the material and leads to reflecting and diffracting X-rays with a random direction, orientation and angles (Figure 3.16). This X-ray interference may occur when the interaction satisfies Bragg's Law, as shown in Equation 3.3. The intensity of the diffracted X-rays was detected and recorded by the X-ray detector before being counted and converted to the peak intensity output. The scanning process was within the range of 2 θ angles, and the analysis was based on each material having a different lattice distance, indicating a unique X-ray diffraction pattern. This pattern, which represents the identity of the material, was then compared through an international standard database for element and chemical identification. These standards have been designated as a reference for comparison with the diffraction peak generated.

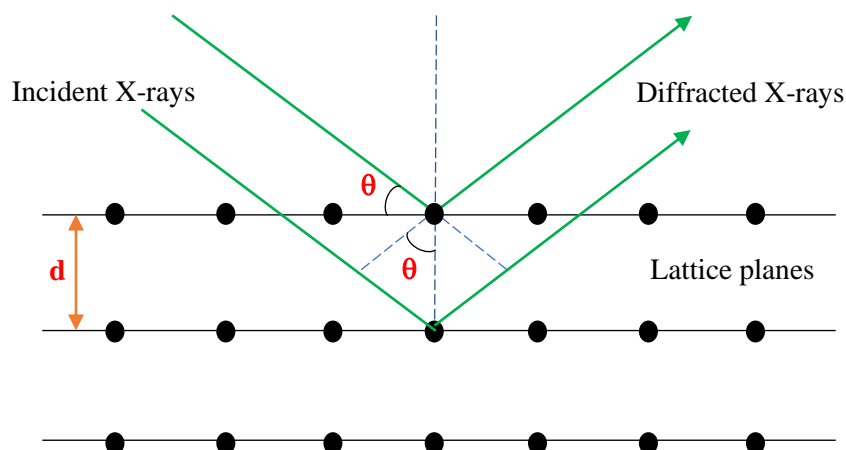


Figure 3.16; X-rays Diffraction at crystalline lattice

The XRD analysis can be expressed by Bragg's Law [209] (equation 3.3), where it relates the radiation wavelength to the diffraction angle and the lattice distance of the sample.

$$n\lambda = 2d\sin\theta \quad (3.3)$$

where n is an integer, the λ represents the wavelength of the incident X-rays, θ is the angles of the incident (the angle between incident X-rays with the lattice plane), and d is the variable distance or spacing between the lattice plane

3.9.3.2 X-Ray Fluorescence (XRF) Analysis

X-Ray Fluorescence is specifically designed for solids, liquids, pellets, beads and loose powders, and each of these materials has different preparation procedures. The measurement principle is based on the fluorescent analysis of X-Rays released from a sample for elemental composition analysis. This non-destructive analytical technique was implemented by XRF Analyser, Panalytical Zetium, provided by Malvern Panalytical Ltd, equipped with software known as SuperQ, designed for elementary and chemical characteristics of materials.

In the present study, a steel cup with an opening size of 6 mm in diameter was used, and this was then placed in the sample trays located at the measurement area. The sample is cut to a suitable size to cover the hole in the steel cup. Once the position of the cups had been identified (used as one of the input parameters), the analysis was carried out under vacuum conditions and repeated three times to obtain a consistent result. The expected result is based on the particular region of the scanning area, the area that was exposed for analysis (depending on the aperture size) and will be projected by the SuperQ program.

3.9.4 Porosity Analysis

3.9.4.1 Volumetric porosity and density measurement

Once successfully fabricated, the characteristics of the porosity of the porous Cu need to be determined, especially the porosity volume fraction. This can be obtained from Equation 3.4.

$$\varepsilon = \left(1 - \frac{\rho_b}{\rho_t}\right) \times 100 \quad (3.4)$$

where ε is the volume percentage of bulk sample porosity, ρ_b is the apparent or bulk density (solid part) and ρ_t is the true density (matrix sample only or skeletal sample) of a solid part without the volume of the pores. The apparent density ρ_b and true density ρ_t , can both be calculated from the known volume and the mass of the sample measured by an electronic balance with a resolution of 0.001 g. The true volume (V_t) of the sample can be obtained directly from the helium pycnometer measurement, while the bulk volume (V_b) relies on the sample dimensions and is calculated using Equation 3.5

$$V_b = \pi * \left(\frac{d}{2}\right)^2 * h \quad (3.5)$$

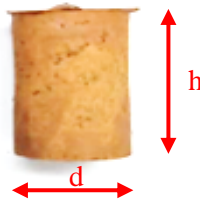


Figure 3.17; Nomenclature used for sample dimensions

where d and h are the diameters and the height of the sample (Figure 3.17). These dimensions were determined by Vernier calliper with 0.001mm resolution. All measurements were repeated three times to obtain average values.

The percentage porosity of the sintered part can also be calculated using Equation 3.6 as the difference between the bulk sample volume (the metal matrix with pore) and the true sample volume (metal matrix only). V_b is the bulk sample volume, and V_t is the true sample volume.

$$\varepsilon, \text{ Porosity (\%)} = V_b (\text{Bulk Sample Volume}) - V_t (\text{True Sample Volume}) \quad (3.6)$$

3.9.4.2 Measurement of density

As mentioned in the previous section, true volume (V_t) was acquired from measurements made by a helium pycnometer. This device uses the gas displacement technique, where the volume of the samples is determined by the amount of displaced helium gas. Helium gas is used as the main measuring medium in the Helium Pycnometer Micromeritics Accupyc II supplied by Micromeritics, USA.

Prior to the analysis exercise, the sample cup and the sample chamber area were cleaned with acetone, and no additional dirt or dust was allowed in the chamber. The sample was cut into small pieces, weighed using a standard analytical balance, and then inserted in the specific sample cup. The helium pycnometer machine has a chamber which can accommodate up to 10 cm³ of volume before being sealed for the measurement. The chamber cap must be tightly closed to avoid any temperature fluctuations and instability and maintain gas pressure. As shown in the schematic diagram (Figure 3.18), the helium gas was introduced into the sample chamber, which filled any pores of the sample structure to achieve equilibrium pressure. The pressure was precisely measured by the pycnometer pressure gauge. Then, the helium gas was allowed to flow into a second empty chamber (also known as the chamber of expansion or reference), and the new equilibrium pressure was measured. From the pressure difference, the volume of the sample can be calculated using Boyle's Law (equations 3.7 and 3.8). The purge fill pressure was set at 10 psi to obtain an average measurement, and 10 cycles of consecutive measurements were performed. It was checked that the results were within the tolerance ranges.

$$V_s = V_c - \frac{V_e}{\frac{P_1}{P_2} - 1} \quad (3.7)$$

$$\rho_s = m_s / V_s \quad (3.8)$$

Where; V_s is sample volume, V_c is the chamber volume, V_e is the expansion chamber volume, P_1 is pressure after fill, P_2 is pressure gauge after expansion, m_s is the weight of the sample, and ρ_s is the density of the sample.

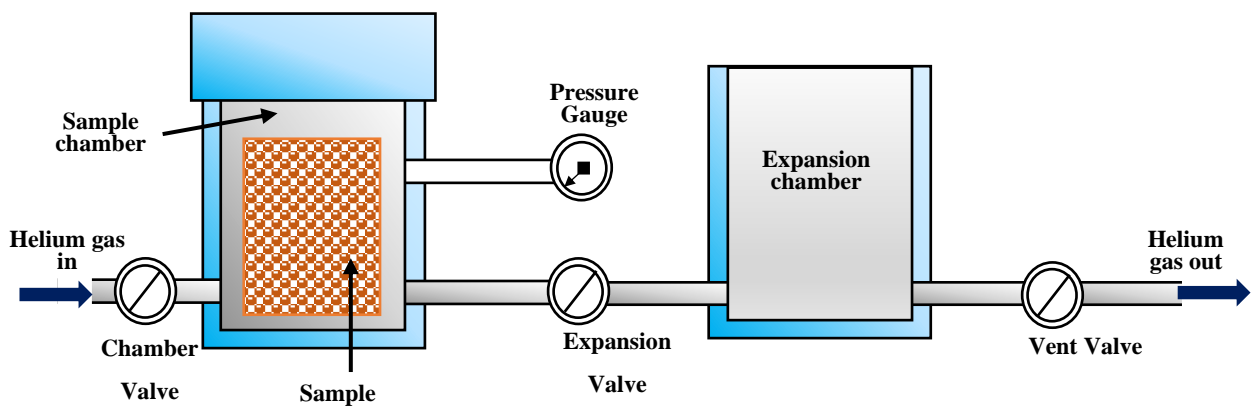


Figure 3.18; Schematic diagram of the main components inside the Helium Pycnometer, Micromeritics Accupyc II

3.9.4.3 Pores size and shape analysis

For the analysis of pore structure using the captured images, the surface porosity, pore size and shape were obtained from selected samples with a cross-sectional area prepared via the standard sample preparation method. Images were obtained via Optical Microscopy (OM) and Scanning Electron Microscopy (SEM) and were utilized for image processing activities. In the case of porous sample characterization, open-source image processing software known as ImageJ was used. This software has been commonly used [213], [214] due to its ability to perform scientific image data analysis on different platforms and file formats. The program can also conduct qualitative and quantitative measurements. It was developed by the National Institutes of Health (www.imagej.nih.gov). In this study, the surface topology of two-dimensional (2D) SEM images was used as an image resource for ImageJ analysis, where porosity, pore size, pore shape and distribution are explored. The porosity results will only be based on the images taken, and the pycnometer needs to be conducted for the volumetric porosity measurement of the sample.

For the image analysis, the image must show a clear contrast between the solid region and the pore area, from which the software can easily determine the difference between the two areas. Any imaging defects spotted on the sample can also be removed manually to avoid inaccuracy of analysis. The analysis process starts by binarizing the images and then continues by applying the individual threshold for each image. When clear contrast is achieved in the images (Figure 3.19), the pores and surface regions are easily distinguished.

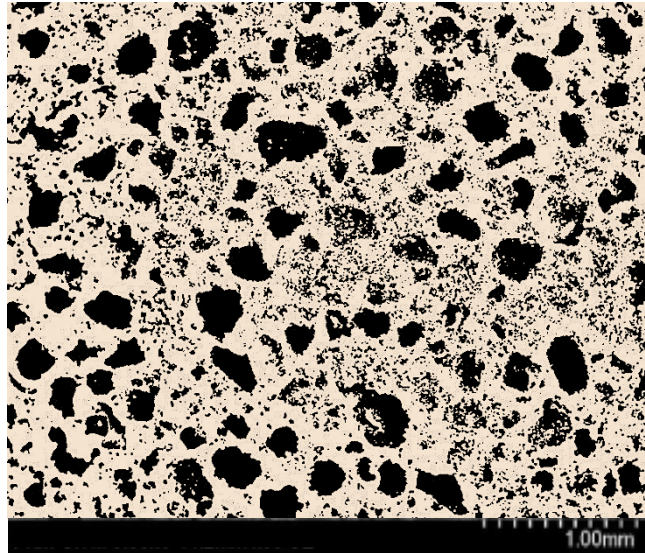


Figure 3.19; An example of a 60% KCl sample for Image J analysis where the colour contrast was applied to the original image to differentiate pores and solid regions

3.9.5 Microstructure analysis

3.9.5.1 Optical Microscope Analysis (OM)

Microstructural research was carried out to examine the formation of pores within the structure of the sintered sample and the porosity. The process involved observation and analysis of images using the Nikon Eclipse LV150 Optical Microscope. The microscope comes with a digital camera that uses its software to capture and store the image, and the analysis will run under polarized light. Optical microscopy was used to examine the sample's macro-pores while the complex structure (including micro-pores) was studied by Scanning Electron Microscopy (SEM).

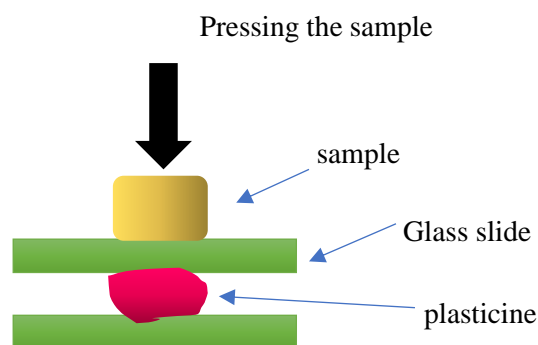


Figure 3.20; Schematic diagram of sample preparation for OM observation

The preparation of the samples began by cutting the sintered samples into a small sizes (about 10 mm diameter and 5 mm height) with a diamond cutter before being cold-mounted by epoxy resin. Thus, to obtain clear images, the sample was placed on a double glass slide with the plasticine in the middle (Figure 3.20) and levelled with a press. The image was then recorded directly using OM software. The grinding and polishing activities were arranged with various grit sizes (p400 to p1200) and 6 μ m diamond suspension to obtain a fine and smooth surface.

3.9.5.2 Scanning Electron Microscopy (SEM)

Scanning Electron Microscopy (SEM) is an effective method for a deeper analysis of sample microstructure. This method is useful in providing information related to morphology, surface texture and features, as well as, for porous metal studies, the formation of pore structure, pore size and shape, porosity and pore distribution. This included the sintered samples and the microstructure of green and debind samples. SEM analysis is also applied to the mechanical sample to test and evaluate the failed components. The SEM analysis was performed using Hitachi SU3500 Electron Scanning Microscope.

The sample surface area was scanned by a high-energy electron beam under vacuum conditions. Then, these electrons penetrate into the sample surface for a few microns, creating an electron-sample interaction that can either be defined as elastic or inelastic. This interaction produces numerous signals containing information related to the surface texture, crystalline structure, chemical element, etc. These signals are known as the Secondary Electron (SE) and the Backscattered Electron (BSE) (Figure 3.21) and will be collected by an appropriate detector before being processed to produce high-quality images. The generated image relates to the signal intensity collected by the detector. Other signals known as characteristic X-Rays are also collected, which provide information on the chemical elements present in the examined sample surface.

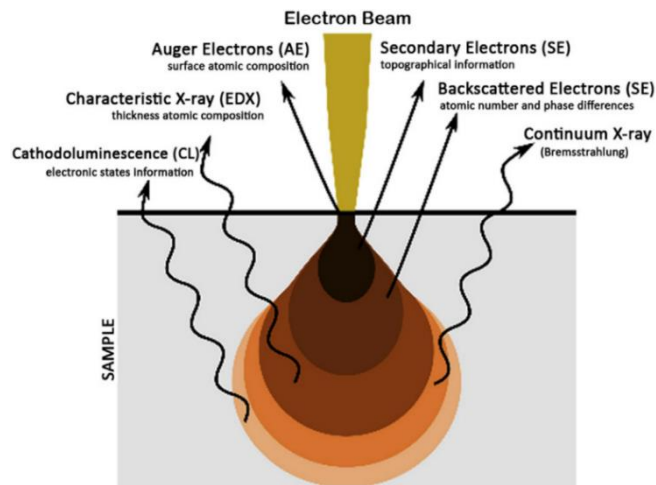


Figure 3.21; The signal produced due to the interaction of the electron beam on the sample surface [215]

In the case of solid porous Cu, the sample must undergo sample preparation such as mounting, grinding and polishing to prepare it for imaging and reveal the internal structure. Powders can be observed in the loose form, which is prepared by spreading the powder onto a carbon sticker. Before the SEM analysis is carried out, a mounted porous sample requires extensive preparation, starting with an ultrasonic bath cleaning process. The process takes about 10 minutes before drying at room temperature. The cleaning process is vital to avoid any unwelcome deposits such as dirt, dust, or other contaminants that may impact the imaging result. To improve conductivity, the dried samples were then coated with a thin layer of conductive gold using a Sputter Coating Machine Polaron SC7620 at 10mA. This process helps to avoid extreme brightness due to a charge accumulation [216] on the surface of the sample that may impair the quality of the image taken.

The samples were fixed to the sample stubs by carbon sticker before being positioned in the measuring chamber of the SEM machine with an acceptable range of SEM working distance. The focused electron beam was scanned across the sample surface with a working distance of 7-10 mm and a spot size of 4.0 with a variety of scanning speeds. The scanning process involves adjusting the contrast and brightness activity, changing the alignment of the lens, focusing the sample with the correct setting and correcting astigmatism to obtain a clearer image. The procedure was performed for the Secondary Electron (SE) configuration at 5kV, and for Backscattered Image (BSE), it was performed at 20kV accelerating voltage. Various ranges of magnification from low to high levels were used to observe and capture high-resolution sample images. Small magnification was used for wider observation of the distribution of macropores, while higher magnification was used for detailed imaging and analysis of micropores.

3.9.5.3 Energy Dispersive X-Ray Spectrometry (EDX)

Since the SEM machine was equipped with an Energy Dispersive X-Ray Microscope (EDX), chemical analysis can be performed on the sample. This non-destructive analysis is crucial for the present study since the sample was exposed to different MIM stages, and, for example, EDX helps to determine whether any KCl elements are still left in the sample, which can indicate the debinding process quality. As SEM interaction with the sample can produce x-rays, EDX also uses the characteristics of X-ray electron beam analysis [217] to provide chemical information. EDX operates by focusing the electron beam on the sample to excite the inner shell electrons of the atom. These electrons will then be ejected from the lower energy of the inner shell and leave behind an electron hole in the atomic structure. This event may attract external electrons from the outer shells to fill the vacancy. The transition of external electrons from high-energy outer shells to low-energy inner shells may release energy in the form of an X-ray due to the different energy of both orbitals [217]. The emitted X-rays that come with a different, characteristic wavelength are then measured by photon-energy sensitive EDX detectors and analyzed using EDX software. The released X-Rays contain the composition of the elements presented in the sample examined.

3.9.5.4 Alicona Infinite Focus optical measurement device

Alicona Infinite Focus is a 3D surface scanner machine which is a fast and accurate optical 3D measurement system. This machine generally measures dimensional accuracy and surface finish characterization, such as surface roughness. This machine is also a cable to differentiate contour profile and depth of surface with a 3D colour image, which the user can estimate the material surface form. This machine is controlled by a software program called Automation Manager, which offers different modes of measurement. This machine is commonly applied for tribology and corrosion applications and the tooling industry.

This 3D image scanning machine is assigned for the present study and is not the in-depth measurement of surface roughness analysis or other surface characterization. This machine was purposely used to observe the image of the surface structure of porous Cu and pre-examine the properties, such as pore size, before proceeding to SEM analysis. Similar to the Optical Microscopy Machine, the selected samples were placed in the measurement platform and then set up the right lighting parameter. The machine captures the image by optical microscope by vertical scanning at 5X optical zoom. Then, using Automation Manager software, the image samples will be analysed accordingly. An accurate 3D surface profile was generated and clearly displayed with different contour profiles (Figure 3.22). By using the pseudocolour variation setting, the surface height of the scanned sample can be evaluated. The porous copper sample must in a flat surface to avoid any blurry image.

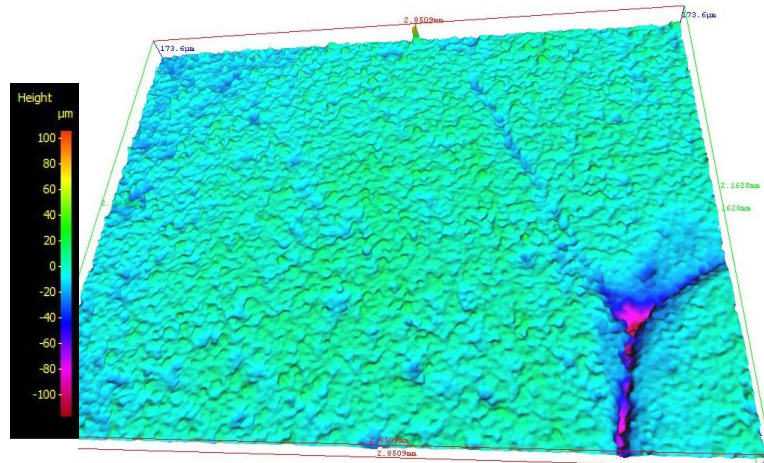


Figure 3.22; Example of a 3D surface image of porous Cu (0% vol. KCl) via Alicona Infinite Focus

3.9.6 Mechanical Testing by Uni-Axial Compression Test

Porous materials are usually known as multifunctional materials with characteristics that are useful for different applications [17]. The assessment of mechanical properties is critical for most multifunctional applications and for all structural applications, specifically for MIM research [218]. It can be inferred that there is a significant correlation between porous structure and mechanical properties. The aim of the fabricated porous samples is to have adequate strength for easy handling and to preserve the integrity of the structure under possible application conditions. Hence the investigation of mechanical properties is crucial in the present study to ensure the sample has the potential to meet these essential requirements.

The porous Cu samples chosen for mechanical tests were cut into uniform sizes with a diameter of 10 mm and a height of 14 mm, giving an aspect ratio of 1.4 (D: H). Before testing, both porous Cu surfaces must be flat to prevent any unbalanced compression force on the sample that could impact the test result. Next, an ultrasonic bath with acetone solution was used to clean the samples for 30 minutes to remove any dirt and residue that had formed during the sample preparation process (such as cutting, grinding and polishing).

Before proceeding with full mechanical testing, a number of tests were carried out to define the test parameters that will be implemented consistently for the entire test. The compression test was carried out using an Instron 382 Universal Testing Machine with the Trapezium X program. Two crosshead platens were mounted and tightened at the measurement platform, specifically designed for compression testing. The sample was positioned in the centre of the lower crosshead platen and was locked securely on the platform,

as shown in Figure 3.23. The compression process was begun by moving the upper crosshead platform downwards and deforming the sample to a certain percentage of strain (this was configured in the software program). The load was transmitted axially to the sample, and the testing data was recorded by the software and used to create graphs of stress against strain, from which mechanical properties can be derived. The compression load cell had a capacity of 100 kN, and loading was performed under 0.5mm/min constant speed rate at room temperature. The monotonic loading test mode allows the load to be applied continuously to the sample until the stress drops due to a sample failure. These tests aimed to measure stiffness and related behaviours such as compressive stress-strain properties. Similar to [219], the yield strength was calculated using the 0.2% offset method for all samples.

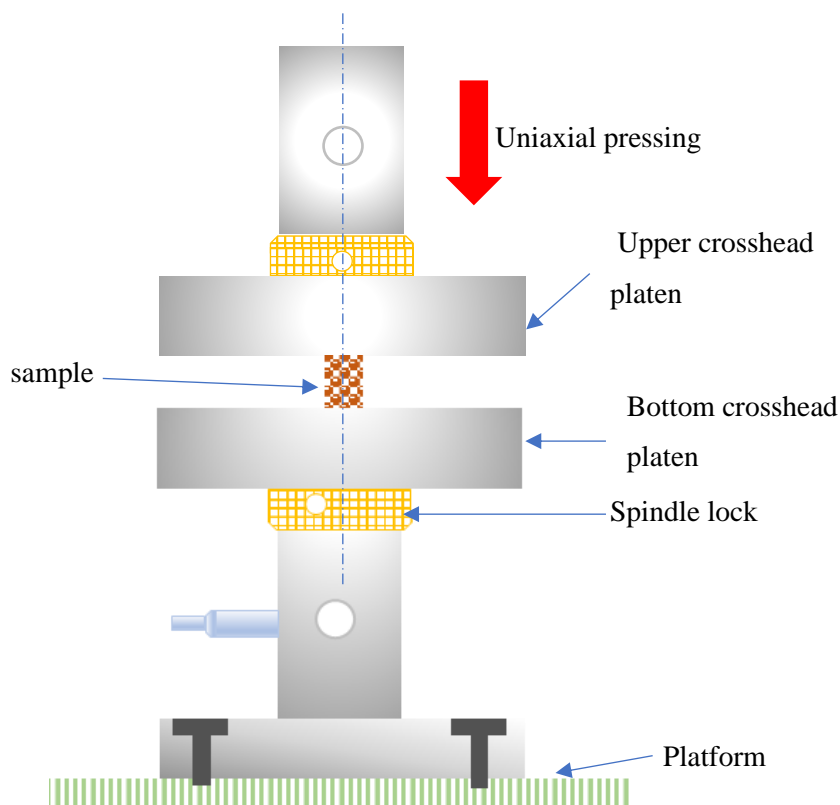


Figure 3.23; A schematic diagram of compression testing

3.9.7 Thermal Test

Due to the lab restriction, limited resources and sample size limitation, a new low-cost testing method (refer to the schematic diagram, Figure 3.24) was designed to examine the thermal properties to evaluate the fabricated sample. The testing is designed in a small-scale prototype that is direct to the actual educational electronic board system. This single-board computer, known as the Raspberry Pi 3, has a functionality of a standard computer and consists of integrated central processing unit (CPU) and graphics processing unit (GPU) chips and is powered by 5 V DC input. Once it connects to the power and other computer peripherals such as a mouse, keyboards and monitor, the Raspberry Pi 3 can work as a normal computer pairing with various operating systems (e.g.; Raspbian, Windows 10, Linux, Android) and can be performed with light performance.

The present Raspberry Pi 3 does not come with its own heatsink system and does not equip with a cooling system. In certain cases, the operating temperature of Raspberry Pi 3 easily increases up to 80-85°C if the system runs with a number of programs simultaneously. The maximum operating temperature is 85°C which may possibly damage the device and prevent the loss of performance of the CPU if the temperature goes up beyond the maximum temperature. Thus, to solve this problem, the raspberry Pie 3 should use an external heatsink to ensure the temperature is below 80°C.

For the present study, the porous Cu is proposed to be applied on the Raspberry Pie 3 system as a heatsink, and the thermal properties are measured in terms of a temperature difference by using temperature coding. The testing required special coding to measure the temperature. The porous Cu was cut into 1 mm height before it was placed on the system core chip before starting the system. Once the system is in running mode, the core temperature of the raspberry pie can be measured directly by using the specific temperature coding. The thermal properties of porous Cu can be evaluated through the different temperatures before and after applying the porous Cu to the system.

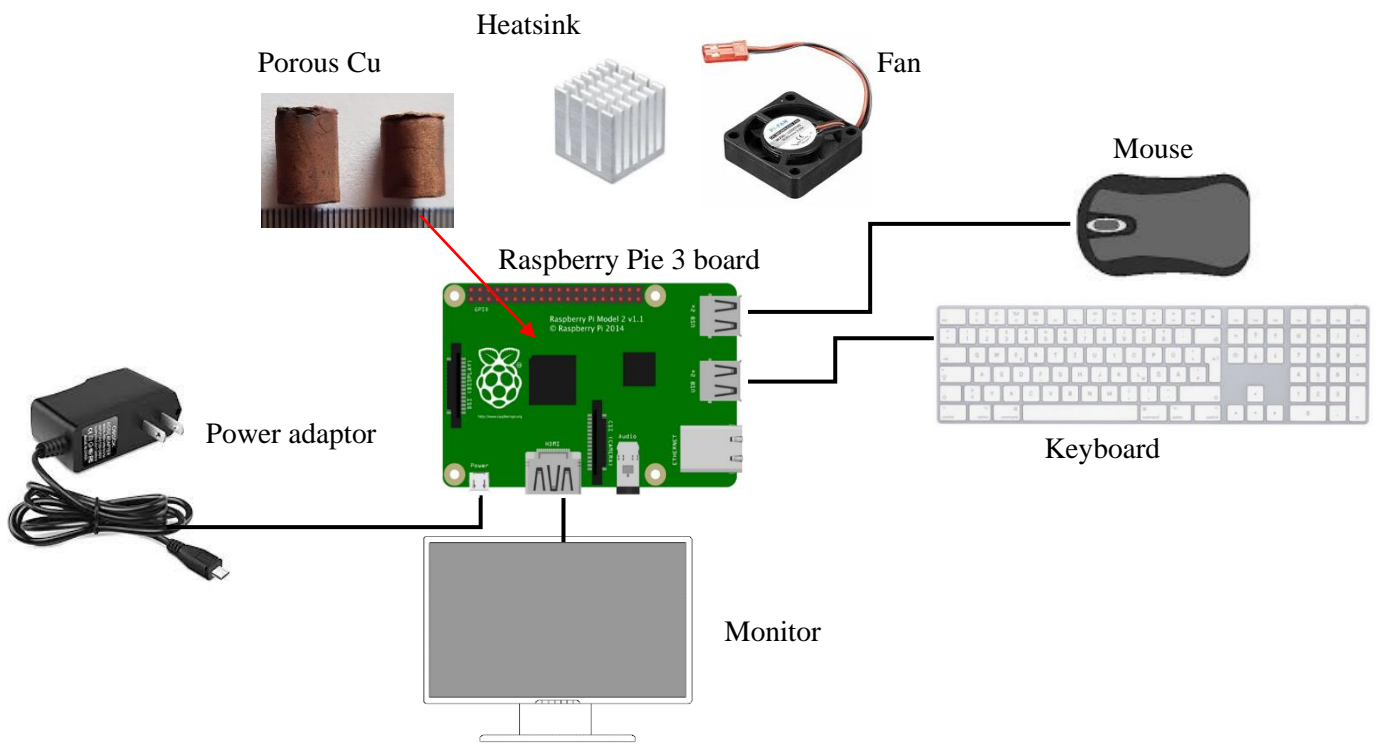


Figure 3.24; A customized thermal testing setup for porous Cu using the Raspberry Pi 3

Chapter 4 COMPACTION AND SINTERING (C&S) METHOD

4.1 Motivation to produce porous Cu via Compaction and Sintering (C&S) Method

The present study aims to develop the porous Cu using the powder metallurgy approach in combination with the space holder technique, as this approach has been proven in developing various porous metals [177], [220]–[222], including some works on porous Cu [53], [83], [189], [223]. In the present study, metal injection moulding (MIM) with Potassium Chloride (KCl) (known as MIM-SH) was selected as the main processing method to produce the porous Cu.

Instead of concentrating on developing porous Cu via MIM-SH, processing by using another method has also been carried out as a means of comparison. The conventional process for porous Cu is commonly conducted via Compaction and Sintering (C&S). This fabrication method provides numerous successful results [53], [96], [99], [224] as it manages to produce porous Cu with various porosity, uniform pores distribution, as well as the shape of the sample, which can be controlled via the specific mould. This additional processing method is still in the same group as MIM-SH, as both are classified under powder metallurgy processes. The investigation will address the challenges of successfully using this manufacturing process and, in particular, will address different key variables such as compaction pressure, sintering conditions and varying the space holder percentage in order to produce porous material.

In addition, previous works on porous copper via C&S approaches commonly employed space holders such as Sodium Chloride (NaCl) [187], [225], potassium carbonate (K_2CO_3) [8], [13], [226], [227], Carbamide [228]. However, there were limited works via C&S with water-based space holders, specifically pairing the KCl (as space holder material) with Cu. The critical information such as processing parameters such as ideal compaction pressure that will not damage the KCl shape, the dissolution routes for KCl and the porous properties obtained with KCl. Thus, this motivates to investigate producing porous Cu via the C&S method with the selected materials, which could extend the knowledge related to porous Cu works. Through this investigation, the compatibility between the pair materials (Cu and KCl) via the C&S method could be verified. The important experiment parameters can be documented, and the manufacturing challenges can be addressed. This information helps prepare the C&S standard laboratory production related to porous Cu with KCl and provides an alternative fabrication process of porous Cu.

4.2 Processing of porous Cu by using the Compaction and Sintering Method

The whole process of porous copper fabrication used here is shown in Figure 4.1, the porous Cu fabrication by compaction method where the space holder material (KCl) is removed after the sintering process. The process is similar to MIM, which requires common powder metallurgy processing stages but without the roles of a binder system. The copper powder and KCl were mixed together with KCl amounts between 10, 20, and 30 vol%. Since both materials have different densities, a small volume percentage of acetone was added to the mixture to assist the mixing process. The process was carried out with a SpeedMixer 800 FZ (Hauschild; by Synergy Devices Ltd., UK). No heat source is needed in this current mixing machine that relies on thermal energy generated by the motion of the material being mixed, which is dependent on speed and time parameters. For this study, a specific mixing program was designed to provide a homogenous mixture between copper and KCl. The main advantage of this mixer machine for this work was that it can perform the mixing process in a short period of time with high speed, up to 2100 rpm.

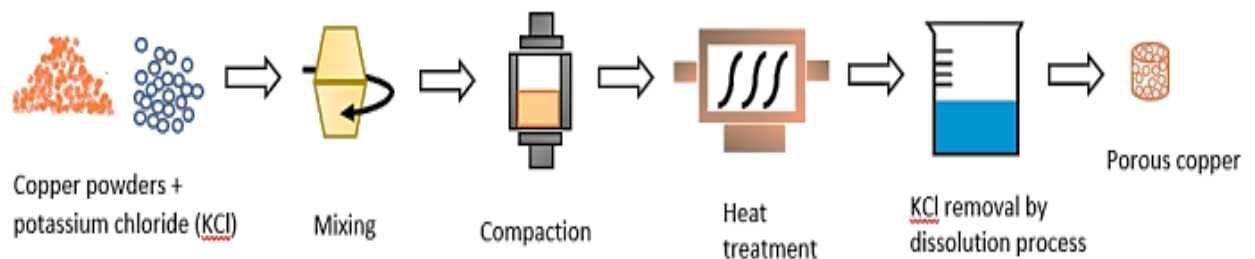


Figure 4.1; The fabrication process of porous copper by compaction and dissolution process

The process is similar to MIM, which requires common powder metallurgy processing stages but without the roles of a binder system. The copper powder and KCl were mixed together with KCl amounts between 10, 20, and 30 vol%. The volume of KCl is set at a lower volume since the pre-trial by 50% volumes compaction has faced difficulty in compacting and requires high energy as the machine was manually operated. The available mould die used in the present study comes with a hole size of 20 mm in diameter and 50 mm in length, as shown in Figure 4.2a, and the Cu powder was completely filled inside the mould with the designated height (Figure 4.2b).

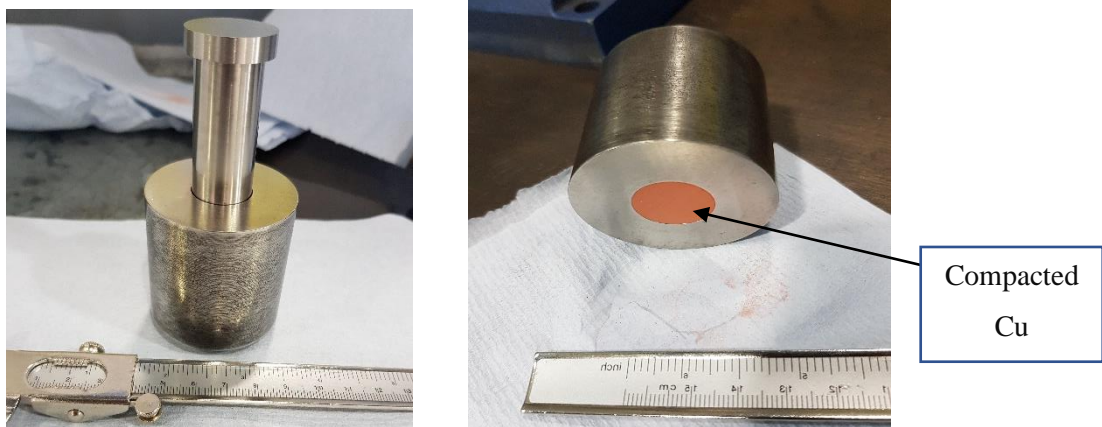


Figure 4.2; Mould die for (a) Compaction and Sintering (C&S) method (b) (a) Mould die set, (b) after the compaction process



Figure 4.3; Manual compaction or pressing machine

The compaction process was carried out by using a Specac Pressing Machine (Figure 4.3), where the process of compaction is manually operated and takes place at low compaction pressure, ranging from 1 tonne (9.81 MPa) to 2 tonnes (25.78 MPa). The maximum compaction pressure is 2 tonnes (25.78 MPa) due to the presence of KCl, and the machine is operated manually. This is because the higher compaction pressure may deform the shape of KCl, which will deteriorate pore development. Furthermore, due to structure fragility, the compaction sample must be handled carefully. Table 4.1 summarises the parameters of mixing fraction and compaction pressure used in this part of the investigation.

Table 4.1; Mixing parameters and compaction pressure

<i>Samples</i>	<i>Compaction pressure</i>	<i>Mixing %Vol. (Cu-KCl)</i>
<i>Pure copper</i>	1 tonne (9.81 MPa) to 2 tonnes (19.61 MPa)	0%
<i>The mixture of copper and KCl</i>	1 tonne (9.81 MPa) to 2 tonnes (19.61MPa)	10, 20, 30%

Since the present porous Cu method produces a pore structure that solely depends on the physical properties of the space holders, thus the sintering temperature must be carefully selected. By considering the melting temperature of KCl (770°C), any temperature above 770° will deteriorate and melt the KCl particles during sintering and, consequently, will lead to the collapse of the KCl and the pores. Therefore, the sintering temperature was set at 750°C to preserve the structure of porous metal (refer to Figure 4.4). A study by [229] reported the successful production of porous copper at a relatively lower sintering temperature, 650°C, giving confidence that the temperature used here would be sufficient for the densification of the Cu to the required extent. The samples were then allowed to cool for 10 minutes before the dissolution process.

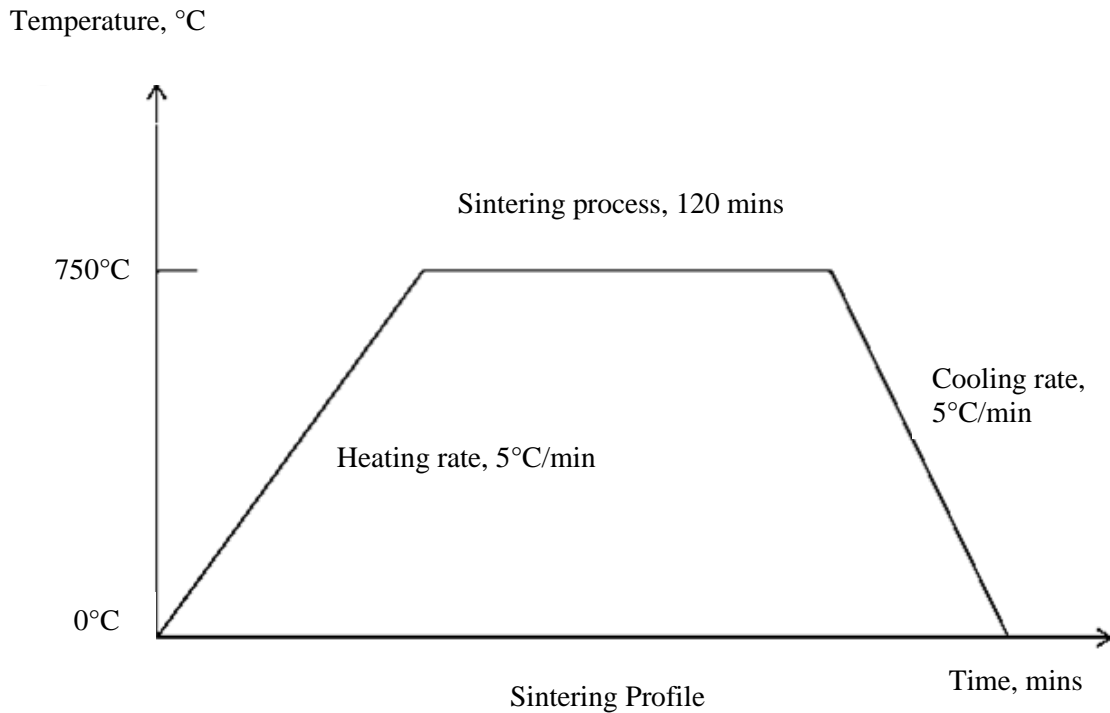


Figure 4.4; Sintering profile used for porous copper production in this work

4.3 Space holder removal

KCl is a soluble space holder, which means it can be removed from sintered samples by water dissolution. The space holder materials need to be removed completely to avoid problems such as corrosion [57]. The approach used here involves the removal of both the space holder and the binder system can be carried out simultaneously by using an ultrasonic bath where the temperature can be controlled precisely as performed by [102]. This heated ultrasonic bath Figure 4.5 has a monitoring and control system that allows the temperature of the water to be controlled accurately. The sintered samples were weighed by using a 0.1 mg resolution analytical balance and then dipped into the ultrasonic bath, which was vibrated ultra-sonically. This process was used with real-time monitoring of weight loss by measuring the weight of samples after certain periods of time (stopping the process and removing them from the bath to do so). The samples were submerged in warm water (60°C) for different periods of time, and the debinding profile can be illustrated. This temperature was set according to DSC analysis. The measurement was taken after the samples had been dried by heated compressed air for 15 minutes, and consistent reading was taken by weighing the samples three times. Finally, by using equation 4.1 given [154], the extent of dissolution at each time was calculated by determining the weight loss reduction rate of samples after a certain timeline.

$$\% W_{\text{loss}} = (W_{\text{initial}} - W_{\text{after}}) / W_{\text{initial}} \times 100 \quad (4.1)$$

W_{initial} is the initial weight of the sample before dissolution; W_{after} is the weight after the samples have been through the dissolution process in a certain period of time.



Figure 4.5; Water leaching process to remove KCl by using ultrasonic bath

4.3.1 Porosity measurement

Most of the previous research generally used compaction methods to produce porous Cu that managed to secure various ranges of porosity [53], [62], [107], [187]. The aim of this study is to determine the porosity of fabricated porous samples based on different percentages of KCl. The porosity of samples can be obtained by the gravimetric method [229] by measuring the density of samples. The mass of samples was calculated by analytical balance, and the geometry of each sample was measured at least three times to find the average. An analytical density balance (Mettler Toledo) was used with the Archimedes principle to measure the density of the porous sample. The porosity percentage can then be calculated according to the following equation 4.2.

$$\text{Porosity (\%)} = [1 - \text{Porous copper density/bulk density}] \times 100 \quad (4.2)$$

4.4 Result and Discussion

The samples were initially mixed (Cu and KCl) without using additional lubricant and compacted at 1-2 tonnes of compaction pressure. The mixture was successfully pressed into the specified mould, however, it was clearly seen that the space holder material was not distributed well, and most of them appeared and congregated at the bottom of the samples Figure 4.6a. Then due to this condition, the sample structure was easy to crack and could not retain its cylindrical shape since the bottom of the sample was fully covered with KCl. This could be explained by the different density that leads the powders to segregate during the compaction preparation. Although the mixing process was done by a high-speed machine that managed to blend the mixture homogenously, the material particles probably separated when preparing the mixture into mould before the compaction was placed. However, this problem can be avoided by adding the mixture with a small amount of acetone during the mixing process. This liquid acts like a ‘binder’ that helps the Cu and KCl to mix well before proceeding to the compaction activities. The sample Figure 4.6b shows good physical behaviour without fracture. Most importantly, no sign of non-uniform distribution of KCl confirms the particles have successfully mixed together with Cu.

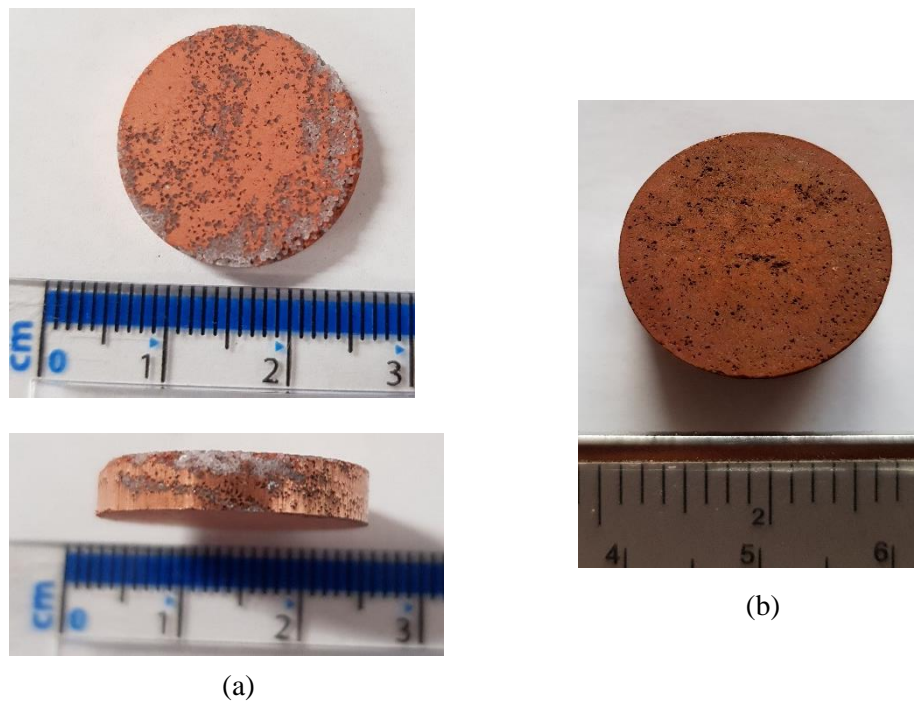


Figure 4.6; Green sample of compacted porous Cu; a) The defect sample (10% vol. KCl) where the space holder was congregated at the bottom of the sample, b) Sample with 20% vol. KCl without defect.

Figure 4.7 shows the appearance of porous copper under a specific compaction pressure range. The purpose of the compaction process is to make the samples to the required shape and give them the mechanical integrity required for handling. The Cu sample without a space holder (0 %vol. KCl) was successfully compacted with compaction pressures from 9.81 MPa to 29.42 MPa (3 tonnes). However, the mixed samples of Cu and KCl can only be compacted until 19.61 MPa, probably due to the KCl particles, which were fractured or deformed above this pressure. As reported in previous studies [143], [144], if the pressure is over the maximum limit of the space holder, it will lead to the fracture of the space holder and subsequently, the original shape changes from spherical to elliptical shape. Other work [138] also support the previous finding where NaCl was deformed at 350 MPa and also shows the same effect. While too high pressures are not suitable, the sample will also show a problem related to its strength if the compaction pressure is not enough. As shown in Figure 4.7a, the samples processed at low pressures are easy to break and difficult to handle. Thus, the adjustment of the pressing pressure is needed where the optimum ranges between 1-2 tonnes (9.81-19.61 MPa) (Figure 4.7b).

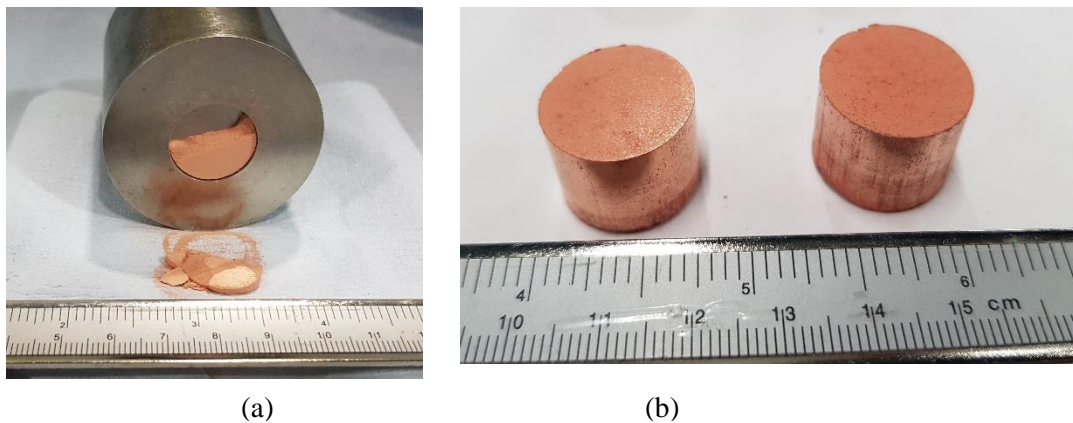
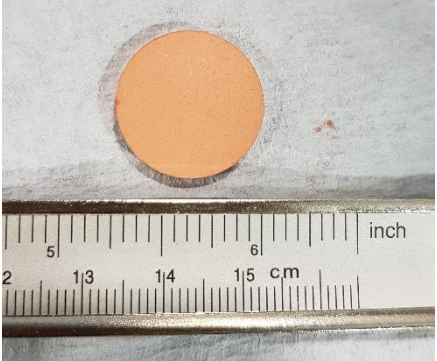

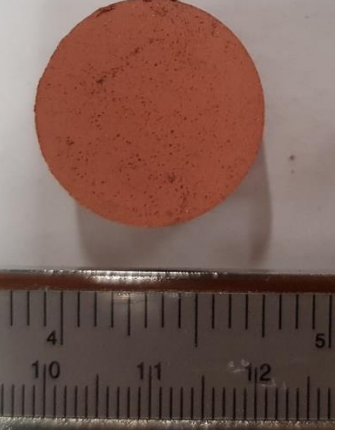




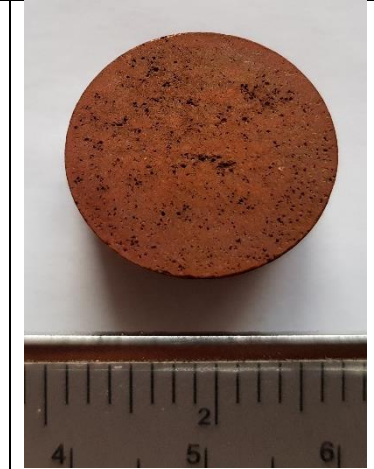
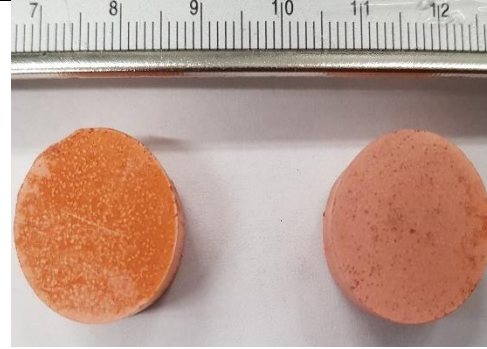
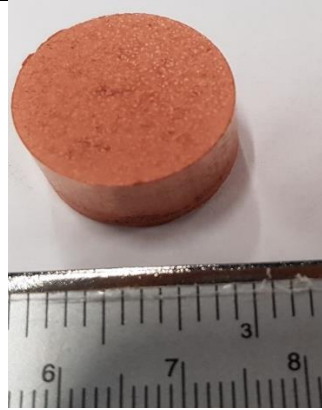
Figure 4.7; (a) the compaction sample with compaction pressure below 9.81 MPa, (b) final compaction copper with the acceptable pressure range (9.81MPa and 25.78MPa)

Table 4.2 shows the porous copper samples in the form of green compacted samples, as-sintered samples and the samples after the leaching process. As clearly seen, the green state compacted Cu samples with no space holder material display a smooth outer surface, while the samples that mixed with KCl, show a pattern of space holder distribution. As-sintered samples do not show a great difference from green compacted samples where the shrinkage was not obvious since the sintering temperature was set at a lower temperature (750°C). The debinded samples clearly showed pore formation within the microstructure, and the shape of the pores replicated the morphology of KCl. The KCl was successfully removed through the dissolution process in 6-8 hours.

Table 4.2; Porous copper with different process parameter

Samples	Green samples (After compaction)	As-sintered samples (under 750°C)	After leaching process
Porous copper without space holder			NIL
Porous copper with 10 vol.% of KCl			

Porous copper with 20 vol.% of KCl



Porous copper with 30 vol.% of KCl

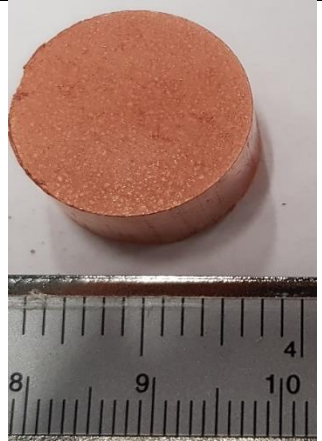


Figure 4.8 displayed the water leaching process for the compaction part that was pressing at 2 tonnes (25.78MPa). It was demonstrated that the present samples successfully removed the space holder particle without any significant defects. This is because all samples were already sintered, and no defect appeared due to this water-leaching process. All sample shows an almost similar trend where they took around 4-5 hours to complete the water leaching process. The process was performed under 60°C of warm water and, within this temperature, accelerated the removal process of KCl.

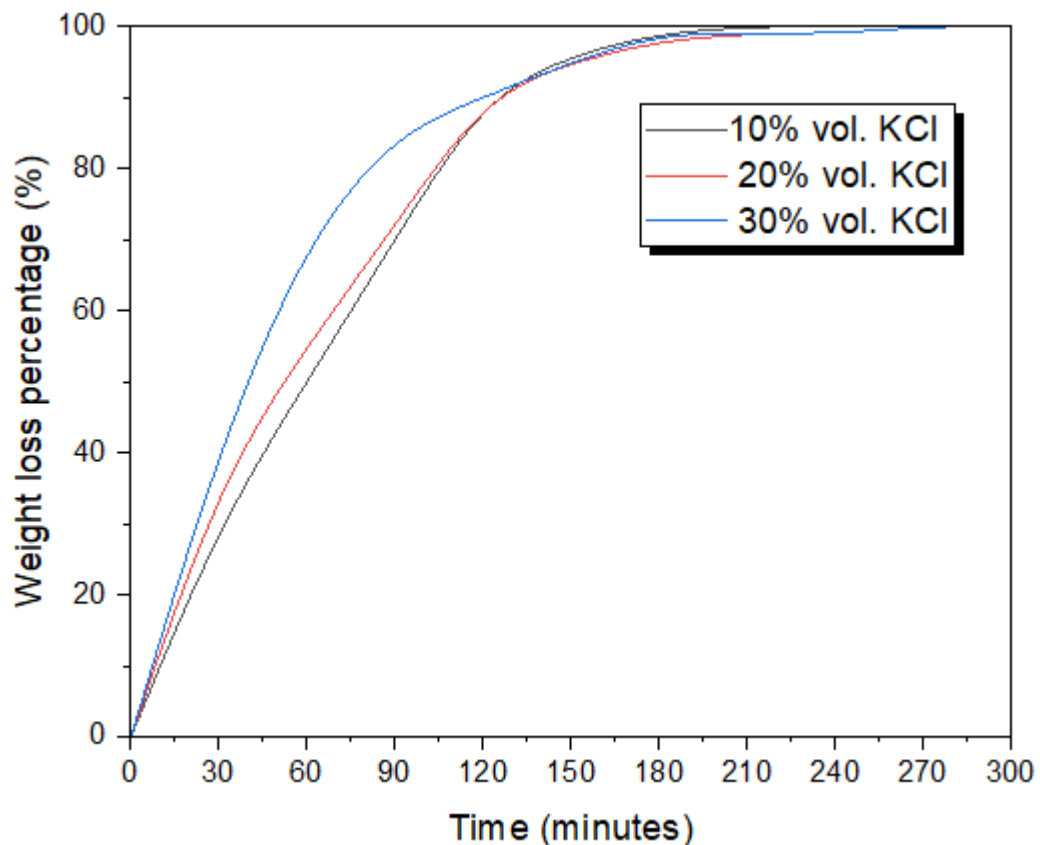


Figure 4.8; The removal of the space holder from the sample that was pressing at 2 tonnes (9.61MPa)

The KCl particles were successfully removed from sintered samples since KCl has good solubility in water [102]. This removal was confirmed by X-ray Florescence (XRF) analysis (Table 4.3). The result shows there is no K or Cl detectable within the microstructure. This means the debinding process was successful in removing all the space holders at 50°C for 6 hours process. As shown in Table 4.3; XRF analysis of leaching samples, there were other elements within the structures in low percentages. This may be contributed to the sintering process and contamination from ceramic containers.

Table 4.3; XRF analysis of leaching samples

Temperature	Sample	Result
750°C	Mixed copper with 10 vol.% KCl	CuO 98.906%, P ₂ O ₅ 0.061%, Al ₂ O ₃ 0.427%, SiO ₂ 0.059%, Ta ₂ O ₅ 0.548%
	Mixed copper with 20 vol.% KCl	CuO 99.577%, Fe ₂ O ₃ 0.018 %, P ₂ O ₅ 0.064%, Al ₂ O ₃ 0.436%, SiO ₂ 0.140%, Ta ₂ O ₅ 0.696%, Rh 0.069%
	Mixed copper with 30 vol.% KCl	CuO 99.592%, Fe ₂ O ₃ 0.031 %, P ₂ O ₅ 0.067%, Al ₂ O ₃ 0.309%,

Table 4.4; The porosity of each porous copper under different compaction pressure and KCl vol. % below shows the result of the porosity percentage of porous copper with different percentages of KCl by weight. The porosity was measured by equation (4.2), and the volume and density of porous samples were determined by the Archimedes method. The result demonstrates that an increasing in space holder weight percentage will increase the porosity percentage of porous copper. In contrast with compaction pressure, the porosity of porous copper was reduced by increasing compaction pressure.

Table 4.4; The porosity of each porous copper under different compaction pressure and KCl vol. %

Compaction pressure (MPa)	KCl vol %	Average Density, (g/cm ⁻³)	Average Porosity percentage (%)
9.81 (1 tonne)	0	8.61	3.90
	10	7.88	12.1
	20	6.73	24.9
	30	5.87	34.5
25.78 (2 tonnes)	0	8.55	4.60
	10	7.91	11.7
	20	6.87	23.3
	30	6.12	31.7

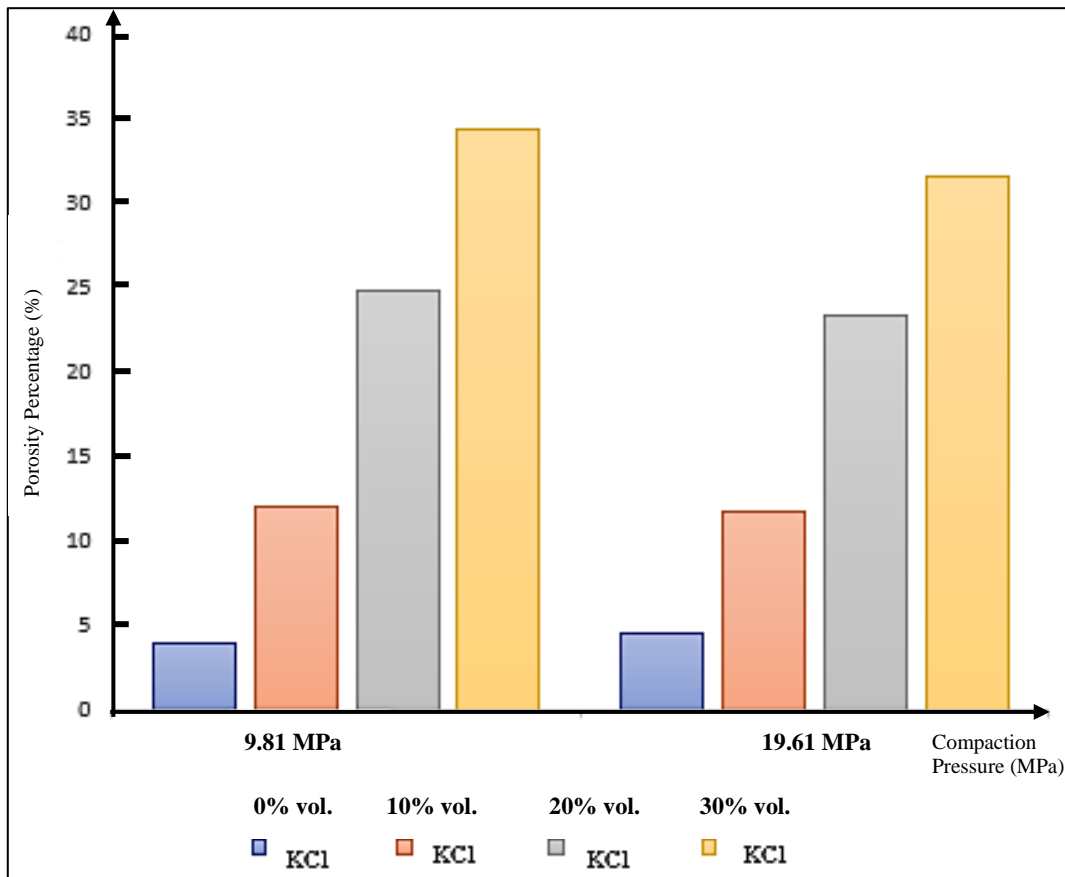


Figure 4.9; The relationship of compaction pressure and KCl volume % towards porosity percentage

Figure 4.9 demonstrates the relationship between compaction pressure and KCl vol. % with porosity. The result shows that the KCl managed to create pores within the microstructures, and as predicted, a higher weight of KCl will create high porosity samples. There is no exact relationship between the porosity percentage and the weight percentage of KCl. Most of the results actually show a slight increase in porosity percentage, around 2 to 4.8 % from the original KCl weight percentage. This is probably due to the effect of the low sintering process and also due to the low compaction pressure compared to the other work [138], [144]. The setting of compaction pressure for this study was selected to be as low as possible in order to create more space and pores within the microstructures.

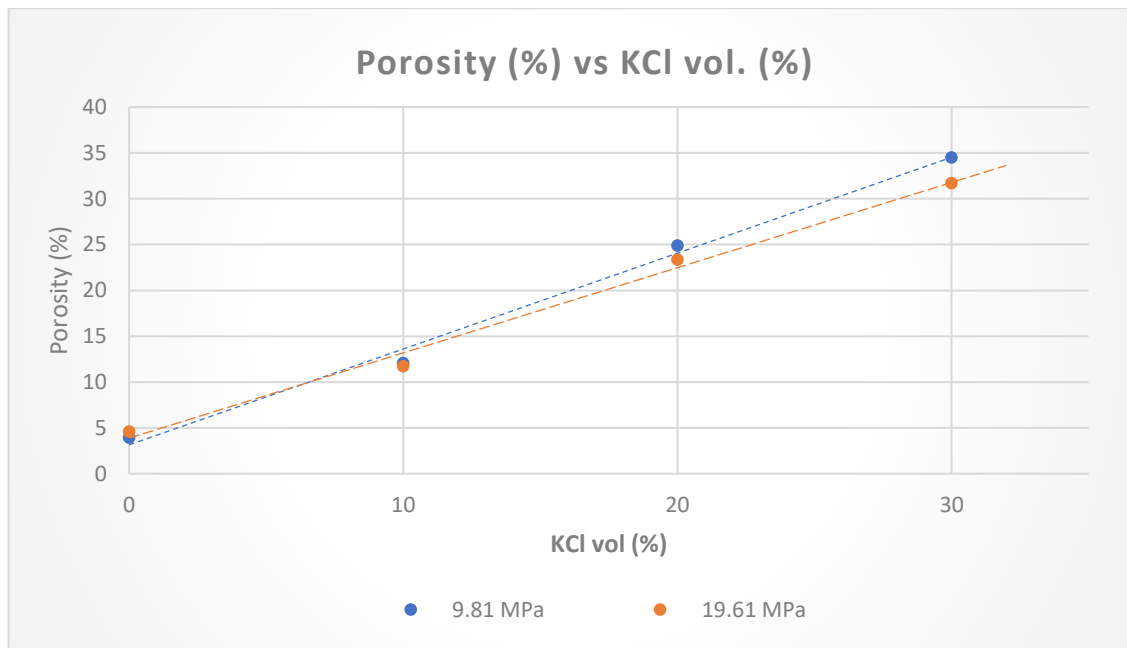


Figure 4.10; The effect of porosity on the variation of KCl amount

As shown in Figure 4.10 clearly displays that increasing the KCl volume % will increase the porosity formation of porous copper. The samples without a space holder have close to 5% of porosity while increasing 10% to 30% vol. of KCl shows a linear trend of porosity formation for both compaction pressures. A similar trend to the previous study, increasing compaction pressure tends to reduce the porosity with 2.8% to 8.1% between the two compaction pressures used here.

4.5 Work planned for porous Metal Injection Moulding (MIM) with Space Holder Technique

The results of the conventional approach to processing porous Cu reveal some promising results in selecting the optimum processing parameter suited for the current study. The porous Cu could be fabricated with low pressing pressure (9.81 and 19.81 MPa) such that the part was perfectly compacted without any defects. In contrast, other research assigned much higher pressure levels ranging from 140MPa [223] to 300 MPa [230]. In the water dissolution process activities, the duration took between 6 and 8 hours, depending on the material employed for the space holder. Previous research revealed that the water-dissolving process might take less time (4 hours) [186] when potassium carbonate was used, but Sharma [231] found that NaCl required more time (12 hours) to dissolve in water. Following the volume of KCl allocated, the manufactured components revealed porosity volume percentages ranging from 3.9% to 34.5% vol. This research

demonstrates that porosity development depends on the space holder features, as it imitates the structure and volume.

However, conventional pressing and sintering processes could limit possible findings on developing porous features. Due to manual operation, the present investigation can only be undertaken at lower volumes of KCl (10-30% vol) as it is hard to handle if the KCl volume reaches 50 %. Furthermore, the manual compaction process contributed to the slow production of the part, resulting in a low number of samples, and the existing die mould could only produce a single sample per process. This situation prolongs the production of porous Cu. In addition, the C&S method is offered with limited shapes of final parts and cannot produce a complex and complicated design.

Thus, employing the MIM method in conjunction with the space holder technique could be the best way to overcome the limitations of the C&S method, as well as to extend the knowledge and information related to this approach and its compatibility with the selected Cu powder, water-based binder, and space holder material, KCl.

4.5.1 The benchmark for porous Cu via Metal Injection Moulding and Space Holder Technique (MIM-SH)

The experiment planning for porous Cu via MIM-SH has been discussed in detail in Chapter 3. The planned work has referred to the previous studies that could possibly work and be compatible with the characteristics of the present materials. Although both the pressing method and the MIM method are in the same class of manufacturing approach (powder metallurgy), these methods show dissimilarity in some aspects, such as the technique used, the appointment of binder materials, the moulding procedure, as well as the selection of materials. Therefore, processing porous Cu by MIM-SH should be conducted carefully to obtain the targeted product without any faults or defects, and benchmarking on the work from the previous studies is necessary.

The work on porous copper via MIM-SH is driven by specific factors, parameters and the outcome from the previous research by MIM-SH. This benchmark for the work of porous Cu can be classified into factors:

(a) The promising binder system: PEG-PMMA-SA

The development of PEG-PMMA-SA binder system for MIM production was developed to improve the debinding process as these binders are water-soluble type binders. This means that the binder components can be removed without using any chemical solvents, as these materials are not environmentally friendly. Furthermore, this binder system can be compatible and paired with numerous

materials such as titanium [232], stainless steel [165], Inconel [193]. Previous work on Cu commonly used paraffin wax as its main binder [159], but it requires using chemical solvents such as Heptane and Hexane. Thus, the fabrication of porous Cu using PEG-PMMA-SA binder is safe, but this work could extend the knowledge and understanding of the suitable parameters that are compatible with Cu material.

(b) The use of a water-based space holder

Space holder materials can be found in many types, shapes and forms. This temporary material is used to preserve 'space' within its structure as the space represents the pores. The created pores imitate the physical properties of the selected space holder. The space holder selection is based on certain factors such as size, shape, volume, removal process, non-toxicity, compatibility, etc. One of the promising space holders is a water-based space holder, which can be removed via water. The most common water-based space holders are Sodium Chloride (NaCl) and Potassium Carbonate (K_2CO_3), which are widely used in many MIM-SH works [176], [186], [233]. There are also some works on Potassium Chloride (KCl) via MIM [139], [177], which give promising results in terms of high porosity and pores formation. Thus, the present work used KCl as space holder material since this material has been successfully proven to generate pores, available in the market and low cost. In addition, using a water-based space holder such as KCl, these substances and the binder could be removed simultaneously. This will reduce the production time of porous Cu.

(c) The introduction of the SpeedMixer Machine

The fabrication of MIM-SH commonly uses the traditional mixing machine such as a sigma or Z-blade mixer, large extruder, twin-screw extruder or torque rheometer. These machines have similarities due to the slow mixing process. Thus, the introduction of a speed mixer machine could reduce the mixing times as works by [193], [232], [234] show promising results. Thus, the present work will employ a SpeedMixer machine to improve the mixing time of the MIM process.

Chapter 5 MIM-SH METHOD: PROCESSING OF POROUS CU FEEDSTOCK

The selection of powders for the injection moulding process considers various important parameters such as particle shape and size, chemical composition, the combination of mixed powder etc., as highlighted by Randall [235]. This section gathers the information from assessments of the main materials used in the present study, including the main powder, space holder material and the binder constituents. Before experimentation, each item was examined in the as-supplied state in terms of physical properties (shape, size, density etc.) and thermal analysis was also carried out on the binder systems, yielding important results for the subsequent process of MIM.

5.1 Characterisation of initial materials

5.1.1 Particle features and shape

In the present study, copper powder (Cu) was used as the main material for the fabrication of the samples. An example image of the as-received powder is shown in Figure 5.1, which indicates the spherical shape with a coarser surface texture. German & Bose [151] have suggested that this type of particle shape increases mouldability qualities due to minimal inter-particle friction, which may improve the flowability behaviour [236]. This condition may assist the MIM process, particularly at the moulding stage. According to Moon [237], a consistent shape of spherical powder will provide higher dimensional accuracy. In addition, the selected Cu has greater than 99% purity to maintain the quality of the final feedstock and encourage good sintering and polymer contact [237].

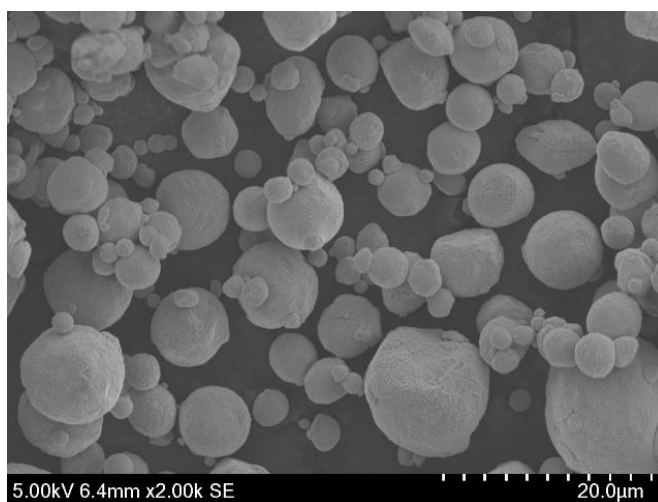


Figure 5.1; Scanning electron micrograph (secondary electron mode) of as-received Cu

Space holders are used to introducing porosity and control its properties such as porosity volume, pores size and shape in the microstructure. The selection of space holders should be compatible with MIM materials (powder and binder system) and their processing parameters. As MIM is commonly conducted at approximately 150-200°C, thus it is necessary to avoid space holders with lower decomposition temperatures. In addition, in the context of this study, water-soluble space holders are preferred since they can be simultaneously removed from the binder components, consequently reducing the production time of porous Cu. Salts like sodium chloride (NaCl) and potassium chloride (KCl) tend to be compatible with these recommendations. KCl is used in the present study since it has higher solubility in water (253.9 g/L at 20°C), which is greater than NaCl. Furthermore, KCl is easy to handle, inexpensive, and non-toxicity.

The size and shape of the space holder should be carefully chosen since these parameters influence feedstock flowability and prevent clogging owing to low MIM process setting (temperature and pressure). These temporary materials can be found in different types, sizes and shapes, such as irregular [139], spherical and cubic [219]. As for the present work, KCl was selected, and SEM observation of the particles shows that the space holder, the KCl has an irregular shape (Figure 5.2), and some of the particles exhibit is nearly cubic shape. Moreover, Shbeh [219] finds that KCl with a cubic shape shows higher viscosity compared to the spherical shape of KCl, and this condition can be adjusted by proper binder selection.

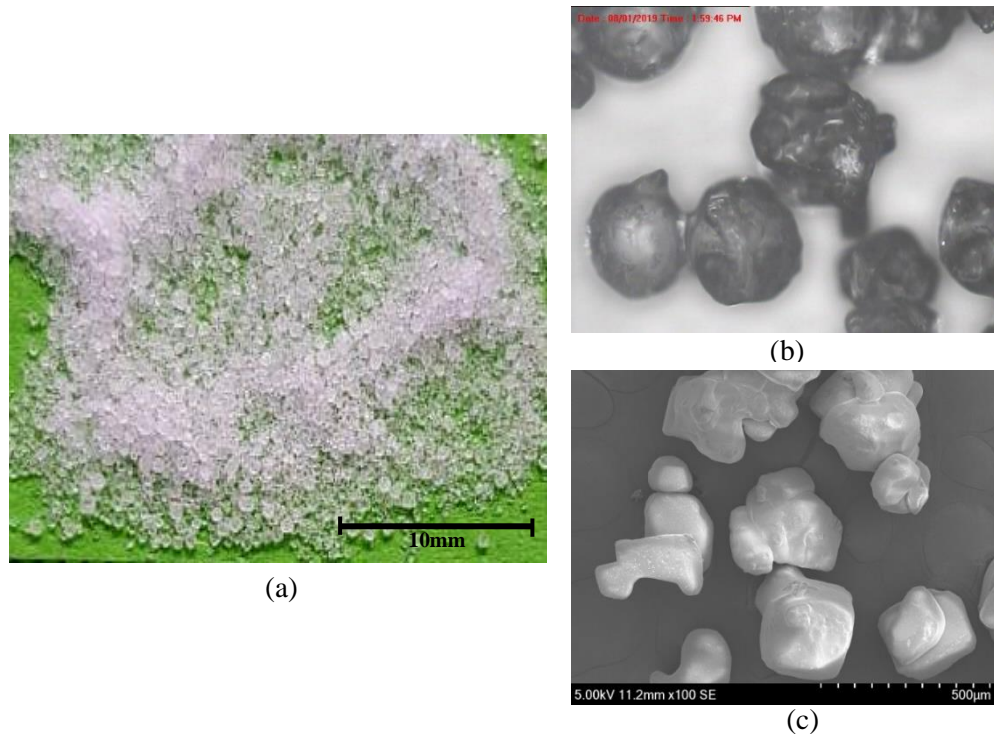


Figure 5.2; The as-supplied space holder material, potassium chloride (KCl), (a) photograph of particles, (b) optical microscope image of KCl by Nikon Optical Microscope, (c) Scanning electron micrograph ((secondary electron mode) of KCl by SEM Hitachi SU 3500

5.1.2 Particle density measurement

As mentioned in Chapter 3, the materials and binders used in the present work were supplied by a range of different suppliers. Some of these materials were provided with materials specifications and descriptions. Generally, the information is included essential data such as particle size, shape, density, percentage of purity, etc. For the present study, the density measurement was performed on both starting materials (copper and space holder- KCl) and binder components to ensure the result was as similar to material specification as possible and to confirm the quality of the materials. Furthermore, the density of each material is essential in identifying the powder loading fraction for feedstock preparation. The arrangement of powder mixture calculation depends on the density of each material, and therefore, an accurate density value is crucial to produce an appropriate feedstock.

The apparent density of the powder can be referred to as the bulk density of the material; the measurement was based on the volumetric displacement method [238] for the present study. As shown in Figure 5.3, the weight of copper was measured by an electronic balance, and the apparent density value was

calculated by dividing the weight and volume of the loosed packed powder according to equation 5.1. The copper powder was in a loose, poured structure without performing any agitation process. For this reason, the value is also referred to as the poured bulk density since the volume was taken after the process of pouring powder into the glass measuring cylinder.

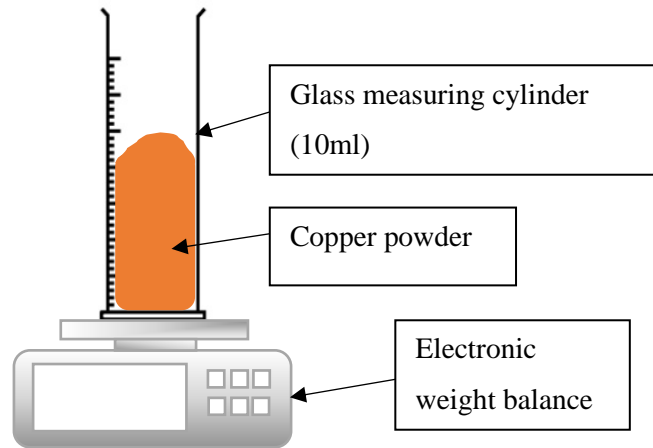


Figure 5.3; Schematic diagram of the apparent density measurement process

$$\rho_d = m / v \quad (5.1)$$

where ρ_d refers to apparent density, m is the weight of powder, and v is the volume of the measurement powder.

For tap density, the measurement was done using a Tap Density Machine with a tapping frequency of nearly 200 taps per minute. The resulting value can be used as guidance for the process of powder loading assessment in order to identify the optimum volume fractions of the constituents in the powder-binder system. The tapping process makes the powder particles reorient and relocate their position with respect to each other, and there is a general tendency for empty space to be filled.

Finally, the true density, also known as the theoretical density, was measured by the gas displacement method using the inert gas, helium. AccuPyc II 1340, Micromeritics, USA (a helium pycnometer) was used to measure the density of these binders. The filling pressure was 10 psi and tested for over 10 cycles. The result of the density measurement for materials is shown in Table 5.1.

Table 5.1; Density measurement of materials

Powder	Apparent Density (g/cm³)	Tapped Density (g/cm³)	Pycnometer Density (g/cm³)
Cu	4.71	5.37	8.92
KCl	-	-	2.01
PEG	-	-	1.22
PMMA	-	-	1.21
SA	-	-	1.01

The apparent density of Cu powder is almost 50% lower than the density measured via the pycnometer. While the tapped density was slightly higher than the apparent density (5.37 g/cm³), it does not match the higher value of the obtained theoretical density. The difference in the powder density value is undeniably caused by the method used to measure the powder, as explained above.

The density measurement for apparent and tapped density requires a particular volume of powder under different conditions; loose and tapped packing conditions. The loose powder condition (for apparent density) indicates the powder particles were not involved in any consolidation process once it was placed into the glass measuring cylinder. It demonstrates that apparent density was calculated on the spatial distribution of particles, with the influence of the inter-particulate void volume. Thus, the low value of apparent density is probably caused by the powder particle arrangement, as the slightest disruption may change the density value. If the powder is highly agglomerated, the result of the apparent density measurement may increase. Moreover, the apparent density relies on the physical features of the powder particles, as low apparent density indicates fine particles and vice versa [236]. The shape of the powder also influences the value of apparent density. [237] claimed that the apparent density of spherical powders can be achieved at 50% of the wrought metal density and will decrease with a less spherical shape. This can be explained by the non-uniformity of powder particles during the packing process leads to a higher surface area-volume ratio. Tapped density measurement was conducted by a mechanical device (tap density machine) that organised and packed the particles under standard conditions and setup. Similar to apparent density, the tapped density also considered the interparticle

voids and the existence of pores but in different conditions. The apparent density is directly measured on loose powder, while tapped density measurement was conducted after the specific tapping steps. Thus, the tapped density is slightly higher than the apparent density, probably due to particle arrangement factors resulting from the tapping process. This condition has decreased the interparticle voids as an outcome of the proper packing and arrangement of the powder particles. Consequently, the void volume of tapped density is significantly reduced and less than the apparent density, resulting in a density value. This information on tapped density is important as it relates to the estimation of the powder-binder ratio. The true density is relating with the accurate volume of the materials that excluding porosity. This means, the true density is basically measured on the actual solid phase of material. The true density is commonly assessed via the gas pycnometer method since its suitable for irregular or fractured shapes. The density measurement is based on the principle of gas displacement, as the volume of gas displaced represents the volume of the samples.

5.1.2.1 Effect of filling pressure of pycnometer on the density measurement

One of the machine parameters of the pycnometer is the helium filling pressure. In general, higher filling pressure uses a larger amount of helium to measure the volume and has the possibility to provide a more accurate result. However, the downside of this setup is that it consumes longer testing time, more than one hour, compared to lower filling pressure, which normally takes around 20-35 minutes per sample. In addition, the slow measurement process also depends on the number of repetition cycles. Therefore, an investigation on the effect of helium filling pressure was carried out to observe the effect on density measurement. For this testing, the number of cycles was set at 10 measurements per sample, and three different filling pressures were used; 10, 15 and 19 psi. The repetition of measurement is necessary to obtain the average reading of density. Figure 5.4 shows the result of the density measurement of KCl.

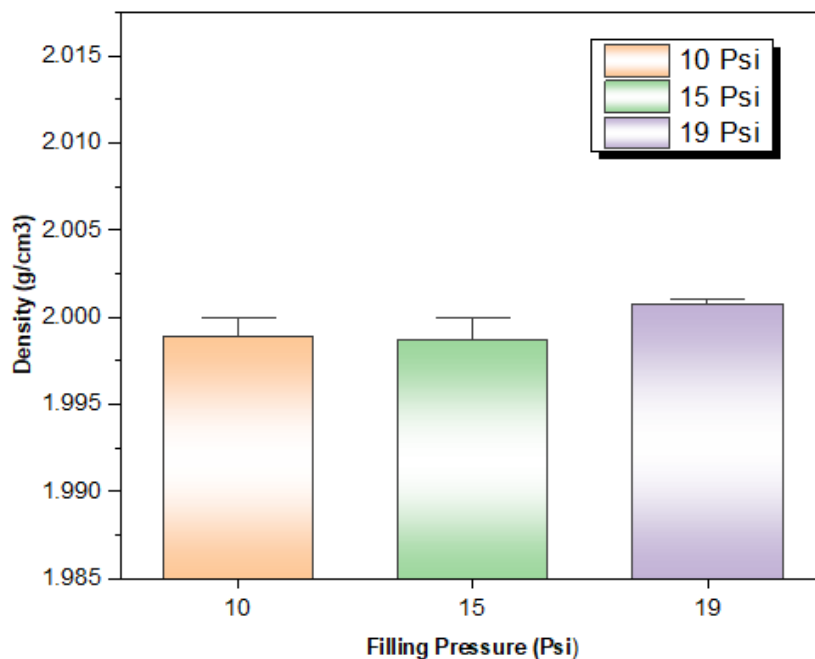


Figure 5.4; Effect of helium filling pressure on density measurement of KCl

The density of KCl with higher pressure (19 Psi) was obtained approximately at 2 g/cm^3 , which takes almost more than one hour to complete the measurement of 10 cycles. However, with lower filling pressure, the measurements only take not more than 30 minutes to achieve readings of around $1.9975\text{-}2 \text{ g/cm}^3$. The results do not show much difference in density measurement for each helium filling pressure. Further testing was conducted on other materials (this analysis was conducted with binder material) to observe whether the results were consistent with those obtained with KCl material. With the same measurement parameters and experimented with three types of filling pressure (10,15,19 psi), the finding also demonstrates similar findings. The density of PEG was approximately between 1.218 and 1.220 g/cm^3 with a relatively slight variation. The finding shows no significant impact on the density measurement with different filling pressure, verifying the similar results on the previous testing on KCl. This is probably associated with the operating principle of the pycnometer, which relies on gas displacement using Boyle's Law's volume-pressure relationship. The change in pressure was detected due to the gas displacement from the sample. The final pressure was recorded at equilibrium conditions, allowing the sample volume to be measured. As a result, this measurement technique is not directly influenced by the filling pressure, as it relies only on the expansion of the gas and pressure variations. However, the experiment demonstrated that the filling pressure affects the measuring time. Therefore, the filling pressure of 10 psi was selected for the rest of the measurements of materials density since it requires less processing time, which has also been used in the previous work [219].

5.1.3 Particle size

The particle size distribution is an assessment of the population of particles, which provides information regarding the particle size and range of the selected material. The information is presented as a mathematical function and statistical distribution of particle size data, which can be interpreted using simple statistical parameters to provide quantified results; the mean (average particle size), median (the particle size which divides the distribution into two equal halves), or mode (particle size with the highest frequency). As stated by [239], the powder qualities, such as particle size and distribution, have a substantial effect on the viscosity of the blend and powder aggregation behaviour, and Seerane [196] found that these attributes have an effect on the difficulty of feedstock moldability. As the current blend primarily consists of Cu powder, the particle size distribution of the Cu and the KCl size is important information, as this can affect blending and is the primary method to control pore size. By doing this analysis, the size of the particles can be controlled following the requirements of the study, and it can be confirmed that the powder qualities are in accordance with supplier specifications. As the MIM method is a powder metallurgy technique, the copper and KCl must be in powder form and will undergo a pressing-moulding process together to create a green sample. The selection of the particle size distribution of the primary powder should be made with care, as prior research has shown that the size of the metal powder can affect the MIM fabrication process, which in turn affects the product [240].

The particle size distribution of Cu powder is found to have an average diameter close to 50 μm , which is similar to the material specification supplied by the manufacturer (Sandvik Malaysia Sdn Bhd). Regarding space holder size, in the present study, KCl was around 315-333 μm . For particle size analysis, the measurement of the KCl particles used was carried out since no specification data were supplied by the supplier. For the present study, the constant KCl particle size is required for the MIM process. Thus, the received KCl powder underwent a sieving process. The sieving was conducted using a sieve shaker with a different mesh of sieve plate, approximately 500 μm , 300 and 150 μm sieves to separate out and classify the powder with different size fractions with uniform particle size. The particle size was measured by a Mastersizer 3000 with the dry analysis method, and the results are shown in Table 5.2.

Table 5.2; KCl particle distribution by Malvern 3000

Number of measurements	Dx (10) (µm)	Dx (50) (µm)	Dx (90)
1	185	316	508
2	187	317	507
3	182	315	515
4	198	333	528
5	196	327	514
6	194	324	510
7	189	322	516
8	185	318	510
9	186	320	513
10	196	330	522
Average	187	321	513

German & Bose [151] claimed that the suitable powder size was in the range of 4 to 20µm, while [237] claimed that finer powder might give better interaction of particles and good packing density. Some other researchers [147] preferred a finer particle size between 2 to 8µm for MIM fabrication since finer powder gives excellent properties such as a good surface finish. The smaller size of powder gives benefits in terms of faster sintering as well as minimising the moulding defects [235], as coarser powder may associate with distortion problems [237]. However, there were also reports on the disadvantages of finer powder particles. Finer powder highly influences shrinkage formation during the sintering process [161], and the trend to use larger particle sizes may contribute to less shrinkage effect [235]. Some work [241] found that the finer powder does not produce an adequate MIM result when it needs to be combined with space holder materials. From the finding, the presence of fine powder in the sample has hindered the space holder material (NaCl) from being appropriately removed during the dissolution process, even when this is carried out for a longer period. The shift to the usage of larger powder particles may also promote the mouldability properties and packing density of the as-sintered part. Moreover, [237] claimed that finer commonly requires an aggressive mixing process, which leads to crack defects during the subsequent moulding process, which in turn, may lower the quality of the fabricated feedstock. Therefore, a new trend in MIM processing study is the tendency to use a larger particle size as it still yields a suitable product, controls the agglomeration effect in finer powder and minimizes shrinkage level [196]. Furthermore, it is more economical due to reduced costs and handling difficulties associated with very fine powders. The previous study [219] has produced a good quality MIM part with a

larger particle size of around 75 μm . Therefore, for the present work, the coarser size of copper powder was preferred (average diameter of 50 μm). However, the preparation of feedstock with coarser powder should be carefully conducted, especially on the estimation of the powder-binder ratio in order to achieve good densification.

In the context of the space holder, the size range of KCl is chosen as previous findings [219] show that with such a size range, the porous sample has an adequate structure and can be handled without deteriorating the microstructure, especially at the green sample stage. Furthermore, the size of KCl is important since it directly affects the size of the pores formed in the microstructure.

From the particle size analysis, the mean size of the space holder (KCl) is almost 6 times larger than that of the Cu powder. Although the size of both particles shows a wide distribution, the size of the space holder should be larger than metal powder as this parameter was commonly used in the production of porous metal, as shown in previous studies on Ti [103], Cu [242], and Mg [200]. Torres [138] recommended that the powder size must be much smaller than the space holder with consent to enhance the sinterability aspect. Budi [59] concluded that in bone tissue engineering, the pore size should be between 200–500 μm to achieve higher permeability to cells and body fluids and have appropriate mechanical properties. In functional applications such as heatsinks, the larger the surface area, the more heat can be transferred. This can be achieved by having an appropriate porosity and reducing the pore size (against the limit of the reduction in permeability of the porous material). In the present study, pre-fabrication of porous Cu with the larger size of space holder is achievable without any sign of poor fabrication in the feedstock itself or the final product. Ideally, the created pore structures replicate the structure of the selected space holder. Thus, larger size space holders should produce more macroporous materials.

5.1.4 The binder constituents

The MIM process uses multi-component binder systems blended with the main metal during processing. These binders will be eliminated by the end of the process, although they play several important roles in MIM samples, such as flowability and the strength of green and debinded samples, as briefly discussed in Chapter 2. The right binder with the proper volume fraction of the selected metal requires a significant amount of work to discover in terms of experiments and analysis. In addition to being cost-effective, recyclable, and compatible with other materials, the selected binder components must also fulfil the many roles assigned to them and address safety issues, reactivity, and decomposition time. Furthermore, as it is vital for the MIM process, particularly when it comes to the debinding and sintering process, the viscosity of the binder and its thermal properties should be considered.

From the previous works [157]–[159], MIM of copper has widely used Paraffin Wax (PW) as a wax type of binder to enhance the flowability of material [243]. However, it has been reported several drawbacks from the viewpoint of processing, such as toxicity [204] and environmental concerns during the debinding process. Thus, the designated binder system (PEG-PMMA-SA) for the current study was chosen from among water-based binder systems that may potentially improve the MIM process for porous Cu. The selection of binder system was chosen based on previously successful binder formulas introduced by [195], [219], [244]–[246] that have been shown to improve processing time and material handling for other metallic materials. The three-component polymeric binder system employed in the present study was inspired by the work of [102], [169] because these types of binders may be simultaneously removed with KCl (a water-soluble substance) using water, which was the goal of the present work. [247] reported that water-soluble PEG exhibits defect-free debinding compared to the wax binder.

Each component of the binder has varied roles, with the first component of the binder system being responsible for the flowability of feedstock. According to Ahn [243], this part of the binder component should be easily removed during the debinding process. Thus, Polyethylene Glycol (PEG) was chosen as the low-viscosity element of the binder system due to its ready availability, high solubility in water, and ease of handling when compared to organic solvents [173]. PEG employment can avoid using organic solvents such as heptane, hexane or acetone, which are hazardous solutions [152], flammable and create environmental issues [248]. In addition, the solubility of PEG in the water meant that its dissolution could be simultaneously performed with the dissolution of KCl. Poly(methyl methacrylate) (PMMA) was chosen for the present work as a second binder (the high viscosity part), which is often paired with PEG in the previous works [164], [169], [244], [249], [250]. PMMA is a thermoplastic polymer that can improve mould strength [245], [246]. The elimination of the first component of binder (PEG) during debinding may result in the formation of many open pore structures that weaken the part shape. Thus, PMMA performed a significant role as the backbone of the binder system to preserve and support the structure and shapes of components during the subsequent process of MIM without tendencies toward collapse and structural alterations. PMMA will be removed through a thermal debinding process, and the diffused gaseous will flow through the open pores due to PEG removal in an earlier debinding process stage.

Finally, the third component of the binder system is a surfactant. According to [251], the absorption of stearic acid onto the powder surfaces through the chemical bonding forms a thin layer on the particle surfaces, resulting in a homogenous structure. Stearic acid serves as a lubricant and significantly lowers the friction among powder particles [252], [253] and the friction between powders and machines or die walls [251]. This condition may improve the dispersion of the Cu powder in the polymeric binder resulting in good mixing. For the present work, a small amount of stearic acid (SA), normally lower than 5 wt.%, was added into the binder system to act as a processing aid for which this chemical is regularly used as a third binder component. The usage of stearic acid in the PEG-PMMA-SA binder system from the previous works [169], [192], [254],

[255] was set in low quantity as increasing amount resulting cracks problems. This binder has a low melting temperature and is removed by the thermal debinding process.

In conclusion, the main binder constituents used in the present work consist of PEG, a backbone polymer- PMMA and SA as a surfactant. This is different from the binder system used previously for MIM copper, which is usually wax. The selection of this binder system can be a good alternative to the wax-type binder that requires specific chemical solvents (e.g.; heptane, hexane) instead of normal water for the debinding process.

5.1.4.1 Thermal analysis of the binder system- TGA and DSC

The essential information that needs to be identified for binder components is their thermal properties, which can be assessed by two types of analysis- TGA and DSC analysis. Both analyses have been fundamentally explained in Chapter 3, and each method gives different findings that are useful for the later setting of parameters for the MIM process.

The first thermal testing performed on binders is Differential Scanning Calorimetry (DSC). The aim of conducting DSC analysis on binder constituents is to analyse the thermal transition behaviour, including the melting temperature (in this study) of these binders and from there, the extrusion temperature setting for later MIM main stages (moulding injection) can be identified. The injection of feedstock requires an appropriate temperature range to ensure all the binder components are melted and can, therefore, easily be extruded. For the present study, the heating rate was set at 5°C/min within the temperature range of 20-210°C under a controlled argon atmosphere. This thermoanalytical technique scans and measures the difference between the amount of thermal energy (heat flow) required to heat the binder and that needed for a reference empty container under the controlled temperature program. The thermogram results can be used to identify features related to the absorption or release of thermal energy from processes occurring in the binder.

Thermo-gravimetric analysis (TGA) provides thermal properties information which is useful for the thermal debinding processing setup [256]. The analysis monitors the change in sample weight as they are subjected to the increasing temperature. Generally, TGA is used in preparation for MIM to identify the optimum decomposition temperature of binder components. It is useful to design the heating cycle of the thermal debinding stage in the sintering cycle. The finding is significant for thermal-type binders, but it is also valuable for the rest of the binder components. Even though both PEG and SA were designed to be eliminated via the water dissolution process, the selection of the right decomposition temperature is useful to ensure all binder constituents are fully removed. In the present study, the backbone polymer binder, PMMA will be eliminated via the heating process, which takes place after the water debinding process of PEG and SA as well

as KCl. These removal routes of binder-SH were proven by [195], [219], [244] as a potential solution for the time-consuming problem in the binder/SH removal process faced in the previous study.

As shown in Figure 5.5, PMMA shows a higher peak melting temperature located by the analysis of the peak position to be at 126.39°C, whereas the PEG and SA recorded at 49.80°C and 65.57°C. These findings indicate that each binder component is expected to be melted close to these respective temperatures. Since the highest melting temperature reaches nearly 127°C, the temperature for the injection process to extrude the feedstock should be set higher than 127°C to guarantee binder melting and thus that the material to be injected can exhibit adequate flowability behaviour. In the present study, the injection temperature cannot, however, be set at a specific temperature at this stage as each powder mixture has a different powder volume fraction and amount of KCl. As reported by [219], the temperature may need to be increased to higher temperatures under these circumstances due to different powder loading and reactions between binder components in the mixture. Therefore, in order to identify an exact optimum temperature for injection, further investigation and testing for each type of powder mixture and injection pressure, holding time, and handling must be considered. Despite this, the result of DSC is an estimation of the initial temperatures to be tested. The final optimum injection temperature range also depends on the rheological behaviour. For this study, the injection temperature was set at approximately 130-175°C. The temperature range is similar to the previous studies [161], [195], [244] that reported good green samples with different metal powders. While for the water debinding process, to ensure the PEG melted, the processing temperature was chosen to be around 50-60°C.

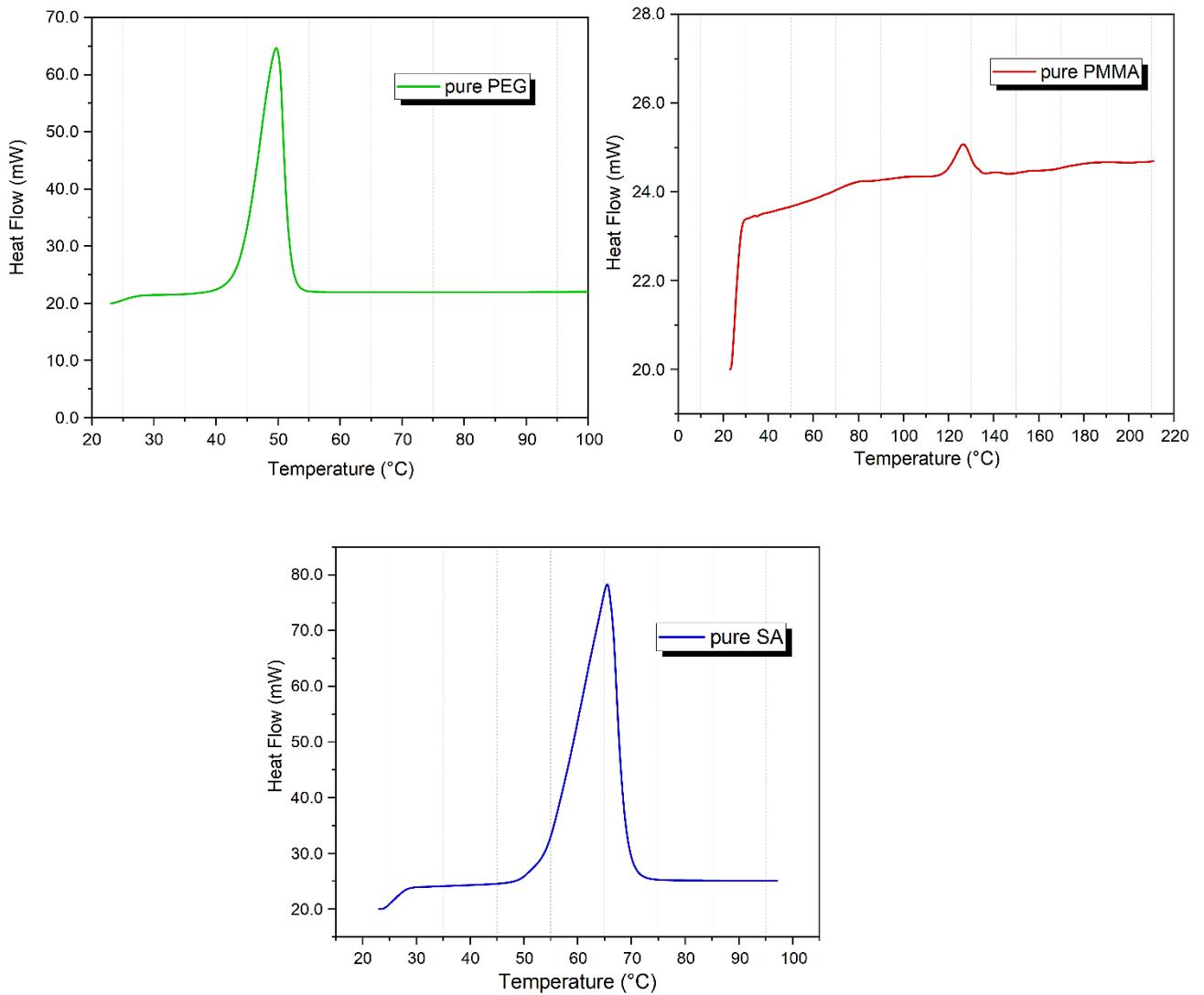


Figure 5.5; DSC thermal analysis on the different binder constituents

Figure 5.6 records the TGA results of the main binder components, which display the weight loss percentage as a function of temperature. It can be clearly seen that each binder component starts to decompose at different temperatures, as PMMA was the first to be lost, followed by SA and PEG. The previous DSC results demonstrated the different melting temperatures of each binder. The decomposition temperature of all binders approximately starts at 50°C-100°C and at nearly 200°C, the weight percentage of PMMA and SA was progressively reduced and almost completely decomposed nearly at 400-450°C (SA) and 460-500°C (PMMA). While PEG was rapidly removed starting roughly at 350°C and completed in the same temperature range for PMMA. The remaining weight of each binder component tends to reach 0 weight percentage as a sufficiently high temperature is achieved. It was noticed that all binders decomposed at a temperature below 460-500°C. With this finding, the debinding process should be performed at a similar temperature or above to guarantee

the elimination of PMMA and remaining binders (PEG and SA) after the water debinding process. The findings of the decomposition behaviour of the binder components were similar to the studies by [195], [219] and the small differences in decomposition pattern may probably be contributed by the factors of different brands, weights or amounts used for the TGA testing. The TGA result of pure binder components is applied for the initial temperature setup of the heating cycle in the thermal debinding process, as the final decomposition temperature range might be changed or adjusted since the heating process will take place with actual feedstock. The decomposition tends to shift into higher decomposition temperature due to the chemical reaction of PMMA and binder components, especially with PEG binder. Hayat [257] identified several factors that influence the removal of PEG, including the molecular weight of PEG, PMMA volume fraction, and the size and shape of the powder used.

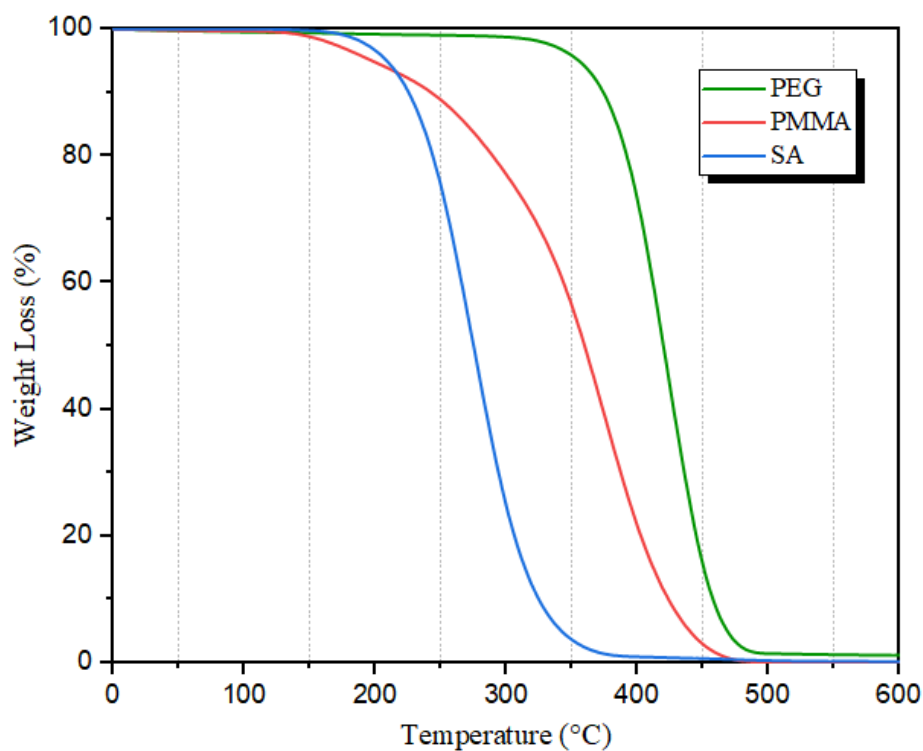


Figure 5.6; TGA analysis of pure binder components

5.1.5 Summary of starting materials properties

The characterisation of powder and binder was carried out in order to analyse the important behaviour such as density, shape and size of particles. Displayed in Table 5.3; is the summary of all material specifications used for the present works.

Table 5.3; The summary of material specifications

Powder	Manufacturer	Particle Density	Particle Size Range	Particle Shape	Melting Point (°C)	Molecular formula	Roles
Cu	Sandvik Malaysia Sdn Bhd, Malaysia	8.92	20 µm	Spherical	1084	-	Parent Material
KCl	Qrec (Asia) Sdn. Bhd, Malaysia	2.01	315-322 µm	Irregular	801	-	Space Holding material
PEG 1500	Alfa Aesar, UK	1.22	-	Flakes-shape solid powder	57-63°C	H(OCH ₂ CH ₂) _n OH	Binder 1-Plasticiser
PMMA	Alfa Aesar, UK	1.21	-	crystalline powder	19-134	[-CH ₂ C(CH ₃)(CO ₂ CH ₃)-] _n	Binder 2-Backbone
SA	System Chemicals, Malaysia	1.01	-	Solid powder	63.16-84.87	C ₁₈ H ₃₆ O ₂	Binder 3-processing aid

5.2 Optimisation of Powder-binder ratio

This section discusses feedstock preparation, focusing on developing a powder-binder loading ratio. MIM production is heavily dependent on the binder system. This is responsible for feedstock flow for part shaping and retaining the structure during subsequent MIM processing stages. The formulation should be in good ratio to ensure the feedstock has appropriate flowability and a good moulding process [157]. An unoptimised solid-binder ratio may potentially introduce part flaws and unwelcome defects such as part distortion, voids within the structure, crack and warpage of the moulding part, slumping of the part during binder removal [202], or poor dimensional control due to the effect of shrinkage of the heating treatment process. Supati [202] claimed that higher powder concentration could reduce the effect of shrinkage in the debinding and sintering process. For example, the present study shows that poor solid loading gave poor results, as displayed in Figure 5.7. The samples cannot retain their shape after two hours of water debinding at 60°C, and the failure occurred in all samples of different KCl compositions. These findings show the importance of the choice of binder system [258] along with other factors such as mechanical and rheological properties. Therefore, the amount of binder must be sufficient to completely coats the solid powders (Cu and KCl) with a thin layer.



Figure 5.7; The structure of Cu feedstocks was clearly deteriorated after two-hour water debinding process at 60°C

According to [259], feedstock with lower powder content tends to show excessive shrinkage on sintering. Previous studies show that the binder system contributes 30-50% of the overall volume of the mixture [149] for successful moulding, which means the solid loading is within 50-70% of the total volume. The amount of solid powders should be maximised, and the binder amount should be sufficient to allow flow behaviour and structure rigidity.

Thus, one of the main investigations of the present study is to determine the optimal solid loading-binder fraction for the development of porous Cu that is compatible with MIM. In general, the investigation of MIM routes starts with a relatively low percentage of solid loading to observe the initial findings in order to establish the standard processing technique. Following this, the solid powder or binder content may increase or decrease until the feedstock shows a promising result. The present work has been carefully carried out systematically to minimise the waste produced from the unsuccessful trials. The feedstock from failed trials is avoided to be used again to maintain the quality of the feedstock. The waste produced from the unsuccessful trials. The feedstock from failure trials is avoided to be used again to maintain the quality of the feedstock.

5.2.1 Tapped density measurement

The investigation of the right powder-binder loading can be performed in many ways. [260] introduced an activation energy technique to identify critical solid loading, while Barbosa [241] describes various methods, including measuring powder tapped density. Seerene [261] applied the tapped density method to identify the maximum powder loading for spherical particles of TiAl4V and concluded that the critical loading is usually 10 to 20% greater than the tap density of powder. Paula [241] claims that this method has difficulty in estimating the changes in the maximum powder loading when dealing with different binder systems. However, the approach can still be applied as a reference for further investigation via systematic analysis.

By knowing the tapped density of powder particles, the critical loading of feedstock can be predicted. The critical loading of feedstock is the maximum amount of powder that can be used in feedstock formulation. It can be used for initial preliminary testing before any adjustment or changes (if needed) for further improvement of the mixture. The critical loading can be measured by dividing the tapped density of powder by the pycnometric density of powder [262], as shown in equation 5.2. The literature considers this relationship to be a preliminary way to estimate the critical solids loading [260].

$$\text{Critical Powder Loading of feedstock, } Cl = \left(\frac{\text{Metal powder tapped density, } \rho_{tap}}{\text{Metal powder pycnometric density, } \rho_{pycno}} \right) \times 100\%$$

(5.2)

In the present work, the tapped density of the sample was 5.37 g/cm^3 which is obtained based on the conducted tapped density measurement process with 200 taps per minute of tapping frequency [197] (briefly discussed in Chapter 3). While for the pycnometric density or known as theoretical density, was calculated at 8.96 g/cm^3 . Then, based according to equation 5.2, the critical loading volume of porous Cu feedstock (Cl) is 59.99%. According to the previous practices depending on the binder system [260], the final feedstock powder loading is generally presented 2-5% below the critical loading. Therefore, the optimal powder loading volume can be estimated at around 54-58%.

5.2.2 The Rule of Mixtures (ROM)

Since the materials in producing MIM porous copper are different; metal (Cu), space holder- potassium chloride (KCl) and polymer (PEG, PMMA, SA), they will combine to give overall properties different from anyone on their own. The Rule of Mixtures (ROM) is applied to estimate the powder-binder mixture either by weight or volume fraction. In the present study, the calculation of powder loading uses a volumetric fraction.

Initially, the density of the mixture was calculated through the theoretical density for the mixtures, which consists of powder and binder components. This can be expressed by using the inverse rule of mixture [235] (equation 5.3).

$$\frac{1}{\rho_f} = \frac{X_b}{\rho_b} + \frac{X_p}{\rho_p} \quad (5.3)$$

where ρ_f is the density of feedstock, ρ_b is the theoretical density of the binder, ρ_p is metal powder density while X_b and X_p represent a weight fraction of binder and metal powder. Thus, the total mixture fraction is equal to 1, as displayed in equation 5.4

$$X_p + X_b = 1 \quad (5.4)$$

The present study uses the volumetric measurement; thus, equation 5.5 shows the calculation of theoretical density in terms of volumetric powder loading as follows;

$$\rho_{mix} = \Phi\rho_p + (1 - \Phi)\rho_b \quad (5.5)$$

where ρ_{mix} is the theoretical powder-binder mixture density, Φ is powder loading volume fraction (%), ρ_p is a density of powder mixture and ρ_b is a binder density. This equation will show a linear relationship between the volume of powder loading and the mixture density.

5.2.3 Discussion on powder-binder ratio investigation

5.2.3.1 Powder loading through Tapped Density Analysis

The sample density was determined by tapping density measurement, which came out to be 5.37 g/cm³. From this, the critical loading volume of porous Cu feedstock (Cl) is 59.99%, according to equation 5.2. Therefore, the optimum powder loading is approximately 54-58%, following the recommendation from [157], [163]. Any value up to 60% of powder loading will probably contribute to the viscosity problem due to high solid loading. These circumstances should be avoided since this characteristic has the possibility to have a problem during the moulding process. Through the investigation, more than 60% of the mixture has demonstrated powdery features, dry and high fragility (Figure 5.8). The lack of binders has prevented the mixture from being well blended as the powders certainly separate due to poor bonding, making them difficult to mould into specific shapes. In the present cases, a good mixture should demonstrate with long cylindrical shape after the moulding process. This finding verified the results of tapping density measurement as the maximum powder loading should exhibit not more than 60% vol.



Figure 5.8; The features of feedstock with more than 60% of powder loading

Ideally, the powder particles should exist in the feedstock at a slightly higher density than they achieve in the tapped density measurement, the interstitial spaces being almost filled with binder at the minimum quantity. The void volume between the tapped volume and the theoretical volume of powder particles (which can be obtained from their mass and density) clearly shows a huge different [263]. When powder particles pack, there will be spaces left between each particle (refer to Figure 5.9). In the case of MIM, the obtained void volume would be an estimation of the amount of binder needed, though this is usually reduced due to the

shearing effect during the mixing and injection process. Previously, the amount of solid powder in MIM Cu processing was between 55-61% vol. [136], [157], [158], [163]. Trials with 80 vol% of binders show drawbacks of low mechanical properties. High solid loading can result in a part with a high amount of metal with lower shrinkage [202] but may not have the proper injection viscosity. Higher levels of binder would leave little metal powder.

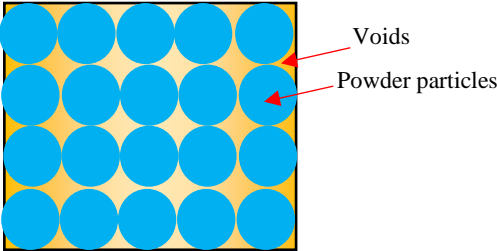


Figure 5.9; A schematic diagram of voids formation within powder particles

This prediction volume was used as an initial starting of powder mixture volume and may vary due to various factors such as the existence of KCl in the mixture, the flowability performances of feedstock and the binder system used. Thus, for further investigation, the next approach of identifying the optimum powder loading, the rule of mixture (ROM), was conducted since the present work has used several types of materials with different densities. The ratio is then systematically investigated with an approach that is careful to conserve material and allows a determination of the optimum powder-to-binder ratio.

5.2.3.2 Powder loading through the Rule of Mixtures (ROM) Technique

Table 5.4 below shows the projected density variation of feedstock for various levels of powder loading. According to the theoretical powder-binder mixture density equation (equation 5.5), the graph of the linear relationship between powder-binder mixture density and powder loading percentage can be drawn.

Table 5.4; The prediction of feedstock density

Powder loading-binder volume (Vol %)	0-100	10-90	20-80	30-70	40-60	50-50	60-40	70-30	80-20	90-10	100-0
The feedstock density (g/cm³)	1.191	1.340	1.629	2.057	2.625	3.332	4.179	5.165	6.291	7.556	8.96

The feedstock density measurement follows the rule of mixtures based on the above equation until it reaches the point below the theoretical value because of void formation. As shown in Figure 5.10, the critical powder loading obtained from equation 5.5 has set the highest limit for the amount of powder. By combining the result of tapped density above, the critical loading line can be estimated at nearly 60%. The shaded area represents the range of optimal loading based on a 2-5% reduction from the powder loading estimation rule proposed by [235], depending on the binder system used.

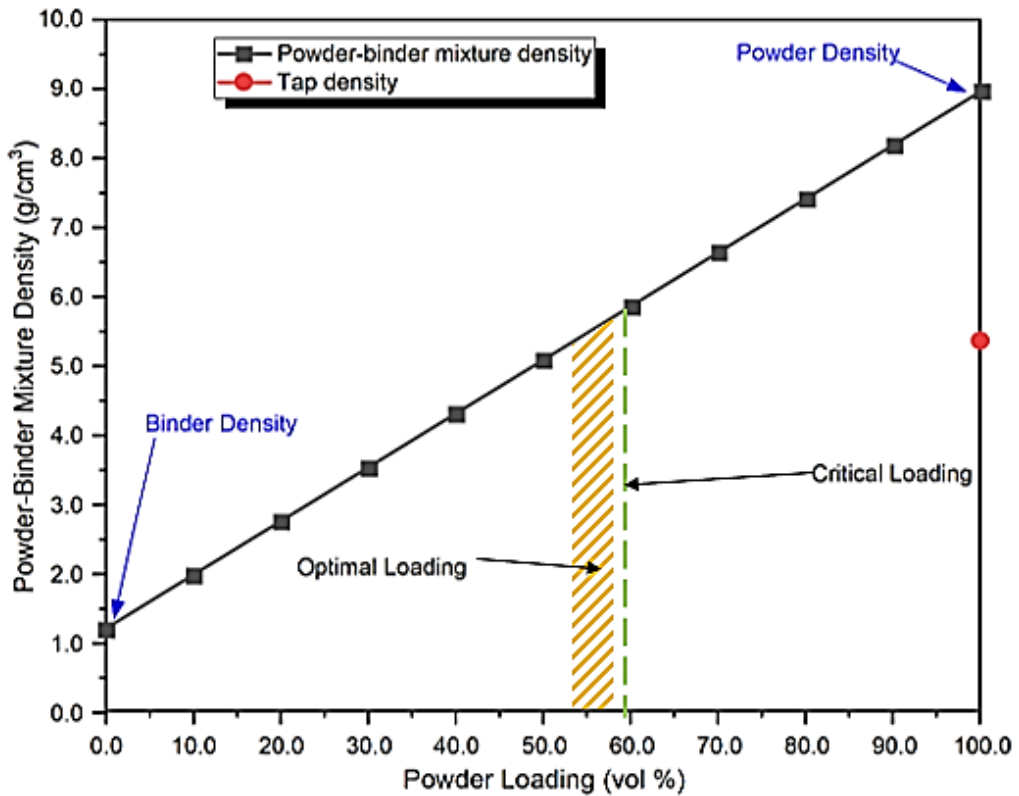


Figure 5.10; The critical and optimal powder loading estimation graph for feedstock preparation.

The critical loading is associated with high mixing viscosity. This figure is also known as a loading curve [235]. The powder loading fraction falls within the shaded area, as this is where the feedstock should show adequate flow behaviour. At high binder concentrations, it shows that the mixture follows the theoretical density line. The critical loading is the point where the particles are closely packed with the minimum binder to fill the gaps between them; beyond this point, the feedstock cannot flow due to high viscosity [151], [159]. Thus, with the finding from the tap density measurement and based on the rule of mixture, the optimum powder loading can be estimated within the range of 54 to 58 % volume, with 60% as critical powder loading. As a rule of thumb, this percentage range can be considered for feedstock preparation. This powder loading fraction is slightly similar to the volume range obtained by previous studies where the solid powder was present in the range between 55-61% vol. [136], [157], [158], [163].

5.2.3.3 The possible situations according to the powder loading identifying process

The proper feedstock formulation is crucial for preparing the feedstock with suitable viscosity. It also offers information about the critical powder loading of the mixture and mixing parameters. The powder loading is recommended at higher composition as more metal (Cu) contents may also enhance the thermal conductivity properties to avoid the shrinkage problem. However, this prediction cannot proceed since the constituents of the MIM ingredient should be balanced with the amount of binders. The factor of powder-particle packing [264] should be considered to estimate the amount of binders to maintain the viscosity level.

From the investigations, the findings can be illustrated according to the schematic diagram (Figure 5.11), which differentiate three different conditions that might happen with the different binder fraction modification. The feedstock that obtained the critical powder loading can be shown in Figure 5.11 (b), as this ratio has the maximum binder concentration suitable for the mixture. The binder is sufficient to fill up the space between the powder particles and has adequate strength to mould the mixture into the long-cylindrical shape of feedstock. This situation displayed the powder particles with the densest packing. The powder loading with 60% volume is represented in this situation with balance volume. This was demonstrated by good shape retention of feedstock with control dimension and suitable for large production of MIM.

However, if the amount of binder is not balanced with the powder loading, this will acquire opposite results that might happen with a lack or excessive binder fraction. The excess binder condition represents the feedstock with lower powder loading, as shown in Figure 5.11 (a). The feedstock was observed and present in a nearly fluid-like shape. This is because a few contacts among the powder particles lead to powder-binder separation [259] and a nonuniform mixture of feedstock. The excess binder affects the subsequent MIM process. The sample demonstrates a flashing problem during the injection process (Figure 5.12), followed by a slumping failure in the debinding process. The problematic shrinkage [264] clearly occurred during the debinding process and the sintering process, and this intricates in controlling the dimension and tolerance of powder particle compact. This could happen if the volume of binders was allocated more than 60%. Alternatively, in the case of a low binder amount, voids may occur in the feedstock (Figure 5.11 (c)). This is because a lower quantity of binder is insufficient to completely fill the spaces between the powder particles and does not fully coat and cover the powders resulting in nearly powdery form feedstock. Finally, the feedstock will be viscous, which complicates the moulding process. This situation happened when the binder amount was adjusted to approximately lower than 35% volume.

The process of determining the right amount of powder loading is complicated and requires a few methods and modifications. Previous works [235], [260] recommend that the optimum powder loading is decided slightly below the critical powder loading levels as Yimin [264] found out that with the optimum

powder loading, the feedstock may obtain benefits such as better rheological properties (which is crucial for moulding process) and acceptable mechanical characteristics. As results from tapped density measurement and the rule of mixtures (ROM) technique, the powder loading can be estimated with 60% of critical powder loading volume, and 54 to 58 % is classified as an optimum range. However, this powder loading ratio requires preliminary testing prior to final MIM production in order to assure the quality of the produced feedstock and minimise material resource waste.

Many trials revealed little difference in the physical qualities of feedstock generated with varying percentages of powder loading, as depicted in Figure 5.13. It also showed that the binder could coat and cover all powder components, despite their physical differences in colour and roughness. The pre-moulding test exhibits no difficulties with the feedstock and no indication of defects such as cracks, segregations of the powder and binder, or warpages problems. Some research [163] utilised a volumetric powder loading of 63% Cu, which produced a satisfactory outcome. While [173] states that the powder content must typically be between 50 and 56% of the volume to provide an appropriate viscosity, which is essential for the injection moulding process. It may exhibit poor sintering ability and result in low part density if the powder volume is less than 50% of the total volume. Therefore, the 60% volume of powder loading was chosen for the current work because larger powder loading fractions may provide superior performances, decrease shrinking problems, and demonstrate good feedstock quality through preliminary testing. This powder volume arrangement contradicts [264], which states that the feedstock may experience poor flowability if the powder loading exceeds the optimal value. This may be explained by several factors, including the various materials used, the various binder types and their constituents, and the various processing settings.

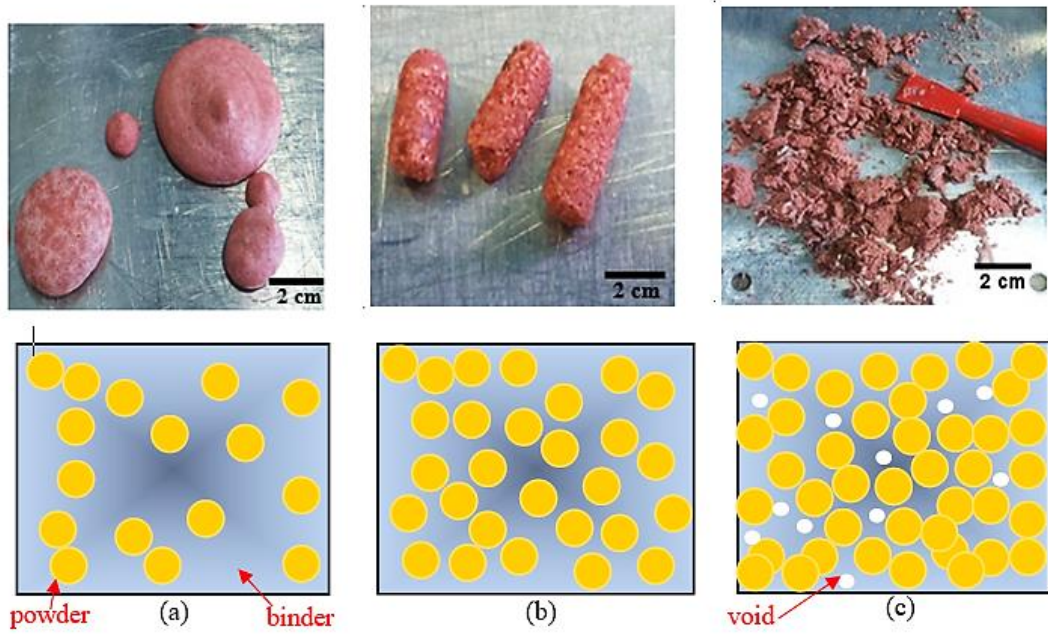


Figure 5.11; Three conditions of the material mixtures, (a) excess binder, (b) critical binder concentration, (c) excess powder

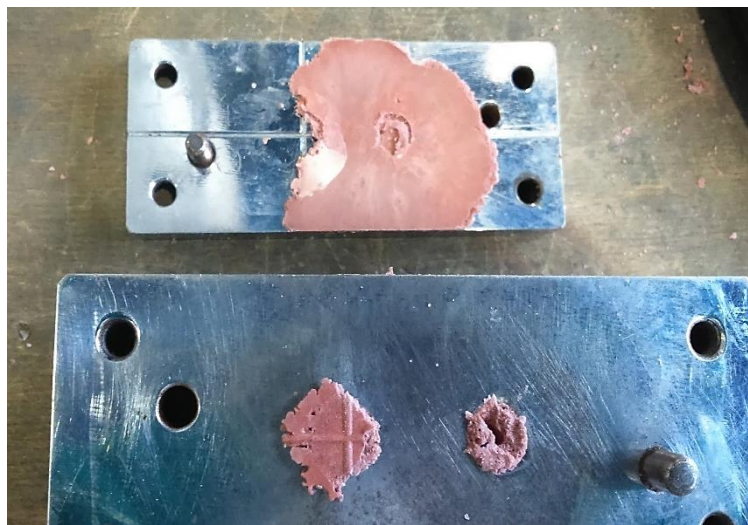


Figure 5.12; Flashing problem on the feedstock due to excessive binder concentration



(a)



(b)

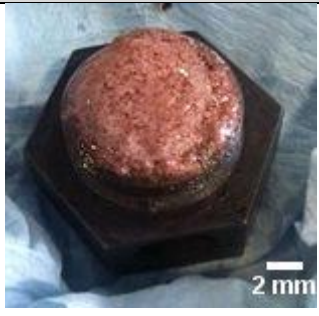
Figure 5.13; Feedstock with different powder loading ratio; (a) Powder loading with 55% volume, (b) Powder loading with 60% powder loading





5.3 Identification of Binder System: PEG-PMMA-SA system

Based on the finding discussed in previous sections, the optimum powder loading lies within the range of 54-58% vol., with critical powder loading at 60% vol. The chosen powder loading fraction is better set at a higher concentration of a powder. Thus in the present case, the high concentration of 60% vol. should be acceptable. According to [259], higher powder concentration helps minimize shrinkage during the sintering process. The percentage of space holder will be added to the solid content within a range of 50-75% vol.

The 40% volume of the binder must then be divided into the three components with the appropriate weight fractions. This process is based on an experimental trial in which any changes in the physical behaviour of the sample can be immediately identified, and the ratio can be modified precisely. As stearic acid (SA) is maintained at a constant weight percentage (5% wt.), the focus of the experiment was on varying the amounts of PEG and PMMA. Based on the findings of [102], [195], [265], [266], the weight percentage of SA was kept at 5% wt. SA is expected to serve as a surfactant and improve the wettability of the mixture throughout the mixing process and does not have a substantial effect on the flowability and structural integrity of the material. While for PEG, the amount of this binder was set at a maximum value of 83% by weight (which was set in reference to [163]) before gradually decreasing to 65% (all tested ratios are shown in Table 5.5). Each result was recorded and analysed until the optimal binder system was determined.

Table 5.5; Examples of findings based on the binder system variation

Solid loading (Solid loading – binder)	Binder system % wt. (PEG-PMMA-SA)	Result	Physical figure
60%-40%	83-12-5 [163]	The feedstock exhibits lower viscosity behaviour	
	81-15-5	Similar result with 83% of PEG content. Lower	

	79-17-5	viscosity. Separation of powder-binder components. No shape of feedstock	
	77-20-5	The feedstock can easily flow out from the injection barrel without any pressure. Poor mould shape.	
	75-20-5 73-22-5 [267]	The feedstock shows good behaviour of viscosity and exhibits a cylindrical shape	 
	70-25-5		
	67-28-5 [102]	Clog in the injection nozzle	-
	65-30-5		

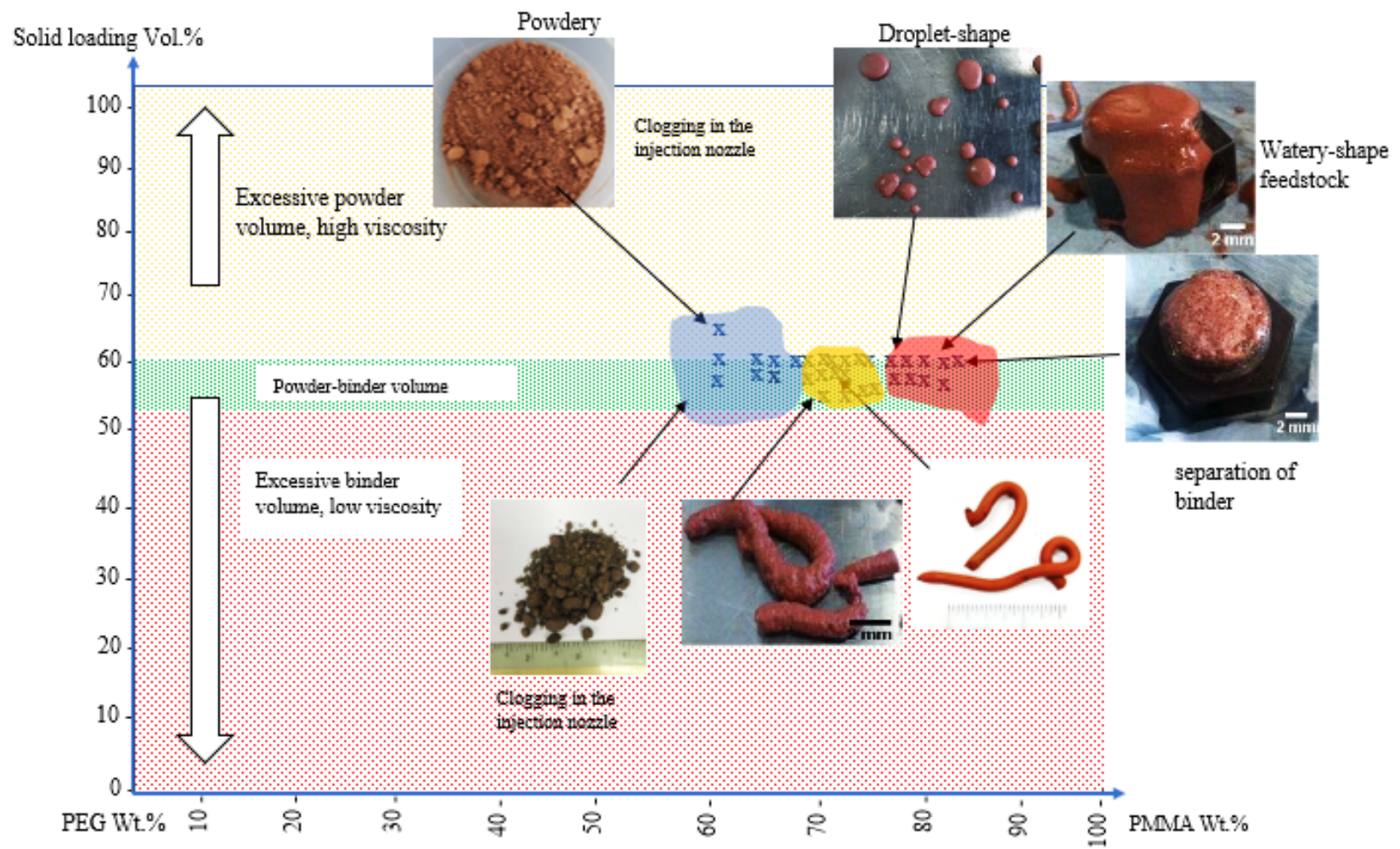


Figure 5.14; Powder-binder ratio versus binder system

In order to find the right amount of each binder component, the present works have been experimentally conducted based on the powder-binder ratio results (explained in the previous section). This means that 40% volume of the binder will be the maximum limit that can be used. Then, the PEG-PMMA-SA ratio was identified in weight percentage which the SA amount is constant at 5% wt. Thus, the trials were based on the varying weight of PEG-PMMA. As shown in Figure 5.14, many tests were conducted with different powder loading volume percentages along with the variation of PEG-PMMA weight percentage.

The green shaded area represents the optimum powder loading with 60% volume as the critical powder loading, which acts as a reference boundary for porous Cu processing. The ranges of the optimum powder loading were obtained from the tapped density measurement and the rule of mixtures (ROM) discussed in the previous section. Therefore, any testing outside of the green area will not be conducted, which will minimize the waste of materials. The experiment was focused on varying the weight of PEG-PMMA, starting with 65% wt. of PEG. The colour-shaded area represents a different outcome where the feedstock has the propensity to clog during the injection (blue area). PEG amount between 65 to 70% wt. demonstrated dry and fragile features. The mixtures were not blended well and were difficult to mould. From the observation, some of the samples showed the separation of KCl-Cu, and the sample tends to be observed with problems associated with flow behaviour when the PEG amount is lower than 70% wt. Although the powder-binder ratio is still within the range of the optimum solid loading amount, it results in powdery-type feedstock, and this is probably due to insufficient PEG amount. The binder is unable to coat the powder particles fully and prepares the powder with a thin layer of bonding. Consequently, the mixtures were prepared with high viscosity, leading to the injection clogs. Thus, it is clearly concluded that the roles of PEG relate to the flowability of feedstock. In the opposite condition, the red boundary area shows an excessive PEG amount. Too much PEG compared to PMMA leads to a watery-type feature that cannot be moulded and retain a shape. At 77% wt. of PEG, the feedstock started to leak from the injection barrel and slowly formed a droplet shape. Then, the results became worst once the PEG amount increased to 83% wt. The feedstocks were displayed with lower viscosity, making them easy to flow, resulting in poor moulding characteristics. This is probably due to powder-binder separation, as the amount of powder is not enough to balance the viscosity of the feedstock. The yellow area is where good quality feedstock fabrication is found where PEG with 70-75% wt. shows promising results with an adequate PEG-PMMA balance ratio. The feedstock shows good viscosity behaviour and exhibits a cylindrical shape. Thus, for the whole process of porous Cu, a binder system with 73-22-5% will be selected as the amount present in the mid-range of the acceptable PEG-PMMA-SA ratio, as previous works [267] shows the promising result of Cu feedstock with a similar ratio.

5.4 Feedstock preparation by Mixing Process

A good feedstock must have the right fraction and give effective MIM processing behaviour, such as homogeneous mixing. [268] defined these two factors; solid loading and mixing procedures, as crucial aspects to specify as part of feedstock development. The binder should coat the particles homogeneously with thin layers without showing signs of binder segregation. This feature is important for successful injection and later stages of the MIM process, such as debinding and sintering. However, this criterion will not be fulfilled without proper mixing. The mixing process can be conducted in a continuous or batch process, should produce a homogenous mixture and be free from agglomeration [269]. Poor mixes will be produced if it is not done properly, as seen in Figure. 5.15. In parts a and b of Figure 5.15, the binder does not bond the particles, and the mix is not homogeneous, leading to poor MIM processing and parts that cannot be corrected at later stages of processing. Figure 5.15c shows the raw shape of feedstock with a good mixture.

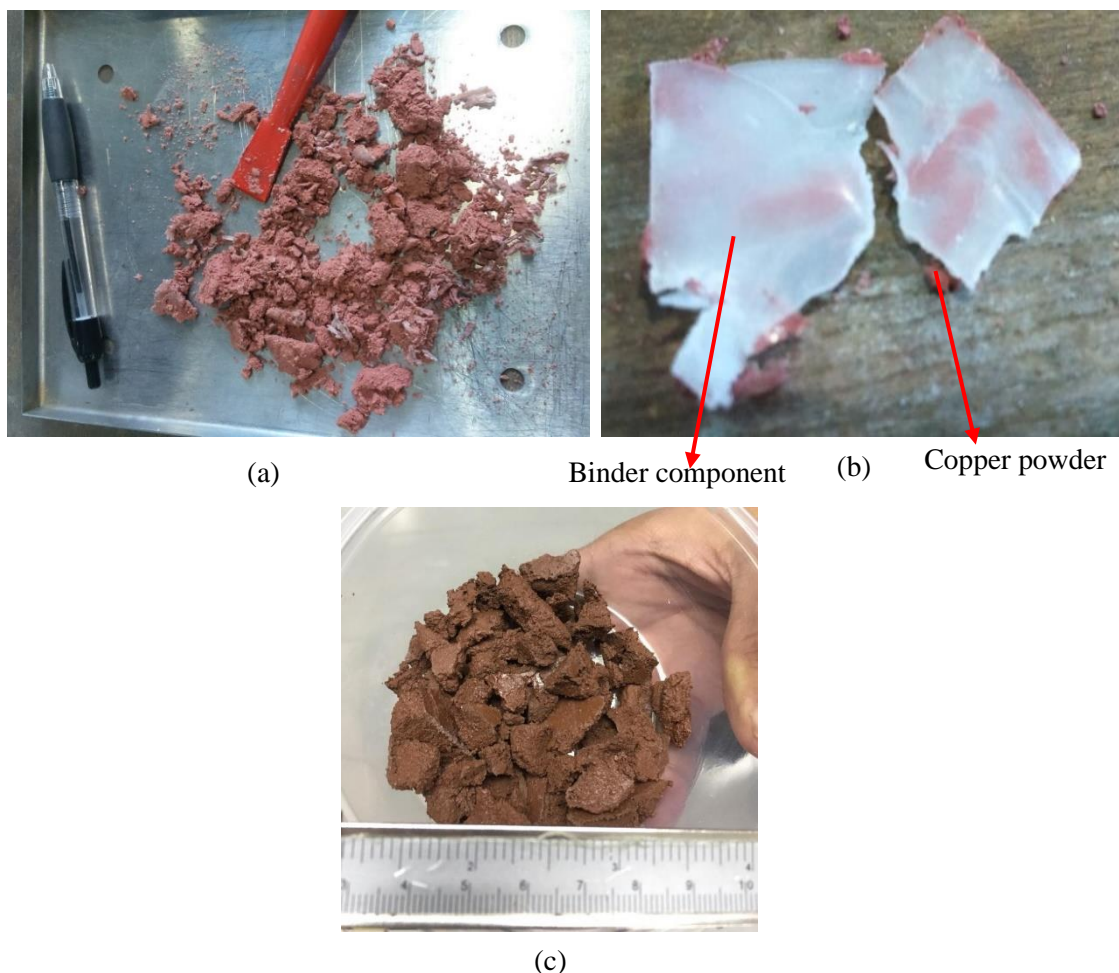


Figure 5.15; Example of the result of poor mixing, (a) The feedstock shows powdery form and incorrect shape, (b) separation of binder and Cu powder, (c) example of the desirable final feedstock of porous Cu

The feedstock mixture must be homogenous and exhibit good flowability behaviour, regardless of the mixing technique employed. Supati [202] outlines the main factors influencing the mixing process, such as the volume of powder loading, mixing temperature, and mixing speed. Suri [270] added the contribution of the mixing machine and its characteristics (including the mixing blade geometry) to the variables that may affect the feedstock properties. Therefore, the choice of mixing machine is important.

The conventional mixing machines (such as a sigma or Z-blade mixer, large extruder, twin-screw extruder or torque rheometer) are similar in terms of low speed of mixing, using a mixing blade, being suitable with a large amount of material (suitable for large production) and having the capability to control the mixing temperature. The features are important when dealing with metal and polymer blends. However, these mixing machines do have limitations. For example, the sigma blade mixer designed with a permanent mixing chamber can cause issues with cleanliness as the chamber can be difficult to clean. Another weakness of many traditional mixing machines, such as sigma blades, is that they usually run at a sluggish mixing speed (approximately 55 rpm [179]). Previous studies took more than one hour [179], [143] [271], and some of the previous works even required longer mixing cycles, approximately 2 to 4 hours, and this process is without the cleaning phase. This concern needs to be resolved because it could lengthen the MIM process and not be suitable for high production. [269] also not recommend the use of a sigma blade due to the low shear mixing process as the higher shear rate of mixing is necessary to crush and knead the binders between the powders. From the perspective of material sensitivity, reactive materials such as titanium can be easily oxidised as the machine is not sealed and may influence the quality of mixing.

Thus, the present study of porous copper fabrication will use a different mixing machine than the traditional mixer. The proposed machine (High-speed mixer- refer to Chapter 3) is very different from the conventional mixing machine with the aim to improve the longer process of MIM. The implementation of a high-speed mixer machine in MIM production should be investigated, as this could save processing time. Such machines can reach 2000 rpm (depending on the type of machine) and could reduce the mixing time by almost 60-75 per cent for that required for conventional machines.

5.4.1 High-Speed Mixing Process with the Introduction of SpeedMixer Machine

The high-speed mixing process offered by the SpeedMixer machine is because of its mixing mechanism. SpeedMixer machine is designed with a dual asymmetric centrifuge (DAC) with a low-weight dual rotor. In contrast to the ordinary centrifuge process, the rotation of the samples relies mainly upon the primary rotation in the central axis, which is controlled by an electrical motor. While in a

DAC, the sample is rotated via the additional rotation around a secondary axis in response to the centrifugal forces resulting from the primary rotation of the mixing arm (refer to Figure 5.16 and Figure 5.17). Both types of rotations occur simultaneously, in the opposite direction to each other. This combination of rotations only needs a few seconds to achieve its maximum speed and blends the final sample uniformly, with a shorter overall mixing time. The SpeedMixer machine can be applied for various tasks such as mixing, homogenisation, milling etc. While it is not directly heated, frictional forces on mixing can generate a significant temperature rise in the mixture. Short runtimes produce less heat than longer processes; without a cooling system, the mixture will cool after the process is completed.

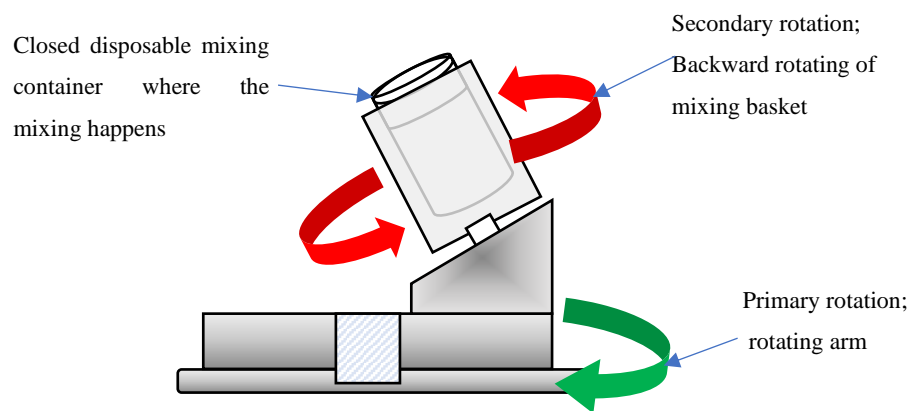


Figure 5.16; SpeedMixer schematic diagram

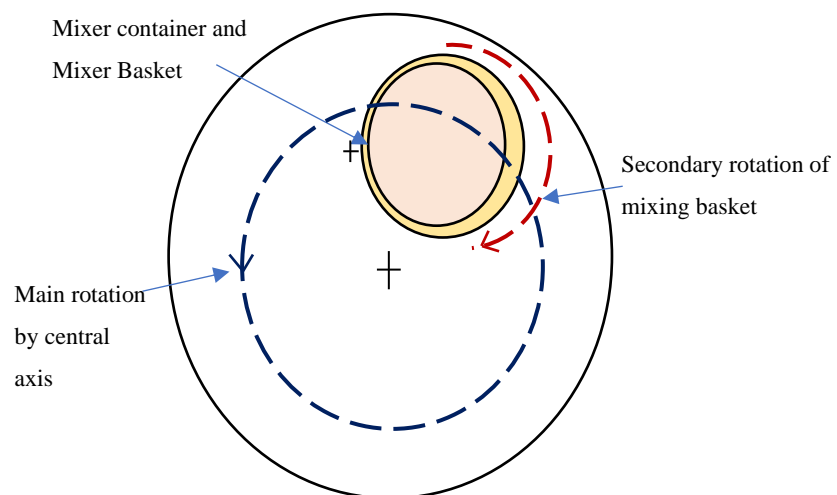


Figure 5.17; Schematic diagram of the top view of SpeedMixer

The other advantage of the SpeedMixer machine is that the mixing process can be carried out with a defined mixing program. Tools or mixing blades are not needed, as they are in many mixer

machines. This avoids the risk and costs of blades being stuck or damaged, and the closed mixing chamber makes cleanliness easier to achieve. The use of standard polypropylene mixing containers further prevents any issues caused by contamination. As the mixing containers are removable and available in different sizes, the machine can also deal with mixes of small volumes, which is highly suitable for research use. To sum up, the use of a SpeedMixer machine can offer many potential advantages for the mixing process and preparation of feedstock.

5.4.2 Challenges for Successful Mixing

The use of the SpeedMixer machine is expected to reduce the processing time, but the correct settings must be determined. The mixing setup should be properly conducted with the right setting since this mixing machine does not have its own temperature controller. The binder needs to be heated efficiently to the point where it can coat and blend with the metal powder. As shown in Figure 5.18, the feedstock exhibited poor mixing due to inadequate heating, which prevented the polymer binder from melting. This result leads to the inhomogeneity of Cu and KCl mixing. The binder components (PEG and SA) melt at a lower temperature (between the range of 50-60°C), but PMMA requires temperatures around 150°C.

The preliminary testing (Figure 5.19) demonstrates that failure will occur at an early stage of the debinding process if PMMA is not consistently mixed. The green samples were degraded after one hour to dissolve in water at 40 degrees Celsius and displayed poor structural integrity. Thus, the other challenge encountered in the present works is ensuring the solid PMMA is distributed, blends well with other materials, and speeds up the mixing process. Previous studies [102], [195] used PMMA in emulsion form to speed up the mixing process. Some work [245] also recommended using PEG in the solution form to obtain homogenous mixing and accelerate the mixing procedure. Although the emulsion PMMA offers some performance advantages, the present works will focus on the solid type of PMMA in order to reduce costs (the powder form is around half the cost of the emulsion), and [269] agreed that emulsion PMMA could give additional cost. Thus, an investigation needs to be conducted to find an optimum mixing parameter (speed, time, sequence of mixing, etc.).

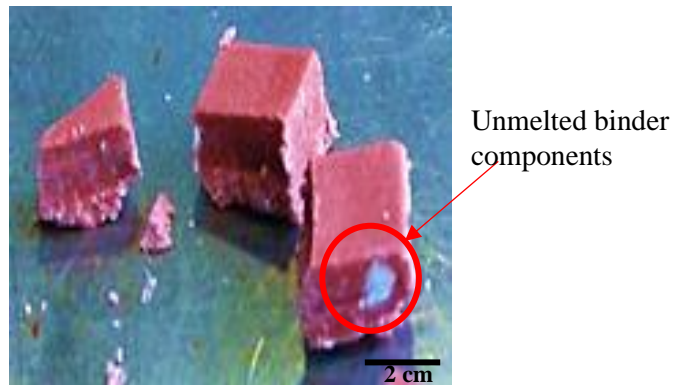


Figure 5.18; Poor mixing due to the binder not blending well with Cu powder.

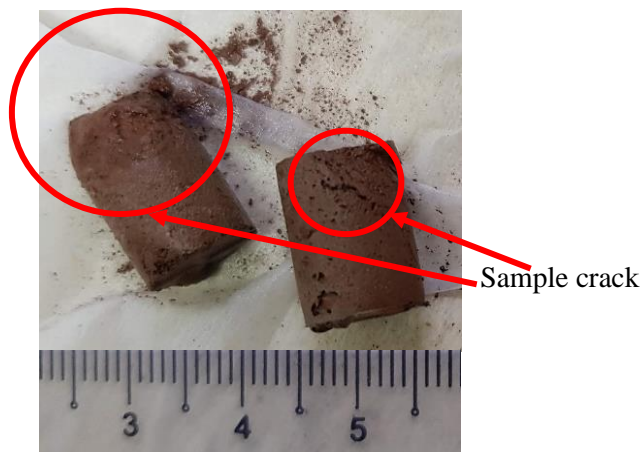


Figure 5.19; Structural failure at the green sample stage after water debinding for one hour at 40°C

5.4.3 Preliminary testing

Initially, it is important to know the actual melting temperature of binder components. Based on the DSC analysis as discussed previously, PEG and SA displayed low melting temperatures, and both recorded at 49.8°C and 65.57°C while PMMA was at 126.39°C. Since the equipment cannot directly determine and control the mixture temperature, the mixing temperature was visually observed and verified by a non-contact infrared digital thermometer.

Preliminary testing was performed to observe how high-speed mixing could melt solid polymer binders. The initial trials were focused on finding the main parameters, such as the speed and time of mixing. Trials with different mixing times (2 to 5 minutes) under lower mixing speeds, approximately 800-1000 rpm, provide no effect on the mixture features. PEG showed no sign of melting and remained

in solid states even mixed with Cu. The result can be seen in Figure 5.20. This finding is probably due to inadequate heating as a result of the low processing temperature. The particles of materials have lower friction due to slow mixing, which could make it difficult to obtain a homogenous mixture.



Figure 5.20; The investigation to find the optimum mixing speed and time to melt the binder. The process was carried out with a variation of speed and time (a) The binder was still in the solid state, (b) The shape of binder particles is clearly seen in the mixture of binder and powder (Cu, KCl)

Then, the mixing process started at a higher speed (around 1200 to 1600 rpm), as a higher speed could increase the processing temperature. However, this step should be avoided since the materials are still in powder form and easily disperse and stick to the wall of the mixing cup if the speed is too fast. The outcome of this investigation was that the mixing speed should start with a higher value as it should be slow at the outset (800 rpm) before gradually increasing. Subsequently, the different mixing parameter needs to be systematically varied to assess their effect on the mixing process. The varied parameters comprised the weight of the mixture used, the mixing sequence (all binders and powders cannot be inserted simultaneously), the mode of mixing (multiphase or single phase) and mixing speed and time.

5.4.4 Findings and discussion on the proposed mixing procedure

Table 5.6 summarises the proposed optimum mixing technique, which includes mixing speed, time, and sequence. Figure 5.21 demonstrates the morphology of the mixing process with different speeds and mixing times. The planned mixing schedule required 21 minutes to complete its mixing cycle, which included both manual mixing and the SpeedMixer Machine. This developed mixing technique has been validated more than three times and has been shown to mix powders effectively into feedstock. It has been carefully established in accordance with the properties of Cu and the water-based binder system, incorporating the optimal flow of mixing speed, time, and mixing components. It has not been tested for other systems and may or may not work for a wider selection of types of metals or binders, depending on the material properties (melting point, particle size and shape, and how rapidly the binders coat the main powder). For example, in previous work on titanium [102], [266], the researcher used different mixing procedures with SpeedMixer, which were probably different from other systems and types of materials.

From the visual inspection, the high-speed mixing process causes the feedstock to scatter and adhere to the container wall. Before the following mixing cycles, this stagnant feedstock on the container wall must be scraped off to guarantee that all feedstock material has been well-mixed. Finally, once the mixing process was completed, the molten feedstock was manually crushed while still soft. If the feedstock starts to cool and solidify, it is very difficult to cut it into small samples (pellet form), and additional heating in an oven at 60°C for 10 minutes is required to soften it.

Table 5.6; The proposed final mixing schedule for porous Cu fabrication

Sequence	Process	Item in the container	Mechanism of Mixing (Using Machine or Manual Mixing)	Speed (rpm)	Time (min)	Remarks
1	Heat the PMMA binder	Binders	SpeedMixer Machine	1000	2	Start the mixing at a lower rpm
2	Add PEG and SA and continue to mix	Binders	SpeedMixer Machine	1000	2	The binders start to appear smooth
3	Mixing process	Binders	SpeedMixer Machine	1200	1	Continue mixing at this speed
4	Mixing process	Binders	SpeedMixer Machine	1400	4	The binders start to melt
5	Add the solid powders to the container	Solid powders and binder	Manual Mix and Stir	NIL	2	Adding the powder once the binder is in the liquid stages and stir it until it looks uniform stage
6	Mixing process	All ingredients	SpeedMixer Machine	1200	2	Start at a lower speed to avoid the dispersion of powder particles
7	Mixing process	All ingredients	SpeedMixer Machine	1400	2	The mixture starts to blend and shows in 'large' particles
8	Mixing process	All ingredients	SpeedMixer Machine	1600	2	Continue mixing at this speed
9	Mixing process	All ingredients	SpeedMixer Machine	1600	2	The mixture starts to melt and shows some viscosity
10	Mixing process	All ingredients	SpeedMixer Machine	1800	2	The feedstock shows paste form shape
TOTAL					21 minutes	

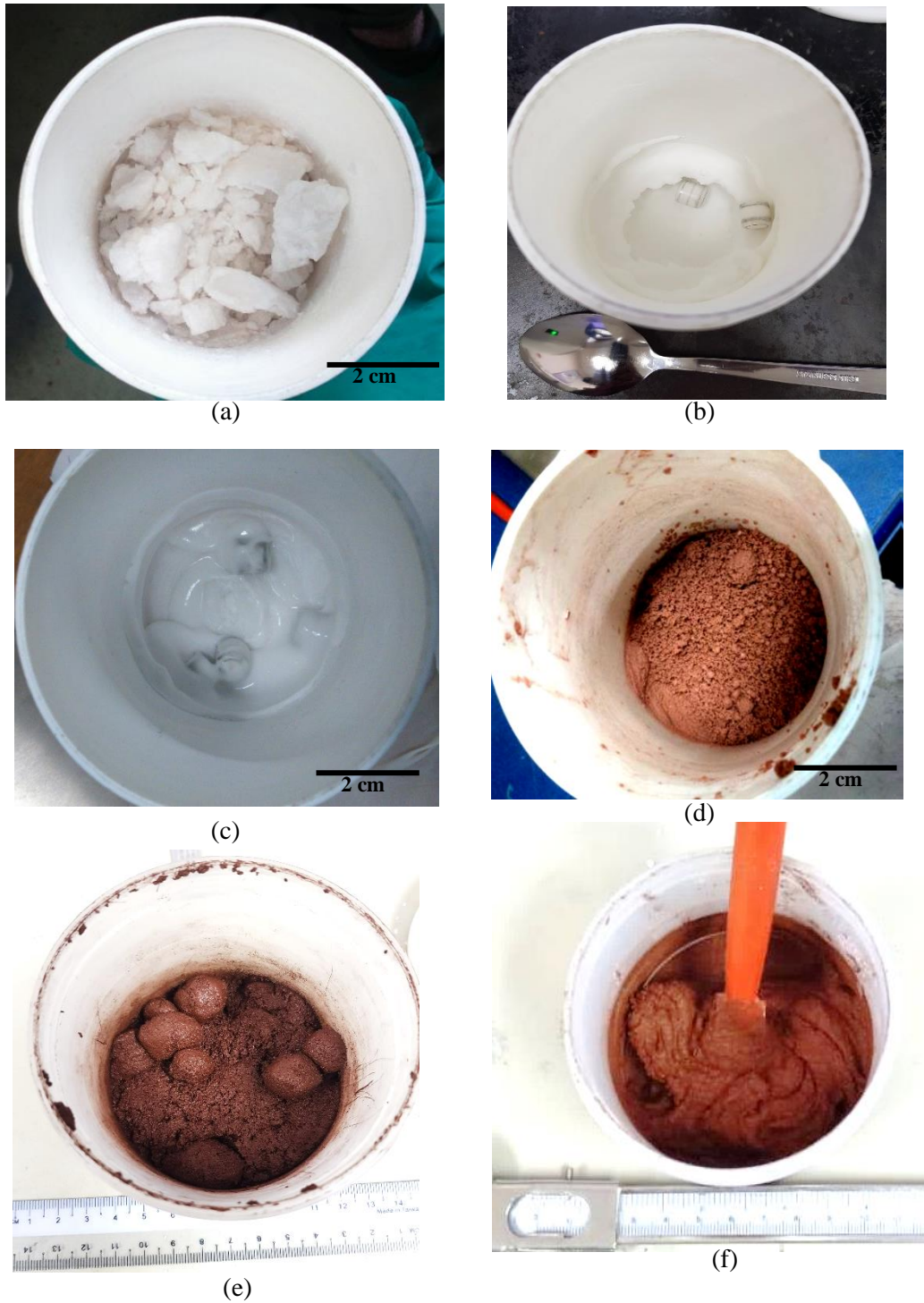


Figure 5.21; The morphology of the mixing process at different speeds and total times, (a) Sequence 1- 1000rpm, total mixing time: 2 min, (b) Sequence 3- 1200rpm, total mixing time: 5min, (c) Sequence 4- 1400rpm, total mixing time: 9 min, (d) Sequence 6- 1200rpm, total mixing time:13 min, (e) Sequence 7- 1400rpm, total mixing time: 15 min, (f) Sequence 10- 1800rpm, total mixing time: 21 min.

The mixing technique was found to have a significant impact on the final mixing results. In the present study, over 90% of mixing process sequences in the optimum method are completed by an automated high-speed mixing machine (SpeedMixer Machine), whereas just one manual mixing process sequence was undertaken (performed at sequence number 5). In general, this is good for process speed and repeatability, though it is possible that the manual step could be a bottleneck in the process or a source of variation in a scaled-up production setting. It is also important that the process steps follow each other promptly so that the material has limited time to cool. The mixing schedule was built in this manner to purposefully melt the binders before blending with Cu powder, as the binders themselves come in solid form. Then, once both powders are blended, the mixing continues with varying speeds and time to guarantee proper mixing. The outcomes will be different if the mixing mechanism is altered, using different speeds, durations, or mixing sequences. Due to insufficient heat, the binder may not melt and remain in solid form (as depicted in Figure 5.18), and burning effects will be apparent on the copper (due to longer mixing time and high speed), which may degrade product quality. In other instances, it can produce very poor results, as shown in Figure 5.19; this was the case when the Cu powder was added early in the mixing sequences and mixed at high speed and for a long period of time. Therefore, determining the proper mixing sequences is essential to enhance homogenous mixing, prevent mixing failures, and reduce material waste.

The present mixing process requires the binder components to be heated in the earlier stages of mixing until mixing sequence 5 where the solid powders (Cu and KCl) start to combine with the melted binders. The mixing speed varies depending on the mixing sequence, where the speed of mixing speed is progressively increased from 1000rpm until mixing sequence 4 with the final speed of 1400rpm. Then, once the solid powder was mixed with the binders in mixing sequence 5, the mixing activity began again with a lower speed of 1200 rpm. The speed value is gradually increased until 1800 rpm at the final mixing sequence 10. Once the solid powders combine with the melted binder (sequence 5), the mixture should be stirred manually for 2 minutes to ensure both materials blend well before automated mixing with the low speed of the SpeedMixer machine. Lower speed helps to avoid the dispersion of powder particles, possibly producing a poor mixing result. The morphology of the mixing process can be seen in Figure 5.21, in which, by the end of the mixing process, the well-mixed feedstock should appear in paste form. By increasing the mixing time and speed, the binder system starts to melt progressively due to heat generation inside the mixing container. A similar finding also happened after sequence 5 where the binder managed to coat the powders.

5.4.4.1 The processing temperature analysis

Since the current mixing machine was not designed with a temperature controller, it is difficult to predict and estimate the right temperature suitable for binder melting. As mentioned in section 5.4.3, a non-contact infrared digital thermometer visually observed and verified the temperature. Figure 5.22 shows the mixing temperature was recorded during the mixing process in order to observe the mixing temperature pattern with different mixing speeds and times. The feedstock temperature is approximately 23°C after 2 minutes of mixing at 1000rpm speed in mixing sequence 1. This low temperature is probably due to the low heat generated in the initial stage of mixing. In this stage, the binder is still in the form of particles. Then, once the mixing speed is set to a high value with a longer mixing time, the mixing temperature gradually increases, and, in this stage, the binder changes its physical state to liquid. This condition is due to the high friction of particles due to high speed, and this will increase the heat. At a certain point, the generated heat is sufficient to melt the binder. The PEG binder melts and turns into smooth paste forms as its melting temperature is about to reach more than 50°C.

After 11 minutes of mixing by SpeedMixer, the mixing process at sequence 5 (Table 5.6) was conducted by manual stirring using a spatula. This process involves the addition of powders (Cu, KCl) to the melted binders. The insertion of powders is not operated with high-speed conditions, which tend to segregate from the binders. Therefore, manual mixing makes it easier to ensure good mixing with deliberate, manual control (it is noteworthy that a degree of skill and experience are required for this step to be successful within the allotted time). In addition, by the manual mixing process, the coating of the binder-powder can be monitored to ensure both materials are mixing well. However, due to this manual stirrer activity, the temperature starts to decrease, probably due to the lower energy of manual mixing, resulting dropped temperature. The slow process of manual mixing makes less shear rate, and low friction among particles produces low heat generation. Then, as expected, during the later stage of mixing, once the mixing process continues using a high-speed machine, the mixing temperature rises rapidly along with the increase in mixing speed and time. This is probably due to the heat generated from high friction between the powder particles and zirconia mixing media. Since the temperature was recorded around 74.5°C, presumably, the stearic acid will be completely melted and mixed uniformly. It can be concluded that the correct mixing process procedure leads to melting the polymer binder materials as desired. Getting the correct mixing temperature is of great importance as it affects the quality of the feedstock. Mixing at lower temperatures means the mixture has a high viscosity and produces cavitation defects. Too high a temperature may result in binder degradation and lowering of the feedstock viscosity, which promotes the powder-binder separation. [169] reported that PEG will oxidise in the air at higher temperatures. According to [272], low-temperature mixing conditions will possess the mixtures with cavitation defects, while too high temperature resulting powder separation [202] from the binder and exhibited with low viscosity.

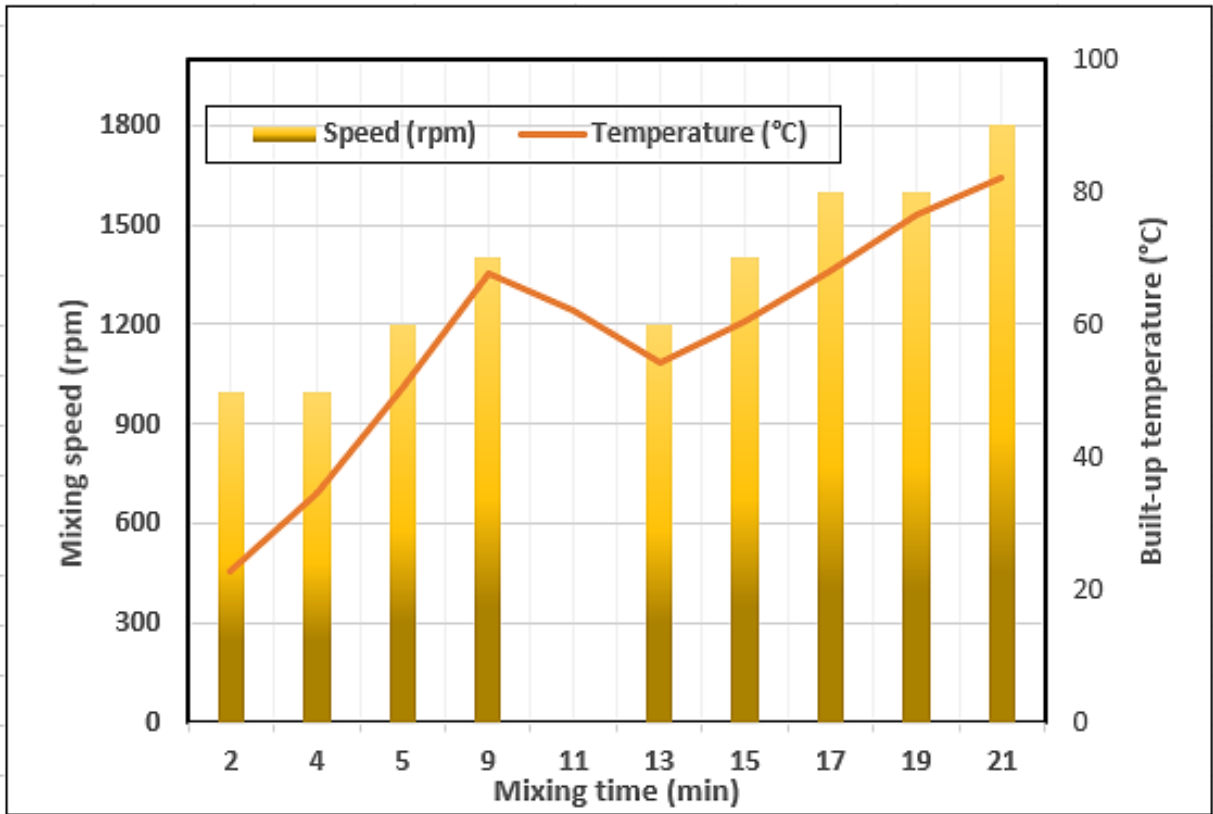


Figure 5.22; Mixing built-up temperature

5.4.4.2 The introduction of cylindrically shaped zirconia

The current mixing machine does not control temperature, making it difficult to ensure the mixture is performed at the appropriate temperature. Furthermore, from the trials, the mixing requires a longer time, even though the speed and time have been altered at the highest condition. Thus, it is necessary to find an alternative solution to promote heat and increase the mixing temperature.

The introduction of dispersion media of cylindrically shaped zirconia (Figure 3.5b in Chapter 3) during mixing shows a significant change to the mixture. As shown in the schematic diagram (Figure 5.23), the zirconia particles are freedom move during the high-speed mixing process. With the use of a number of zirconia particles and under high-speed conditions, the binders will easily be melted and well mixed with the powders. This combination assisted in increasing the mixing temperature. This zirconia media acts as ‘mixing blades’ that stir and blend the mixture. This external media also helps generate heat among particles from the friction between the mixing media and the mixture constituents.

However, the usage of zirconia dispersion media needs to be controlled and not be used for certain situations. Firstly, due to high-speed mixing, the dispersion of this external material will break up the KCl, changing its original geometrical shape and affecting the particle size distribution. This situation will impact the morphology of the targeted pores, changing the pore size and the porosity properties. A few trials show that the formation of pores was not uniform, and the porosity was far lower than the expected value. As mentioned, the formation of the pores depends on the physical properties of KCl. Thus, this problem can be overcome by limiting the usage of zirconia dispersion media. This material will be added to the mixture at the early stage of mixing, mixing sequences 1 to 4 (refer to Table 5.6), purposely to melt the binder. Then, these zirconia particles will remove at mixing sequence 5 where the KCl starts to be introduced to the mixture. In the second situation, due to high-speed rotation, the generation of energy is high, and as a result of the high thermal conductivity of Cu itself, it will create too much heat. This excessive heat can easily be transported to the polypropylene container, causing melting and resulting in big holes at the bottom of the container (Figure 5.24). Instead of altering the mixing speed and time (as the designated parameters visually demonstrate with a good result), the usage of zirconia was exceptional in the second phase of mixing (mixing sequences 5 to 10). This decision can protect the container from defects caused by excessive heat.

In conclusion, zirconia dispersion media will assist in generating heat during the mixing process and help in melting solid binders. However, the use of these materials must be controlled and restricted to specific phases of mixing rather than the entire mixing process.

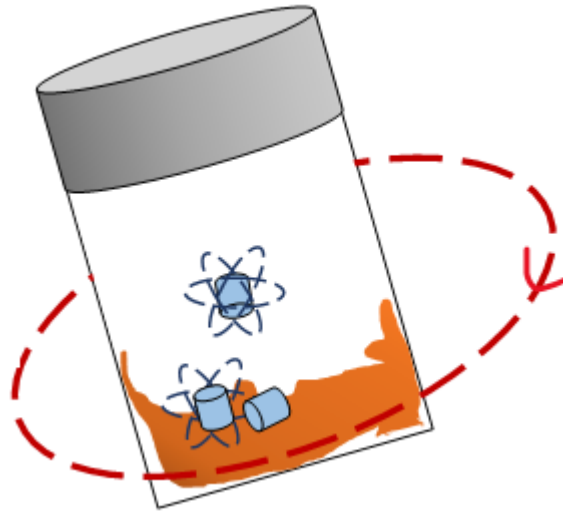


Figure 5.23; The schematic diagram of the movement of zirconia dispersion media inside the mixing container



Figure 5.24; A hole at the bottom of the mixing container, caused by overheating from high energy generation with mixing media used

5.4.4.3 The mixing speed and time

The determination of the proper mixing speed and time is crucial for the current study. This is due to the fact that the existing mixing machine (SpeedMixer) lacks a temperature controller, which is essential when working with polymer binders. Previous work [271] used the sigma-blade machine because it is equipped with a temperature controller to achieve the desired temperature, and this benefit counterbalances its slow mixing process. Therefore, the correct combination of the primary mixing parameter is essential to find the right point where the binders can melt.

This mixing speed should not begin at its maximum speed to prevent the dispersion and scattering of powders onto the walls of the container, which hinders the mixing process and produces unsatisfactory results. Mixing should ideally begin at a lower speed (1000 rpm) and progressively increase to a maximum speed of 1800 rpm. Although the SpeedMixer machine is designed with a maximum speed of 2000-2500 rpm, the machine begins to vibrate and will stop automatically under specific situations. With varying mixing times, the optimum mixing speed was determined to be within the range of 1000 rpm to 1800 rpm. According to Table 5.6, various mixing times, ranging from 2 to 4 minutes per mixing sequence, were assigned to each mixing sequence. The binder requires 9 minutes of mixing time (combined time from sequences 1 through 4) to melt and become ready to combine with powders. Previous research [169] recommended higher mixing times when dealing with PMMA. With the assistance of zirconia dispersion media, the binder is crushed and kneaded due to the high shear rate [269] before it begins to melt as a result of the heat generated during the mixing process. The mixing time and speed adjustment were made based on observations from visual inspection at two-minute intervals of mixing time.

The mixing time and speed must be correctly regulated to prevent undesirable consequences such as overheating and the production of stagnant binders on the container wall. This circumstance prevents the feedstock from becoming a uniform mixture. Observation revealed that, as a result of the higher speed, the agglomeration of feedstock decreased. This finding is similar to the [273], which provides a good indication of the mixing quality, but the high speed must be controlled because it traps air in the feedstock. The designed mixing speed and time are comparable to previous work [102], [274] since the researcher also completed the mixing process at 1300 to 1800 rpm for 16 minutes to achieve a homogenous mixture. However, according to some research [192], the mixing parameters (speed and time) were marginally lower. The mixing was performed at 600 rpm for less than eight minutes. This is probably due to the different materials employed, as the PEG content was larger (83%) than in current works.

5.4.4.4 Mixing Procedure

According to Table 5.6, the mixing procedure consists of 10 mixing sequences with different mixing speeds and times. The proposed mixing procedure is designed to obtain the molten stage of molten binders before the solid powders are added to the mixture. It is quite challenging since the SpeedMixer machine cannot control the temperature. Therefore, the mixing procedure is planned and designed with the right parameter combination in terms of speed, time, and sequence.

Although all the materials (powders, binder, KCl) need to blend, it is not right if all of these materials are mixed together without a proper plan. According to [272], mixing should start with heating a high-melting binder. This means PMMA material will be added at the initial mixing steps, followed by the remaining binders (PEG and SA). Once the binders were observed under the molten stage, the powders (Cu and KCl) were added to the mixture. Based on the observation, the temperature of the mixture was decreased with the addition of powders. This is probably because of the high heat capacity of the binder [272]. The sequence of material added in the present work is also similar based on the recommendation from [102] with the aim to get PMMA melts in the first place. Furthermore, these designated steps were proven to promote heat from the friction of materials. The arrangement is designed to prevent defects such as overheating (Figure 5.24) caused by the early addition of Cu powder due to its high thermal conductivity of Cu.

5.4.4.5 Weight of Mixture

In terms of mixing weight, although the container can accommodate around 200-250g of materials per mixing session, the present study used no more than 150g. The machine starts to vibrate and will automatically stop if the weight approaches 200g. This will not only slow down the mixing process but may also affect the mixture quality. The total weight used was sufficient for small-scale laboratory trials.

5.4.4.6 Mode of mixing

One of the advantages of SpeedMixer Machine, it offers different types of mixing modes. The mixing mode can be described as the mixing patterns and has two different modes: single-phase mixing and multi-phase mixing. The symbol of this function can be shown in Table 5.7. The main difference between these mixing modes is in their mixing pattern.

Table 5.7; Mixing Mode Phase Symbol

Type of phase mode	Symbol
Multi-Phase	-----
Single-Phase	⌈⌋⌈⌋⌈⌋⌈⌋⌈⌋⌈⌋⌈⌋⌈⌋⌈⌋⌈⌋⌈⌋

In Multi-Phase mode, this non-stop mixing approach can accelerate the mixing process without interruption, and it will end once all designated mixing cycles have been completed. However, in the context of current work, this method is unsuitable and results in numerous mixing failures. This continuous process precludes the user from frequently checking the mixture condition. Trials revealed that the mixture had flaws from overheating and processing because of this 'non-stop' mixing method. It is impossible to validate the temperature of the mixture, particularly in the middle of mixing cycles, and some trials result in excessive heating. As shown in Figure 5.25, the defect samples were obtained using the Multi-Phase Mode. The result shows a poor mixture that exhibits a fragile and powdery form. This happened because the mixture was not well blended and the separation of materials. A good mixture should consist of a smooth paste or dough. In addition, the colour of the mixture changed from orange to dark brown. This is probably due to the process of continual mixing, which causes the sample to oxidise due to excessive heat.



Figure 5.25; Defect samples obtained from the Multi-Phase Mode Mixing

In contrast, the Single-Phase mode is more flexible because it allows the user to pause the mixing process before beginning a new cycle. This sample could be immediately visually evaluated and examined. Then, specific changes, particularly to the mixing parameter, might be made if the mixtures were found to have faults, abnormalities, or physical changes. This method allows for more ‘freedom’ in the design of mixing cycles, as the present investigation involved many types of materials. In addition, this mixing mode can prevent potential material waste as soon as possible without waiting for the mixing cycles to complete. Due to its benefits, Single-Phase Mode will be chosen as the mixing mechanism in this work.

5.4.4.7 Summarisation of Mixing Parameters

Therefore, based on the preliminary testing and observations, the proposed mixing parameters can be summarised as shown in Table 5.8.

Table 5.8; Propose mixing parameters

Item	Parameter	Description
The usage of external mixing media particles	Four cubes of cylindrically shaped zirconia	The usage of the external mixing media was proven to speed up the melting of polymer binders
Mixing speed range	1000 – 1800 rpm	This is the ideal range of mixing speed. The speed initially starts at a low speed (800 rpm) before gradually increasing up to 1800 rpm.
Weight of mixture	100-150 gram	This weight range shows a homogenous mixture of feedstock.
Mode of mixing	Single-phase mixing method (mixing mechanism offered by SpeedMixer Machine)	The single-phase mixing method is used since this method allows the user to regularly check and monitor the mixing result in the middle of the mixing cycle.

5.5 Feedstock Characterisation

5.5.1 Physical observation

During the mixing process, the feedstock exhibited soft, malleable and paste form and had acceptable viscosity behaviour (Figure 5.26a). In this condition, it is easy to mould and shape, and the findings were similar for all feedstocks made with different KCl volumes. It also demonstrated that the feedstock without KCl has less viscosity than those with KCl. It was observed that the molten feedstock with zero KCl volume was easy to handle and injected into the specific mould. This is probably because both feedstocks have different densities and flowability behaviour.

The molten feedstock needs to be granulated and crushed into small particles (Figure 5.26b) for easy handling and storage. This process needs to be conducted straight away after the mixing process. If the feedstock is solidified before being converted into small particles, it is difficult to cut and requires additional cutting since the solidified feedstock exhibits a rigid structure. However, the size of solidified feedstock must be less than the size of the injection barrel for easy feeding into the moulding machine. The feedstock is kept in a closed container to avoid contamination. This dark-orangish colour feedstock shows uniform characteristics with no sign of binder-powder separation. Figure 5.27 demonstrates the physical characteristic of feedstock.

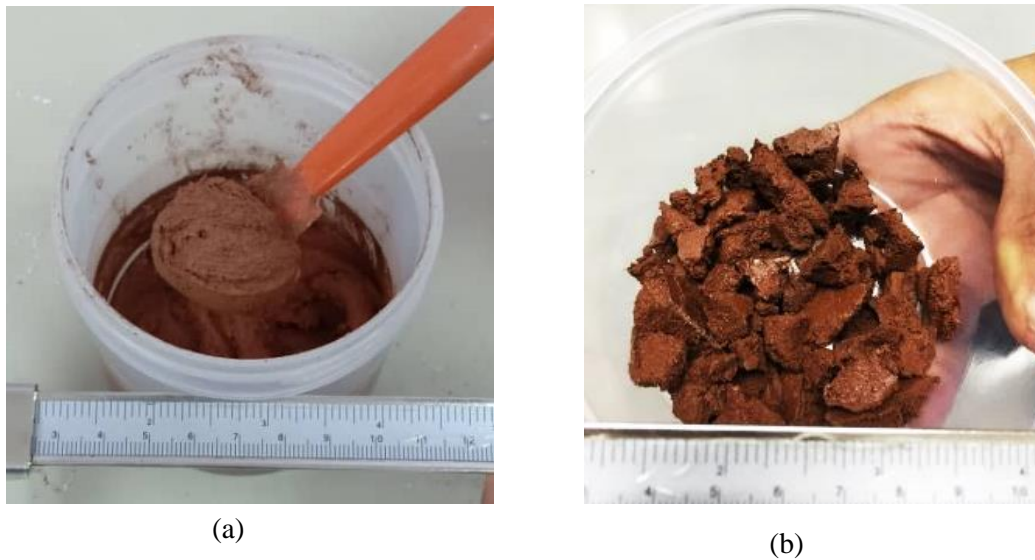


Figure 5.26; The feedstock particles after the mixing process; (a) Molten feedstock, (b) Solidified feedstock

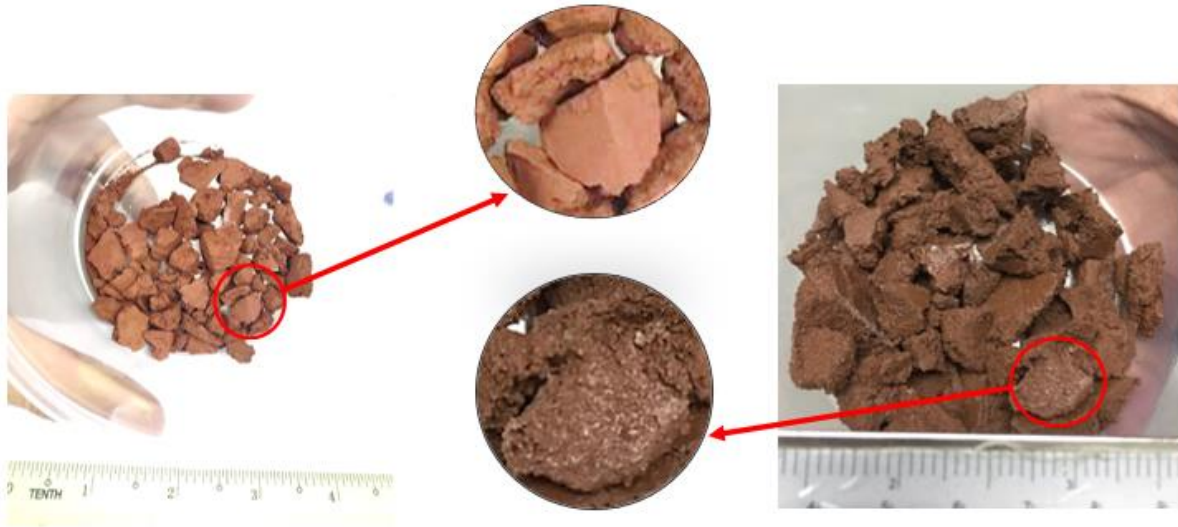


Figure 5.27; Physical observation on feedstock made with different KCl volumes, (a) Feedstock with 0% vol. of KCl, (b) Feedstock with 60% vol. of KCl

As shown in Figure 5.28a, the schematic diagram of the feedstock contains three main elements- Cu, KCl and binder constituents. Figure 5.28b shows the actual cross-sectional of the feedstock with 60% of KCl via SEM imaging. The space holder material is visibly distributed uniformly within the feedstock structure and ready for moulding.

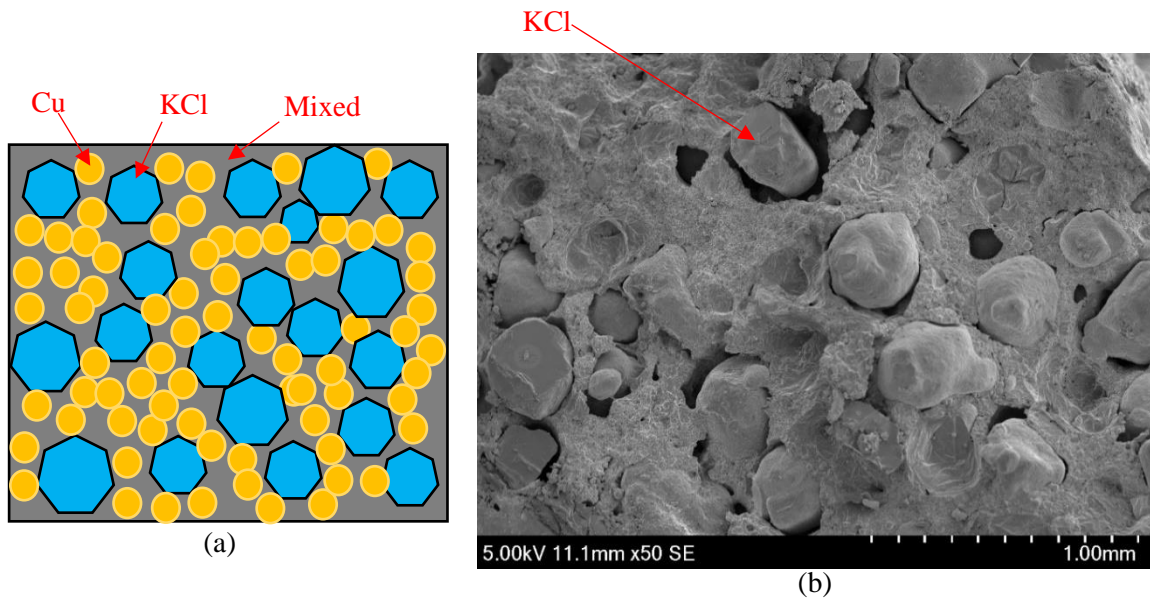


Figure 5.28; The present study of Cu-KCl-Binder mixture, (a) Schematic diagram of the mixture, (b) Example of SEM image of cross-sectional feedstock with 60% KCl

5.5.2 Thermal Analysis on feedstock sample

The thermal behaviour of the materials used in the MIM production of porous Cu must be analysed in order to design and interpret the process correctly. The properties, such as the temperature of melting and decomposition, are essential to understand since these features will correspond to the flow behaviour and mouldability of feedstock. The previous thermal analysis (Section 5.1.4.1) concentrated on pure binder components. Therefore, it is recommended to repeat similar tests on the feedstock to evaluate for changes in its melting point and temperature of decomposition.

DSC analysis was performed under a similar parameter under the controlled argon atmosphere within the temperature range of 20-210°C and 5 °C/min heating rate. As shown in Figure 5.29, the DSC curves were plotted for the MIM feedstock with 40% vol. binder. The DSC result of the pure binder component can be referred to in the previous section 5.1.4.1. The feedstock has a consistent proportion of binder and KCl. The DSC analysis of PEG, SA, and PMMA gives temperatures of 49.80°C, 65.57°C, and 126.39°C, respectively. These results indicate that each component of the binder is expected to melt close to these temperatures. However, when DSC experiments were conducted on the actual feedstock in which all binder components were combined, as indicated in Figure 5.29, the PEG and PMMA melting temperatures were slightly increased. The new peak melting point of PEG has been determined to be 62.1 °C, while PMMA is 137.3 °C.

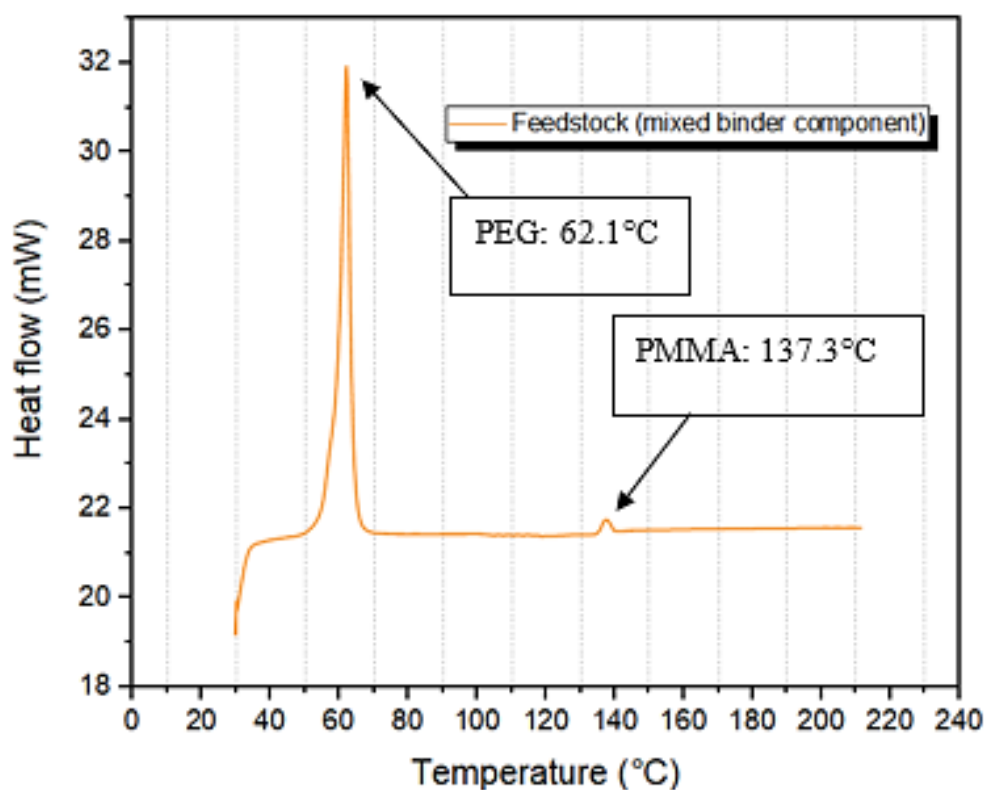


Figure 5.29; DSC thermal analysis on feedstock

Previous TGA analyses on pure binder components determined that all binder components decomposed completely within the specified range. All binders started to lose weight at 50°C-100°C, and the PMMA amount was progressively reduced and almost completely decomposed at 460-500°C. However, modifying the final decomposition temperature range is necessary since the heating process will involve actual feedstock. Based on the result (Figure 5.30), the TGA study done on feedstock was slightly higher than pure PMMA due to chemical interactions in the mixed feedstock. However, the decomposition temperature of the binder is still between 460 and 500 degrees Celsius. The removal of PEG and PMMA may be more difficult at a fixed temperature. Hayat [257] discovered a number of parameters that influence the removal of PEG, such as the molecular weight of PEG, the volume fraction of PMMA, and the size and shape of the powder used. Consequently, for the current investigation, thermal debinding will be performed at a temperature range of 460-500°C, which is suitable for removing the remaining binder components, including PEG and SA. The findings of the decomposition behaviour of the binder components were comparable to those of other research [195], [219], and the small differences in decomposition pattern may be attributable to the factors of different purity weights or amounts used during TGA testing.

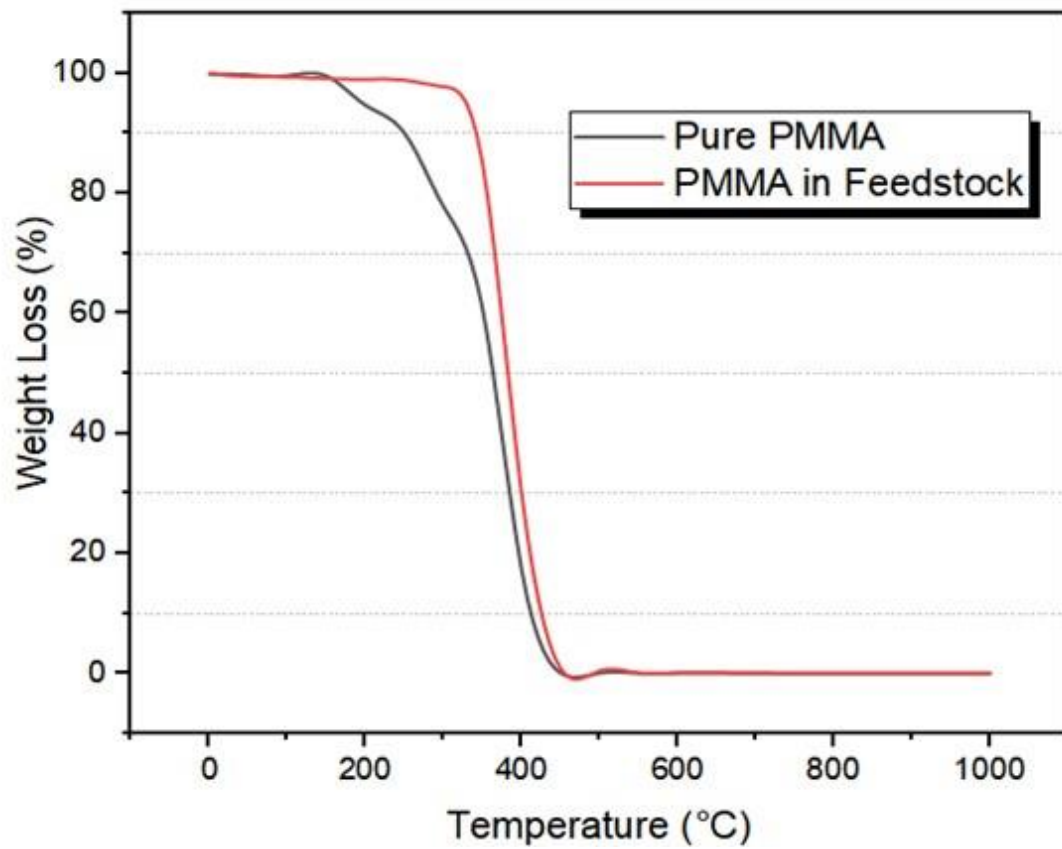


Figure 5.30; TGA analysis comparison between pure PMMA and feedstock

5.5.2.1 Discussion on thermal analysis of feedstock

It is important to understand the thermal behaviour, since the MIM process involves thermal processes in moulding, debinding, and in sintering processes. For the present study, the data are specifically used to identify the optimal range of injection temperature since the feedstock has been made with different types of materials (Cu, binders, KCl), and the injection process temperature cannot be selected with reference to the behaviour of a single material on its own. The temperature could be increased, as in [219], due to different powder loading and reactions between binder components in the mixture. The DSC results, therefore, give an estimate for the initial temperatures to be tested. DSC and TGA have been conducted on the feedstock, and the findings act as a guideline to estimate the optimum processing parameters during debinding, as well as the sintering process. The data show different ranges of melting points for each of the binder's components once these binders were blended into feedstock form.

From Figure 5.29, two endothermic peaks were clearly shown (feedstock sample), indicating the melting temperature of the PEG and PMMA. The first endothermic peak was detected around 61-62 °C, which corresponds to the PEG component of the binder melting. However, this peak was much lower than the second endothermic peak observed between 135-137°C. This range indicates the melting phase of PMMA, and the finding was comparable with previous work [102]. In addition, PEG might be evaporated during the high-speed mixing or hot extrusion process of the injection phase. This finding can be verified by the result of mixing built-up temperature (Figure 5.22) during the high-speed mixing process. The evaporation of PEG might occur during the 'rest' periods in the mixing sequence. The melting temperature of the PEG was increased from 49.8°C on its own (pure form, Figure 5.5) to 62.1°C (feedstock form, Figure 5.29), while PMMA shifted from 126.4°C to 137.3°C. This is believed to be because of the interaction between PEG and PMMA during the feedstock preparation and is similar to that seen before [102], where this change was interpreted as showing an indication of binder interaction at the structural level due to the mixing of crystalline (PEG) and amorphous (PMMA). PEG is a crystalline solid, and the melting point relies on the molecular weight, while PMMA is an amorphous polymer that has a glass transition temperature of 106°C [169]. According to [275], the interaction between PMMA-PEG can develop crystalline-amorphous regions once the PEG content is more than 35 wt.% (where it can form a network), which corresponds to the new melting point peak. [276] claimed that the shifted peak in the feedstock mixture is due to the compatibility effect of each binder. However, other work [169] has reported that the PEG component tends to segregate from the amorphous component.

Lastly, it also noticed that the peak for SA is not detected for the present study, probably due to a small amount of SA in the feedstock mixture (a similar finding to a previous study [277]). As a conclusion from the DSC finding, the injection temperature range for investigation was set at 130-175°C to ensure all binder components were likely to be melted. This temperature range is similar to that used in previous studies [161], [195], [244], which reported good green samples using different metal powders. For the water debinding stage of the process, the processing temperature was chosen to be 50-60°C to ensure the PEG component is completely removed. The samples are expected to retain their shape due to the roles of PMMA, as this binder component was also not affected by the water dissolution process.

Although PEG and SA were mainly designed to be eliminated via water dissolution, the other binder component, PMMA, required a thermal debinding process. Thermo-gravimetric analysis (TGA) provides thermal properties information which is useful for the thermal debinding processing setup [256]. The analysis monitors the change in the weight of the sample as it is subjected to increasing temperature. TGA analysis estimates the amount of binder removed from the feedstock under different conditions. In the present study, this thermal analysis was used to predict the optimum decomposition temperature of binder components. It is useful to design the heating cycle of the thermal debinding stage. Even though both PEG and SA were ideally to be eliminated via the water dissolution process, the selection of the right decomposition temperature is important to ensure all binder constituents are completely removed during the thermal debinding.

It was demonstrated that the PMMA in feedstock would start to have a high rate of weight loss (Figure 5.30) once the processing temperature reached 375°C, and this continued until it reached 460-500°C. This finding showed that PMMA would be completely removed at the highest decomposition temperature, 460-500°C. There were slight changes in the PMMA decomposition temperature between pure PMMA and PMMA in feedstock form, as shown in Figure 5.6 and Figure 5.30. Pure PMMA displayed a lower decomposition temperature compared to PMMA in the feedstock. This result might be due to the chemical interaction between the binders. Hayat et al. reported [257], [278] that many factors affect the removal process, such as PMMA percentage as well as powder properties.

In conclusion, the findings from the thermal analysis are important to accurately design the debinding process of the binder components, together with KCl (the space holder material). The combination of removal routes of water dissolution (for KCl, PEG and SA) and thermal decomposition for PMMA can be a potential solution for the time-consuming problem in the binder/SH removal process and is consistent with findings from other material processing [195], [219], [244].

Chapter 6 MIM-SH METHOD: POROUS CU PRODUCTION

6.1 Introduction

As the finished feedstock has displayed a good mixture, the injection process should be carried out efficiently without encountering difficulty during the moulding process and relatively easy to inject. However, the injection process parameters should be examined in order to find the optimum parameter.

6.2 Pre-injection process - Free flow injection (without using mould)

Although the feedstock was displayed with a good quality mixture and no sign of defects, pre-injected activity should be conducted as compulsory practice before the actual injection is taken place. This process purposely identifies the best possible condition of feedstock that should be injected at the right time and proper temperature. Furthermore, this practice is essential to observe the flow shape of feedstock that should be in proper shape based on the recommendation of a previous study [195]. Then, the feedstock shape is physically examined, giving an initial prediction of the successful injection process, and the sample can proceed to the next MIM stages.

This free flow injection process instructs that the feedstock is injected out from the injection barrel without being subjected to specified mould and die. This pre-injection was performed at the temperature range between 150°C to 180°C, where the polymer was estimated to melt and flow. The feedstock was injected around 2-5 mm under different settings and repeated to obtain optimum conditions. The pre-injection process will be assessed in terms of the shape of the flowing feedstock and the holding time.

6.2.1 Identifying the shape of flow feedstock

As shown in Figure 6.1a, the feedstock was presented with long-cylindrical shapes once it was extruded under the specific injection parameters. This finding was similar to the suggestion from [195], as the feedstock should maintain a desired cylindrical shape. Furthermore, the feedstock should be in continuous flow after it is injected. These findings indicate that the binders were well-mixed with Cu and KCl and show

a homogenous mixture, as there is no sign of powder-binder separations. The report from [163] discussed the physical properties of injected feedstock. The characteristic of feedstock that displayed with long-cylindrical shape demonstrated good flowability and was easy to inject into the mould with certain pressure. Therefore, the subsequent trials were performed with a specific mould to verify the claim from [163]. As predicted, the results show positive outcomes that the feedstock was successfully injected and filled the mould (Figure 6.1b). The feedstock demonstrated excellent viscosity as they filled the mould without any sign of defects such as flashing or clogging in the inlet of the mould. Additionally, the feedstock appears to be compatible with the lower injection pressure of the existing injection moulding machine. This finding is important since the injection moulding machine cannot be conducted with high pressure.

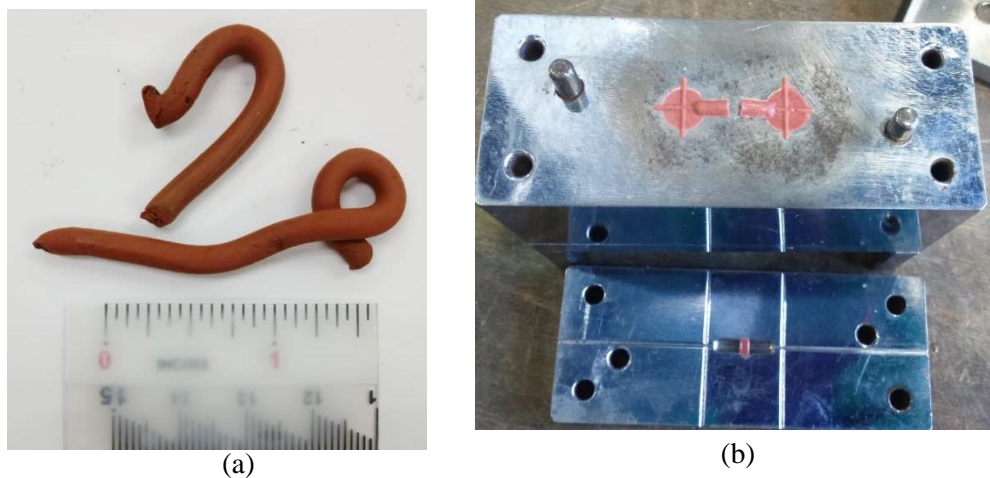


Figure 6.1; Cu feedstock, (a) Good feedstock quality in the form of continuous flow cylindrical shape, b) The feedstock was successfully filled inside the mould.

Furthermore, this pre-injection process helps to screen and examine the feedstock. As the present works have limited material resources, this screening activity may reduce the potential waste from the defects feedstock and avoid the processing failure for later stages of metal injection moulding. Some trials show poor injection processes, as shown in Figure 6.2. The injected feedstocks were not in a continuous cylindrical shape. The feedstocks were displayed with a watery-look of feedstock (Figure 6.2a), droplet-look feedstock (Figure 6.2b) and feedstock with binder separation (Figure 6.2c). These defects probably happened to certain factors. The powder-binders recipe is probably not a proper ratio, as the PMMA amount is insufficient to retain the shape of feedstock and appears in the molten stage. The improper mixing procedure might also cause this failure. The mixing is probably conducted with a lower speed (800-1000 rpm) under the low mixing time. The feedstock displayed with powder-binder separation is probably due to high mixing temperature [202] that leads to an inhomogeneous mixture.

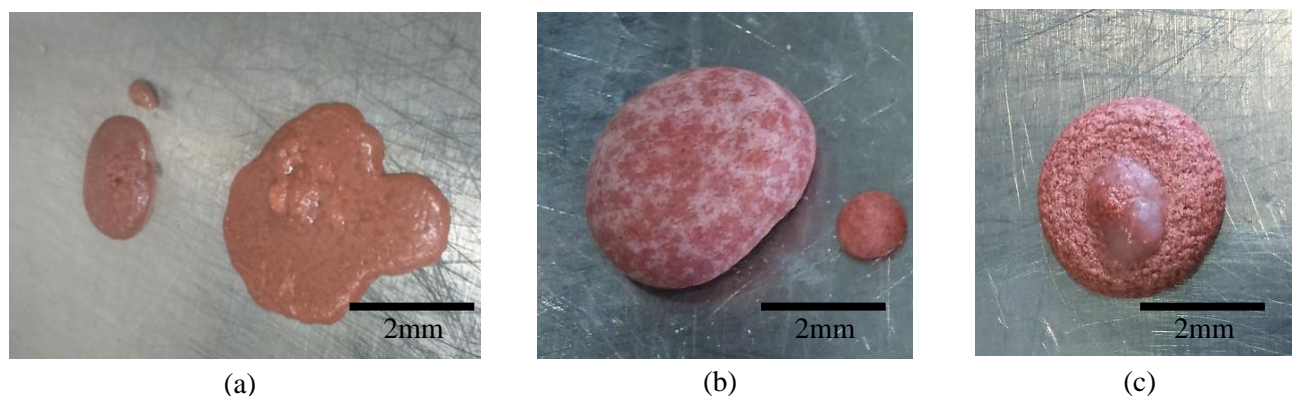


Figure 6.2; Example of defects on the feedstock during the pre-injection process, a) Watery-look of feedstock which easily flows out without given an injection pressure, b) Droplet-look feedstock that flows out without injection pressure, c) Binder separation from the feedstock

6.2.2 Identifying the optimum holding time for feedstock melting

Before starting the injection process, it is necessary to heat the injection barrel to a specific temperature. With this condition, the feedstock will get enough heat to melt and be easy to flow. This process takes 20-40 minutes to gradually rise from zero temperature to the proper temperature range but will not take long for the subsequent cycles. This condition is probably suitable for the current custom-made vertical injection moulding and may differ from other injection mouldings. Then, the crushed feedstock particle will be inserted into the heating barrel and held for some time before initiating the injection process. Then, the investigation to find the suitable holding time was carried out for the injection moulding parameter.

From the trials (as displayed in Table 6.1), the optimum condition for feedstock holding time is between 10-15s before the injection process takes place. In this condition, the binder got enough heat to melt and then easily flow with a small injection pressure setup for this study (45 MPa). This can be explained by the heat transfer from the heated barrel to the feedstock, which requires a certain amount of energy to melt the feedstock. Once the equilibration temperature occurs between the feedstock and the heated barrel, the feedstock gets enough energy to transition from the solid to the liquid phase of the feedstock. This indicates that the PEG binder has reached a melting point within 10-15 seconds, allowing them to melt. It also states that if the Cu feedstock does not receive enough heat, it will not melt uniformly and will exhibit high viscosity behaviour. The feedstock could not be injected and flowed due to its high viscosity which caused a clog problem at the mould nozzle, and the feedstock got trapped inside the heated barrel. The finding is shown in




Figure 6.3, where the Cu feedstock was stuck and could not be injected. Based on the observation, all feedstock particles added to the heated barrel had already melted but possessed a high viscosity. The Cu feedstock was also blocked at the injection nozzle, as expected.



Figure 6.3; The Cu feedstock trapped inside the heated barrel.

On the other hand, prolonged holding times for Cu feedstock may cause it to be overheated due to excessive heat exposure. This overheated feedstock commonly happened on the remaining feedstock inside the hot barrel and appeared in dark brown colour (refer to Table 6.1). Although the feedstock was demonstrated with a long-continuous shape, this parameter should be avoided to prevent contamination. Most of the finding shows sign of burning and the colour changing into dark brown if the holding time is more than 16s. Thus, for the present study, the amount of supplied feedstock should be adjusted before filling in the barrel to cater to one injection shot. This condition will prevent the left-over feedstock inside the injection barrel. For the new cycle of injection, the new feedstock will be used.

Table 6.1; The identifying of the optimum time for filling the feedstock inside the heating barrel

Holding time	Observation	Image	Comment
0-9 s	The Cu feedstock is still in a solid state before it starts to melt. Difficult to inject.		Not recommended for injection process where it may lead to feedstock clog in the barrel as well as at the head of the nozzle
10-15 s	This is the optimum condition where the Cu feedstock melts with a certain viscosity.		Recommended time for injection.
16 s onward	The Cu feedstock current exposed overheating, which leads to burning, and the colour changes from orange to dark brown.		The feedstock can be injected but not recommended. Longer injection time.

6.3 The Injection processes

The vertical injection machine employed in this study (discussed in Chapter 3) is easy to operate and control. The investigation of the injection process will focus on determining the optimal injection temperature and other variables, such as injection holding time and sample handling. The current machine was built with a constant injection pressure of 45 MPa. Therefore, each sample was injected at the same pressure. In addition to identifying these parameter characteristics, the proposed injection process arrangement should minimise any potential defects that may occur during the moulding process.

The good quality of the mould sample could be predicted based on the quality of the mixture. Once the injection setting was properly checked, the injection process was conducted with constant pressure and the temperature was set according to the findings from the DSC value. Each injection can produce two green samples per injection process, which was repeated with different space holder variations. As demonstrated in Figure 6.4a, the shape of the final green sample should appear cylindrical. Figure 6.4 (b) displays the sample failures with sample distortion failure.

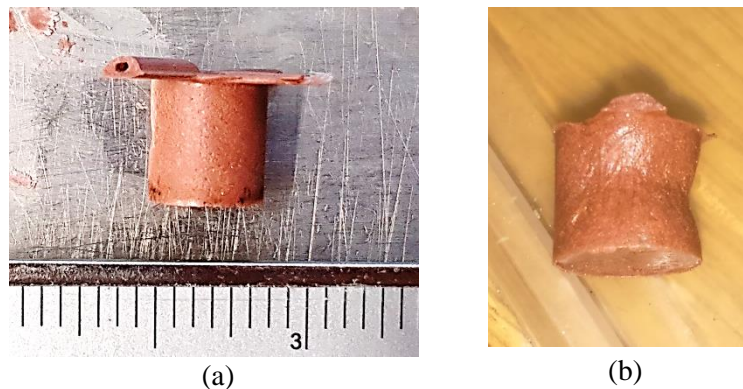


Figure 6.4; Green sample, a) good quality of the green sample, b) failure sample.

The injection moulding is the ‘heart process’ of metal injection moulding which transform the prepared feedstock particles into the specific mould part. This part can be called the green sample, representing the actual products without undergoing debinding and heat treatment processes. In this stage, the structure of the green part still consists of the elements of binders and powders. The size of the moulded part is not the same as the final part, and it will allow shrinkage during the sintering process. The temporary space holder and binder will be eliminated through the subsequent process, and the final part will consist only metal structure. In the present injection moulding process, it is crucial to successfully inject the feedstock into the desired mould and maintain the tight tolerance of the green sample.

The solid feedstock particles were supplied to the injection barrel as it was being heated at a specific temperature. The chosen injection temperature is selected based on the findings of thermal analysis (DSC) that are sufficient for the feedstock to melt. From the pre-injection process findings, the feedstock is required to 'hold' inside the heated barrel for 10-15s. The holding time is necessary to allow the feedstock to melt with proper viscosity before the injection process is taken place. Then, the molten feedstock will be injected into the cavity of the mould, where cooling and solidification happen. The shape of the solidified green sample is based on the mould design. According to [155], two main moulding parameters; pressures and temperatures, need to be controlled and optimized in order to achieve fewer defects on the green sample. Improper injection moulding preparation leads to defects such as flashing, warping and uneven density. Aslam [155] indicated that the injection relies on the factors of the quality of feedstock and mould design.

6.3.1 Identifying the optimum injection temperature range

According to the thermal analysis result presented in the previous section, the injection temperature could be set up between 150-170°C that suits the current binder system. This temperature range should be enough to melt the binder fully, and the injection process can be performed. Although the temperature setup is based on thermal analysis findings, a few systematic tests need to be performed to identify the suitable injection temperature since each sample comes with a different space holder amount. This variation may affect the flowability of feedstock, and the injection temperature may be different for each condition.

Table 6.2; Injection testing to identify the suitable injection temperature for different sample conditions.

Injection temperature, °C	KCl variation, Vol %				
	75	70	60	50	0
Below than 150	Clogged and cannot proceed for injection				
150-160	Good flow	Good flow	Good flow	Clogged	Clogged
160-165	Good flow	Good flow	Good flow	Clogged	Clogged
165-170	Good flow	Good flow	Good flow	Good flow	Good flow



Figure 6.5; The feedstock 'stuck' at the inlet and cannot flow to the mould.

As displayed in Table 6.2, the finding shows that all samples are suitable for injection at the temperature range of 165-170 °C. If the injection temperature is low, the injection faces a problem where the feedstock clogs and cannot flow through the mould (Figure 6.5). The feedstock was not getting enough heat to melt and exhibited in partially melted shape with low temperature. Then, with high viscosity, it is difficult for the feedstock to flow easily through the inlet and then clogged.

According to the findings, samples containing no KCl are difficult to inject at low injection temperatures. This indicates that these samples can be injected between 165 and 175 degrees Celsius. As KCl particles were added to the mixes, the injection temperature decreased, as 75% of KCl may be injected between 150 and 165 degrees Celsius. This can be explained by the feedstock densities. The higher the KCl volume added, the less Cu. Consequently, this mixture has a low viscosity due to its low density. It requires a minimum temperature range to create adequate heat in order to melt the combination. Nonetheless, samples with the highest Cu content tend to have greater viscosity. This circumstance demands extra energy to turn the solid feedstock into a liquid state. However, in certain experiments, increasing KCl content makes the sample difficult to inject. This is probably due to the characteristics of KCl. As the size of KCl (315-333m), which is six times larger than the size of Cu, and the variance in its volumes, effective binders are required. To achieve the desired viscosity, binders must be able to cover all particles. The investigation revealed that some components were not well combined, resulting in inadequate viscosity. Thus, the mixing parameters were modified to produce a more effective mixture. The current findings are comparable to the previous study [279]. More space holders were added, less metal powder and the wettability of the mixture became higher and less viscosity. The viscosity varies due to the metal-space holder variation, but the binders were maintained. Higher content of space holder, less heat to be used to melt the mixture.

The injection temperature for all samples in the present study was chosen between 165-170°C. This high injection temperature range allows all samples to be injected at the same temperature, reducing the injection time as all samples can be injected simultaneously. In addition, since the injection process can be proceeded within the temperature range, therefore no need to implement the injection of more than 170°C. This direction can prevent the waste sample since the present study has limited material resources. The injection temperature and pressure may vary according to different factors, such as materials, binder system, and machine capabilities. Previous work [280] suggested that the injection moulding temperature should not be more than 200 °C as it is believed to be the common melting point for binders. [249] managed to produce parts with good strength with an injection temperature of 145°C on stainless steel using similar PEG-PMMA-SA binders. This value was slightly lower than the current works, probably due to certain factors. Their water-based binder system was designed with different volumes (73% PEG, 25% PMMA and 2% stearic acid), and the PEG comes with higher mol. weight (PEG 4000). Then, their works used 4 ml acetone (per gram of PMMA) in feedstock, which is believed to improve the viscosity of feedstock. The use of these parameters probably contributes to the lower injection temperature.

6.3.2 Identifying the holding time for moulding process



Figure 6.6; The green sample that does not completely fill up the mould and solidified

Although the main injection parameter has been identified, some trials show defects, as shown in Figure 6.6. According to [281], these incomplete defects were caused by low temperature and pressure. Without proper parameter values, it is hard for the melted feedstock to flow and fill the cavity before solidification occurs. However, in the context of current works, pressure factors can be neglected since the work used constant pressure value. Furthermore, the temperature was set according to DSC and TGA thermal analysis, as the temperature represents the melting point of the binder. Therefore, this can be further investigated on a different parameter, such as injection holding time.

Once the melted feedstock was injected into the mould, the next consideration was to identify the duration that the green sample required to cool inside the mould before it could be pulled out properly without any shape defect. This aspect is essential to ensure the green sample has sufficient holding time to be moulded and fill the cavity, and with the right holding time, the sample can be ‘cool’ and maintain its desired shape. During the investigation, the testing showed that if the green sample was pulled out too early, the sample tended to stick and clog inside the mould. This is because the sample is still in the ‘molten stage’, does not solidify enough and is still not in good shape during this stage. Immediate removal process to pull out them before the right holding time will result in clogging problems, and the sample was not in ‘maturity’ condition with poor quality shape. This normally happens if the holding time before the injection is below 15s and below 19s (holding time after the injection), as shown in Figure 6.6.

If the combination holding time before injection (10-15s) and after injection (20-40s), the sample has a good shape, and no defect is observed on the sample. It is believed that the sample has sufficient time to mould and complete the filling before it can be injected and has a good cylindrical shape. Then, however,

if the removal process is quite late, which is more than the 40s, the end sample comes with a burning sign. This is probably because the sample was exposed to the heat from the injection heating barrel, which affected the structure. Thus, the injection holding time for the present study should be performed between 20-40s. The investigation of the injection holding time can be referred to in Table 6.3.

Table 6.3; Identifying the injection holding time

Holding time (before injection)	Injection time (constant)	Injection holding time (after injection)	Observation
Below than 9s	1-2 s	Below than 10 s	Clogged, poor shape design
Below than 9s	1-2 s	10-15 s	Clogged poor shape design
10-15s	1-2 s	Below than 10 s	Sample with defect, crack
10-15s	1-2 s	10-19s	Sample with defect
10-15s	1-2 s	20-40s	Good shape
10-15s	1-2 s	More than 40s	Burning sign

The flow of injected feedstock can be described in the schematic diagram (Figure 6.7). According to [282], the flow of melted polymer in the cavity can be discussed into three regions. The front region represents the melted polymer that flows with a free surface with a constant velocity under the equilibrium shape. The polymer will flow and fill the cavity, and the speed depends on the injection pressure. The fountain region can be defined as the slip stage where polymer moves slower as it is near the mould wall. The lubricant region is contradictory to the fountain region, as this region is a non-stop stage of the flow. Once the melted feedstock flows into the cavity, the layer of the frozen wall will be created near the cavity wall. The heat from the feedstock will be transferred to the cavity wall, reducing its temperature. Due to the continuous decrease of feedstock temperature, the polymer of the frozen wall turns into a solid phase and starts the solidification process. With the given pressure (from the injection), the hot surface of melted polymer will get close to the frozen wall that will avoid an air gap. The longer holding time is allocated, the melted feedstock has time to flow and fill each mould cavity under specific pressure.

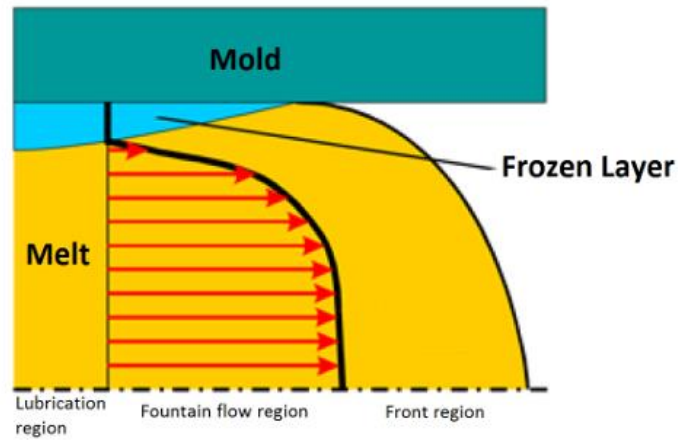


Figure 6.7; The polymer flow inside the cavity during the injection process [282]

The injection holding time is the time required for the injected materials to solidify and cool within the mould. This parameter must be precisely defined because, without sufficient cooling, samples tend to be deformed. It is believed that mould design may contribute to cooling the heated feedstock. As the feedstock is injected into the mould cavity, the heat from the molten feedstock could be transferred to the cold mould. The sample then solidified evenly. This relates to the surface area of the mould. With a larger surface area provided by the mould, more heat may be transferred, and the sample can be adequately cooled. Without correct mould design, improper heat transmission will occur.

6.4 Assessment of the sample

6.4.1 Moulding evaluation

The sample can be assessed after conducting the injection process, and the whole process was not taken much time. The moulding machine was relatively easy to handle, but needed to be aware of the heating barrel. The moulding evaluation was performed with the aim of minimising the possible defects during the moulding process. Although the injected sample was acceptable and showed the good results (refer to Figure 6.8a), in some conditions, it was observed that some of the injection processes showed defects, with both giving different end products. Figure 6.8b shows the sample with short-shot defects that generally occurred during the initial injection moulding stage. This condition happened due to incomplete die filling, probably from lower feedstock viscosity. This problem is probably because of the low injection temperature that leads to this defect. Therefore, this problem can be solved by increasing the injection temperature, and the injection process must be conducted within the optimum holding time. However, in another condition, if the temperature is set too high and together with the given injection pressure, it will lead to other defects known as flashing (Figure 6.8c). The feedstock could easily flow due to low viscosity and can flow out between the two platens gap and leave the waste of feedstock because of the further pressing of the injection piston. The feedstock not only fills the cavity but is also easy to flow out. This problem can be solved by controlling the injection temperature and allocating the right amount of feedstock to the heating barrel.

According to German and Bose [283], the large density difference between the powder and the binder facilitated the separation powder-binder. When the flow direction changes during mould filling, denser powders with greater momentum tend to continue along the original flow path and distribute unevenly in the cavity. The powder-binder separation could be influenced by a poor debinding process that may lead to uneven shrinkage.

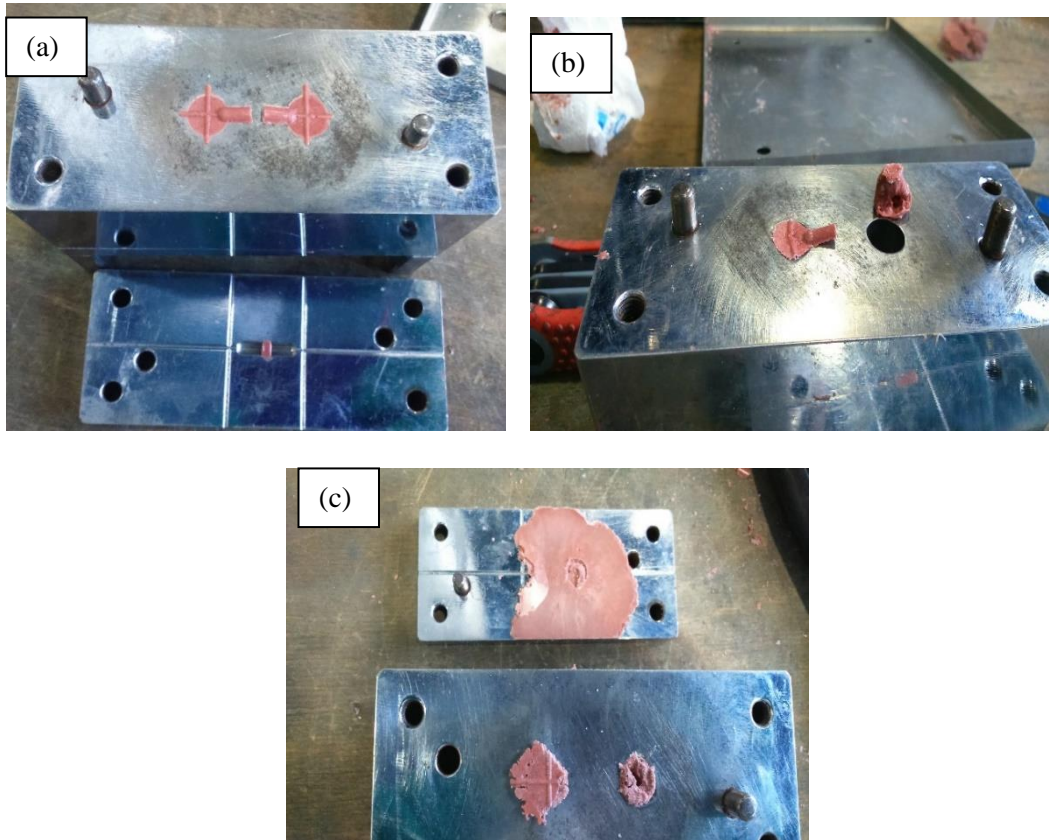


Figure 6.8; Mould parts quality checking, a) good mould sample, b) and c) defect samples of short shot and flashing

6.4.2 Physical observation

Figure 6.9 below shows the transformation process from feedstock to a green sample of porous Cu. The green sample was successfully injected without any sign of defects using the final injection parameter investigated earlier. The injection parameter consists of holding time before and after the injection process, injection temperature, and pre-injection feedstock flows shape with constant injection pressure. The operating injection pressure was set at a constant amount based on the laboratory requirement for any case of the injection process. This prevents pressing with too high pressure that may lead to unwelcome conditions.



Figure 6.9; The transformation of feedstock into a green sample after the injection moulding process. The sample was made with 50% vol. KCl

According to the mould design, the green sample has an excellent cylindrical shape with 14 mm high and 10mm in diameter. Furthermore, there was no change in the colour of the sample (orange colour), and the sample is ready for the following MIM process (debinding). Most of the green sample shows similar physical conditions, although each was made with different KCl volumes. The samples are easy to handle and do not easy to damage their structure. It is believed they are still in the good green polymer stage.

6.4.3 Microstructure analysis

The green sample was cut in half, and the image of the inside structure was captured by SEM analysis. This assessment aims to check the condition of the space holder within its structure since the green sample was injected with a certain amount of pressure during the injection moulding process. This examination is essential to ensure the space holder particle is still in its original shape and size, thus not affecting the pore design.

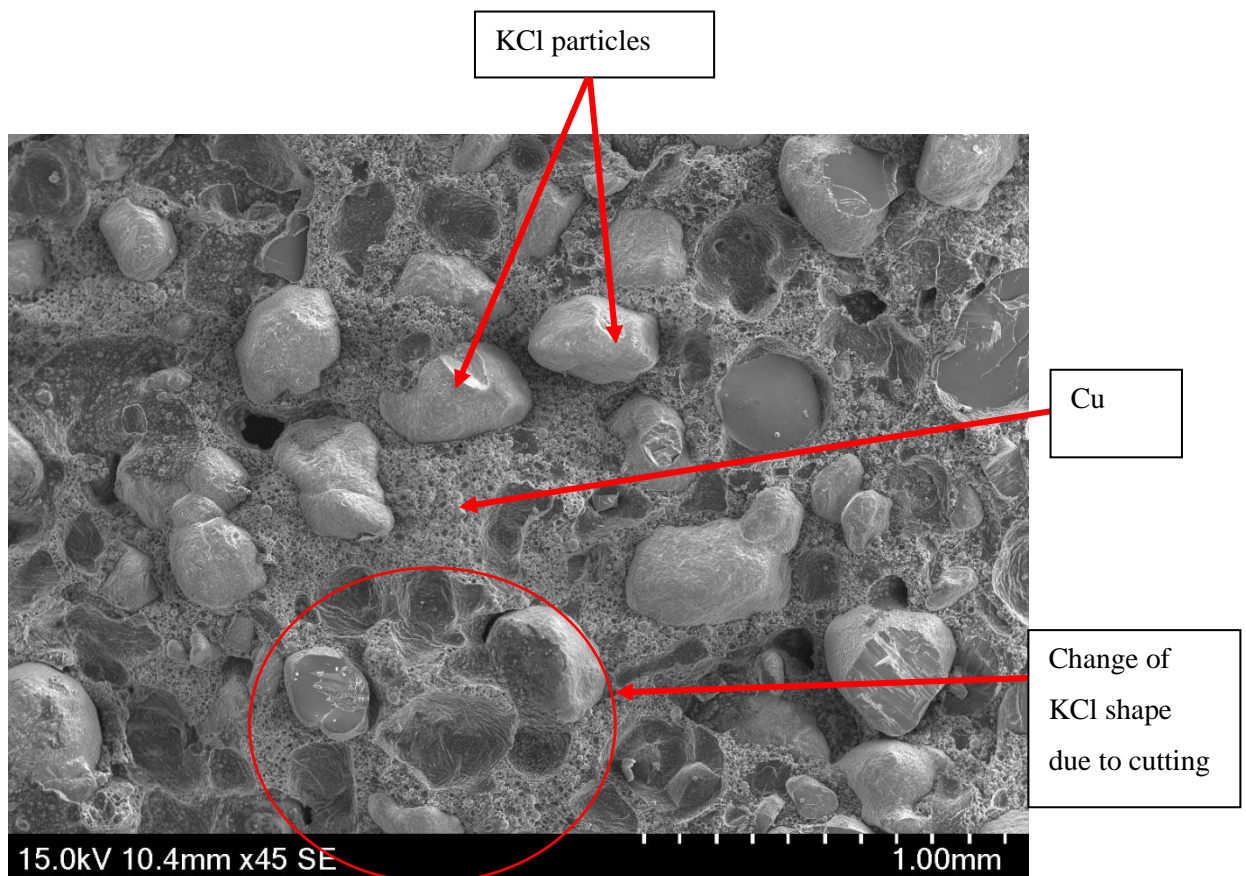


Figure 6.10; SEM image of green sample of porous Cu that made with 50% KCl

From the observation (Figure 6.10), most of the sample made with different KCl shows similar findings with a good shape of KCl. The irregular space holder particle maintains its original shape without any sign of damage or size changes. The KCl was distributed well through the structure and mixed well with Cu and binder system. Some KCl was cut due to the cutting process and not because of the MIM processing failure.

6.5 Debinding Process

The binder will be removed just like a space holder as they are worked to assist the process and not as a part of the final product. These temporary materials must be removed in order to meet the objective of the present work. The intended porosity and pore structure could be produced as the binder supported the MIM process while being held in place by the removal space holder [284], [285].

The green part by the MIM process was mixed with binders, but these components were not part of the final MIM product. It must undergo a removal process. Once these binders are progressively eliminated, the left part without the component of the binder will proceed for densification through a heating process. The removal process can be a pre-requisite process to examine how good the quality of the green part should withstand and surpass the 'hardest' process of leaching without destroying its shape and design.

Since the binders were already integrated with the main element, selecting a suitable removal process should be carefully reviewed. This is to ensure the process will not deteriorate the physical shape of the part and no chemical reaction on the primary metal that will downgrade the performance of the fabricated MIM part. The raise issue may not only be around the perimeter to keep the end product in good shape (Figure 6.11), but how efficient the removal process and how fast it can be carried out should be considered for any candidate for removal method. The removal process may take much time, which may not be ideal for large-scale production. The consequences of the poor debinding process could contribute to defects such as blistering, warping, and skin over the period. While too short of a removal process period may contribute to problems such as residue where the left binder or space holder material could affect the material composition and performance. Thus, identifying the right and efficient debinding process is necessary to guarantee the good quality of the end product. Figure 6.11 demonstrated a good dissolution process and the removal of the space holder during the simultaneous water-dissolving process, and the pores were displayed within the microstructure.

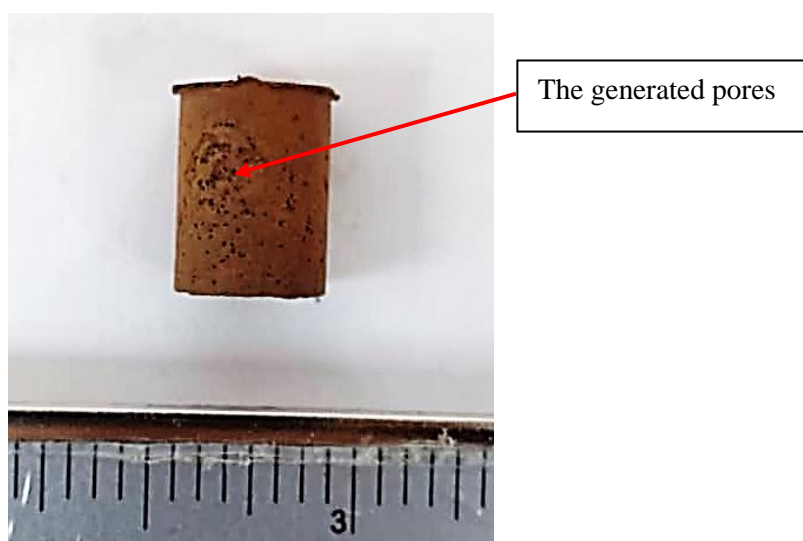


Figure 6.11; Debinded sample (made with 60% vol. KCl) after 2 hours of the water dissolution process

6.5.1 Water dissolution of the space holder and debinding process

Unlike other binders that require chemical solvent and water dissolution for their debinding process and needs to be conducted separately, the use of water-soluble binder such as PEG-PMMA-SA has shortened the removal process. This is because binder and KCl were eliminated simultaneously using the water-leaching process. The process of debinding was discussed clearly in Chapter 3. For the present study, the removal process was conducted in warm water with a temperature of 60°C and was also used in the previous research [250]. Too low-temperature processing will prolong the removal process of PEG and KCl.

Furthermore, this condition (low dissolution temperature) will probably increase PEG residue formation, which may affect the quality of the sample. However, if the water temperature was more than 70°C, the sample was easy to destroy due to the high temperature. Then, the samples were also assessed through two different water debinding techniques; the static dissolution process and the ‘force dissolution’ process by putting the rotating magnetic bars inside the beaker. The weight loss can be measured according to equation 6.1 [154]

$$\% W_{\text{loss}} = (W_{\text{initial}} - W_{\text{after}}) / W_{\text{initial}} \times 100 \quad (6.1)$$

W_{initial} is the initial weight of the sample before dissolution; W_{after} is the weight after the samples have been through the dissolution process in a certain period.

The water dissolution process for porous Cu is relatively challenging because, in this stage, the sample exhibits very fragile conditions and improper handling could destroy the sample structure. In addition, the process consumes much time and contributes almost 60-70% of the total time of MIM production. In some studies of the MIM process, the water debinding process can be taken up to 72 h [218]. In addition, previously MIM Cu sample was made with paraffin wax as a primary binder [159], requiring more time for binder removal. Therefore, the present study offers the removal process in one stage by using water-soluble polymer (PEG) as the main binder and KCl that is friendly to water.

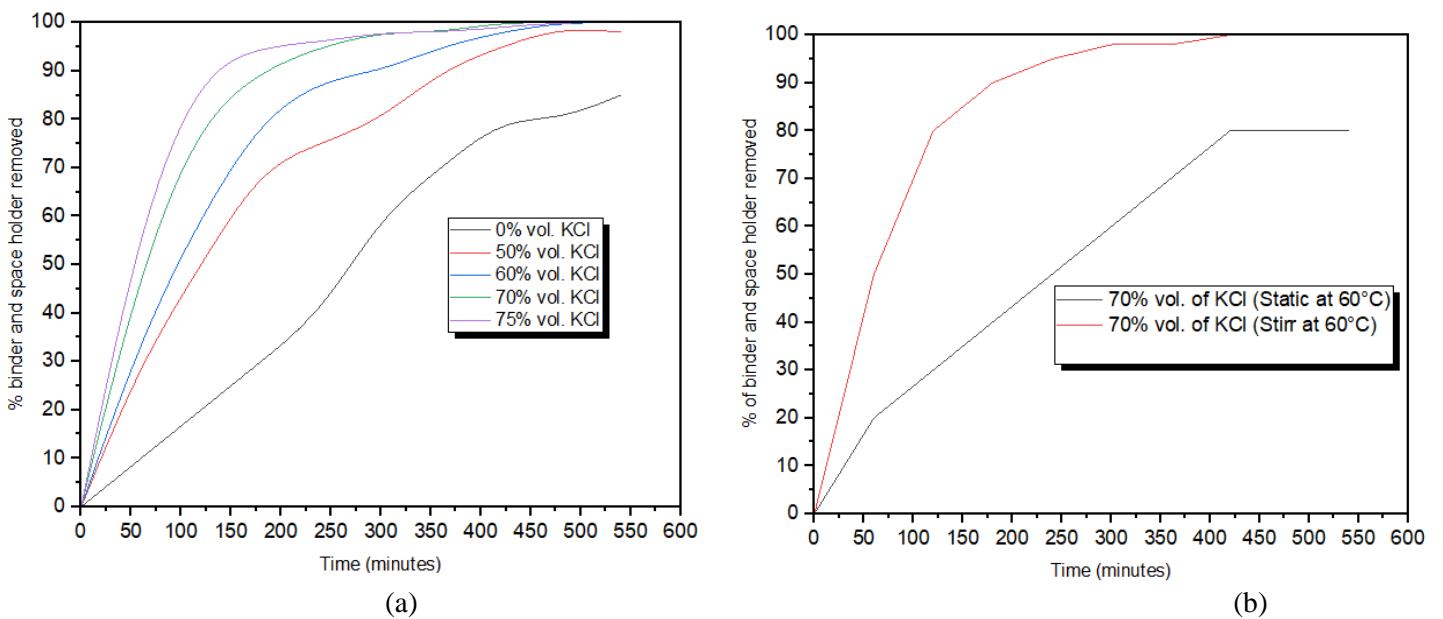
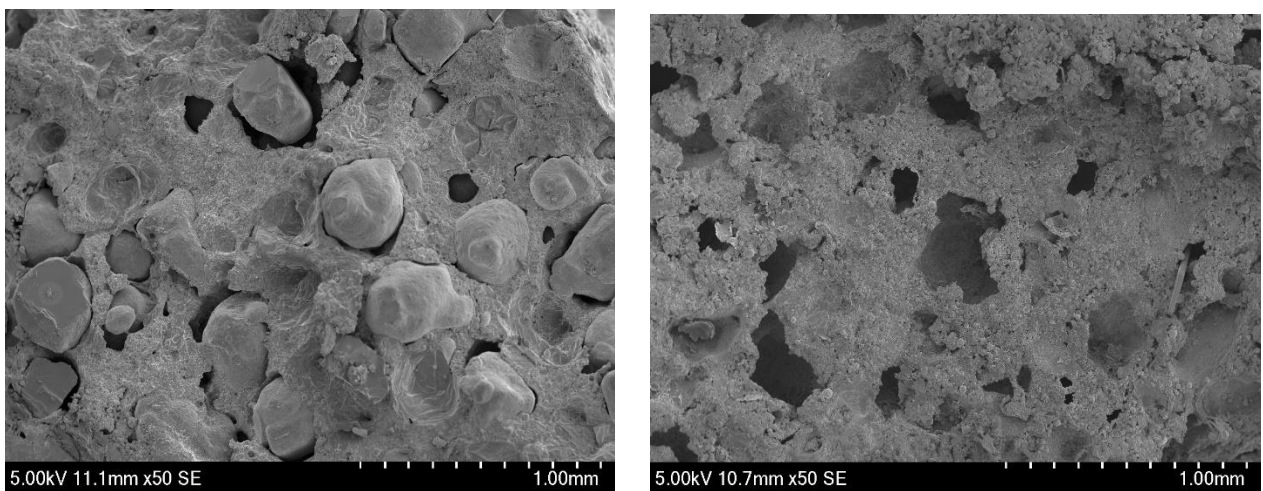


Figure 6.12; Results of water debinding and dissolution, (a) samples with different vol% of KCl at 60°C, (b) samples with 70% vol KCl that test at different dissolution technique

From the result (Figure 6.12a), the sample with the highest KCl amount shows a rapid removal process compared to the rest of the sample, where the PEG and KCl were completely removed around 8 hours. At the same time, the sample made without a space holder shows the slowest process of water debinding and dissolution. The finding shows that the existence of a large amount of KCl within the sample microstructure has encouraged the removal of the process. This is due to the weight loss combined between KCl and binders. KCl is also one of the most accessible space holders to dissolve with water. While in Figure 6.12b shows the different techniques of the removal process in which one of the samples was removed statically under warm water at the temperature of 60°C and the other sample was immersed in sample condition with an additional rotating magnetic bar. The result clearly demonstrated that the sample with the stirring condition was rapidly removed compared to the sample

with the static condition. The KCl and PEG were dissolved faster with a stirring condition where this condition improves the dissolution process.

Figure 6.13 below shows the transformation microstructure of the copper green part before and after the debinding process. The green part was blended copper powder with KCl particles with a size range between 300-400 μm . It is clearly seen that, before proceeding to the water dissolution process, the space holders were distributed within the microstructure. After the dissolution process, all KCl particles were removed, leaving pores behind. The pores displayed a similar shape to KCl, but in some areas, the pores were shown differently. This is probably due to the cutting process during the experiments. The binder was also not entirely removed since the process took only 3 hours, from a total of 9 to 10 hours.



(a)

(b)

Figure 6.13; (a) Cross-sectional of green part 60% powder loading 40% binder with 60% volume KCl, (b) Cross-sectional of debind sample after 3 hours water leaching process at 60°C (sample 60% powder loading 40% binder with 60% volume KCl)

6.5.2 Sample observation and microstructure analysis

Water debinding and dissolution is one of the crucial MIM processes, and the sample exhibited a very fragile structure due to water exposure. Without a good powder loading-binder ratio, the sample will be easy to destroy (Figure 6.14a). This failure happens probably because of the poor distribution of PMMA. This binder component plays an important role in maintaining the structure while removing other binders and KCl. Moreover, poor handling of debinded samples is one of the factors that contribute to structural failure. In this stage, the samples appeared with smooth and soft structures. Any hard press or larger forces that are subjected to the samples will easily damage the structure. This can be avoided by using special tools to handle the sample.

With further modification, the sample finally has a good ratio and can withstand the underwater leaching process. As shown in Figure 6.14b, the sample was displayed with good structure, maintaining the shape and most importantly, there were pores distributed around the sample body. This finding indicates that the KCl was successfully removed during the water-leaching process. Figure 6.15 demonstrates the microstructure of the porous sample after completing almost 90% of the dissolution process at 60°C.

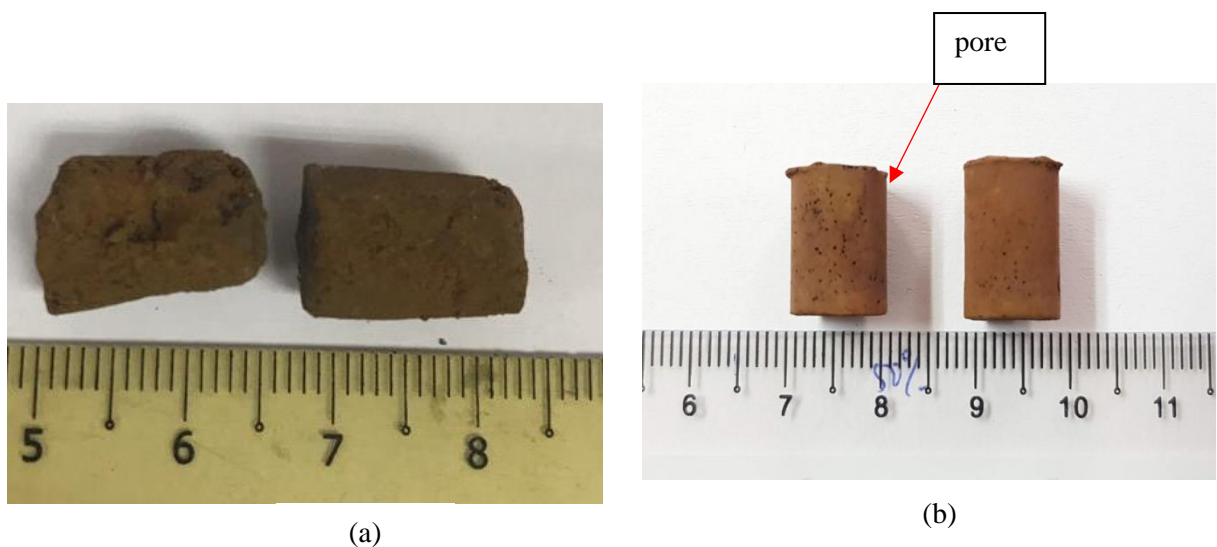


Figure 6.14; Porous Cu sample after water debinding process, (a) poor sample, (b) good sample with 50% vol. KCl after 8 hours debinding process at 60°C.

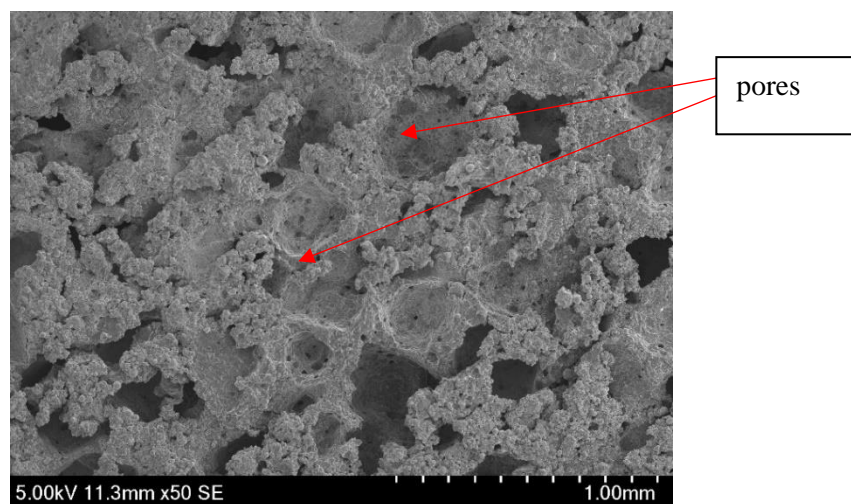


Figure 6.15; SEM image of porous Cu (70%.vol. KCl) after the water leaching process

The SEM image of the debinded sample (Figure 6.15) shows that many pores appeared within the microstructure. This finding reflects the space created by the removal of KCl. The findings also indicate that the KCl was successfully removed with the designated parameters (dissolution temperature, the method during the water leaching process. Furthermore, the sample structure was not affected by the elimination of PEG and KCl since PMMA plays its role in retaining the sample shape. XRD and EDS analyses were performed on the samples to observe whether the PEG was still present in the sample structure. The result shows no sign of the KCl residue element with the microstructure (Figure 6.16). This analysis verified the SEM analysis as KCl has managed to create pores as expected.

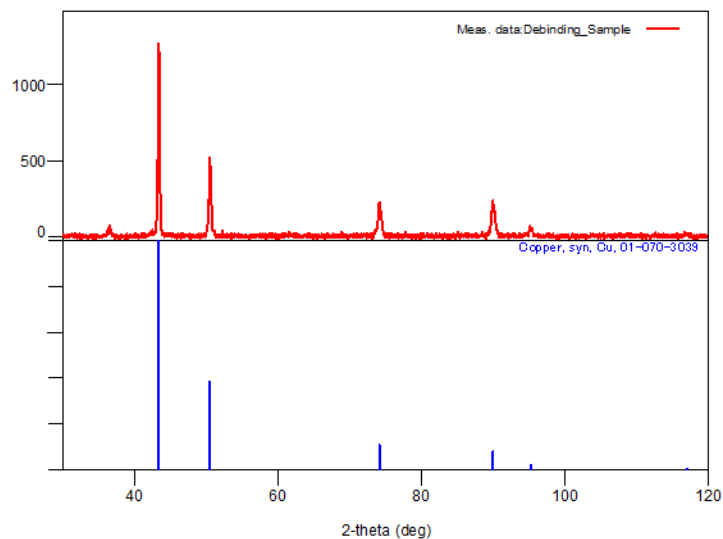


Figure 6.16; XRD analysis on the debinded sample

6.5.3 The binder removal without water leaching process.

This approach technically avoids the involvement of the water-leaching process. This contradicts what was intended (refer to Chapter 3), in which the binder and space holder were chosen specifically for their water-friendly removal behaviour. According to TGA analysis, by 450°C, all binder components will be decomposed. PMMA is maintained under thermal degradation as it would be in the original plan but not for the remaining binder components (PEG and SA), as water leaching is suitable for them. However, this approach forces all the binders to be removed under a one-shot thermal decomposition process. While the KCl will be terminated after the sintering process and not in the green part stage as previously performed for all water-based space holders [218], [219] with the MIM process. This means the KCl will be removed at the end of the processing cycle (refer to Figure 6.17), similar to the finding [189], but the porous Cu processing is without the involvement of the binder element. The objective of the process is to observe whether this approach may become an alternative removal process appropriate for the present porous Cu process since all binders can be eliminated before reaching the sintering temperature. This means all binder are thermally decomposed before water leaching process take place on KCl. The samples were tested at 450°C (thermal decomposition temperature) for 1 and 2 hours to ensure no remaining binder left before proceeding for densification stage at 850°C and water leaching process).

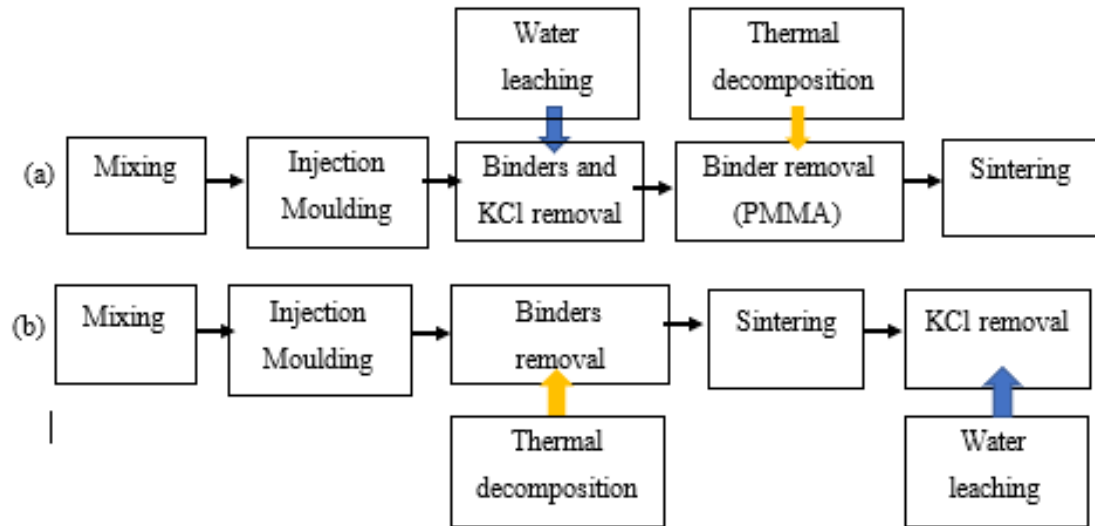


Figure 6.17; The flow of Porous Cu by MIM process, a) Water leaching process involvement in binder and KCl removal process, b) Water leaching at the end of the processing cycle for KCl removal

As a result, without going through the water debinding process, the binder appeared with burning signs, and dust covered the samples (Figure 6.18a) compared to the samples where the water leaching process removed PEG. This result shows a similar output for all samples even though the process was conducted with different heating times. Based on the observation, the tested sample maintains its shape in a positive perspective, reflecting the good mixing with the suitable composition. In addition, it also displayed many tiny pores distributed around the sample as a result of the binder-burning process. The pores are not expected from KCl since the samples were not going through the water-leaching process yet. The downside of this approach is that the sample was burned, and the whole body turned black. This finding probably occurred due to the high temperature of binders. However, this phenomenon does not have a high impact on the sample where the PEG and KCl were removed earlier before the thermal process took place (refer to Figure 6.18b). The sample is a bit cleaner, and the orangish colour of Cu is displayed. However, the worst finding is that almost all samples tested by this approach demonstrate internal cracks and are easy to break, as shown in Figure 6.19. Both samples in either bar or cylinder shape give similar defects; the samples come with poor structural integrity. The handling of the sample becomes difficult due to its high fragility even after the sintering process. In vice versa, this trend did not happen in samples undergoing the water leaching process for PEG and KCl. These samples show no sign of crack but come in different sizes due to the sintering process.

This can be explained since there was no path or channel for the decomposition gas from the binder to flow out from the samples during the heating process. In the present sample, all binders (PEG, PMMA and SA) were decomposed and vaporised simultaneously during the heating process. Each binder may create an open channel to decompose out from the structure, and at the same time, the distributed KCl particles may block some channels. Due to this problem, combining many open channels created due to each binder degradation causes an internal stress pressure that could contribute to internal structure failure. Thus, most of the samples come with cracks and low structural integrity. On the other hand, using the water dissolution process to get rid of binders (PEG and SA) alongside KCl may give samples advantages in preparing the open pores channel earlier before proceeding to the heating process. The pore channel may help the remaining thermal binder. PMMA decomposed easily through the open pore channel (created by the previous binder and KCl) without creating a new channel that may give internal stress problems and lead to structure fragility.

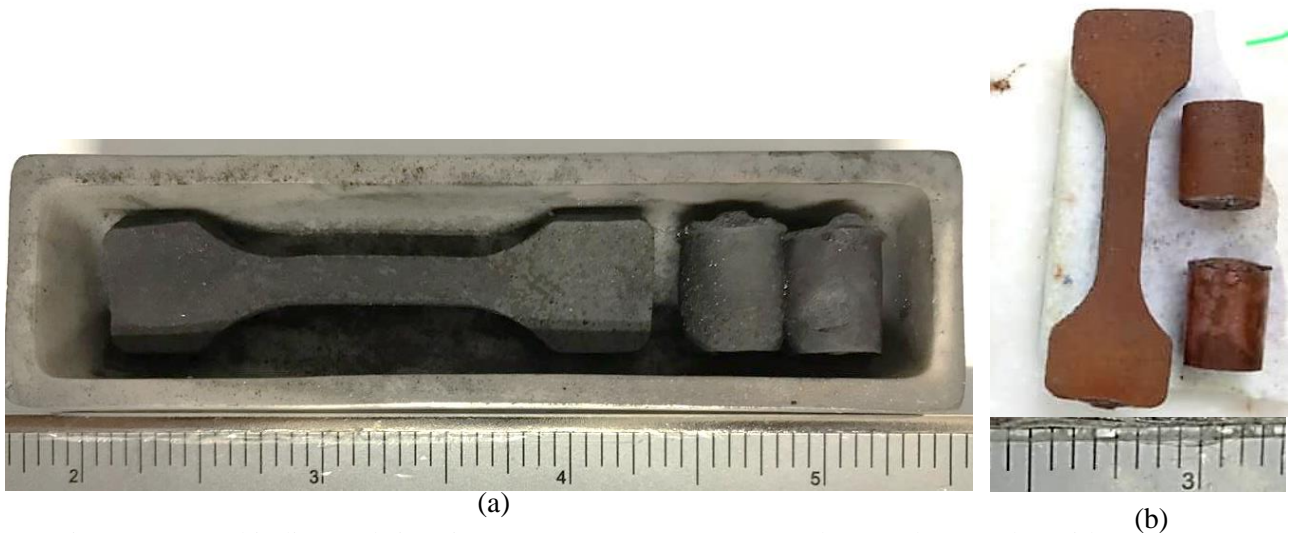


Figure 6.18; Debinding and sintering process on porous Cu samples, a) The samples without water debinding process, b) The sample with water leaching process on binder and KCl.

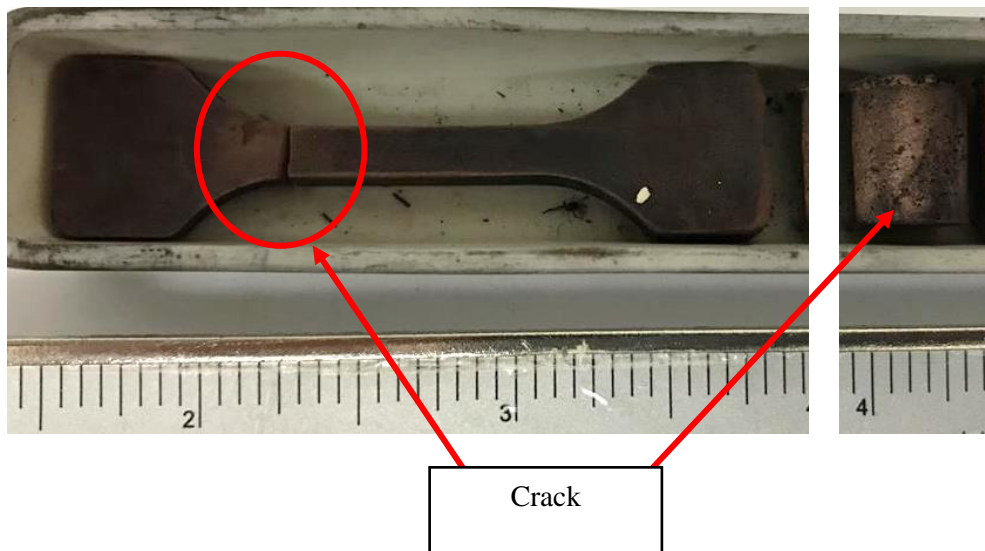


Figure 6.19; Crack problem on the sample that sintered without water debinding process.

6.6 Sintering Process

The sintering or densification process is important to improve and strengthen the sample structure. The process enhances the density of the sample and creates a strong bonding among the particles. The process involves the removal of binder (PMMA), sample shrinkage and reduction of sample porosity. The sintering normally occurs near the melting temperature, which in the present study, the temperature was placed at 800 and 850°C. This is because, with a lower sintering temperature but still acceptable, it could increase the formation of porosity within the microstructure.

At the initial testing stage, the sintered sample was destroyed after the sintering process (Figure 6.20a). The sample was sintered at 980°C for 3 hours under the argon atmosphere. From the failure observation and investigation, this defect was because of poor powder loading ratio, the amount of PEG set more than 80% wt. from the total binder system. Because of that, the amount of PMMA is insufficient to maintain the sample structure during the sintering process. Therefore, the amount of PEG-PMMA was adjusted (discussed in Chapter 5) to obtain a good structure. The samples were observed with a good cylindrical shape for the following sintering trials, but the entire body turned black. The sample was burned during the sintering process (Figure 6.20b). This problem indicates that the sintering temperature should be reduced from 980°C to 850°C. Finally, with a few adjustments in terms of sintering temperature and sintering profile, a good sample managed to be produced (refer to Figure 6.21ab). The SEM image captured on the selected sample shows the sintering neck formation between the microstructure, indicating the excellent bonding between particles (Figure 6.21).



Figure 6.20; The poor-quality sample after the sintering process, a) The sample consists of too much PEG, b) The sintering was performed with high sintering temperature

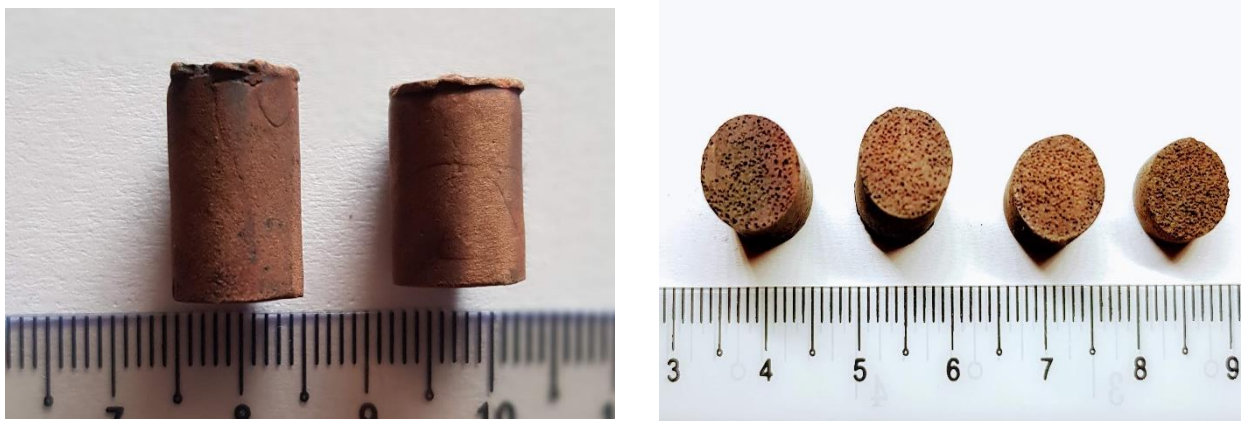


Figure 6.21; Good sintered sample, (a) Porous Cu without space holder, (b) Porous Cu made with different amount of space holder.

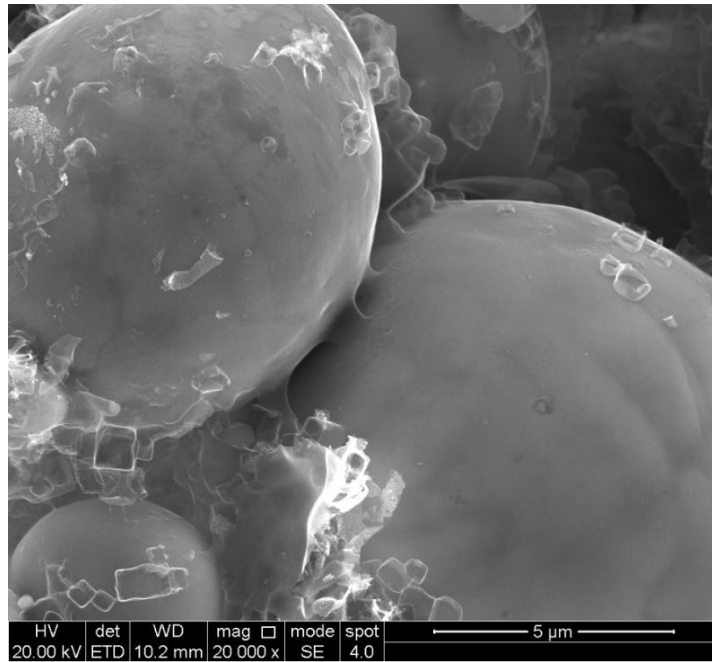


Figure 6.22; SEM image of the porous sample that shows the sintering neck formation


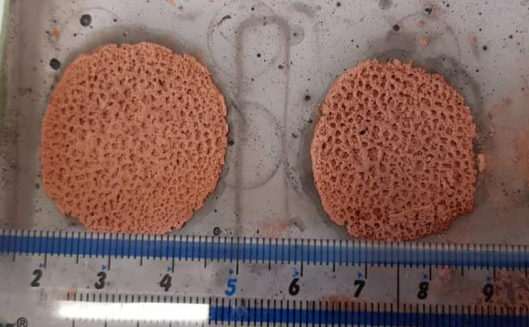
Sintering is a high-temperature consolidation process that often occurs near 70-90% [155] of the melting temperature of the material. The contact point between particles was formed due to the injection process and will create bonds through particle fusion. This situation will enhance the mechanical properties and change the physical properties of samples in terms of volume, density and porosity. The sintering process parameter commonly includes the sintering temperature, time, material properties, and machine capabilities. The sintering process can be classified into different stages. During the first phase, a neck forms at the particle contact point. Then, pore rounding occurred during the middle stages of neck development. At this stage, density grows dramatically. In the last stage, grains continue to increase in size, the number of pores decreases, and enhanced densification.


Sintering always referred to the process of mechanical improvement through the bonding among particles. However, the sintering process commonly relates to shrinkage problems. The shrinkage happens as the effect of the diffusion process and commonly results in size reduction. The sintering has two different types of transport mechanisms. The surface transport mechanism refers to the atoms at the surface that move from one particle to another. This activity leads to neck growth, and then densification takes place. While in bulk transport mechanism mainly refers to the movement of atoms from inside the structure to the surface. This transportation mechanism leads to densification through grain boundary diffusion.

6.6.1 Preliminary Testing

Table 6.4 summarize the investigations that have been conducted in order to find the optimum sintering parameter. The findings may be different according to different conditions. It can be concluded that the roles of sintering temperature and the quality of mixtures lead to these problems. As the sintered sample melted, the sample made with higher PEG components showed poor structural integrity. The low amount of PMMA fails to retain the original cylindrical shape of the sample. Then, it was noticed that if the sample was sintered under the highest temperature may expose the samples to extreme heat. The sample appeared with a burning sign. Thus, this can be remedied by lowering the sintering temperature.

Table 6.4; Samples trials to find sintering parameters

Type of samples	Sintering Temperature and Time	Findings and Observation	Visual observation	Possible reason
Sample with 80% PEG	850 °C, 2 hours		The sample melted and was not in the desired shape.	Poor mixing ratio
Sample with a high water-based binder (PEG) 76-85% vol of PEG binder	850 °C, 2 hours		The sample melted and was not in the desired shape.	The sample consists of too much PEG

<p>Sample sintered at high temperature, almost near to melting temperature (960°C)</p>	<p>960°C, 2 hours</p>		<p>Poor shape, burning sign</p>	<p>Extreme sintering temperatures</p>
----------------------------------------------------------------------------------------	---------------------------	------------------------------------------------------------------------------------	---------------------------------	---------------------------------------

Chapter 7 POROUS COPPER ASSESSMENT

7.1 Physical Analysis

From the observation, most of the sintered parts show a good structure and maintain their original cylindrical shape (Figure 7.1a) even though they were relatively exposed to high temperatures between 800-850°C. All samples from 0 to 75% vol. of KCl show physical similarity where they can retain their shape. Thus, through the MIM method, the sample can be produced with a near-net shape, and this finding also relates to the good mixture ratio of powders and binders during the sample preparation. Furthermore, the uniform distribution of pores was clearly seen throughout the whole body (Figure 7.1b) of the sample. These findings indicate the good mixing process of the Cu powder and KCl via a high-speed mixing machine.

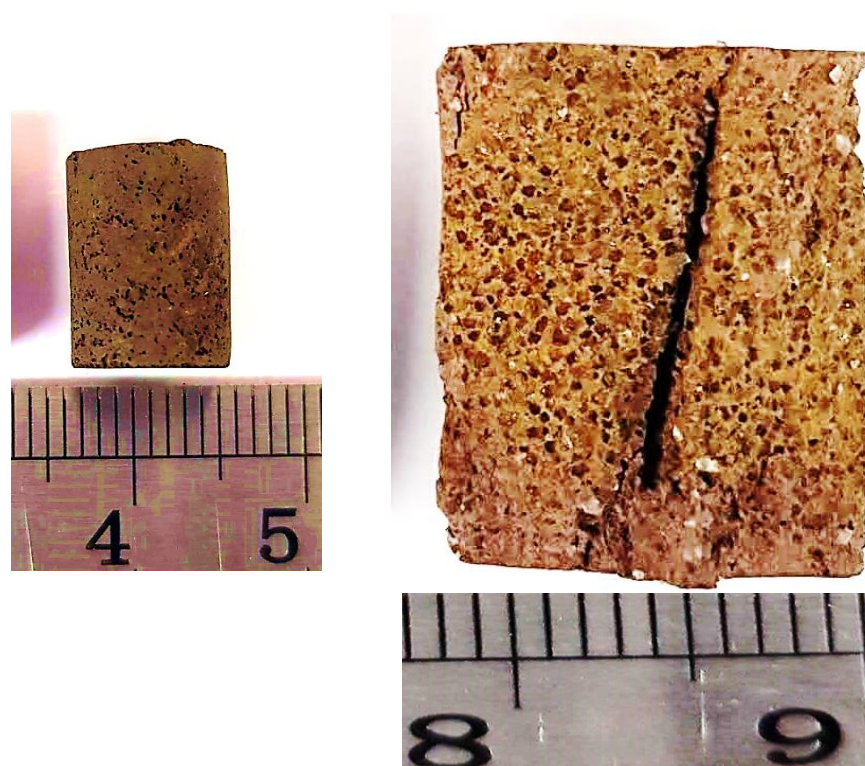


Figure 7.1; (a) Sintered porous Cu made with 60% vol. KCl, (b) Cross-section of sintered sample (60% vol. KCl)

Although all of the samples were successfully manufactured without any structural failure, there were some minor defects on select samples during the inspection session, such as cracking issues (Figure 7.2) and changing their shapes. The issue might be traced to the shrinking issue being caused by density decrease. Furthermore, it is believed that this fracture developed during the binder removal procedure as a result of heat decomposition and diffusion from the inside to the exterior of the sample structure. This typically happens during the initial stage of sintering cycles. Interestingly, the crack could be occurred earlier during the injection moulding, probably due to insufficient injection pressure and improper debinding process. Some of the green samples have appeared with tiny cracks that might be formed on the sample in some cases, the crack is too small and difficult to detect earlier before proceeding to the heating process.

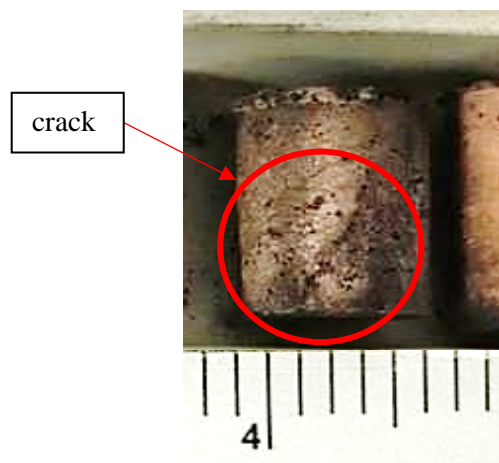


Figure 7.2; Sample crack after the sintering process

Apart from that, in some cases, the sintered part is not produced in a good cylindrical shape. This defect could be explained for several reasons; firstly, the non-uniform filling of feedstock into injection moulding die. The injection die should be fully filled before being injected into the mould. This might cause the injected green sample to gradient density. Secondly, this problem might be due to an insufficient debinding process. The debinding process purposely removes the binders but, without adequate removal time, has trapped the residue binder in the sample structure. Thus, during the subsequent heating of the sintering process, this residue starts to melt, which might change the shape of the sample. These problems can be controlled by frequently examining the green and debinded sample before the sintering process.

7.2 Microstructure Analysis

As the MIM processing technique is known to produce samples with high-density and near-net shape, voids formation is not allowed where this condition leads to poor mechanical properties. The purpose of the current study, however, was to intentionally find the opposite outcome. The porous Cu samples are successfully fabricated and managed with a certain amount of porosity. The sample is mainly fabricated with different levels of porosity and sintering process. The present section specifically discusses the microstructural analysis focusing on porosity properties.

The fabricated samples aim at a certain level of voids or porosity with the roles played by the space-holding technique, as shown in Figure 7.3. The pores formation relies on the physical properties of KCl once this holding material is successfully removed. All generated samples duplicate the physical characteristic of space-holding material, and the finding is in line with the previous study outcome [286]. The result shows that the pores formed from the process were similar to the space holder shape.

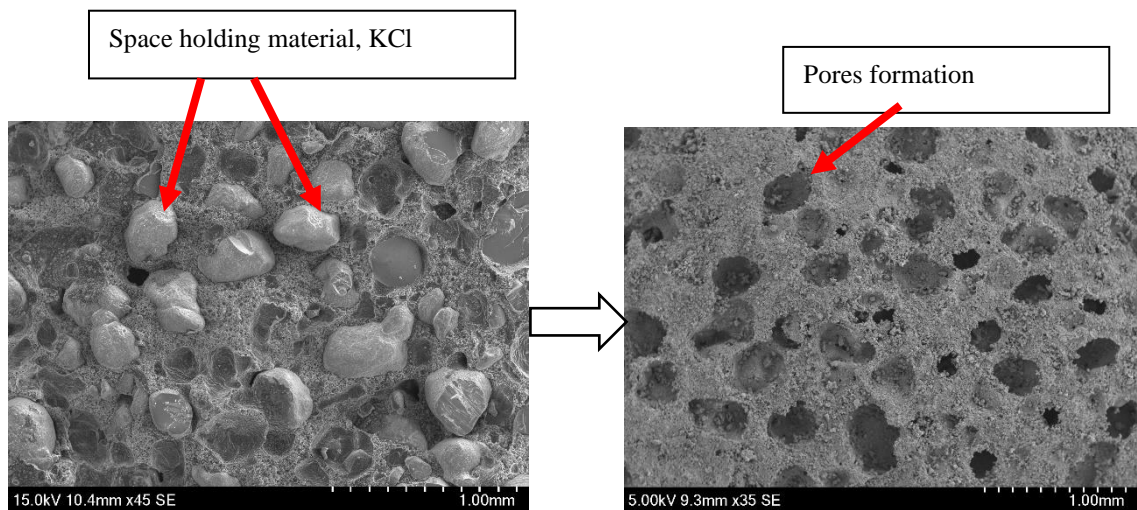


Figure 7.3, A comparison of green sample stage (with 70% KCl) with sintered sample where it shows the pore generating by space holding method

7.2.1 Porous structure morphology

Most of the samples showed macropores created by the space holder approach, and there were tiny pores within the microstructure, most likely from the sintering process (micropore). Figure 7.4 below is randomly taken from pre-trial samples that were made after 2 hours heating process at 850°C. With 80% vol. KCl volume, the purpose of obtaining porous Cu with high porosity. The sintered sample was too fragile, and a crack area could be founded at certain parts of the sample. Besides the crack formation probably caused by high porosity, the main point is that porous Cu can possibly be made via MIM fabrication in combination with the space holder technique. The sample was completely porous and came with a porous network as it combines many connected pores. The open pores structure is generally irregular, expecting to imitate the shape of KCl. The porosity of Cu samples is approximately greater than the expected porosity designed KCl volume, with the size of pores also about similar to or slightly larger than the original size of KCl. This pattern is believed from the factor of the removal of binders prior to various MIM stage processes, including water leaching and thermal debinding. These factors might ready the sample with greater porosity, and [233] also mentioned the roles of binder and sintering towards pore formation.

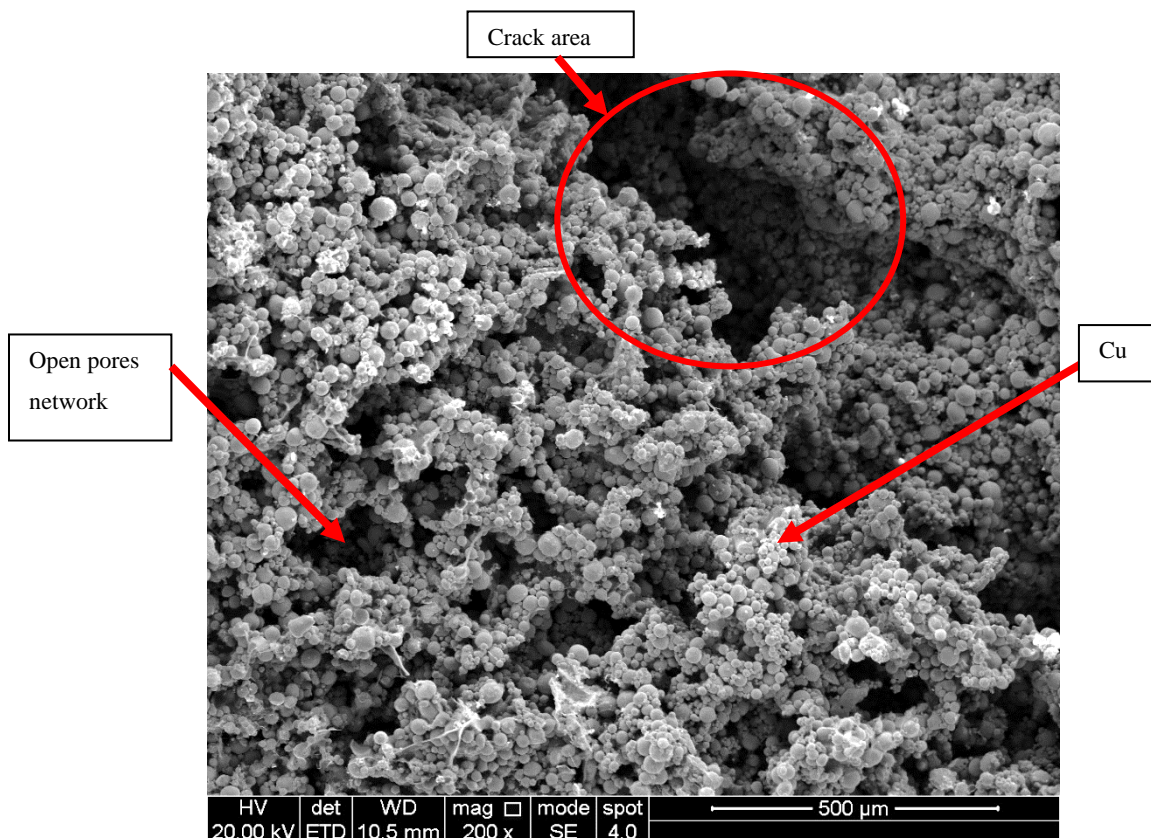


Figure 7.4; Cross-sectional samples with extreme KCl volume after the sintering process

Due to the high fragility sample with 80% vol. KCl, then the space holding material was adjusted to 75% vol. KCl (as shown in Figure 7.5), where all samples were created with better strength and not too fragile as the previous setup. This gives benefits for handling activities where the sample should withstand minimum stress. Similar to previous findings, the pores were well distributed with irregular shapes and various sizes. Therefore, the highest volume of KCl can be obtained in the current study is up to 75%, besides numerous fabrications at 50, 60 and 70% vol.

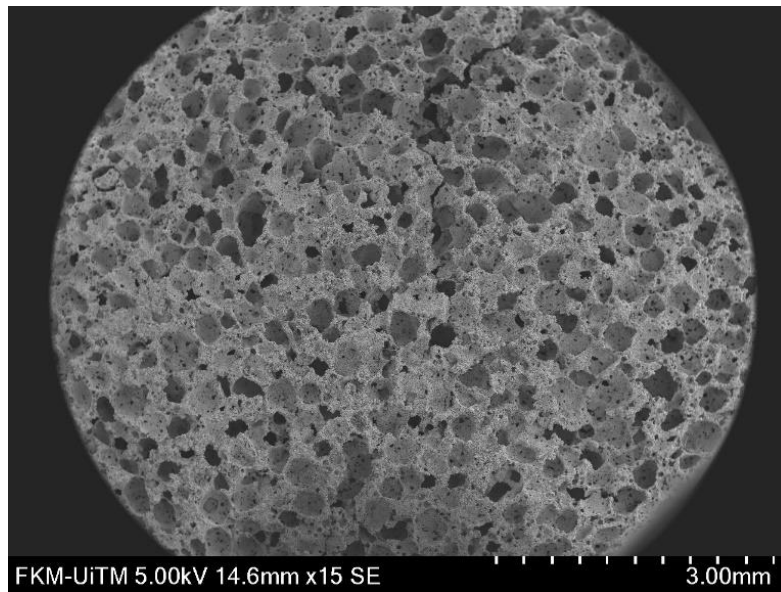


Figure 7.5; Porous Cu with 75% vol. KCl sintered at 850°C for 2 hours sintering process

Figure 4 shows a cross-section of the 3D isometric image surface of porous Cu measured via Alicona Infinite Non-contact Profiler. This machine was traditionally designed to analyze the surface roughness, but the 3D images are useful for the present study to observe the distribution of pores and their physical characteristics. Figure 4 (a) demonstrates the 3D image of samples with 70% vol. KCl compared to samples without any space-holding material. The finding supports the SEM images above, where the KCl particles are uniformly distributed throughout the structure, and the shape of the irregular pores replicates the shape of KCl. The depth of pores varied as the image taken from the cut sintered sample. Figure 4 (b) is clearly 'clean' without any pores as it was made with 0% of KCl. The blue colour line is probably the crack area of the sample due to cutting activities.

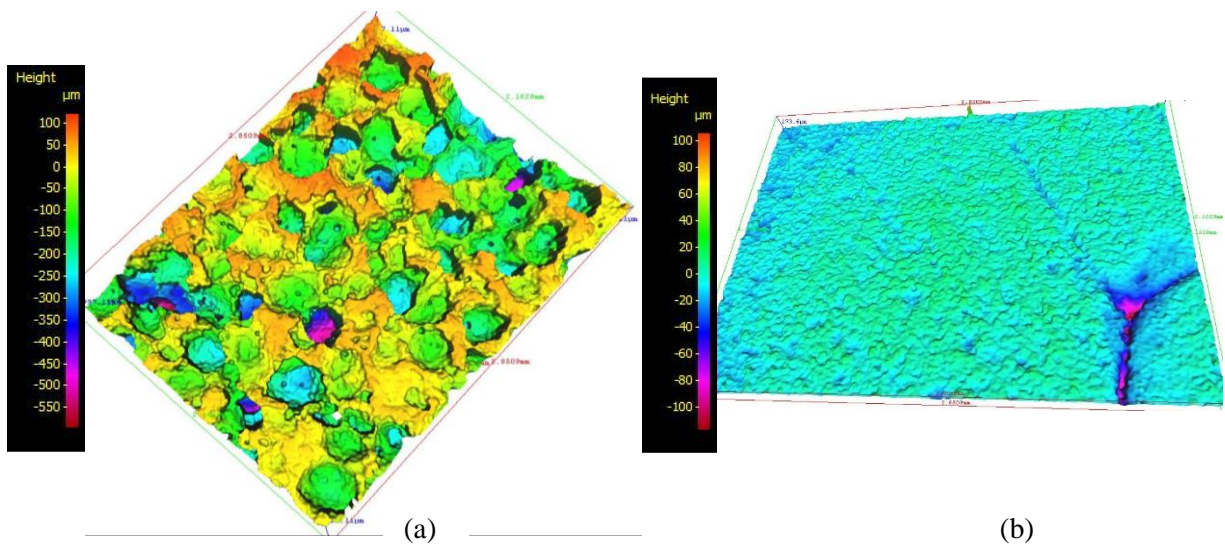


Figure 7.6; 3D isometric surface image of porous Cu measured by Alicona Infinite non-contact Profiler, a) Sample with 70% vol. KCl, b) Sample with no space holding material

Figure 7.7 below shows the SEM images for all samples with a variation of KCl volume percentage that sintered at 850°C for 2 hours of the sintering process. In general, all pore shapes are similar to KCl shapes and uniformly distributed except for samples without KCl.

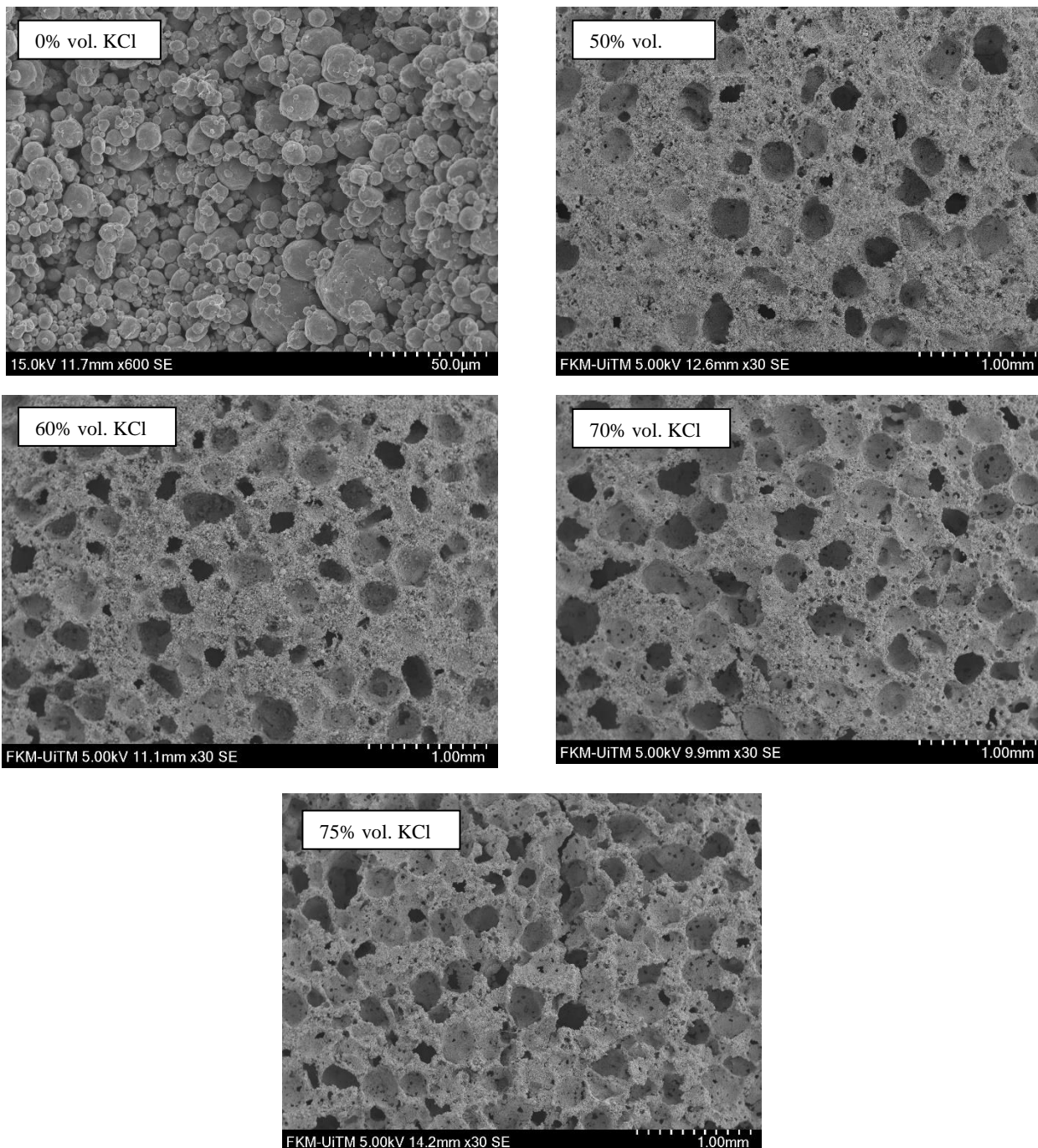


Figure 7.7; SEM images of various porous Cu sintered at 850°C for 2 hours sintering process

7.2.2 Pore size analysis

The pore size can be initially estimated and counted directly on the SEM images during the imaging session, as shown in Figure 7.8. The SEM software is complete with measurement tools that are able to manually draw and measure the size of the pores. However, this procedure is just for the initial prediction of pore size measurement and not for final analysis since the measurement was manually performed with a tendency of human error and skip measurement. For the present study, the result may give the initial prediction data before the actual pore size analysis is carried out via image analyzer software.

As shown in Figure 7.8, the size of pores was simply drawn on the SEM image, and it will automatically calculate the size. According to the image (sample with the highest KCl fraction (75%)), the pore size is mainly as small as 192 μm , and 412 μm is the highest value. Most of the measured pore size was exhibited between 250-380 μm . The size range was slightly different from the actual KCl size, which calculated an average of 321 μm using the Mastersizer particle analyser. The pore size and shape change was probably affected after going through all MIM stages where the samples were exposed to injection moulding pressure and mixing process friction. In addition, the heating process might be a possible factor in reducing pore size. This phenomenon happens due to shrinkage activities during the sintering process [183].

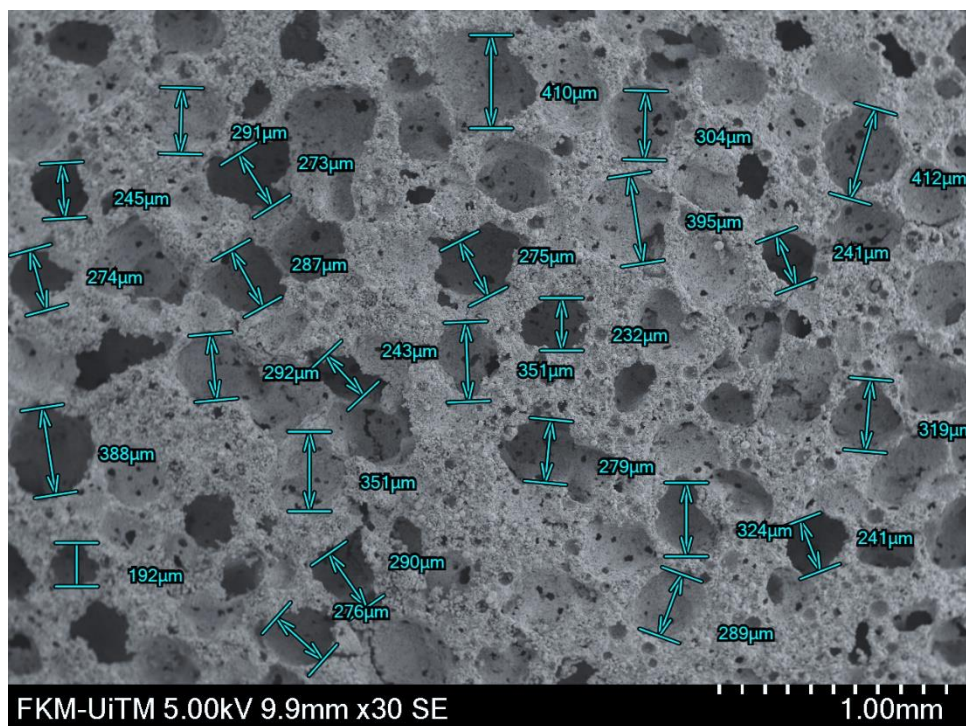


Figure 7.8; Manual measurement of pore size using SEM software

The pore size distribution of the samples was then measured using image analyzer software known as ImageJ. The brief procedure has been explained in Chapter 3, where this method relies on SEM images as the main source for the image analyzer software. Ten SEM images of each sample were evaluated with constant size and scale before being converted into greyscale before turning into binary mode, as shown in Figure 7.9. The two-contra image consists of black pixels representing pores, while the white pixels correspond to dense areas. Then the image will be analysed using particle analysis instructions. Figure 7.10 shows the pores distribution of each sample.

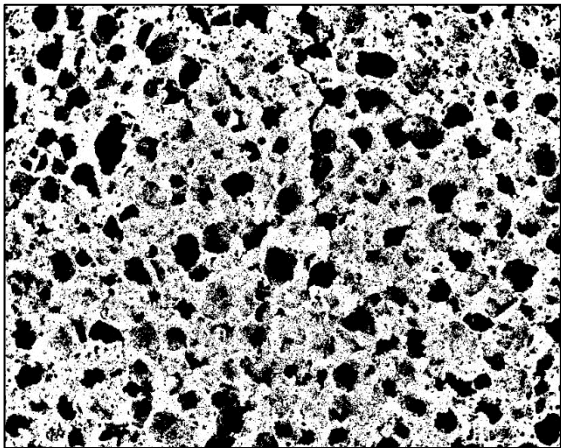


Figure 7.9; Example of Binary mode image of 75% vol. KCl sample

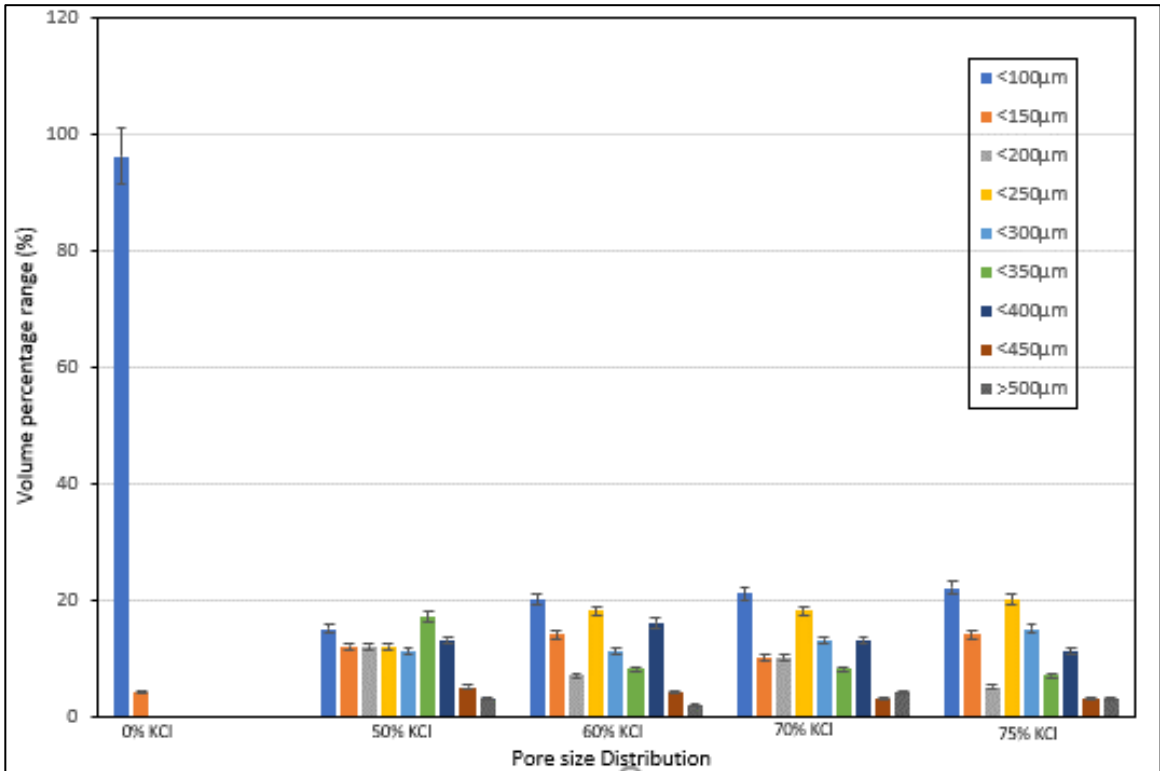


Figure 7.10; Pore distribution of porous Cu

The distribution of pores in porous Cu reflects how well the pores are distributed within its structure. During the production procedure, these pores are distributed uniformly. It has been observed that there is a significant difference between samples fabricated with and without space holders. Two prominent pore size patterns were seen in the sample produced with zero volume percent KCl. More than ninety percent of the distribution of the pore sizes was presented at 100 μm , as was clearly observed. It is believed that the formation of these pore size distributions was caused by the fabrication process (injection moulding) and the effect of the sintering process, resulting in micropore formation. The pores were formed between the copper particles. In contrast to this group, the pore size distribution for the samples made with KCl has shown variation in of pores size distribution. It revealed that the pattern of pore size distribution was identical and uniformly dispersed throughout all samples, despite the fact that these samples were created with different volumes of KCl. These pores were created on purpose using KCl and are classified as macropores. Two important pieces of information may be obtained from this pore size distribution. Firstly, the pore sizes were spread equally, and there was no dominant pore size. Most of the pores appeared in a variety of sizes, with a small percentage of pores with a diameter greater than 450 μm . This is probably due to the combination of several pores that increase its size. Secondly, the pores were proportional to the size of KCl. This indicates that the porous copper was successfully performed with the assistance of KCl.

7.2.3 Porosity analysis

Based on Figure 7.11, the porous Cu sample created without a space holder consists of low porosity, around 8.67 to 12.5%. This generated porosity is probably due to an incomplete MIM sintering process that produces micro-size pores. While each sample was fabricated with space holder materials, the samples were obviously displayed with high porosity percentages, 59.33%, 67.67%, 75.33% and 80.67%, respectively, that, made with 50% vol KCl to 75%KCl. This amount is almost 4-7 times higher than the sample made without a space holder. In addition, the obtained porosities were not exactly similar to the KCl vol.%, which is generally higher than the expected amount. This can be assumed; that his finding has contributed to the removal of binders during the water leaching and sintering processes that leave a huge number of pores. While as expected, a slight difference in the porosity of the sample was seen as the sintering temperature was raised. The porosity percentage is between 8.67 % for the samples that were made with the lowest KCl vol. % and 86.7 % for the samples with 75% vol. KCl.

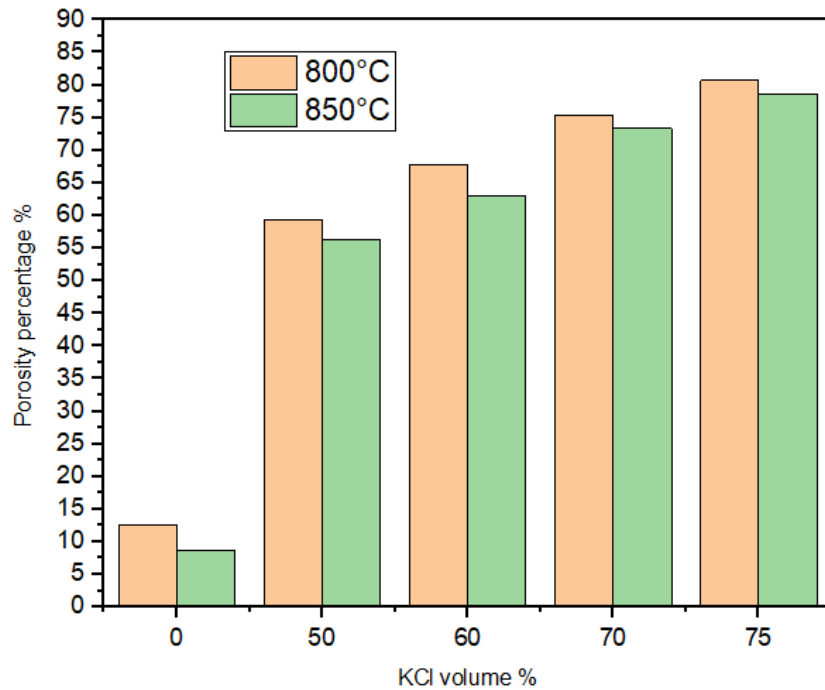


Figure 7.11; The porosity of the sample under two different sintering temperatures

7.3 Mechanical Properties of Porous Cu

It should be noted that samples containing space holder material should have a greater number of pores in their structure. With increased porosity, the fabricated sample may have decreased strength and may be unsuitable for mechanical handling. Thus, it is necessary to evaluate the mechanical properties of these samples to fully understand their mechanical behaviour, particularly for those fabricated samples with a higher porosity structure.

The strength of porous metal structures can be assessed on their mechanical properties under a particular load. The investigation of mechanical properties of porous metal, particularly porous Cu, has been performed widely [12], [100], [287]. Theoretically, the larger the porosity, the lower its strength; however, it depends on various factors. According to [288], pore shapes and porosity control the mechanical properties of the porous structure.

In the case of porous Cu, because it has been widely used for functional applications, it appears that it is not required for samples in this category to be subjected to high-stress levels. The finding contrasts with structural application [56], where the samples are purposely designed to meet the maximum amount of strength. However, the information on the mechanical properties of present porous Cu is still relevant and essential, which gives the thought of the acceptable range of strength that these samples can withstand and

endure. With the information obtained from the mechanical analysis, these fragile samples should be treated and carefully handled. In addition, the information may give a minimal amount of stress that the sample can resist. Therefore, compression testing (Figure 7.12) was performed for the current porous Cu samples. A brief description of the performed compression testing is explained in Chapter 2.

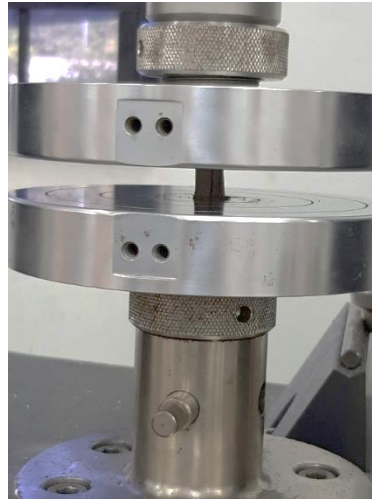


Figure 7.12; Compression experiment on porous Cu sample

7.3.1 Mechanical stress-strain curve toward porosity differentiation

Figure 7.13a shows the mechanical behaviour of porous Cu once completed the sintering phase and its similarity to the typical stress-strain curve. The present compressive stress-strain curves represent samples with different space holder volumes after being sintered for 2 hours at 850°C.

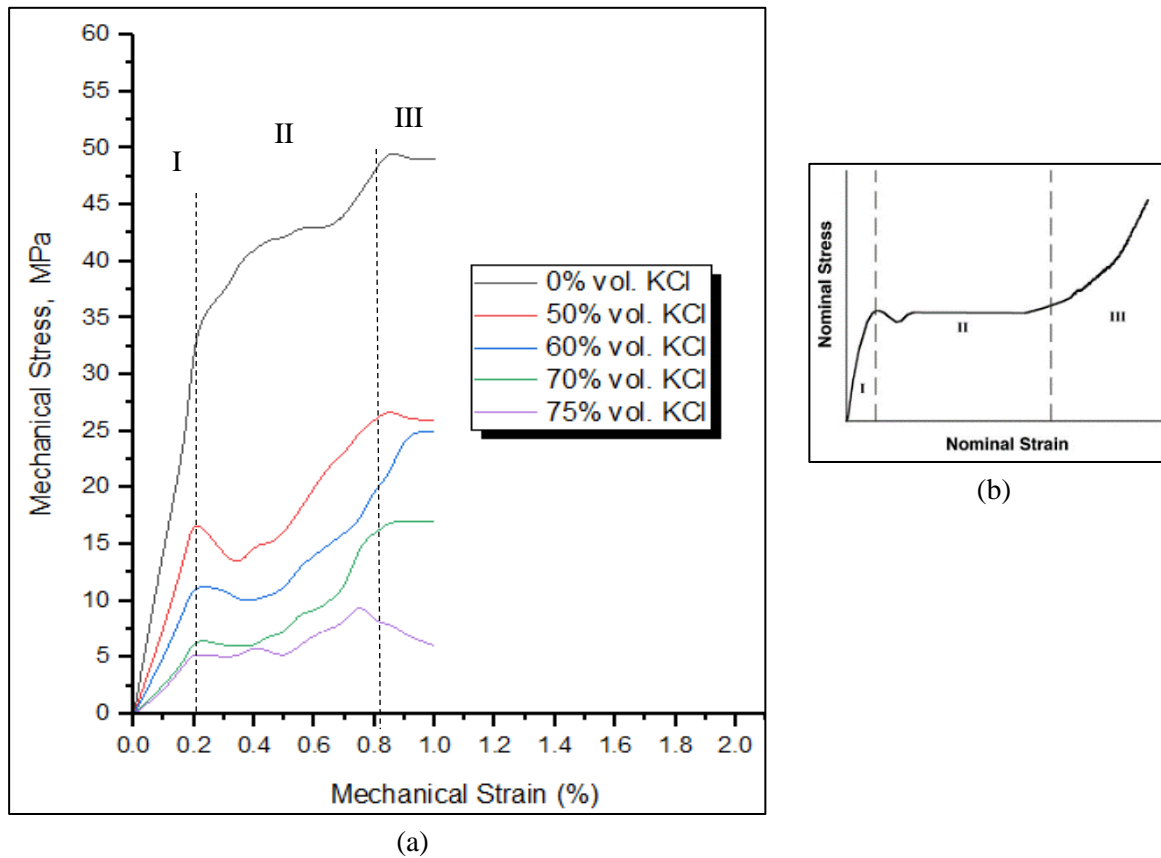


Figure 7.13; (a) Compressive Strength curve of porous Cu with variation porosity, 2 hours sintering at 850°C, (b) Typical stress-strain curve for porous metal deformation [289]

Based on the result (Figure 7.13a), an increase in sample porosity has decreased the maximum stress the sample can achieve. All porous Cu samples made with space holder material show almost similar mechanical behaviour and not much difference in the pattern. This outcome is probably because these samples come with similar pore shapes and the same processing method sintered with similar heating conditions. However, a slightly different porous Cu sample was prepared without a space holder, but this trend is similar for those with low porosity [12]. It is noticeable; the result is comparable to the typical design of a stress-strain curve for porous structure [289] (Figure 7.13b) and was identical to the typical compressive deformation curve

reported on porous Cu studies on different space holder PMMA [225], [58], CaCO₃ [290], K₂CO₃ [13], NaCl [291].

The deformation process of porous Cu starts with the subjected load was distribute evenly to the whole area of the sample. Based on Figure 7.13, most of the sample achieved maximum stress at the lower strain range (0.2%). Then, the applied stress was localized on the structure's weak spot and gradually spread throughout the entire area. When the strain rate reaches 0.2%, the stress exceeds the maximum yield stress and initiates plastic deformation. Further increment in strain rate was then making the pores collapse before the densification stage took place. For the present study, the mechanical behaviour of porous Cu is summarised according to this stress-strain curve.

1. *Linear elasticity region (Region I)*. The graph shows the steady slope linear line for both types of samples. They displayed a similar pattern to the linear graph since they managed to withstand the given stress within a low strain rate before the structure failure occurred afterward. This structure failure probably occurred on the weakest wall structure before entering the long plateau stage. According to [292], the cell edge is the main mechanism to control the formation of linear elasticity, and [293] reports that the deformation of the porous Cu mechanism starts with bending and buckling before the stress concentrates on cell nodes and finally collapses on the final stage of deformation. The stress-strain graph is proportional to Hook's Law, and the Young Modulus, E, represents the slope of this linear region. The Cu sample (0% vol. KCl) shows higher stress, approximately 35.34 MPa at 2% strain. While for porous samples (50-75% vol. KCl), the stress value is noticeably approximately 5.32, 6.81, 11.46, and 17.63 MPa with the range of a similar strain rate. It clearly shows that the sample without KCl amount has greater strength than the rest of the samples. For a sample with 0% KCl, this is probably contributed by a denser area within its structure to cater to the impact of compression.

Plastic deformation region (Region II). In this region, the slope decreases due to deformation before it shows a long steady deformation stage. This stage is also known as the plateau curve. Based on the graph, it is clearly seen that the porous sample generally exposes the yield stress at the strain of 0.2% with associated stress as low as 5.32 to below 40 MPa. The stress was subjected to samples until it reached a maximum level that the sample structure could hold, then the sample was gradually deformed, and the cell wall began to collapse. When the pores touch the opposing walls, the structure density rises. Most porous samples had a long plateau region curve before reaching the densification stage. This region usually happens on porous material, as similarly reported in the previous study [140]. The result demonstrates that the porous structure displayed steady deformation until it reached the densification stage. This finding contradicts the sample made without a space holder, which had a densification stage earlier. Their plateau region is much shorter and keeps increasing after the yielding. As reported by [125], this plateau region begins to disappear with the reduction of porosity amount, and the stress pattern flows sharply.

2. *Densification stage (Region III)*. In this stage, the parts start to fracture as they no longer endure higher compressive stress. The graph pattern shows a rapid increase for both types of samples alongside the given stress. The cell wall is close contact with each other due to the rising flow of stress. The sample with 75% vol. of KCl easily collapsed and cracked formed within its whole body due to high porosity.

The strength of the porous Cu is attributed to the maximum compression strength that the sample can withstand. This parameter is influenced by their microstructure, such as pores size, distribution, and shape [111],[58]. As shown in Figure 7.14ab, there was a large difference in microstructure between porous Cu made with 0% vol. KCl and 75% vol. KCl. A large number of pores and irregular shapes in the sample microstructure may increase the weakest point of the structure where the stress can penetrate and break through. The stress can easily outbreak the sharp edge of the pores and gradually reduce the structure strength. As a result, this condition encourages fracture formation, and then the sample collapses. In contrary conditions, the sample with low porosity certainly prepares with lower pores and void area and has strong structure bonding. With a density of 8.66 g/cm^3 , nearly reaching the net density of solid Cu and a structure with very low porosity (3.33% vol. porosity), the sample managed to absorb the high stress and was able to slow down until it reached its limits. The high-density solid structure has 'delayed' cell collapse and achieved compressive strength almost 5 times higher than the highest porous Cu sample. These findings were obedient to previously reported studies [58] for those samples with smaller porosity. The small micropores exhibited on the structure were rapidly reduced due to the cell pressing of the deformation process that closed these pores and subsequently improved their density.

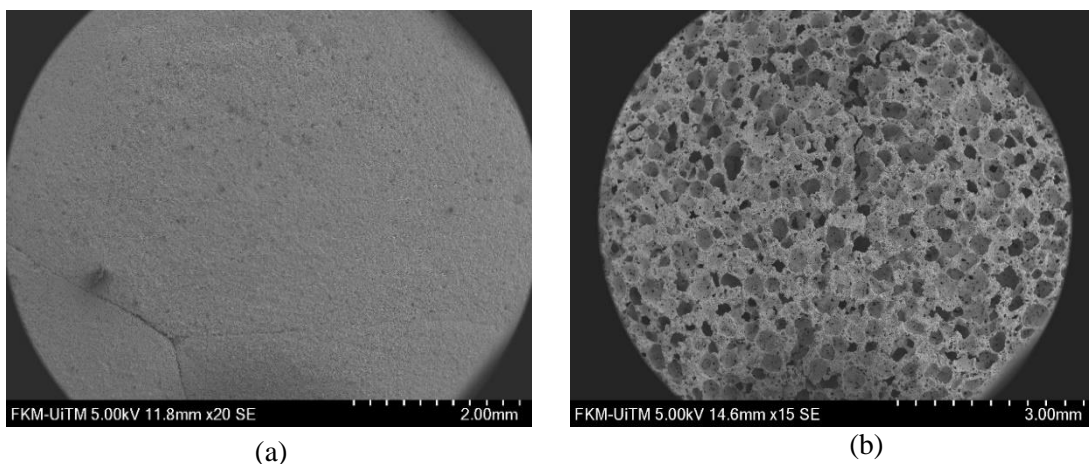


Figure 7.14; SEM images of porous Cu made with different space holder volumes, (a) 0% vol. KCl (b) 75% vol. KCl

7.3.2 Compression Yield Strength of Porous Cu

The compressive strength of porous metal generally relies on its yield strength and density, which can be expressed from the Gibson-Ashby model equation [288]. Considering the proposed model designed for a porous material, relative density is the important feature that influences compressive strength. This summarised that the relative density and yield strength of porous metal corresponding to compressive deformation could be expressed in equation 7.1;

$$\frac{\sigma_y}{\sigma_{ys}} = C \left(\frac{\rho}{\rho_o} \right)^{3/2} \quad (7.1)$$

where σ_y and σ_{ys} are the yield stress of porous metal and the yield stress of the cell wall of solid metal. Both can be represented as the relative yield stress. While ρ and ρ_o are the density of porous and dense materials, which can correlate to the relative density (ρ/ρ_o). C is constant where the Gibson-Ashby model states a C value of 0.3 associated with porous metal and polymers.

For the present study, the compressive stress for each sample was measured from the experiment. The result can be referred to in Table 7.1;

Table 7.1; Yield stress and relative density of porous Cu samples

Type of sample	Porosity (Vol.%), fraction	Relative density, $\left(\frac{\rho}{\rho_o} \right)$	Yield Stress, σ_o . (MPa)
0 % of KCl, 800°C	12.50,	0.875	34.5
50% of KCl, 800°C	59.33	0.41	16.2
60% of KCl, 800°C	67.67	0.32	11.1
70% of KCl, 800°C	75.33	0.25	6.5
75% of KCl, 800°C	80.67	0.19	5.2
0 % of KCl, 850°C	8.66	0.91	46.6
50% of KCl, 850°C	56.3	0.44	20.4
60% of KCl, 850°C	63.0	0.37	15.23
70% of KCl, 850°C	73.33	0.27	8.34
75% of KCl, 850°C	78.70	0.21	6.2

7.4 Thermal Assessment of Porous Copper

Instead of assessing the sample microstructure and its strength via mechanical testing, the porous Cu sample has been assessed on its thermal properties. The porous Cu was commonly dedicated to the functional application related to thermal properties, such as in the heat exchanger and heatsink. Therefore, for the present study, it is significant to understand and examine the capability of the current fabricated porous Cu toward thermal properties. Previously, the investigation on the thermal properties of porous copper was extensively conducted in many ways and methods, either by air or water, as an intermediate test medium for heat transfer. The variation of sample porosity has notably influenced the thermal performance.

For the present study, there were certain limitations and difficulties in thermal testing on the fabricated samples. Instead of the testing cost and the restriction access to laboratory equipment due to the Coronavirus disease (COVID-19) pandemic, the sample also comes with a small size that makes it impossible to fit into the standard experimental jig in the laboratory. Most sample sizes are too small to suit the standard laboratory thermal testing apparatus. The apparatus and tools for thermal measurement were developed for sample sizes of more than 100 mm, whereas the current work produces samples of approximately 14 mm. This will probably influence the outcome of the measurement, which may lead to inaccurate thermal analysis. Therefore, it is necessary to identify the simplest ways to examine the thermal properties and the suitable physical shape of the sample. Due to these factors, the developed thermal test is an alternative way to validate the thermal properties of the sample and was not intentionally designed in a complex thermal test. The outcome is enough to give information related to thermal behaviour.

The simple alternative testing method was designed that fulfill the sample feature shape, and most importantly, the test was directly applied to the actual application. The porous Cu sample was transformed into a heatsink and placed on the electronic board of the Raspberry Pi 3 system. With a program that was specifically developed for the present testing and suitable with the Raspbian Operating System (ROS), the thermal behaviour can be calculated in terms of temperature difference. A brief description of the performed thermal testing is explained in Chapter 3. The use of Raspberry Pi 3 as a measurement tool was designed specifically for this project as this measurement instrument is capable of handling small sample sizes. In addition, because Raspberry Pi 3 is compatible with various peripheral devices, the samples will be tested directly on the actual electronic application in order to measure thermal properties.

7.4.1 Temperature difference towards porosity and SH amount

As discussed in Chapter 3, the thermal analysis can be measured through the temperature difference of the core electronic chip of Raspberry Pi 3. The temperature of the core electronic chip can be measured by

using a special coding system. The testing started with the initial temperature measurement of the electronic chip after the system was in running mode. The reading of temperature can be calculated using the coding system, where the results represent the actual temperature of the electronic system. The Raspberry Pi 3 system was not equipped with any heat transfer devices in order to transfer the heat obtained from the operation. Thus, the present porous Cu was placed on the chip and sealed with a thermal paste to avoid thermal dissipation. The porous Cu works as a heatsink as it is expected to transfer the heat and reduce the temperature of this electronic chip. The thermal properties of porous Cu can be evaluated through the different temperatures before and after applying the porous Cu to the system.

The temperature readings from the thermal study performed on the Raspberry Pi 3 system are summarised in Table 7.2. This small and compact testing process was capable of measuring the temperature difference of the electronic chip. Each measurement will be repeated three times and averaged to ensure measurement consistency. From the results, it was determined that the temperature readings of the chip significantly changed before and after the porous copper implementation. The use of porous Cu is required to minimise the high processing temperature of the Raspberry Pi 3 processor. According to the data, the standard working system kept consistent temperatures between 73 and 81 degrees Celsius. These temperature readings are slightly higher under the standard operating mode system. If the system operates with more than five applications, the temperature rises rapidly. The system will shut down automatically if the operating temperature exceeds 90 degrees Celsius. In order to ensure the safety of the current measurement work, Raspberry Pi 3 will only operate in standard mode, resulting in a steady temperature value between 73 and 81 degrees Celsius.

After the porous copper is tested into the Raspberry Pi 3 system, the temperature reading significantly reduces. It can be summarized that with the application of porous copper, the temperature was reduced as it managed to have lower reading once it was tested on porous copper made with 60% KCl. From the findings, it can be concluded:

- 1) The normal temperature of the Raspberry Pi 3 processor was constantly between 73 and 81°C.
- 2) Longer testing time does not give impact the temperature readings. The temperature reading still demonstrated a constant value.
- 3) The introduction of porous copper decreased the temperature by approximately 50 percent compared to its normal temperature (porous copper manufactured with 60 percent KCl). Each porous copper with a different KCl volume has successfully reduced the temperature. This is due to the ability of porous copper to function as an efficient heatsink. Porous copper efficiently transfers heat through its pores from the Raspberry Pi 3 processor. The formation of pores within the microstructure of porous copper increases its surface area. More heat may be transmitted out due to the larger surface area, resulting in a drop in temperature.

- 4) Porous copper made with a larger quantity of KCl can transfer out more heat, as seen by the decrease in temperature pattern. The temperature decreased by approximately 10°C for each KCl addition. However, the findings from samples with 70 and 75% KCl have demonstrated different temperature patterns. The temperature started to increase, which indicates less heat could be transferred. This can be explained by the lower amount of copper. A higher amount of copper will provide better thermal conductivity. The copper amount represents the lowest value (25 to 35 vol. %)
- 5) The lowest temperature is obtained with samples containing 50-60% KCl. This is due to the balance between the amount of copper and the creation of pores that promote heat transport.
- 6) It also demonstrated that the sample made with 0% KCl could reduce the temperatures to around 10-15 °C lower than the usual reading.
- 7) The measurement of temperature is within the standard operating of Raspberry Pi 3. The temperature is expected to increase if the system runs with many software and applications.

Table 7.2; Temperature different variations of the operating temperature of Raspberry Pie 3 (average value)

Testing Time (Min)	Normal temperature (without KCl) (°C)	Porous Cu (0%vol.KCl) (°C)	Porous Cu (50%vol.KCl) (°C)	Porous Cu (60%vol.KCl) (°C)	Porous Cu (70%vol.KCl) (°C)	Porous Cu (75%vol.KCl) (°C)
5	75.8	60.5	57.2	47.3	50.5	55.6
10	76.9	63.3	58.1	46.1	51.2	56.6
15	77.7	64.0	58.3	45.4	53.3	54.4
20	78.1	65.2	59.4	45.1	54.4	58.5
25	81.0	66.5	59.4	45.2	56.1	55.5
30	74.3	67.2	58.5	45.1	55.3	52.6
35	73.4	66.0	58.6	45.2	52.0	53.4
40	77.5	62.1	59.1	45.3	51.3	54.3
45	78.9	65.5	58.9	45.2	53.5	55.0
50	78.9	64.3	59.1	45.2	53	55.0

Chapter 8 CONCLUSION

The main purpose of the present work is to investigate the usage of Metal Injection Moulding in combination with the Space Holder Technique for the fabrication of porous Cu. The work is motivated by the aim to discover an appropriate technique for porous Cu fabrication that can provide high-accuracy shapes while also producing parts with varying percentages of porosity. In addition, the Compaction and Sintering (C&S) method was employed to provide more information on the manufacture of porous Cu. The work can be concluded as below:

1. The MIM process is comprised of four primary stages: mixing, water debinding, injection moulding, and sintering.
2. The MIM feedstock preparation using a SpeedMixer machine is based on a Dual Asymmetric Centrifuge (DAC), which can produce a sample in a short period of time due to the high mixing speed. The mixture was successfully blended for approximately 21 minutes at a varied speed of 1000rpm to 1800rpm. A zirconia dispersion media was used as a mixing blade during the mixing operation in order to increase the mixing temperature. The Single-Phase Mixing technique is preferred as the sample can be checked regularly during the two-minute gap between each mixing step. With the usage of a high-speed mixing machine, it is possible to obtain a homogenous feedstock, and from the observations, the space holder materials were evenly dispersed. Since the mixing machine was not equipped with a temperature controller, the mixing process temperature was measured manually with an infrared thermometer.
3. The optimum powder loading-binder mixture ratio was obtained through systematic investigation, with 60 % vol. of solid powder and 40 % vol. of the binder. While the weight fraction of the binder system consisted of 75%wt.PEG, 25%wt. PMMA, and 5%wt.SA. The solid loading ratio was determined using a combination of Tapped density measurement and the Rules of Mixture (ROM). For identifying PEG-PMMA-SA, the selection parameter was achieved by performing critical assessments on each binder component.
4. The temperature for injection moulding and the water leaching process can be estimated using DSC and TGA analysis on the feedstock. The findings are important to predict the suitable processing

temperature to ensure the parts can be manufactured with good quality and avoid repeating processes due to defective parts.

5. For the moulding procedure, a pre-injection step was required in order to assess the flowability of the feedstock at the given injection temperature. By identifying the optimal holding period before and after injection moulding, the sample defects during injection moulding can be avoided. The temperature of injection moulding was also carefully examined, with the feedstock capable of being injected at temperatures ranging from 165 to 170 degrees Celsius.
6. The selection of the water removal leaching approach was intended to eliminate PEG and KCl simultaneously, and the process was suited to be carried out in 60°C warm water. The removal of binder and space holder material has been expedited compared to a static dissolution procedure using a rotating magnetic bar. The water leaching procedure took around 7 to 8 hours.
7. The porosity percentage of the sample ranged from 59.33% to 67.67% and 75.33% to 80.67% when prepared with 50% vol KCl to 75% KCl. The sample sintered at a higher temperature (850°C) achieved less porosity than the sample sintered at a lower temperature (800°C).
8. The compressive stress-strain curves of the porous Cu were similar to the typical curves for porous metal. The stress-strain curve can be separated into three regions: the zone of linear elasticity, plastic deformation, and deformation.

Chapter 9 RECOMMENDATIONS AND FUTURE WORKS

The current study successfully delivered porous copper using powder metallurgy procedures in combination with the space holder technique. This technology has been shown here to be capable of creating a porous structure by physically following the structure of the designated space holders, and the size, shape and volume of porosity may therefore be easily controlled within certain limits. Furthermore, the introduction of improved processing techniques in the Metal Injection Moulding process (MIM), such as high-speed mixing, may significantly improve the speed of the MIM production process. This high-speed approach can minimize mixing time by over 50-80 percent compared to standard mixing machines such as sigma-blade mixing machines. Additional improvements to process time can be gained by the improvement of the debinding process, where the space holder and binder were successfully eliminated in a simultaneous process employing water dissolution. This can save cost by decreasing the processing time and reducing the quantity of dissolution solution used.

The knowledge of the process and material properties acquired from this study can be utilized to develop components incorporating this material for applications such as computer heatsinks. To achieve this goal, additional research and development would be required:

1. *Further variation of space holder parameters to establish process limits.*

The present work employed one type of space holder material - potassium chloride (KCl). Thus, the current information obtained may be limited to this type of material, and using other space holders may produce very different behaviour. Although effective as a space holder in this research, other space holders could be lower cost or easier to handle in industrial quantity. Thus, the investigation could be extended to assess other candidates, including those removed thermally as well as by water, or other solvents, dissolution (for example, Potassium Carbonate (K_2CO_3)). Furthermore, the present study used a constant size of space holder (50 μ m diameter), but variable pore size may be useful in optimizing heat transfer behaviour. Thus, for future work, a range of sizes can be explored, for example between 10 μ m to 70 μ m, to verify how this translates to pore size in the porous structure, and the effect on properties. The size range of space holders could be generated by milling larger powders and sieving. The effect of the space holder shape could also be explored, as previous research has suggested this contributes to the properties seen.

2. Varying injection moulding pressure.

For the MIM process, rather than using a constant injection moulding pressure, it is recommended to vary the pressure in order to find the potential optimum parameter. The current works have focused on a constant low injection pressure value (45 MPa). Although this was sufficient to inject the feedstock, higher injection pressure may increase the efficiency of the process and decrease defects associated with partial mould filling. This could become more important if more complex shapes, as could be required for real components, were produced. The potential disadvantage of higher pressures is that they could lead to fracture of the space holder particles and, thus, undesirable alterations to the porous structure.

3. Varying the Powder-Binder Loading and Binder system.

For a broader understanding of the method, attempts to produce foams with different Powder-Binder loading ratios and even different binder systems to the PEG-PMMA-SA system could be valuable. The present study found 60% vol. of Cu and 40% vol. of binder was effective. However, if processing could be developed to allow higher levels of Cu powder within the ratio, this could lead to better thermal conductivity and reduce the amount of shrinkage. Shrinkage was not a problem with the samples made in this work, but with more complex shapes, it could lead to processing inconsistencies.

4. Sample size scale up.

To properly test the thermal behaviour using most standard equipment, larger samples would be needed. The current specimens are up to 10mm × 14mm, which is insufficient for accurate thermal testing. An increase in the size of the samples, up to a volume of the order of magnitude of 1000 cm³, would also permit the production of example components for a range of applications, which is an enabling process for the last area of recommended development.

5. Demonstrator component production and testing.

To properly evaluate the effectiveness of the process and material for applications, it would be necessary to produce an example component, perhaps of slightly reduced size or geometrical complexity, but one that would allow testing of its performance to be made and directly compared to current solutions (such as finned aluminium heat sinks). A challenge with complex components would be the need to manufacture a bespoke mould for the injection, which would be expensive. This could be mitigated by the formation of a basic shape and machining in the green state or after sintering with non-contact machining techniques such as Electro-Discharge Machining.

REFERENCE

- [1] R. A. Hardin and C. Beckermann, "Integrated design of castings: Effect of porosity on mechanical performance," *IOP Conf. Ser. Mater. Sci. Eng.*, vol. 33, no. 1, 2012.
- [2] M. Safiuddin, A. Kaish, C.-O. Woon, and S. Raman, "Early-Age Cracking in Concrete: Causes, Consequences, Remedial Measures, and Recommendations," *Appl. Sci.*, vol. 8, no. 10, p. 1730, Sep. 2018.
- [3] J. L. Huang, N. Warnken, J. C. Gebelin, M. Strangwood, and R. C. Reed, "On the mechanism of porosity formation during welding of titanium alloys," *Acta Mater.*, vol. 60, no. 6–7, pp. 3215–3225, 2012.
- [4] J. Qin, Q. Chen, C. Yang, and Y. Huang, "Research process on property and application of metal porous materials," *J. Alloys Compd.*, vol. 654, pp. 39–44, 2016.
- [5] J. Banhart, "Aluminum foams: On the road to real applications," *MRS Bull.*, vol. 28, no. 4, pp. 290–295, 2003.
- [6] L. P. Lefebvre, J. Banhart, and D. C. Dunand, "Porous metals and metallic foams: Current status and recent developments," *Adv. Eng. Mater.*, vol. 10, no. 9, pp. 775–787, 2008.
- [7] Y. S. Lee and S. K. Hyun, "Centrifugal casting for unpressurized fabrication of lotus-type porous copper," *Mater. Lett.*, vol. 78, pp. 92–94, 2012.
- [8] L. P. Zhang and Y. Y. Zhao, "Fabrication of high melting-point porous metals by lost carbonate sintering process via decomposition route," *Proc. Inst. Mech. Eng. Part B J. Eng. Manuf.*, vol. 222, no. 2, pp. 267–271, 2008.
- [9] H. Zhang, L. Chen, Y. Liu, and Y. Li, "Experimental study on heat transfer performance of lotus-type porous copper heat sink," *Int. J. Heat Mass Transf.*, vol. 56, no. 1–2, pp. 172–180, 2013.
- [10] J. L. Johnson, L. K. Tan, R. Bollina, P. Suri, and R. M. German, "Evaluation of copper powders for processing heat sinks by metal injection moulding," *Powder Metall.*, vol. 48, no. 2, pp. 123–128, 2005.
- [11] B. S. Zlatkov *et al.*, "Recent advances in PIM technology I," *Sci. Sinter.*, vol. 40, no. 1, pp. 79–88, 2008.
- [12] Y. M. Z. Ahmed, M. I. Riad, A. I. Zaky, M. Abdel-Aziz, and M. M. H. Shalabi, "Investigation on the mechanical properties of sintered porous copper compacts," *China Particuology*, vol. 5, no. 6, pp. 391–394, 2007.
- [13] Y. Y. Zhao, T. Fung, L. P. Zhang, and F. L. Zhang, "Lost carbonate sintering process for manufacturing metal foams," *Scr. Mater.*, vol. 52, no. 4, pp. 295–298, 2005.
- [14] J. Banhart, "Manufacture, characterisation and application of cellular metals and metal foams," *Prog. Mater. Sci.*, vol. 46, no. 6, pp. 559–632, 2001.
- [15] K. Ishizaki, S. Komarneni, and M. Nanko, *Porous materials: process technology and applications*, 1st ed., vol. 27. Springer US, 1998.

- [16] L. Stanev, M. Kolev, B. Drenchev, and L. Drenchev, "Open-cell metallic porous materials obtained through space holders - Part I: Production methods. A review," *J. Manuf. Sci. Eng. Trans. ASME*, vol. 139, no. 5, pp. 1–21, 2017.
- [17] M. F. Ashby, A. Evans, N. A. Fleck, L. J. Gibson, J. W. Hutchinson, and H. N. . Wadley, "Metal foams: a design guide," *Mater. Des.*, vol. 23, no. 1, p. 119, 2002.
- [18] J. Banhart, "Manufacturing Routes for very low specific," *Jom*, no. December, pp. 22–27, 2000.
- [19] J. Y. Chen, C. Y. Yang, and P. Y. Chen, "Synthesis of hierarchically porous structured CaCO₃ and TiO₂ replicas by sol-gel method using lotus root as template," *Mater. Sci. Eng. C*, vol. 67, pp. 85–97, 2016.
- [20] K. Ishikawa, "Bone substitute fabrication based on dissolution-precipitation reactions," *Materials (Basel)*, vol. 3, no. 2, pp. 1138–1155, 2010.
- [21] A. Mansourighasri, N. Muhamad, and A. B. Sulong, "Processing titanium foams using tapioca starch as a space holder," *J. Mater. Process. Technol.*, vol. 212, no. 1, pp. 83–89, 2012.
- [22] M. Shbeh *et al.*, "Incorporation of HA into porous titanium to form Ti-HA biocomposite foams," *J. Mech. Behav. Biomed. Mater.*, vol. 96, no. November 2018, pp. 193–203, 2019.
- [23] A. I. Taub and A. A. Luo, "Advanced lightweight materials and manufacturing processes for automotive applications," *MRS Bull.*, vol. 40, no. 12, pp. 1045–1053, 2015.
- [24] R. Goodall Dr, "Porous metals: Foams and sponges," *Adv. Powder Metall. Prop. Process. Appl.*, pp. 273–307, 2013.
- [25] C. Y. Zhao, "Review on thermal transport in high porosity cellular metal foams with open cells," *Int. J. Heat Mass Transf.*, vol. 55, no. 13–14, pp. 3618–3632, 2012.
- [26] T. Hipke, J. Hohlfeld, and S. Rybandt, "Functionally Aluminum Foam Composites for Building Industry," *Procedia Mater. Sci.*, vol. 4, no. 371, pp. 133–138, 2014.
- [27] Y. J. Chen, B. Feng, Y. P. Zhu, J. Weng, J. X. Wang, and X. Lu, "Fabrication of porous titanium implants with biomechanical compatibility," *Mater. Lett.*, vol. 63, no. 30, pp. 2659–2661, 2009.
- [28] A. Nouri, P. D., and C. We, "Biomimetic Porous Titanium Scaffolds for Orthopedic and Dental Applications," *Biomimetics Learn. from Nat.*, pp. 415–451, 2010.
- [29] M. Wolff, J. G. Schaper, M. Dahms, T. Ebel, K. U. Kainer, and T. Klassen, "Magnesium powder injection moulding for biomedical application," *Powder Metall.*, vol. 57, no. 5, pp. 331–340, 2014.
- [30] F. Matassi, A. Botti, L. Sirleo, C. Carulli, and M. Innocenti, "Porous metal for orthopedics implants," *Clin. Cases Miner. Bone Metab.*, vol. 10, no. 2, pp. 111–115, 2013.
- [31] Z. J. Wally, W. van Grunsven, F. Claeyssens, R. Goodall, and G. C. Reilly, "Porous titanium for dental implant applications," *Metals (Basel)*, vol. 5, no. 4, pp. 1902–1920, 2015.
- [32] T. W. Pelletiers and W. K. Daye, "Properties and Selection of Powder Metallurgy Copper and Its Alloys," in *ASM Handbook; Powder Metallurgy*, vol. 7, ASM International, 2015, pp. 539–543.
- [33] T. W. Pelletiers and W. K. Daye, *Production of Copper and Copper Alloy Powders*, vol. 7. ASM International, 2015.

- [34] T. W. P. Li, W. K. Daye, A. Ecker, G. Schumacher, and M. Products, “Properties and Selection of Powder Metallurgy Copper and Its Alloys,” *Powder Metall.*, vol. 7, pp. 539–543, 2018.
- [35] T. W. Pelletiers, W. K. Daye, A. Ecker, G. Schumacher, and M. Products, “Production of Copper and Copper Alloy Powders,” *Powder Metall.*, vol. 7, pp. 544–554, 2018.
- [36] W. K. Daye and T. W. Pelletiers, *Pressing and Sintering of Copper Powders*, vol. 7. ASM International, 2015.
- [37] P. Chokratanasombat and E. Nisaratanaporn, “Preparation of ultrafine copper powders with controllable size via polyol process with sodium hydroxide addition,” *Eng. J.*, vol. 16, no. 4, pp. 39–46, 2012.
- [38] J. Dunkley Dr, “Advances in atomisation techniques for the formation of metal powders,” in *Advances in Powder Metallurgy: Properties, Processing and Applications*, vol. 3, pp. 3–18, 2013
- [39] J.R. Davis, *Introduction and Overview of Copper and Copper Alloys*, 2nd ed. ASM International, 2018.
- [40] R. Konečná and S. Fintová, “Copper and Copper Alloys: Casting, Classification and Characteristic Microstructures,” in *Copper Alloys – Early Applications and Current Performance – Enhancing Processes*, Luca Collini, Ed. IntechOpen, 2012.
- [41] M. Zhang, L. Liu, S. Liang, and J. Li, “Evolution in Microstructures and Mechanical Properties of Pure Copper Subjected to Severe Plastic Deformation,” *Met. Mater. Int.*, vol. 26, no. 10, pp. 1585–1595, 2020.
- [42] L. Liu, J. Lyu, T. Zhao, and T. Li, “Preparations and Properties of Porous Copper Materials for Lithium-Ion Battery Applications,” *Chem. Eng. Commun.*, vol. 203, no. 6, pp. 707–713, 2016,
- [43] L. Bie, X. Luo, L. Kang, D. He, and P. Jiang, “Commercial Copper Foam as an Effective 3D Porous Electrode for Nonenzymatic Glucose Detection,” *Electroanalysis*, vol. 28, no. 9, pp. 2070–2074, 2016.
- [44] Z. Ling *et al.*, “Review on thermal management systems using phase change materials for electronic components, Li-ion batteries and photovoltaic modules,” *Renew. Sustain. Energy Rev.*, vol. 31, pp. 427–438, 2014.
- [45] D. J. Thewsey and Y. Y. Zhao, “Thermal conductivity of porous copper manufactured by the lost carbonate sintering process,” *Phys. Status Solidi Appl. Mater. Sci.*, vol. 205, no. 5, pp. 1126–1131, 2008.
- [46] T. Ogushi, H. Chiba, and H. Nakajima, “Development of lotus-type porous copper heat sink,” *Mater. Trans.*, vol. 47, no. 9, pp. 2240–2247, 2006.
- [47] GoodFellow Company, “Product Summary of Lost Carbonate Sintering (LCS) Porous Copper Foam [Cited 2018 21/06/2018],” Available from: <https://www.goodfellow.com/uk/en-gb/information/larger-quantities/514/553/metals/lcs-copper-foam>.
- [48] H. Nakajima, T. Ikeda, and S. K. Hyun, “Fabrication of lotus-type porous metals and their physical properties,” *Adv. Eng. Mater.*, vol. 6, no. 6, pp. 377–384, 2004.

- [49] Z. Li, T. Yang, Q. Jin, Z. Li, Y. Jiang, and R. Zhou, “Compressive behaviours of lotus-type porous copper fabricated by Gasar process,” *Procedia Eng.*, vol. 31, pp. 337–342, 2012.
- [50] A. E. Simone and L. J. Gibson, “The compressive behaviour of porous copper made by the GASAR process,” *J. Mater. Sci.*, vol. 32, no. 2, pp. 451–457, 1997.
- [51] M. A. Atwater, L. N. Guevara, K. A. Darling, and M. A. Tschopp, “Solid State Porous Metal Production: A Review of the Capabilities, Characteristics, and Challenges,” *Adv. Eng. Mater.*, vol. 20, no. 7, pp. 1–33, 2018.
- [52] S. Xie and J. R. G. Evans, “High porosity copper foam,” *J. Mater. Sci.*, vol. 39, no. 18, pp. 5877–5880, 2004.
- [53] M. H. Shahzeydi, A. M. Parvanian, and M. Panjepour, “The distribution and mechanism of pore formation in copper foams fabricated by Lost Carbonate Sintering method,” *Mater. Charact.*, vol. 111, no. November, pp. 21–30, 2016.
- [54] A. Bansiddhi and D. C. Dunand, “Shape-memory NiTi foams produced by replication of NaCl space-holders,” *Acta Biomater.*, vol. 4, no. 6, pp. 1996–2007, 2008.
- [55] M. Lu and Y. Zhao, “Mechanical properties of LCS porous steel: Comparison between dissolution and decomposition routes,” *TMS Annu. Meet.*, vol. 2, no. June, pp. 137–142, 2010.
- [56] B. Zhao, A. K. Gain, W. Ding, L. Zhang, X. Li, and Y. Fu, “A review on metallic porous materials: pore formation, mechanical properties, and their applications,” *Int. J. Adv. Manuf. Technol.*, vol. 95, no. 5–8, pp. 2641–2659, 2018.
- [57] A. Kennedy, “Porous Metals and Metal Foams Made from Powders,” in *Powder Metallurgy*, no. August, K. Kondoh, Ed. Rijeka, Croatia: InTech, 2012, pp. 31–46.
- [58] E. Zhang and B. Wang, “On the compressive behaviour of sintered porous coppers with low to medium porosities - Part I: Experimental study,” *Int. J. Mech. Sci.*, vol. 47, no. 4-5 SPEC. ISS., pp. 744–756, 2005.
- [59] B. Arifvianto and J. Zhou, “Fabrication of metallic biomedical scaffolds with the space holder method: A review,” *Materials*, vol. 7, no. 5, pp. 3588–3622, 2014.
- [60] H. Nakajima, “Fabrication, properties and application of porous metals with directional pores,” *Prog. Mater. Sci.*, vol. 52, no. 7, pp. 1091–1173, 2007.
- [61] N. Kränzlin and M. Niederberger, “Controlled fabrication of porous metals from the nanometer to the macroscopic scale,” *Mater. Horizons*, vol. 2, no. 4, pp. 359–377, 2015.
- [62] Q. Z. Wang, W. J. Liu, D. M. Lu, and C. X. Cui, “Open-celled porous Cu prepared by replication of a new space-holder,” *Mater. Lett.*, vol. 142, no. 4–5, pp. 52–55, 2015.
- [63] S. Kishimoto, Q. Wang, Y. Tanaka, and Y. Kagawa, “Compressive mechanical properties of closed-cell aluminum foam-polymer composites,” *Compos. Part B Eng.*, vol. 64, pp. 43–49, 2014.
- [64] T. Miyoshi, M. Itoh, S. Akiyama, and A. Kitahara, “ALPORAS aluminum foam: Production process, properties, and applications,” *Adv. Eng. Mater.*, vol. 2, no. 4, pp. 179–183, 2000.
- [65] L. Espinal, “Porosity and Its Measurement,” in *Characterization of Materials*, Elton N. Kaufmann,

Ed. John Wiley & Sons, Inc, 2012.

- [66] I. H. Oh, N. Nomura, and S. Hanada, "Microstructures and mechanical properties of porous titanium compacts prepared by powder sintering," *Mater. Trans.*, vol. 43, no. 3, pp. 443–446, 2002.
- [67] D. C. Dunand, "Processing of titanium foams," *Adv. Eng. Mater.*, vol. 6, no. 6, pp. 369–376, 2004.
- [68] P. S. Liu and K. M. Liang, "Functional materials of porous metals made by P/M, electroplating and some other techniques," *J. Mater. Sci.*, vol. 36, no. 21, pp. 5059–5072, 2001.
- [69] H. W. Seeliger, "Aluminium foam sandwich (AFS) ready for market introduction," *Adv. Eng. Mater.*, vol. 6, no. 6, pp. 448–451, 2004.
- [70] J. Banhart, "Aluminium foams for lighter vehicles," *Int. J. Veh. Des.*, vol. 37, no. 2–3, pp. 114–125, 2005.
- [71] A. Fuganti, L. Lorenzi, A. Grønsund, and M. Langseth, "Aluminium foam for automotive applications," *Adv. Eng. Mater.*, vol. 2, no. 4, pp. 200–204, 2000.
- [72] S. R. Mohamed, S. A. C. Ghani, and W. Sawangsri, "Mechanical properties of additive manufactured cocrmo meta-biomaterials for load bearing implants," *J. Tribol.*, vol. 21, no. July 2018, pp. 93–107, 2019.
- [73] B. R. Levine and D. W. Fabi, "Porous metals in orthopedic applications - A review.," *Materwiss. Werksttech.*, vol. 41, no. 12, pp. 1001–1010, 2010.
- [74] J. M. Baloyo, "Open-cell porous metals for thermal management applications: fluid flow and heat transfer," *Mater. Sci. Technol. (United Kingdom)*, vol. 33, no. 3, pp. 265–276, 2017.
- [75] K. Diao and Y. Zhao, "Heat transfer performance of sintered Cu microchannels produced by a novel method," *Int. J. Heat Mass Transf.*, vol. 139, pp. 537–547, 2019.
- [76] Z. Xiao and Y. Zhao, "Heat transfer coefficient of porous copper with homogeneous and hybrid structures in active cooling," *J. Mater. Res.*, vol. 28, no. 17, pp. 2545–2553, 2013.
- [77] C. Y. Zhao, T. J. Lu, H. P. Hodson, and J. D. Jackson, "The temperature dependence of effective thermal conductivity of open-celled steel alloy foams," *Mater. Sci. Eng. A*, vol. 367, no. 1–2, pp. 123–131, 2004.
- [78] K. Boomsma, D. Poulidakos, and F. Zwick, "Metal foams as compact high performance heat exchangers," *Mech. Mater.*, vol. 35, no. 12, pp. 1161–1176, 2003.
- [79] S. Mao, N. Love, A. Leanos, and G. Rodriguez-Melo, "Correlation studies of hydrodynamics and heat transfer in metal foam heat exchangers," *Appl. Therm. Eng.*, vol. 71, no. 1, pp. 104–118, 2014.
- [80] M. A. White, "Physical Properties of Materials," in *Physical Properties of Materials*, 3rd ed., Boca Raton: CRC Press, 2018.
- [81] A. Moloodi, R. Raiszadeh, J. Vahdati-Khaki, and A. Babakhani, "An assessment of the process of Self-propagating High-Temperature Synthesis for the fabrication of porous copper composite," *J. Alloys Compd.*, vol. 487, no. 1–2, pp. 413–419, 2009.
- [82] K. S. Lee, W. S. Kim, and J. M. Si, "Optimal shape and arrangement of staggered pins in the channel of a plate heat exchanger," *Int. J. Heat Mass Transf.*, vol. 44, no. 17, pp. 3223–3231, 2001.

- [83] A. M. Parvanian and M. Panjepour, “Mechanical behavior improvement of open-pore copper foams synthesized through space holder technique,” *Mater. Des.*, vol. 49, no. August 2013, pp. 834–841, 2013.
- [84] X. Lu and Y. Zhao, “Effect of flow regime on convective heat transfer in porous copper manufactured by lost carbonate sintering,” *Int. J. Heat Fluid Flow*, vol. 80, no. June, p. 108482, 2019.
- [85] Z. Qu, T. Wang, W. Tao, and T. Lu, “Experimental study of air natural convection on metallic foam-sintered plate,” *Int. J. Heat Fluid Flow*, vol. 38, pp. 126–132, 2012.
- [86] R. Singh, A. Akbarzadeh, and M. Mochizuki, “Sintered porous heat sink for cooling of high-powered microprocessors for server applications,” *Int. J. Heat Mass Transf.*, vol. 52, no. 9–10, pp. 2289–2299, 2009.
- [87] P. X. Jiang, M. Li, T. J. Lu, L. Yu, and Z. P. Ren, “Experimental research on convection heat transfer in sintered porous plate channels,” *Int. J. Heat Mass Transf.*, vol. 47, no. 10–11, pp. 2085–2096, 2004.
- [88] Y. Ould-Amer, S. Chikh, K. Bouhadeh, and G. Lauriat, “Forced convection cooling enhancement by use of porous materials,” *Int. J. Heat Fluid Flow*, vol. 19, no. 3, pp. 251–258, 1998.
- [89] L. Stanev, M. Kolev, B. Drenchev, and L. Drenchev, “Open-cell metallic porous materials obtained through space holders - Part II: Structure and properties. A review,” *J. Manuf. Sci. Eng. Trans. ASME*, vol. 139, no. 5, 2017.
- [90] A. Güner, M. M. Arıkan, and M. Nebioglu, “New approaches to aluminum integral foam production with casting methods,” *Metals (Basel)*, vol. 5, no. 3, pp. 1553–1565, 2015.
- [91] A. M. Matz, B. S. Mocker, D. W. Müller, N. Jost, and G. Eggeler, “Mesostructural design and manufacturing of open-pore metal foams by investment casting,” *Adv. Mater. Sci. Eng.*, vol. 2014, 2014.
- [92] B. Matijasevic and J. Banhart, “Improvement of aluminium foam technology by tailoring of blowing agent,” *Scr. Mater.*, vol. 54, no. 4 SPEC. ISS., pp. 503–508, 2006.
- [93] L. Drenchev, J. Sobczak, S. Malinov, and W. Sha, “Gasars: A class of metallic materials with ordered porosity,” *Mater. Sci. Technol.*, vol. 22, no. 10, pp. 1135–1147, 2006.
- [94] F. C. Neto *et al.*, “An Overview of Highly Porous Titanium Processed via Metal Injection Molding in Combination with the Space Holder Method,” *Metals (Basel)*, vol. 12, no. 5, 2022.
- [95] Y. Zhou, Y. Li, and J. Yuan, “The stability of aluminum foams at accumulation and condensation stages in gas injection foaming process,” *Colloids Surfaces A Physicochem. Eng. Asp.*, vol. 482, pp. 468–476, 2015.
- [96] H. Ran, Z. Liu, P. Feng, C. Xu, J. Wang, and F. Akhtar, “Processing, microstructure and properties of hierarchically porous Cu,” *Mater. Express*, vol. 6, no. 3, pp. 271–276, 2016.
- [97] H. Sazegaran and M. Hojati, “Effects of copper content on microstructure and mechanical properties of open-cell steel foams,” *Int. J. Miner. Metall. Mater.*, vol. 26, no. 5, pp. 588–596, 2019.
- [98] M. Khodaei, M. Meratian, O. Savabi, and M. Razavi, “The effect of pore structure on the mechanical

- properties of titanium scaffolds,” *Mater. Lett.*, vol. 171, pp. 308–311, 2016.
- [99] C. Waters, M. Salih, and S. Ajinola, “Porosity comparative analysis of porous copper and OOF modelling,” *J. Porous Mater.*, vol. 22, no. 4, pp. 989–995, 2015.
- [100] C. Waters, S. Ajinola, and M. Salih, “Dissolution sintering technique to create porous copper with sodium chloride using polyvinyl alcohol solution through powder metallurgy,” *Am. J. Eng. Appl. Sci.*, vol. 9, no. 1, pp. 155–165, 2016.
- [101] W. Niu, C. Bai, G. B. Qiu, and Q. Wang, “Processing and properties of porous titanium using space holder technique,” *Mater. Sci. Eng. A*, vol. 506, no. 1–2, pp. 148–151, 2009.
- [102] M. M. Shbeh and R. Goodall, “Design of water debinding and dissolution stages of metal injection moulded porous Ti foam production,” *Mater. Des.*, vol. 87, pp. 295–302, 2015.
- [103] M. M. Shbeh and R. Goodall, “Open Celled Porous Titanium,” *Adv. Eng. Mater.*, vol. 19, no. 11, pp. 1–17, 2017.
- [104] X. Lin and A. R. Kennedy, “Structure-property-processing relationships for stainless steel foams made by mechanical aeration of powder slurries,” *Adv. Eng. Mater.*, vol. 17, no. 6, pp. 839–845, 2015.
- [105] H. X. Dong *et al.*, “Formation of porous Ni-Al intermetallics through pressureless reaction synthesis,” *J. Alloys Compd.*, vol. 484, no. 1–2, pp. 907–913, 2009.
- [106] F. Xie, X. He, S. Cao, and X. Qu, “Structural and mechanical characteristics of porous 316L stainless steel fabricated by indirect selective laser sintering,” *J. Mater. Process. Technol.*, vol. 213, no. 6, pp. 838–843, 2013.
- [107] Q. Z. Wang, C. X. Cui, S. J. Liu, and L. C. Zhao, “Open-celled porous Cu prepared by replication of NaCl space-holders,” *Mater. Sci. Eng. A*, vol. 527, no. 4–5, pp. 1275–1278, 2010.
- [108] H. Lee, “Powder Metallurgy Based Porous Metal Biomaterials,” *J. Powder Metall. Min.*, vol. 02, no. 02, p. 1000109, 2013.
- [109] D. Demirskyi, D. Agrawal, and A. Ragulya, “Neck formation between copper spherical particles under single-mode and multimode microwave sintering,” *Mater. Sci. Eng. A*, vol. 527, no. 7–8, pp. 2142–2145, 2010.
- [110] C. A. Calow and C. R. Tottle, “The measurement and form of porosity in the loose sintering of copper compacts,” *Powder Metall.*, vol. 8, no. 15, pp. 1–19, 1965.
- [111] B. Jiang, N. Q. Zhao, C. S. Shi, X. W. Du, J. J. Li, and H. C. Man, “A novel method for making open cell aluminum foams by powder sintering process,” *Mater. Lett.*, vol. 59, no. 26, pp. 3333–3336, 2005.
- [112] B. Ye and D. C. Dunand, “Titanium foams produced by solid-state replication of NaCl powders,” *Mater. Sci. Eng. A*, vol. 528, no. 2, pp. 691–697, 2010.
- [113] J. Jakubowicz, G. Adamek, and M. Dewidar, “Titanium foam made with saccharose as a space holder,” *J. Porous Mater.*, vol. 20, no. 5, pp. 1137–1141, 2013.
- [114] M. Hakamada, Y. Yamada, T. Nomura, Y. Chen, H. Kusuda, and M. Mabuchi, “Fabrication of

- porous aluminum by spacer method consisting of spark plasma sintering and sodium chloride dissolution,” *Mater. Trans.*, vol. 46, no. 12, pp. 2624–2628, 2005.
- [115] F. Zhang, E. Otterstein, and E. Burkel, “Spark plasma sintering, microstructures, and mechanical properties of macroporous titanium foams,” *Adv. Eng. Mater.*, vol. 12, no. 9, pp. 863–872, 2010.
- [116] A. Ibrahim, F. Zhang, E. Otterstein, and E. Burkel, “Processing of porous Ti and Ti5Mn foams by spark plasma sintering,” *Mater. Des.*, vol. 32, no. 1, pp. 146–153, 2011.
- [117] A. Jinnapat and A. Kennedy, “The Manufacture and Characterisation of Aluminium Foams Made by Investment Casting Using Dissolvable Spherical Sodium Chloride Bead Preforms,” *Metals (Basel)*, vol. 1, no. 1, pp. 49–64, 2011.
- [118] F. García-Moreno, “Commercial applications of metal foams: Their properties and production,” *Materials (Basel)*, vol. 9, no. 2, pp. 20–24, 2016.
- [119] E. Chevalier, D. Chulia, C. Pouget, and M. Viana, “Fabrication of porous substrates: A review of processes using pore forming agents in the biomaterial field,” *J. Pharm. Sci.*, vol. 97, no. 3, pp. 1135–1154, 2008.
- [120] Y. Y. Zhao and D. X. Sun, “Novel sintering-dissolution process for manufacturing Al foams,” *Scr. Mater.*, vol. 44, no. 1, pp. 105–110, 2001.
- [121] D. P. Mondal, H. Jain, S. Das, and A. K. Jha, “Stainless steel foams made through powder metallurgy route using NH₄HCO₃ as space holder,” *Mater. Des.*, vol. 88, pp. 430–437, 2015.
- [122] M. T. Dehaghani, M. Ahmadian, and B. H. Beni, “Fabrication and characterization of porous Co-Cr-Mo/58S bioglass nano-composite by using NH₄HCO₃ as space-holder,” *Mater. Des.*, vol. 88, pp. 406–413, 2015.
- [123] N. Bekoz and E. Oktay, “Effects of carbamide shape and content on processing and properties of steel foams,” *J. Mater. Process. Technol.*, vol. 212, no. 10, pp. 2109–2116, 2012.
- [124] H. Bafti and A. Habibolahzadeh, “Production of aluminum foam by spherical carbamide space holder technique-processing parameters,” *Mater. Des.*, vol. 31, no. 9, pp. 4122–4129, 2010.
- [125] E. E. Aşik and Ş. Bor, “Fatigue behavior of Ti-6Al-4V foams processed by magnesium space holder technique,” *Mater. Sci. Eng. A*, vol. 621, no. 2011, pp. 157–165, 2015.
- [126] T. Aydoğmuş and Ş. Bor, “Processing of porous TiNi alloys using magnesium as space holder,” *J. Alloys Compd.*, vol. 478, no. 1–2, pp. 705–710, 2009.
- [127] M. Sharma, G. K. Gupta, O. P. Modi, B. K. Prasad, and A. K. Gupta, “Titanium foam through powder metallurgy route using acicular urea particles as space holder,” *Mater. Lett.*, vol. 65, no. 21–22, pp. 3199–3201, 2011.
- [128] G. Adamek and J. Jakubowicz, “Tantalum foam made with sucrose as a space holder,” *Int. J. Refract. Met. Hard Mater.*, vol. 53, pp. 51–55, 2015.
- [129] Q. Z. Wang, D. M. Lu, C. X. Cui, and L. M. Liang, “Compressive behaviors and energy-absorption properties of an open-celled porous Cu fabricated by replication of NaCl space-holders,” *J. Mater. Process. Technol.*, vol. 211, no. 3, pp. 363–367, 2011.

- [130] S. B. Jamaludin, C. X. Yi, A. Abdullah, and K. Hussin, "Effect of space holder and compaction pressure on the porosity of sintered copper," *Adv. Mater. Res.*, vol. 795, pp. 82–86, 2013.
- [131] G. L. Hao, Q. P. Xu, F. S. Han, W. D. Li, and S. M. Bai, "Processing and damping behaviour of porous copper," *Powder Metall.*, vol. 52, no. 2, pp. 145–150, 2009.
- [132] N. Michailidis, F. Stergioudi, P. Seventekidis, A. Tsouknidas, and D. Sagris, "Production of porous copper with high surface area for efficient water purification," *CIRP J. Manuf. Sci. Technol.*, vol. 13, pp. 85–89, 2016.
- [133] Y. Chen, D. Kent, M. Bermingham, A. Dehghan-Manshadi, and M. Dargusch, "Manufacturing of biocompatible porous titanium scaffolds using a novel spherical sugar pellet space holder," *Mater. Lett.*, vol. 195, pp. 92–95, 2017.
- [134] R. Siti Athirah, M. Mazlan, N. Amalina, A. Jumahat, and M. H. Ismail, "Processing of Porous Copper by Powder Metallurgy Route with Different Types of Space Holder Materials (SHMs)," *Adv. Mater. Res.*, vol. 1113, no. September, pp. 110–115, 2015.
- [135] R. L. Lehman, J. S. Gentry, and N. G. Glumac, "Thermal stability of potassium carbonate near its melting point," *Thermochim. Acta*, vol. 316, no. 1, pp. 1–9, 1998.
- [136] A. A. Mahaidin *et al.*, "Effect of Sintering Cycle on Physical and Mechanical Properties of Open Pore Cell Copper Foam," *Procedia Chem.*, vol. 19, pp. 546–551, 2016.
- [137] D. X. Sun and Y. Y. Zhao, "Simulation of thermal diffusivity of Al/NaCl powder compacts in producing Al foams by the sintering and dissolution process," *J. Mater. Process. Technol.*, vol. 169, no. 1, pp. 83–88, 2005.
- [138] Y. Torres, J. J. Pavón, and J. A. Rodríguez, "Processing and characterization of porous titanium for implants by using NaCl as space holder," *J. Mater. Process. Technol.*, vol. 212, no. 5, pp. 1061–1069, 2012.
- [139] A. M. Laptev, N. F. Daudt, O. Guillon, and M. Bram, "Increased Shape Stability and Porosity of Highly Porous Injection-Molded Titanium Parts," *Adv. Eng. Mater.*, vol. 17, no. 11, pp. 1579–1587, 2015.
- [140] N. A. Jamal *et al.*, "Fabrication and compressive properties of low to medium porosity closed-cell porous Aluminum using PMMA space holder technique," *Materials (Basel)*, vol. 9, no. 4, pp. 1–13, 2016.
- [141] Y. Bi, Y. Zheng, and Y. Li, "Microstructure and mechanical properties of sintered porous magnesium using polymethyl methacrylate as the space holder," *Mater. Lett.*, vol. 161, pp. 583–586, 2015.
- [142] D. F. Heaney, J. D. Gurosik, and C. Binet, "Isotropic forming of porous structures via metal injection molding," *J. Mater. Sci.*, vol. 40, no. 4, pp. 973–981, 2005.
- [143] H. I. Bakan, "A novel water leaching and sintering process for manufacturing highly porous stainless steel," *Scr. Mater.*, vol. 55, no. 2, pp. 203–206, 2006.
- [144] O. Smorygo, A. Marukovich, V. Mikutski, A. A. Gokhale, G. J. Reddy, and J. V. Kumar, "High-porosity titanium foams by powder coated space holder compaction method," *Mater. Lett.*, vol. 83,

- pp. 17–19, 2012.
- [145] A. Laptev, M. Bram, H. P. Buchkremer, and D. Stöver, “Study of production route for titanium parts combining very high porosity and complex shape,” *Powder Metall.*, vol. 47, no. 1, pp. 85–92, 2004.
- [146] G. Kotan and A. Ş. Bor, “Production and characterization of high porosity Ti-6Al-4V foam by space holder technique powder metallurgy,” *Turkish J. Eng. Environ. Sci.*, vol. 31, no. 3, pp. 149–156, 2007.
- [147] K. F. German, R. M., Hens, “Key Issues in Powder Injection Molding,” *Ceram. Bull.*, vol. 70, no. 8, pp. 1294–1302, 1991.
- [148] D. F. Heaney, “Handbook of Metal Injection Molding,” in *Handbook of Metal Injection Molding*, D. F. Heaney, Ed. Elsevier Science & Technology, 2012, pp. 1–286.
- [149] I. U. Mohsin, D. Lager, C. Gierl, W. Hohenauer, and H. Danninger, “Simulation and optimisation for thermal debinding of copper MIM parts using thermokinetic analysis,” *Powder Metall.*, vol. 54, no. 1, pp. 30–35, 2011.
- [150] A. T. Sidambe, “Biocompatibility of advanced manufactured titanium implants-A review,” *Materials (Basel)*, vol. 7, no. 12, pp. 8168–8188, 2014.
- [151] B. A. German, Randall M., “German RM, Bose A. Injection Molding of Metals and Ceramics, Metal Powder Industries Federation, Princeton, New Jersey, USA, 1997,” *Met. Powder Ind. Fed.*, 1997.
- [152] A. Royer, T. Barriere, and J. C. Gelin, “The degradation of poly(ethylene glycol) in an Inconel 718 feedstock in the metal injection moulding process,” *Powder Technol.*, vol. 284, pp. 467–474, 2015.
- [153] P. Thomas-Vielma, A. Cervera, B. Levenfeld, and A. Várez, “Production of alumina parts by powder injection molding with a binder system based on high density polyethylene,” *J. Eur. Ceram. Soc.*, vol. 28, no. 4, pp. 763–771, 2008.
- [154] S. J. Park, D. Kim, D. Lin, S. J. Park, and S. Ahn, “Rheological characterization of powder mixture including a space holder and its application to metal injection molding,” *Metals (Basel)*, vol. 7, no. 4, p. 120, 2017.
- [155] M. Aslam, F. Ahmad, P. S. M. B. M. Yusoff, K. Altaf, M. A. Omar, and R. M. German, “Powder injection molding of biocompatible stainless steel biodevices,” *Powder Technol.*, vol. 295, pp. 84–95, 2016.
- [156] W. J. Tseng, D. M. Liu, and C. K. Hsu, “Influence of stearic acid on suspension structure and green microstructure of injection-molded zirconia ceramics,” *Ceram. Int.*, vol. 25, no. 2, pp. 191–195, 1999.
- [157] G. Goudah, F. Ahmad, O. Mamat, and M. A. Omar, “Preparation and characterization of copper feedstock for metal injection molding,” *J. Appl. Sci.*, vol. 10, no. 24, pp. 3295–3300, 2010.
- [158] S. M. Jabir *et al.*, “Analysis of the Rheological Behavior of Copper Metal Injection Molding (MIM) Feedstock,” *Procedia Chem.*, vol. 19, no. December, pp. 148–152, 2016.
- [159] L. Moballeggh, J. Morshedean, and M. Esfandeh, “Copper injection molding using a thermoplastic binder based on paraffin wax,” *Mater. Lett.*, vol. 59, no. 22, pp. 2832–2837, 2005.
- [160] J. L. Johnson, L. K. Tan, R. Bollina, P. Suri, and R. M. German, “Evaluation of copper powders for

- processing heat sinks by metal injection moulding,” *Powder Metall.*, vol. 48, no. 2, pp. 123–128, 2005.
- [161] A. Royer, T. Barrière, and J. C. Gelin, “Development and characterization of a metal injection molding bio sourced inconel 718 feedstock based on polyhydroxyalkanoates,” *Metals (Basel)*, vol. 6, no. 4, p. 89, 2016.
- [162] N. Nor Amalina, R. Izyan, W. Nor Aini, J. Aidah, and I. Muhammad Hussain, “Viscosity analysis of copper powder mixed with palm stearin based binder,” *Appl. Mech. Mater.*, vol. 660, no. August, pp. 259–264, 2014.
- [163] M. D. K. Bahrin, N. ‘Aini Wahab, N. A. Nordin, M. H. Ismail, and I. N. Ahmad, “Influence of space holder on rheological behavior of copper feedstocks for metal injection molding,” *J. Teknol.*, vol. 76, no. 6, pp. 91–95, 2015.
- [164] M. H. I. Ibrahim, N. Muhamad, and A. B. Sulong, “Rheological Investigation of Water Atomised Stainless Steel,” *Int. J. Mech. Mater. Eng.*, vol. 4, no. 1, pp. 1–8, 2009.
- [165] M. A. Omar, R. Ibrahim, M. I. Sidik, M. Mustapha, and M. Mohamad, “Rapid debinding of 316 L stainless steel injection moulded component,” *J. Mater. Process. Technol.*, vol. 140, no. 1-3 SPEC., pp. 397–400, 2003.
- [166] N. Chuankrerkkul, P. F. Messer, and H. A. Davies, “Flow and void formation in powder injection moulding feedstocks made with PEG/PMMA binders Part 1 - Experimental observations,” *Powder Metall.*, vol. 51, no. 1, pp. 66–71, 2008.
- [167] G. Chen, P. Cao, G. Wen, and N. Edmonds, “Debinding behaviour of a water soluble PEG/PMMA binder for Ti metal injection moulding,” *Mater. Chem. Phys.*, vol. 139, no. 2–3, pp. 557–565, 2013.
- [168] A. T. Sidambe, I. A. Figueroa, H. G. C. Hamilton, and I. Todd, “Metal injection moulding of CP-Ti components for biomedical applications,” *J. Mater. Process. Technol.*, vol. 212, no. 7, pp. 1591–1597, 2012.
- [169] M. D. Hayat, T. Li, G. Wen, and P. Cao, “Suitability of PEG/PMMA-based metal injection moulding feedstock: an experimental study,” *Int. J. Adv. Manuf. Technol.*, vol. 80, no. 9–12, pp. 1665–1671, 2015.
- [170] M. A. Omar, H. A. Davies, P. F. Messer, and B. Ellis, “The influence of PMMA content on the properties of 316L stainless steel MIM compact,” *J. Mater. Process. Technol.*, vol. 113, no. 1–3, pp. 477–481, 2001.
- [171] M. H. Ismail, R. Goodall, H. A. Davies, and I. Todd, “Porous NiTi alloy by metal injection moulding/sintering of elemental powders: Effect of sintering temperature,” *Mater. Lett.*, vol. 70, pp. 142–145, 2012.
- [172] N. S. Manam, “Experimental Study of Solvent Debinding on Water Soluble PEG Behavior for Water Atomised SS 316L Compact,” *Natl. Conf. Postgrad. Res. 2016*, pp. 187–192, 2016.
- [173] J. González-gutiérrez, G. B. Stringari, and I. Emri, “Powder Injection Molding of Metal and Ceramic Parts,” *Some C*, 2012.

- [174] S. T. Lin and R. M. German, "Extraction debinding of injection molded parts by condensed solvent," *Powder Metall. Int.*, vol. 21, no. 5, pp. 19–24, 1989.
- [175] A. C. Gonçalves, "Metallic powder injection molding using low pressure," *J. Mater. Process. Technol.*, vol. 118, no. 1–3, pp. 193–198, 2001.
- [176] L. jian CHEN, T. LI, Y. min LI, H. HE, and Y. hua HU, "Porous titanium implants fabricated by metal injection molding," *Trans. Nonferrous Met. Soc. China (English Ed.)*, vol. 19, no. 5, pp. 1174–1179, 2009.
- [177] N. de F. Daudt, M. Bram, A. P. C. Barbosa, A. M. Laptev, and C. Alves, "Manufacturing of highly porous titanium by metal injection molding in combination with plasma treatment," *J. Mater. Process. Technol.*, vol. 239, pp. 202–209, 2017.
- [178] M. Köhl, M. Bram, A. Moser, H. P. Buchkremer, T. Beck, and D. Stöver, "Characterization of porous, net-shaped NiTi alloy regarding its damping and energy-absorbing capacity," *Mater. Sci. Eng. A*, vol. 528, no. 6, pp. 2454–2462, 2011.
- [179] T. K. Tatt, N. Muhamad, A. Muchtar, A. B. Sulong, and H. S. Yunn, "Rheological behaviour of novel feedstock for manufacturing porous stainless steel via (MIM)-PSH," *J. Teknol. (Sciences Eng.)*, vol. 59, no. SUPPL.2, pp. 187–191, 2012.
- [180] M. Shbeh, "Titanium Foams via Metal Injection Moulding in Combination with a Space Holder," 2018.
- [181] K. Prashanth, K. Zhuravleva, I. Okulov, M. Calin, J. Eckert, and A. Gebert, "Mechanical and Corrosion Behavior of New Generation Ti-45Nb Porous Alloys Implant Devices," *Technologies*, vol. 4, no. 4, p. 33, 2016.
- [182] K. Nishiyabu, S. Matsuzaki, and S. Tanaka, "Fabrication of micro porous metal components by metal injection molding based powder space holder method," *High Temp. Mater. Process.*, vol. 26, no. 4, pp. 257–267, 2007.
- [183] J. F. Nie *et al.*, "Development of Porous Aluminium by Metal Injection Moulding," *Mater. Forum*, vol. 28, pp. 376–382, 2004.
- [184] E. Carrenõ-Morelli, M. Rodríguez-Arbaizar, A. Amherd, and J. E. Bidaux, "Porous titanium processed by powder injection moulding of titanium hydride and space holders," *Powder Metall.*, vol. 57, no. 2, pp. 93–96, 2014.
- [185] A. Info, "Australian Journal of Basic and Applied Sciences Production of Stainless Steel Foams using the Powder Space Holder-Metal Injection Moulding (PSH-MIM) Method," vol. 9, no. 19, pp. 80–84, 2015.
- [186] A. Noorsyakirah *et al.*, "Application of Potassium Carbonate as Space Holder for Metal Injection Molding Process of Open Pore Copper Foam," *Procedia Chem.*, vol. 19, no. December, pp. 552–557, 2016.
- [187] N. A. Nordin, M. H. Ismail, and N. M. F. N. Jafar, "Porous copper fabricated through powder metallurgy route using NaCl space holder," *Appl. Mech. Mater.*, vol. 446–447, no. March 2015, pp.

- 335–338, 2014.
- [188] A. M. Parvanian, M. Saadatfar, M. Panjepour, A. Kingston, and A. P. Sheppard, “The effects of manufacturing parameters on geometrical and mechanical properties of copper foams produced by space holder technique,” *Mater. Des.*, vol. 53, pp. 681–690, 2014.
- [189] M. Mosalagae, R. Goodall, and M. Elbadawi, “Tape Casting And Lost Carbonate Sintering Processes For Production Of Heat Sinks For Portable Electronics,” *Adv. Mater. Lett.*, vol. 8, no. 7, pp. 807–812, 2017.
- [190] M. D. Hayat, “Development of PEG based binders for metal injection moulding with special focus on titanium,” The University of Auckland, New Zealand, 2015.
- [191] X. Yang, C. Jia, Z. Xie, W. Liu, and Q. Liu, “Water-soluble binder system based on poly-methyl methacrylate and poly-ethylene glycol for injection molding of large-sized ceramic parts,” *Int. J. Appl. Ceram. Technol.*, vol. 10, no. 2, pp. 339–347, 2013.
- [192] E. Hnatkova, B. Hausnerova, A. Hales, L. Jiranek, F. Derguti, and I. Todd, “Processing of MIM feedstocks based on Inconel 718 powder and partially water-soluble binder varying in PEG molecular weight,” *Powder Technol.*, vol. 322, pp. 439–446, 2017.
- [193] A. Hales, “Metal Injection Moulding of Inconel 718 using a Water Soluble Binder System,” The University of Sheffield, UK, 2015.
- [194] T. K. Tatt, N. Muhamad, C. H. Che Haron, and A. B. Sulong, “Influences of temperature and pressure to the green defects,” *Int. J. Mech. Eng. Technol.*, no. 1, pp. 186–192, 2019.
- [195] M. H. Ismail, N. Muhamad, and M. A. Omar, “Characterization of Metal Injection Molding (MIM) Feedstock Based on Water Soluble Binder System,” *J. Kejuruter.*, vol. 20, no. 1, pp. 11–18, 2008.
- [196] M. Seerane, P. Ndlangamandla, and R. Machaka, “The influence of particle size distribution on the properties of metal-injection-moulded 17-4 PH stainless steel,” *J. South. African Inst. Min. Metall.*, vol. 116, no. 10, pp. 935–940, 2016.
- [197] S. Y. Heng, N. Muhamad, A. B. Sulong, A. Fayyaz, and S. M. Amin, “Effect of sintering temperature on the mechanical and physical properties of WC-10%Co through micro-powder injection molding (μ PIM),” *Ceram. Int.*, vol. 39, no. 4, pp. 4457–4464, 2013.
- [198] M. A. Omar, I. Subuki, N. S. Abdullah, N. M. Zainon, and N. Roslani, “Processing of Water-atomised 316L Stainless Steel Powder Using Metal Injection Processes,” *J. Eng. Sci.*, vol. 8, pp. 1–13, 2012.
- [199] R. M. Kumar and B. R. Golla, “Effect of Space Holder on Porosity, Structure and Mechanical Properties of Al Processed via Powder Metallurgy,” *Trans. Indian Inst. Met.*, vol. 74, no. 9, pp. 2379–2386, 2021.
- [200] S. F. Aida, H. Zuhailawati, and A. S. Anasyida, “The Effect of Space Holder Content and Sintering Temperature of Magnesium Foam on Microstructural and Properties Prepared by Sintering Dissolution Process (SDP) Using Carbamide Space Holder,” *Procedia Eng.*, vol. 184, pp. 290–297, 2017.

- [201] B. Lee *et al.*, “Space-holder effect on designing pore structure and determining mechanical properties in porous titanium,” *Mater. Des.*, vol. 57, pp. 712–718, 2014.
- [202] R. Supati, N. H. Loh, K. A. Khor, and S. B. Tor, “Mixing and characterization of feedstock for powder injection molding,” *Mater. Lett.*, vol. 46, no. 2–3, pp. 109–114, 2000.
- [203] M. E. Dizlek, M. Guden, U. Turkan, and A. Tasdemirci, “Processing and compression testing of Ti6Al4V foams for biomedical applications,” *J. Mater. Sci.*, vol. 44, no. 6, pp. 1512–1519, 2009.
- [204] G. Wen, P. Cao, B. Gabbitas, D. Zhang, and N. Edmonds, “Development and design of binder systems for titanium metal injection molding: An overview,” *Metall. Mater. Trans. A Phys. Metall. Mater. Sci.*, vol. 44, no. 3, pp. 1530–1547, 2013.
- [205] M. F. F. A. Hamidi, W. S. W. Harun, N. Z. Khalil, S. A. C. Ghani, and M. Z. Azir, “Study of solvent debinding parameters for metal injection moulded 316L stainless steel,” *IOP Conf. Ser. Mater. Sci. Eng.*, vol. 257, no. 1, 2017.
- [206] P. C. Dawson, “Flow Properties of Molten Polymers,” in *Mechanical Properties and Testing of Polymers: An A–Z Reference*, Springer Science & Business Media, 1999, pp. 88–95.
- [207] H. M. Ng, N. M. Saidi, F. S. Omar, K. Ramesh, S. Ramesh, and S. Bashir, “Thermogravimetric Analysis of Polymers,” *Encyclopedia of Polymer Science and Technology*, no. November. JohnWiley & Sons, pp. 1–29, 2018.
- [208] C. de Blasio, “Thermogravimetric analysis (TGA),” in *Green Energy and Technology*, R. B. P. Joseph D. Menczel, Ed. John Wiley & Sons, 2019, pp. 91–102.
- [209] A. A. Bunaciu, E. gabriela Udriștioiu, and H. Y. Aboul-Enein, “X-Ray Diffraction: Instrumentation and Applications,” *Crit. Rev. Anal. Chem.*, vol. 45, no. 4, pp. 289–299, 2015.
- [210] C. Giannini, M. Ladisa, D. Altamura, D. Siliqi, T. Sibillano, and L. De Caro, “X-ray Diffraction: A powerful technique for the multiple-length-scale structural analysis of nanomaterials,” *Crystals*, vol. 6, no. 8, pp. 1–22, 2016.
- [211] K. Guo *et al.*, “Experimental Investigation on Steel Foams Fabricated by Sintering-Dissolution Process,” *Mater. Manuf. Process.*, vol. 31, no. 12, pp. 1597–1602, 2016.
- [212] J. Vargas-Martínez, J. E. Estela-García, O. M. Suárez, and C. A. Vega, “Fabrication of a porous metal via selective phase dissolution in Al-Cu alloys,” *Metals (Basel)*, vol. 8, no. 6, 2018.
- [213] J. Schindelin, C. T. Rueden, M. C. Hiner, and K. W. Eliceiri, “The ImageJ ecosystem: An open platform for biomedical image analysis,” *Mol. Reprod. Dev.*, vol. 82, no. 7–8, pp. 518–529, 2015.
- [214] J. Schindelin *et al.*, “Fiji : an open-source platform for biological-image analysis,” *Nat. Methods*, vol. 9, no. 7, pp. 676–682, 2012.
- [215] M. Ezzahmouly *et al.*, “Micro-computed tomographic and SEM study of porous bioceramics using an adaptive method based on the mathematical morphological operations,” *Heliyon*, vol. 5, no. 12, p. e02557, 2019.
- [216] A. Ul-Hamid, *A Beginners’ Guide to Scanning Electron Microscopy*. Springer, 2018.
- [217] M. Scimeca, S. Bischetti, H. K. Lamsira, R. Bonfiglio, and E. Bonanno, “Energy dispersive X-ray

- (EDX) microanalysis: A powerful tool in biomedical research and diagnosis,” *Eur. J. Histochem.*, vol. 62, no. 1, pp. 89–99, 2018.
- [218] N. Tuncer, M. Bram, A. Laptev, T. Beck, A. Moser, and H. P. Buchkremer, “Study of metal injection molding of highly porous titanium by physical modeling and direct experiments,” *J. Mater. Process. Technol.*, vol. 214, no. 7, pp. 1352–1360, 2014.
- [219] M. M. Shbeh and R. Goodall, “Open pore titanium foams via metal injection molding of metal powder with a space holder,” *Met. Powder Rep.*, vol. 71, no. 6, pp. 450–455, 2016.
- [220] T. K. Tatt, N. Muhamad, A. Muchtar, A. B. Sulong, and K. Y. Shia, “Production of porous stainless steel using the space holder method,” *Sains Malaysiana*, vol. 50, no. 2, pp. 507–514, 2021.
- [221] M. Bram, C. Stiller, H. P. Buchkremer, D. Stöver, and H. Baur, “High-porosity titanium, stainless steel, and superalloy parts,” *Adv. Eng. Mater.*, vol. 2, no. 4, pp. 196–199, 2000.
- [222] M. Rafi Raza, A. Bakar Sulong, N. Muhammad, M. Niaz Akhtar, and J. Rajabi, “Effects of Binder and Processing Parameters on Processability of Porous Ti/HA Composite through Powder Injection Molding,” *Adv. Mater. Res.*, vol. 1133, pp. 90–94, 2016.
- [223] X. F. F. Tao, L. P. Zhang, and Y. Y. Y. Zhao, “Mechanical response of porous copper manufactured by lost carbonate sintering process,” *Mater. Sci. Forum*, vol. 539–543, no. PART 2, pp. 1863–1867, 2007.
- [224] R. Siti Athirah, M. Mazlan, N. Amalina, A. Jumahat, and M. H. Ismail, “Processing of Porous Copper by Powder Metallurgy Route with Different Types of Space Holder Materials (SHMs),” *Adv. Mater. Res.*, vol. 1113, no. July, pp. 110–115, 2015.
- [225] Y. Hangai, K. Zushida, H. Fujii, R. Ueji, O. Kuwazuru, and N. Yoshikawa, “Friction powder compaction process for fabricating open-celled Cu foam by sintering-dissolution process route using NaCl space holder,” *Mater. Sci. Eng. A*, vol. 585, pp. 468–474, 2013.
- [226] A. M. Parvanian, M. Saadatfar, M. H. Shahzeydi, and M. Panjepour, “Pore engineering of copper foams made by space holder technique through XMCT characterization,” pp. 10–12.
- [227] M. A. El-Hadek and S. Kaytbay, “Mechanical and physical characterization of copper foam,” *Int. J. Mech. Mater. Des.*, vol. 4, no. 1, pp. 63–69, 2008.
- [228] J. Xiao, Y. Li, J. Liu, and Q. Zhao, “Fabrication and Characterization of Porous Copper with Ultrahigh Porosity,” 2022.
- [229] C. Vincent, J. F. Silvain, J. M. Heintz, and N. Chandra, “Effect of porosity on the thermal conductivity of copper processed by powder metallurgy,” *J. Phys. Chem. Solids*, vol. 73, no. 3, pp. 499–504, 2012.
- [230] Y. M. Z. Ahmed, M. I. Riad, A. S. Sayed, M. K. Ahlam, and M. E. H. Shalabi, “Correlation between factors controlling preparation of porous copper via sintering technique using experimental design,” *Powder Technol.*, vol. 175, no. 1, pp. 48–54, 2007.
- [231] M. Sharma, O. P. Modi, and P. Kumar, “Synthesis and characterization of copper foams through a powder metallurgy route using a compressible and lubricant space-holder material,” *Int. J. Miner.*

- Metall. Mater.*, vol. 25, no. 8, pp. 902–912, 2018.
- [232] A. T. Sidambe, W. Xu, I. Todd, I. A. Figueroa, and H. Hamilton, “Rapid debinding of a titanium injection molded component,” *Proc. Euro Int. Powder Metall. Congr. Exhib. Euro PM 2008*, vol. 2, pp. 275–280, 2008.
- [233] M. I. Jamaludin, N. A. A. Kasim, N. H. M. Nor, and M. H. Ismail, “Development of porous Ti-6Al-4V Mix with palm stearin binder by metal injection molding technique,” *Am. J. Appl. Sci.*, vol. 12, no. 10, pp. 742–751, 2015.
- [234] M. H. Ismail, N. H. M. Nor, H. A. Davies, and I. Todd, “Feedstock flow characterization and processing of porous niti by metal injection moulding (MIM),” *J. Teknol.*, vol. 76, no. 11, pp. 97–105, 2015.
- [235] R. M. German, “The characteristic of powders for injection moulding,” in *Powder Injection Moulding*, Metal Powder Industries Federation, 1990, pp. 61–70.
- [236] D. F. Heaney, “Powders for metal injection molding (MIM),” in *Handbook of Metal Injection Molding*, 2012, pp. 50–63.
- [237] A. P. Moon, S. Dwarapudi, K. S. Sista, D. Kumar, and G. R. Sinha, “Opportunity and challenges of iron powders for metal injection molding,” *ISIJ Int.*, vol. 61, no. 7, pp. 2015–2033, 2021.
- [238] C. J. Boukouvalas, M. K. Krokida, Z. B. Maroulis, and D. Marinou-Kouris, *Density and porosity: Literature data compilation for foodstuffs*, vol. 9, no. 4. 2006.
- [239] B. Hausnerova, T. Kitano, I. Kuritka, J. Prindis, and L. Marcanikova, “The role of powder particle size distribution in the processability of powder injection molding compounds,” *Int. J. Polym. Anal. Charact.*, vol. 16, no. 2, pp. 141–151, 2011.
- [240] A. Dehghan-Manshadi, M. J. Birmingham, M. S. Dargusch, D. H. StJohn, and M. Qian, “Metal injection moulding of titanium and titanium alloys: Challenges and recent development,” *Powder Technol.*, vol. 319, pp. 289–301, 2017.
- [241] A. P. Cysne Barbosa, *Development of the 2-Component-Injection Moulding for Metal Powders*, vol. 127. 2011.
- [242] C. Salvo, C. Aguilar, S. Lascano, L. Pérez, M. López, and R. V. Mangalaraja, “The effect of alumina particles on the microstructural and mechanical properties of copper foams fabricated by space-holder method,” *Mater. Res. Express*, vol. 5, no. 5, p. 56514, 2018.
- [243] S. Ahn, S. J. Park, S. Lee, S. V. Atre, and R. M. German, “Effect of powders and binders on material properties and molding parameters in iron and stainless steel powder injection molding process,” *Powder Technol.*, vol. 193, no. 2, pp. 162–169, 2009.
- [244] A. T. Sidambe, I. A. Figueroa, H. Hamilton, and I. Todd, “Improved processing of titanium alloys by metal injection moulding,” *IOP Conf. Ser. Mater. Sci. Eng.*, vol. 26, no. 1, p. 012005, 2011.
- [245] M. Y. Anwar, P. F. Messer, B. Ellis, and H. A. Davies, “Injection moulding of 316l stainless steel powder using novel binder system,” *Powder Metall.*, vol. 38, no. 2, pp. 113–119, 1995.
- [246] H. I. Bakan, Y. Jumadi, P. F. Messer, H. A. Davies, and B. Ellis, “Study of processing parameters for

- MIM feedstock based on composite PEG-PMMA binder,” *Powder Metall.*, vol. 41, no. 4, 1998.
- [247] B. Hausnerova, I. Kuritka, and D. Bleyan, “Polyolefin backbone substitution in binders for low temperature powder injection moulding feedstocks,” *Molecules*, vol. 19, no. 3, pp. 2748–2760, 2014.
- [248] Davit Bleyan, “Binder Systems for Powder Injection Moulding Polymerní,” Tomas Bata University in Zlin, 2015.
- [249] A. B. Sulong, N. Muhamad, A. Arifin, and K. B. Yong, “Optimizing injection parameter of metal injection molding processes using the feedstock of 16 μm stainless steel powder (SS316L), PEG, PMMA and stearic acid,” *J. Appl. Sci. Res.*, vol. 8, no. 6, pp. 2998–3003, 2012.
- [250] N. Chuankrerkkul, P. F. Messer, and H. A. Davies, “Application of polyethylene glycol and polymethyl methacrylate as a binder for powder injection moulding of hardmetals,” *Chiang Mai J. Sci.*, vol. 35, no. 1, pp. 188–195, 2008.
- [251] T. -Y Chan and S. -T Lin, “Effects of Stearic Acid on the Injection Molding of Alumina,” *Journal of the American Ceramic Society*, vol. 78, no. 10, pp. 2746–2752, 1995.
- [252] A. Arockiasamy *et al.*, “Effect of additives on sintering response of titanium by powder injection moulding,” *Powder Metall.*, vol. 54, no. 3, pp. 420–426, 2011.
- [253] I. Subuki, M. H. Ismail, A. Amir, and M. A. Omar, “Effect of stearic acid on rheological properties of 316L feedstock for metal injection moulding,” *J. Teknol. (Sciences Eng.)*, vol. 59, no. SUPPL.2, pp. 173–177, 2012.
- [254] M. H. Ismail, R. Goodall, H. A. Davies, and I. Todd, “Formation of microporous NiTi by transient liquid phase sintering of elemental powders,” *Mater. Sci. Eng. C*, vol. 32, no. 6, pp. 1480–1485, 2012.
- [255] M. D. Hayat, G. Wen, T. Li, and P. Cao, “Compatibility improvement of Ti-MIM feedstock using liquid surfactant,” *J. Mater. Process. Technol.*, vol. 224, pp. 33–39, 2015.
- [256] M. T. Zaky, F. S. Soliman, and A. S. Farag, “Influence of paraffin wax characteristics on the formulation of wax-based binders and their debinding from green molded parts using two comparative techniques,” *J. Mater. Process. Technol.*, vol. 209, no. 18–19, pp. 5981–5989, 2009.
- [257] M. D. Hayat, G. Wen, M. F. Zulkifli, and P. Cao, “Effect of PEG molecular weight on rheological properties of Ti-MIM feedstocks and water debinding behaviour,” *Powder Technol.*, vol. 270, no. Part A, pp. 296–301, 2015.
- [258] R. M. German, “Progress in titanium metal powder injection molding,” *Materials (Basel)*, vol. 6, no. 8, pp. 3641–3662, 2013.
- [259] L. Liu, N. H. Loh, B. Y. Tay, S. B. Tor, Y. Murakoshi, and R. Maeda, “Mixing and characterisation of 316L stainless steel feedstock for micro powder injection molding,” *Mater. Charact.*, vol. 54, no. 3, pp. 230–238, 2005.
- [260] J. M. Contreras, A. Jiménez-Morales, and J. M. Torralba, “Experimental and theoretical methods for optimal solids loading calculation in MIM feedstocks fabricated from powders with different particle characteristics,” *Powder Metall.*, vol. 53, no. 1, pp. 34–40, 2010.
- [261] M. N. . Seerane, H. K. Chikwanda, W. Focke, and R. Machaka, “Investigating the Powder loading of

- gas atomised Ti6Al4V powder using an ‘in-house’ binder for MIM,” *Adv. Met. Initiat. Precious Met.* 2013, pp. 49–56, 2013.
- [262] S. Ali Afraz, “Master’s Thesis - Mechanical, microstructural and corrosion performance for MIM materials,” 2005.
- [263] M. Behi, “High Solid Loading Aqueous Base Metal/Ceramic Feedstock for injection Molding,” p. 14, 2001.
- [264] Y. Li, L. Li, and K. A. Khalil, “Effect of powder loading on metal injection molding stainless steels,” *J. Mater. Process. Technol.*, vol. 183, no. 2–3, pp. 432–439, 2007.
- [265] S. N. Kane, A. Mishra, and A. K. Dutta, “Preface: International Conference on Recent Trends in Physics (ICRTP 2016),” *J. Phys. Conf. Ser.*, vol. 755, no. 1, 2016.
- [266] A. T. Sidambe, I. A. Figueroa, H. Hamilton, and I. Todd, “Metal injection moulding of Ti-64 components using a water soluble binder,” vol. 4, no. 4, pp. 56–62, 2010.
- [267] S. N. Kane, A. Mishra, A. K. Dutta, and P. Sen, “Preface,” *J. Phys. Conf. Ser.*, vol. 365, no. 1, p. 011001, 2012.
- [268] J. Hidalgo, A. Jiménez-Morales, and J. M. Torralba, “Torque rheology of zircon feedstocks for powder injection moulding,” *J. Eur. Ceram. Soc.*, vol. 32, no. 16, pp. 4063–4072, 2012.
- [269] S. J. Park, Y. Wu, D. F. Heaney, X. Zou, G. Gai, and R. M. German, “Rheological and thermal debinding behaviors in titanium powder injection molding,” *Metall. Mater. Trans. A Phys. Metall. Mater. Sci.*, vol. 40, no. 1, pp. 215–222, 2009.
- [270] P. Suri, S. V. Atre, R. M. German, and J. P. de Souza, “Effect of mixing on the rheology and particle characteristics of tungsten-based powder injection molding feedstock,” *Mater. Sci. Eng. A*, vol. 356, no. 1–2, pp. 337–344, 2003.
- [271] T. K. Tatt, N. Muhamad, A. Muchtar, A. B. Sulong, and N. M. Cherng, “Influence of sintering parameters on the compressive yield strength of stainless steel foams produced by the space holder method,” *Sains Malaysiana*, vol. 45, no. 4, pp. 653–658, 2016.
- [272] S. V. A. R.K. Enneti, V.P. Onbattuvelli, “Powder binder formulation and compound manufacture in metal injection molding (MIM),” in *Handbook of Metal Injection Molding*, 2nd ed., Woodhead Publishing, 2019, pp. 57–62.
- [273] A. Arifin and A. B. Sulong, “Effect of mixing parameters on the mixing time and density of composite HA/Ti6Al4V feedstock for powder injection molding,” *MATEC Web Conf.*, vol. 101, 2017.
- [274] M. Mosalagae, C. M. Brambila Renteria, M. Elbadawi, M. Shbeh, and R. Goodall, “Structural characterisation of porous copper sheets fabricated by lost carbonate sintering applied to tape casting,” *Mater. Charact.*, vol. 159, 2020.
- [275] S. Lin-Jian and L. Guoqin, “Morphology and thermal behaviour of poly(methyl methacrylate)/poly(ethylene glycol) semi-interpenetrating polymer networks,” *J. Chil. Chem. Soc.*, vol. 56, no. 4, pp. 918–921, 2011.

- [276] J. M. Adames, “Characterization of Polymeric Binders for Metal Injection Moulding (MIM) Process,” The University of Akron, 2007.
- [277] A. P. C. Barbosa, M. Bram, D. Stöver, and H. P. Buchkremer, “Realization of a titanium spinal implant with a gradient in porosity by 2-component-metal injection moulding,” *Adv. Eng. Mater.*, vol. 15, no. 6, pp. 510–521, 2013.
- [278] M. D. Hayat, T. Li, and P. Cao, “Incorporation of PVP into PEG/PMMA based binder system to minimize void nucleation,” *Mater. Des.*, vol. 87, pp. 932–938, 2015.
- [279] A. Manonukul, N. Muenya, F. Léaux, and S. Amaranan, “Effects of replacing metal powder with powder space holder on metal foam produced by metal injection moulding,” *J. Mater. Process. Technol.*, vol. 210, no. 3, pp. 529–535, 2010.
- [280] M. Aslam *et al.*, “Investigation of Rheological Behavior of Low Pressure Injection Molded Stainless Steel Feedstocks,” *Adv. Mater. Sci. Eng.*, vol. 2016, 2016.
- [281] Ç. Karataş, A. Sözen, E. Arcaklioglu, and S. Erguney, “Investigation of mouldability for feedstocks used powder injection moulding,” *Mater. Des.*, vol. 29, no. 9, pp. 1713–1724, 2008.
- [282] Y. Liu, *Heat Transfer Process between polymer and cavity wall during injection molding*. 2014.
- [283] R. M. German and A. Bose, “Injection Molding Of Metals And Ceramics. Princeton, New Jersey: Metal Powder Industries Federation,” p. 1997, 1997.
- [284] Y. Torres, S. Lascano, J. Bris, J. Pavón, and J. A. Rodriguez, “Development of porous titanium for biomedical applications: A comparison between loose sintering and space-holder techniques,” *Mater. Sci. Eng. C*, vol. 37, no. 1, pp. 148–155, 2014.
- [285] A. Laptev and M. Bram, “Manufacturing hollow titanium parts by powder metallurgy route and space holder technique,” *Mater. Lett.*, vol. 160, pp. 101–103, 2015.
- [286] B. Jiang, N. Q. Zhao, C. S. Shi, and J. J. Li, “Processing of open cell aluminum foams with tailored porous morphology,” *Scr. Mater.*, vol. 53, no. 6, pp. 781–785, 2005.
- [287] M. Sabzevari, S. A. Sajjadi, and A. Moloodi, “Physical and mechanical properties of porous copper nanocomposite produced by powder metallurgy,” *Adv. Powder Technol.*, vol. 27, no. 1, pp. 105–111, 2016.
- [288] M. F. A. Lorna J. Gibson, *Cellular Solids: Structure and Properties*, 2nd ed. Cambridge University Press, 1999.
- [289] C. M. Cady, G. T. Gray, C. Liu, M. L. Lovato, and T. Mukai, “Compressive properties of a closed-cell aluminum foam as a function of strain rate and temperature,” *Mater. Sci. Eng. A*, vol. 525, no. 1–2, pp. 1–6, 2009.
- [290] Y. Saberi and H. Oveisi, “High porosity micro- And macro-cellular copper foams with semi-open cell microstructure toward its physical and mechanical properties,” *Mater. Res. Express*, vol. 7, no. 1, 2019.
- [291] M. A. Salih, “Processing And Modeling Of Porous Copper Using Sintering Dissolution Process,” North Carolina Agricultural and Technical State University Follow, 2014.

- [292] Z. Esen and Ş. Bor, "Characterization of Ti-6Al-4V alloy foams synthesized by space holder technique," *Mater. Sci. Eng. A*, vol. 528, no. 7–8, pp. 3200–3209, 2011.
- [293] M. Hakamada, Y. Asao, T. Kuromura, Y. Chen, H. Kusuda, and M. Mabuchi, "Density dependence of the compressive properties of porous copper over a wide density range," *Acta Mater.*, vol. 55, no. 7, pp. 2291–2299, 2007.